CONCEPTUAL DESIGN OF A NEW TWO-SEATER WING-IN GROUND EFFECT CRAFT

By

AHMAD AFIFI BIN AHMAD PUA'AT

Thesis Submitted to the School of Graduate Studies, Universiti Putra Malaysia, in Fulfilment of the Requirements for the Degree of Doctor of Philosophy

March 2024

FK 2024 9

Abstract of thesis presented to the Senate of Universiti Putra Malaysia in fulfilment of the requirement for the degree of Doctor of Philosophy

CONCEPTUAL DESIGN OF A NEW TWO-SEATER WING-IN GROUND EFFECT CRAFT

By

AHMAD AFIFI BIN AHMAD PUA'AT

March 2024

Chair : Md Amzari bin Md Zhahir, PhD
Faculty : Engineering

Wing-in-Ground (WIG) crafts are a concept with the potential to revolutionize transportation. They leverage the ground effect to achieve high speeds and efficiency, offering advantages over traditional airplanes and ships. However, there are significant design problems that hinder their widespread adoption such as instability when transiting from inside ground effect (IGE) zone to outside ground effect (OGE) zone. This consequence in drastic change in pressure distribution around the lifting surfaces and causes the location of center of pressure (COP) to migrate along the chord. This phenomenon results in flight instability in longitudinal direction and requires fast response from the pilot to control the hoverwing. Hence, the thesis focused on developing a new conceptual design of two-seater wing in ground effect (WIG) craft based on center of pressure migration investigation. The initial task is to conduct Computational Fluid Dynamic (CFD) simulations on various types of airfoils incorporated with rectangle and inverse delta wing geometries, and UH18-SPW Hoverwing to investigate COP migration behavior based on pressure

distribution around lifting surfaces. Then, the next task to develop a new conceptual design of a two-seater WIG craft based on the established design requirements and verifies the aerodynamic performance of UH18-SPW Hoverwing using CFD software by comparing it to the result of UH18-SPW wind tunnel test data produce by Steven Morris, 2008. After that, a design with minimum COP migration was produce as final outcome. Using the data obtained previously the next step is to analyze and compare the performance of the proposed WIG craft design iteration with respect to baseline design references. The result of the analysis is plotted using excel spreadsheet for better visualization. The aerodynamic performance comparison between the new two-seater WIG craft design and the baseline reference design reveals a significant difference. The new design exhibits a 99% reduction in center of pressure migration, suggesting a significant improved in longitudinal stability. However, this comes at the cost of a substantial trade-off. The new design generates a substantial decrease in maximum lift coefficient of 43% than the baseline. Furthermore, the new design experiences a 48.6% decrease in maximum drag coefficient, which translates to lesser fuel consumption and improved overall efficiency. These findings highlight the need to carefully balance stability improvements with the crucial aspects of lift generation and drag reduction in the design process for WIG craft.

Keywords: Wing-in-Ground, inside ground effect, outside ground effect, hoverwing, center of pressure

SDG: GOAL 9: Industry, Innovation and Infrastructure, GOAL 11 Sustainable Cities and Communities, GOAL 13 Climate Action

Abstrak tesis yang dikemukakan kepada Senat Universiti Putra Malaysia sebagai memenuhi keperluan untuk ijazah Doktor Falsafah

REKA BENTUK KONSEP BAHARU KAPAL WING-IN-GROUND EFFECT DUA TEMPAT DUDUK

Oleh

AHMAD AFIFI BIN AHMAD PUA'AT

March 2024

Pengerusi : Md Amzari bin Md Zhahir, PhD
Fakulti : Kejuruteraan

Wing-in-Ground (WIG) Kraf adalah konsep yang berpotensi untuk merevolusikan pengangkutan. Mereka memanfaatkan kesan darat untuk mencapai kelajuan dan kecekapan tinggi, menawarkan kelebihan berbanding kapal terbang dan kapal tradisional. Walau bagaimanapun, terdapat masalah reka bentuk yang ketara yang menghalang penggunaan meluas mereka seperti ketidakstabilan apabila beralih dari zon kesan tanah dalam (IGE) ke zon kesan tanah luar (OGE). Akibat ini dalam perubahan drastik dalam pengagihan tekanan di sekeliling permukaan angkat dan menyebabkan lokasi pusat tekanan (COP) berhijrah di sepanjang kord. Fenomena ini mengakibatkan ketidakstabilan penerbangan dalam arah membujur dan memerlukan tindak balas pantas daripada juruterbang untuk mengawal lelayang. Tugas awal adalah untuk menjalankan simulasi Computational Fluid Dynamic (CFD) pada pelbagai jenis airfoil yang digabungkan dengan geometri sayap delta segi empat tepat dan songsang, dan UH18-SPW Hoverwing untuk menyiasat tingkah laku penghijrahan COP berdasarkan taburan tekanan di sekitar permukaan angkat. Kemudian, tugas seterusnya untuk membangunkan reka bentuk konsep baharu pesawat WIG berdasarkan keperluan reka bentuk yang ditetapkan dan mengesahkan prestasi aerodinamik UH18-SPW Hoverwing, menggunakan perisian CFD. Data prestasi aerodinamik daripada kajian ini kemudiannya dibandingkan dengan hasil data ujian terowong angin UH18-SPW yang dihasilkan oleh Steven Morris, Perbandingan prestasi aerodinamik antara reka bentuk kraf WIG dan reka bentuk rujukan garis dasar mendedahkan perbezaan yang ketara. Reka bentuk baharu mempamerkan pengurangan 99% dalam penghijrahan pusat tekanan, mencadangkan peningkatan yang ketara dalam kestabilan membujur. Walau bagaimanapun, reka bentuk baharu menjana pengurangan ketara dalam pekali angkat maksimum sebanyak 43% daripada garis dasar. Tambahan pula, reka bentuk baharu mengalami penurunan 48.6% dalam pekali seret maksimum, yang diterjemahkan kepada penggunaan bahan api yang lebih rendah dan kecekapan keseluruhan yang dipertingkatkan. Penemuan ini menyerlahkan keperluan untuk mengimbangi penambahbaikan kestabilan dengan teliti dengan aspek penting penjanaan daya angkat dan pengurangan seretan dalam proses reka bentuk untuk kraf WIG.

Kata Kunci: Wing-in-Ground, zon kesan tanah dalam, zon kesan tanah luar, hoverwing, pusat tekanan

SDG: MATLAMAT 9**:** Industri, Inovasi dan Infrastruktur, MATLAMAT 11 Bandar dan Komuniti Lestari, MATLAMAT 13 Tindakan Iklim

ACKNOWLEDGEMENTS

بِسْمِ اللَّه الرَّحْمَنِ الرَّحِيمِ

Alhamdulillah to Allah S.W.T because of His will and blessing, providing me with a great health, strength and patience that in the end I have successfully finished this thesis. A thousand thank you to Dr. Md Amzari Bin Md Zhahir, Dr. Ezanee Gires, Dr. Mohd Faisal Bin Abdul Hamid, Re. Lt. Kol. Assoc. Prof. Mohamed Tarmizi Bin Ahmad and Ir.Dr.Abdul Aziz Hassan for his guidance alongside me through finishing this thesis. Their wide knowledge and wisdom have been of great value for me on doing this thesis. To Innopeak (M) Sdn Bhd, I would like to take the opportunity to thank those people who spent their time and shared their knowledge for helping me to complete my thesis as best as possible. Without their advice and encouragement, I might not finish this thesis. With a million thanks, I stand here indebted to my late father, Ahmad Pua'at Mustapha, my mother, Hamidah Bahari, and my wife, Nurul Qusna Mohd Zaki. Their unwavering support, both moral and financial, fueled my pursuit of knowledge and experience. It is with profound gratitude that I dedicate this valuable thesis to them. This journey wasn't just about acquiring fundamental knowledge; it was a crucible that forged me into someone capable of inheriting and passing on the lessons gleaned over years of dedicated study. As I reach this milestone, the completion of my Doctor of Philosophy, my heart overflows with appreciation for their unwavering belief in me.

Thank you,

This thesis was submitted to the Senate of Universiti Putra Malaysia and has been accepted as fulfilment of the requirement for the degree of Doctor of Philosophy. The members of the Supervisory Committee were as follows:

Md Amzari bin Md Zhahir, PhD
Senior Lecturer
Faculty of Engineering
Universiti Putra Malaysia
(Chairman)

Ezanee bin Gires, PhD
Senior Lecturer
Faculty of Engineering
Universiti Putra Malaysia
(Member)

Mohd Faisal bin Abdul Hamid, PhD
Senior Lecturer
Faculty of Engineering
Universiti Putra Malaysia
(Member)

Mohamed Tarmizi bin Ahmad
Associate Professor, LT. COL (RE)
Faculty of Engineering
Universiti Pertahanan Nasional Malaysia
(Member)

Abdul Aziz Hassan, PhD
Professor Adjung,Ir
Fakulti Teknologi dan Informatik Razak
Universiti Teknologi Malaysia
(Member)

____
ZALILAH MOHD SHARIFF, PhD
Professor and Dean
School of Graduate Studies
Universiti Putra Malaysia

Date: 13 January 2025

TABLE OF CONTENTS

LIST OF TABLES

LIST OF FIGURES

LIST OF ABBREVIATIONS

ACV	Air cushion vehicle
AR	Aspect Ratio
AOA	Angle of Attack
CAD	Computer aided design
CD	Coefficient of drag
CFD	Computational fluid dynamic
CG	Center of gravity
CL	Coefficient of lift
CM	Coefficient of moment
CSSRC	China shipbuilding scientific research center
COP	Center of pressure
FAST	Functional analysis system technique
HC	Height to Chord
HPC	High performance computer
IGE	In ground effect
IMO	International maritime organization
L/D	Lift to drag ratio
LE	Leading edge
LLT	Lifting line theory
OGE	Out of ground effect
PAR	Power augmented ram
PUGH	Decision making matrix
QFD	Quality function deployment

RAN	Reynold average navier
RC	Remote control
SES	Surface effect ship
TE	Trailing edge
UH	Universal hovercraft
UPM	University Putra Malysia
VG	Vortex generator
Re	Reynold Number
VLM	Vortex lattice method
WIG	Wing in ground effect

CHAPTER 1

INTRODUCTION

1.1 General Preamble

A Wing in Ground effect (WIG) [1] craft is an aircraft operating in proximity of non-compressible surfaces level or ground [2]. It is classified as a marine vessel under the International Maritime Organization (IMO) [3]. Consequently, flying a WIG craft would be similar to consistently piloting an aircraft in landing or take off conditions which will lead to accident. However, the benefits gain [4] due to this phenomenal outweighs its downsides and this statement is widely stated in many studies and publishing papers. Presently, while it is not widely reported, a lot of past WIG craft are either sank in when too close to the sea or back flip when descendent too high [5] making them difficult to be commercialize. It is strongly believed that the accidents involving the WIG crafts are caused by their stability issues hence the design problem, particularly in the longitudinal direction. The latest commercially successful WIG craft known today is called Hoverwing (UH18-SPW). However, it is only limited to small payload. During ground effect phenomenal, the air flow under the wing becomes restricted due to interferences by the ground surfaces. At lower angle of attack, the impact on pressure gradient will also allow separation (stall) to occur [6]. An increased in pressure, moving aft on the wing to nearer to the center of the wing will result in reducing the upper surface lift and increasing aft portion of the lower surface lift will result in a lateral shift of the center of pressure. An aircraft designed [7] to balance in free flight will experience pitch down moment when it transitions into ground effect. Conversely, an aircraft designed to balance in ground effect will experience a pitch up moment when transitioning out of ground effect. In extreme proximity to the surfaces, air below the wing is trapped to some degree and reduces the cord wise lower surface flow, thus increasing the static pressure. The effect on the upper surface flow is being reduced due to the reduced Lower Surface flow. As a result, at a lower angle of attack (AOA) the upper Surface flow separates from the wing would occur in free air. Occasionally, in accordance to wing profile, a venturi could occur between the wing and the ground thus accelerating the air flow underneath the wing [8]. The negative effect on lift of this flow can outweighs the benefit of the air being trapped. Under exceptional circumstances, the net aerodynamic lift can even be negative. It is also worth noting, more energy loss will occur when pressure is lost due to the high pressure directly below the wing compresses the layer of air beneath it. Adding the non-compressible surfaces will stop the movement of downwash. The wing in ground effect produces approximately double the amount of lifting force as the wing in free air. It is widely disseminated that this effect is directly proportional to the cord length, x and inversely proportional to elevation, h and is known as Ram Effect [9]. As a result, a WIG craft of comparable size should be able to transport almost two times the weight of its body. A smaller aircraft generates vortex smaller than average vortex, therefore flying close to the surface will also yield less vortex reduction. Aside from that, for both aircraft and WIG craft [10], the center of pressure, COP and the center of gravity, CG are located about the same place. It is safe to assume that the COP location of free flight is about 25% of its wing chord and turn to 50% of its wing chord when the same wing [11] transiting into ground effect zone. The latest research done by the Royal Thai Navi shows the COP location of free flight is about 34% of its wing chord and turn to 41.5% of its wing [12] chord when the same wing transiting into ground effect zone. This is due to when the craft separates from the ground, the COP moves forward on the wing and the front nose wants to pitch up [13]. A WIG craft designed to operate in ground effect zone will meet disastrous result in these circumstances.

Therefore, it is imperative that the migration of COP need to remain relatively lesser in order for the WIG craft to safely descend higher. This means that as the COP migration become lesser, the WIG craft will be able to transit higher with more prominent pitch stability. Aside from that, other solution to compromise this challenge is a WIG craft needs to incorporate horizontal stabilization [14]. The Joerg tandem wing design is an exception of this problem since the front and rear wing supported the craft. During takeoff, the front wing reduces lift by moving into free air thus becoming stabilizing force for the craft and the rear wing remains in ground effect mode at the same time. As a result, there is no need for additional horizontal stabilizer. Regrettably to this day knowledge, this type of WIG craft become unstable [15] as it transiting out of ground effect zone.

1.2 Background of the study

This study delves into the design challenges faced by Wing-in-Ground Effect (WIG) craft. The investigation will explore various configurations and architectures employed in WIG design including UH18-SPW, aiming to understand the impact of these choices on performance and functionality. Additionally, the study will investigate the use of Computational Fluid Dynamics (CFD) software in simulating WIG performance. This combined approach aims to shed light on the complexities of WIG design and the valuable role of CFD software in optimizing these unique vehicles.

1.2.1 WIG Design Challenges

High speed sea transport [16] has been the main society's development since centuries ago. During the last half century, the rapid growth [12] of fast passenger transportation ships around and between many coastal cities has become noteworthy development due to demand in both work and travel pleasure [17]. For that reason, the study of WIG craft has continued to this day in order to improve transportation capacity [18]. However, until now not even one WIG craft has ever reached satisfying acceptance as mainstream transport vehicles [19]. It is by the author assumption that the reason behind this is because WIG craft need a high-power capacity in order to take off thus affecting the investment and operational cost. The second reason would be when WIG craft travel in ground effect, it tends to have experienced pitch up moment (longitudinal instability). This resulting in control difficulty and potential accident [20] such as back flip and crash might be possible to occur [21]. Such cases will need a pilot to take over the craft manually. All of these issues pointed to WIG craft having a design problem and possible solution lies on the developing a new design concept of WIG craft that can cater these issues.

1.2.2 Different Embodiment of WIG Architecture

To solve longitudinal stability problem, most WIG craft are designed [22] to have huge tail unit located relatively high and far away from the central main wing such as airplane, composite and lippisch types as shown in Figure 1.1. The tail area of the best craft is varied between 22% to 30% of the main wing area [23]. This type of arrangement requires a relatively huge fuselage [24] which reduces the lift to drag ratio, L/D. It is widely known in aerodynamic study that the best option to increase L/D is to increase the Aspect Ratio, AR of the wing [25]. However, there is an opinion that a low AR is sufficient for a WIG craft to operate and has the possibility to perform sharp turning maneuvers at high roll angle without any contact from water surfaces [26]. Low AR also increases the efficiency of Power Augmented Ram (PAR) system. A composite wing type as shown in Figure 1.1 is designed to have side wings of high AR located above the main wing [27] and the wing is subdivided into two sections along the span. One wing is used for PAR system and the other to generate lift in cruise mode. Due to this arrangement, the AR increases by two or three to five times and possibly higher. Noted that the derivative đh/đU also increases as the limitation of AR increase [23]. This reduces the "Binding" between the WIG craft and the level surfaces. This can also cause the WIG craft to jumps in a vertical direction due to wind gust or thrust increase.

Type	Figure
Orlyonok	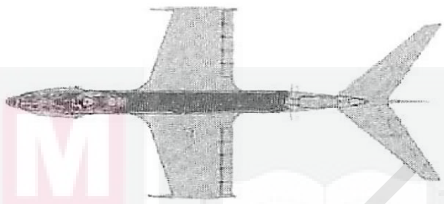
Composite Wing	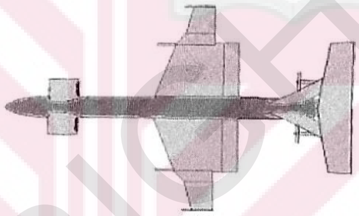
Lippisch	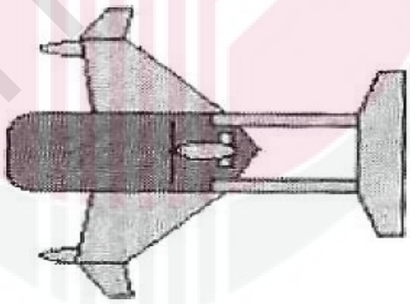
Tandem	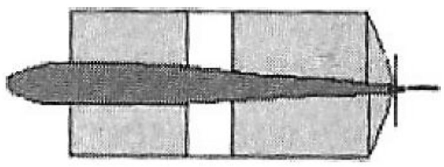

Ivolga

Bixel

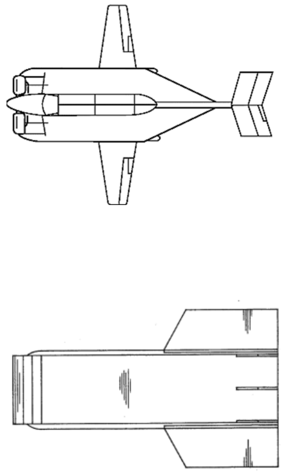

Figure 1.1: Different lifting surfaces of WIG craft

For a lippisch type, the main wing is designed with a low pressure loading by embodied a combination of anhedral, tapered cord, and forward sweep as shown in Figure 1.1. Such a WIG craft is relatively stable in flight. The propulsion system can be mounted above the hull or near tail. Additional stability and control in higher ground effect is achieved by incorporated the outer winglets with dihedral [28]. A tandem wing type is linked by two end plates [29] and formed a streamline channel of flow as shown in Figure 1.1. This configuration increases efficiency of ground effect usage and static stability of the WIG craft motion over the rough sea and during landing in weave conditions. For Ivolga type, the craft has a traditional aviation control system such as tailplane, fin, rudder, and wing ailerons as shown in Figure 1.1 [28]. The central wing frontal surface is configured in reverse V shape, flaps at rear part of the wing and a slender side buoy in catamaran form. This type of WIG craft has both longitudinal and transverse steps for good hydrodynamic performance especially during takeoff mode. To the present day, UH18-SPW hoverwing is the only WIG craft that has already demonstrated its potential to be a safe, efficient, and versatile aircraft. It is a promising new technology that has the potential to change the way human travel. The UH18-SPW hoverwing WIG craft is an amphibious aircraft. This means that the aircraft can operate on both land and water. It is a type of WIG craft that utilizes a hoverwing to generate lift. The hoverwing is a large, wing-like structure that is located underneath the fuselage of the aircraft. As the aircraft moves forward, air is forced between the hoverwing and the ground, creating a cushion of air that lifts the aircraft off the ground. The UH18-SPW hoverwing craft is designed for use in a variety of applications, including search and rescue, surveillance, and transportation. The UH18-SPW hoverwing craft is a unique and innovative aircraft that has the potential to revolutionize the way human travel. As for Bixel type, it is a combination of hovercraft [30] and ground effect technology. It is a flat double wing type of craft and claimed to have the ability to travel near level surface at a safe distance over water or land masses [31].

The flat double wing has a retractable wing and capable of longer time hovering and remain at faster speed before transition into true flight. It also incorporated with a hovercraft air containment wall mounted at the bottom of the body which allows the craft to be lifted out of the water [32]. The air containment wall is a structure with a flat bottom. This gives a water ski effect for emergency stopping and landing [31]. Bixel craft also has a thin air fence attached to the inside of the containment wall. This allows it to operate at zero degree Angle of Attack, AOA in a hovercraft mode. For maneuvering control, Bixel craft flight control used conventional aircraft type and mounting two or three large stabilizers with a rudder at the rear of the body.

1.2.3 CFD software used in WIG simulations

Computer Fluid Dynamic or CFD is a fast-growing application in the field of applied sciences. Before when computer is not advanced enough to solve large numerical problem, analytical and experimental method was used in solving fluid dynamic problems [33]. Both methods are either too simplified or too cost consuming. This is a different case today since the computer technology has improve tremendously such as High-Performance Computer (HPC) and able to solve complex fluid dynamic problem in relatively short time [34]. CFD uses numerical methods and algorithms to solve and analyze problems that involve fluid flows. Generally, CFD method of flow calculation is governing equations, discretization, numerical methods, boundary conditions, solution process, post-processing, validation and verification [35]. CFD calculates fluid flow by discretizing the governing equations, applying appropriate boundary conditions, solving the resulting system of equations using numerical methods, and then analyzing the obtained results through post-processing techniques [36]. The accuracy of CFD simulations depends on the quality of the discretization, the appropriateness of the numerical methods, and the fidelity of the boundary conditions used in the simulation. There are several CFD softwares capable of conducting ground effect study nowadays [37] available such as XFLR5, Solidwork Flow simulation, Autowing Code, Comsol Multiphysics CFD and Ansys Fluent.

1.3 Problem Statement

The wing in ground effect technology has been around since 1960s. However, to this day none of the vessel has yet to be commercialize although the projected market potential for large WIG craft is huge. This is possibly due to the range of power needed for takeoff and cruising is high which affects the investment and operational cost. Therefore, it is crucial to have a lifting surface that has the least amount drag force in order to accommodate power to take off. The second reason would be the stability of the WIG craft when transiting from in ground effect (IGE) to out of ground effect (OGE) which cause the WIG craft to back flip and crash. Third reason would be even IGE condition, the WIG craft will also be subjected to the possibility of back flip due high pressure build up underneath craft when in high-speed cruising.

In 1989, Charles Bixel claimed to solve the commercialization issue of a WIG craft by patented his own design called Bixel hoverwing. Unfortunately, there is a lack of aerodynamic analysis data presented by him to support his claimed. Presently several small prototypes were produce including two seats recreational hoverwing [38] called UH18-SPW by Universal Hovercraft. Normally, a WIG craft will only fly IGE zone however the "hop" maneuver for obstacle clearance introduces complexities, demanding COP behavior analysis at various angles and heights. Hence the investigation of center of pressure (COP) migration need to done to address this problem. Generally, COP is more pronounce at low altitudes and high speed. It is a complex phenomenon that is not fully understood. However, it is an important factor to address when designing and operating WIG craft. While some WIG architectures might be well-studied, others might be relatively unexplored. Existing research has focused on a narrow range of WIG architectures. This gap could be addressed by exploring unconventional designs or investigating how existing architectures can be adapted for different purposes.

1.4 Objective of study

In this proposal there are several objectives that need to be achieved. These are as follows:

1. To investigate the COP migration profile for existing reference WIG aircraft with various type of airfoil.
2. To develop a new conceptual design of a two-seater WIG aircraft based on established design requirements
3. To analyze and compare the performance of the proposed WIG aircraft design with respect to baseline design references

1.5 Research Question

There is several research questions that need to be highlight in this thesis and they are:

1) Question: What is the quantification used to represent the relationship between COP migration and longitudinal stability performance of a WIG craft?

2) Question: What is the best method to identify the configuration of lifting surfaces of two-seater Hoverwing for better longitudinal stability performance?
3) Question: How can the aerodynamic performances and stability of the proposed lifting surfaces configuration for two-seater Hoverwing be determine?

1.6 Scope of study

- The chosen turbulent model equation for this study is k-epsilon (k-ε) combine with wall function (Y +) due to the k-ε model is more suitable to predict flow behavior for large space compare to k-omega (k- ω) model which usually use to predict small and narrow space such as flow in pipe. The k- ω model will be used to predict the collision space between the WIG craft floor and level surface (ground effect region). The chosen Re number is based on UH18-SPW take off speed, wing chord, and kinematic viscosity. Hence in CFD simulation the converted speed is higher due to the scale of the model become smaller.
- The research assumption is based on Re number of full scales hoverwing which is more than 9 million (velocity of 25 m/s). Therefore, when converted to small scale hoverwing for aerodynamic simulation the velocity increase significantly (146m/s) while maintaining the same Re number.

- Due to the limitation of wind tunnel velocity output, the same velocity as per simulation (146 m/s) cannot be conducted for the small scale hoverwing.
- To verify patent claims for Bixel Hoverwing COP migration in and out ground effect using XFLR5 software.
- To do software verification on UH18-SPW with Naca4412 using Solidworks Flow Simulation and compared result with UH18-SPW wind tunnel test analysis data produce by Steven Morris, 2008.
- To propose a conceptual design of new two-seater WIG craft configuration by using Solidworks workbench. Each surface component and arrangement will be done related to external flow only.
- Due to the lack of equipment to produce more accurate result such high performance computer, only preliminary aerodynamic data were produced as thesis final analysis.
- Some information is confidential and cannot be published as it the company private and confidential work.

1.7 Significant of study

This study addresses the challenges to minimize the operational power requirement and stability of current WIG Craft configuration and explore the UH18-SPW and Bixel hoverwing as possible alternative to exploit the market potential of fast marine transport since both of this solution has lack aerodynamic data published. The author strongly believes that UH 18 SPW and Bixel hoverwing is the answer to the questions mark that has not been solve since the beginning of Russian military research on ground effect which started on 1960s. Therefore, the author would like to verify his hypothesis by exploring the Bixel hoverwing patent aerodynamic performances. The success of this thesis will create a design and manufacturing capability and supply chain which can further develop different air/marine transportation and commercialization purpose. It will develop new aerospace industry segment for special aircraft which is uniquely designed to operate in the ground effect environment [39]. Currently, SE-STRIDER SDN BHD is in a process of developing a Technology Demonstrator prototype and a preliminary concept model was exhibit at LIMA2023 in Malaysia Industry Government for High Technology (MIGHT) pavilion as shown in Figure 1.2. It received excellent interest reception among local and international visitors to invest in the project. With MIGHT as a backbone supporter, SE-STRIDER is working with Universiti Kuala Lumpur Malaysian Institute of Marine Engineering Technology (MIMET), Universiti Teknologi Malaysia (UTM), and 3DNaval Innovation to develop the prototype. The result of this study will be compared with SE-STRIDER CFD simulation. On receiving funding, a wind tunnel experiment will be carried out to validate the simulation results and modified the configuration and profiles for the first prototype. Included in the team, there are also Mejor Syed Abdullah (Airfish 8 pilot) and Lt. Kol. Assoc. Prof. Mohamed Tarmizi to conduct the flight test of the prototype.

Figure 1.2: New Hoverwing Concept exhibition at LIMA2023 (Courtasy by SE-STRIDER)

CHAPTER 2

LITERATURE REVIEW

2.1 Wing in Ground effect (WIG) craft

The ground effect [40] has already been known since the early days of aviation where experimental Wing in Ground Effect (WIG) craft was built in Scandinavia before the Second World War. The Russian Rostislav Alexeiev and German Alexander Lippisch was two individual that contributed to the first series of WIG craft [41] development. These two individuals while having a different background have encountered the same problems and have come out with a different solution. Alexeiev who has a background as a ship designer has thought that the WIG craft as a hydrofoils boat with its wings just above the surface. For Lippisch, he was intrigued by the potential to increase the efficiency of aircraft to fly close to the surface based on his background as an aeronautical engineering.

2.1.1 Early Design Contribution

Experimental WIG

There are two major research and development of ship speed enhancement taken place in Russia in the twentieth century. The first initiative was in 1940s and aimed at reducing wave making resistance at high speed. The second initiative was in 1950s and aimed to glide the marine craft above water by lifting it out of water surfaces completely. The first experimental WIG craft is the SM-1 and was designed by Alexeyev together with his team in 1960. SM-1 has a twin wing in a tandem arrangement and a gross weight of 2.8 tons as shown in Figure 2.1. SM-1 has a 20-meter-long cigar shape fuselage and a tandem wing at the center and aft. It has a side plate in a form of wing tip floats installed on the main wing and tail to reduce tip vortices and increase L/D ratio of the craft. SM-1 had a three crew and was flight tested on calm water at 200 km/h on 22th July 1961. From the trial, SM-1 shows unsteadiness in pitch [42] due to its rear wing operated directly in the unsteady slipstream of the forward wing. SM-1 crashed in Jan 1962 from engine failure when it climbed maneuvers.

Figure 2.1: SM-1 [28]

The second configuration was designed after SM-1 and named as SM-2 in March 1962 as shown in Figure 2.2. It is similar to SM-1 except that in this new arrangement, one main wing supported the craft in ground effect mode and another horizontal tail stabilizer was mounted at the top of the vertical fin to maintain positive longitudinal stability. SM-2 was damaged in a hanger fire and was given the name SM-2P after modification of installing high mounted rectangular tail wing and new jet engine. This SM-2P configuration was stable in-flight test.

Figure 2.2: SM-2 [28]

Later in 1962, SM-3 was developed and has a longer, low AR of main lifting wing and smaller tail as shown in Figure 2.3. It has a three crew in an enclosed cockpit and the main engine was moved right forward to the nose of the fuselage. The exhausts from the engine jet were blown underneath the main wing. SM-3 shows insufficiency for steady flight in yaw stability when flying above 1.5 meter. It is clear at this point that low AR of the main wing was only suitable for small ground clearance concept. Later on, SM-3 was succeeded in by the SM-4 in 1963 as shown in Figure 2.4. SM-3 was based on the SM-2 configuration but using a larger jet engine in bow driving the lift enhancing system. SM-4 showed a successful performance and encouraged the design bureau to develop a very large WIG craft which was known as the KM (also known as “Caspian Sea Monster” by the west) in late 1963 (see Figure 2.5). A 1:4 test model of KM was built in the same time called SM-5.

Figure 2.3: SM-3 [28]

Figure 2.4: SM-4 [28]

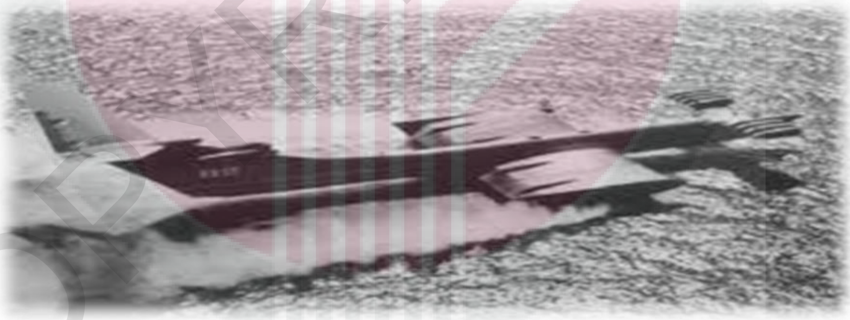

Figure 2.5: KM a.k.a Caspian Sea Monster [28]

Another noteworthy experimental WIG craft [43] to mention is the Buchon-1. It has the velocity of 200 to 250 km/h, the vehicle length is 13 meter and has a 0.5 to 3 m of an altitude range. The Buchon-1 is mainly for commercialization applications and civilian transport. It is incorporated with reverse delta wing [44] form and a wing section of S shape camber line [45].

Due to blended wing shape, its fuselage produces more lift and horizontal stability. The canard also helps during the takeoff and landing producing a high AOA at low velocity. The canard also generated positive lift during takeoff and landing. Buchon-1 also embodied an elevator and rudders which effective even in slow forward speed. Its catamaran hull design reduces the hydrodynamic drag and the propulsion system is placed in a spray free region reducing the maintenance cost and increases the system durability. Figure 2.6 show the Buchon-M1 [46] configurations produce in Russia.

Figure 2.6: Buchon M-1 model during wing tunnel test in Russia [46]

In china, more than 40 small scale model of PARWIG was built at China Shipbuilding Scientific Research Center or CSSRC in the late 1960s for experimental purposes. These models were tested out in a wind tunnel of MARIC in Shanghai and also in the towing tank of CSSRC in Wu-Xi. The successful of this test lead to the development of a full-size craft in late 1970s. Figure of PARWIG is as shown in Figure 2.7.

Figure 2.7: CSSRC PARWIG [28]

In Germany, the development of experimental WIG craft was started by Dr. G.W Jorg. He began with fostering ram air cushion underneath the wing by incorporating a negative delta wing form. In his early experiment, the single ram air wing was replaced by two identical parallel wings in a tandem arrangement due to this configuration has higher efficiency, improved stability, and reduced total resistance. After several years of development took place, the German Ministry of Transport approved the Tandem Airfoil Flair, TAF Boat as a ship or boat [47]. Figure 2.8 shows the main configuration of TAF VIII-3.

Figure 2.8: TAF VIII-3 photo [28]

Large Russian Ekranoplan

Initially WIG craft that being design by Alexeiev has two wings and it was set as a tandem wing. The first full scale of WIG craft from the Design Bureau was a tandem craft SM-1, but after that the tandem concept was soon rejected in favors of ekranoplan design. Having a high take off speed, rough ride quality and poor maneuverability is the reason why the tandem concepts were rejected. SM-2P was the first ekranoplan built in 1962 and has featured low aspect ratio wing, high T-tail, and also the aerodynamics of the wing that will assist at takeoff [48].

Figure 2.9: Lun type enkranoplan [49].

All these designs are to decreased speed and load at takeoff and made the craft amphibious to accommodate Power Augmented Ram, PAR-system [50]. As shown in Figure 2.9, the 400 lun that was built in 1987 [51] is the most recent large ekranoplan with missile launcher on top of the hull. After that the second craft were created and being renamed Spasatel. After the collapse of Soviet Union, it has become impossible for the Russian to keep developing or keep maintaining the big ekranoplan.

2.1.2 Current Design

Small type of WIG craft [52] has more opportunities in commercialization purposes whether in tourism, logistic and human transportation. For that reason, the design bureau started focusing on smaller ekranoplan for non-military use.

Russian

The design bureau started focusing on smaller ekranoplan [52] for nonmilitary use. Since the dissolvent of Soviet Union, Volga Shipyard has been the one to continue producing enkranoplans and smaller enkranoplan for nonmilitary use is still under development. The development of eight seat Volga 2 was introduced in 1985 [53].

German

Alexander Lippisch, also known as a father of delta wing who designed the ME 163 rocket powered delta wing airplane, develop the X-112 WIG craft with inversed delta wing and T-tail in 1963. This design has proved to be stable, efficient in ground effect and was successfully tested. Soon the six seat X-114 were develop by German company called Rhein Flugzeugbau [54] as shown in Figure 2.10.

Figure 2.10: Rhein Flugzeugbau X-114 in flight [53].

Later Hanno Fischer completed two models. Figure 2.11 shows the two-seater Airfisch 3 [54], and the six-seater FS-8 [55]. The FS-8 was to be developed by Fischer Flugmechanik for a Singapore-Australian joint venture called Flightship.

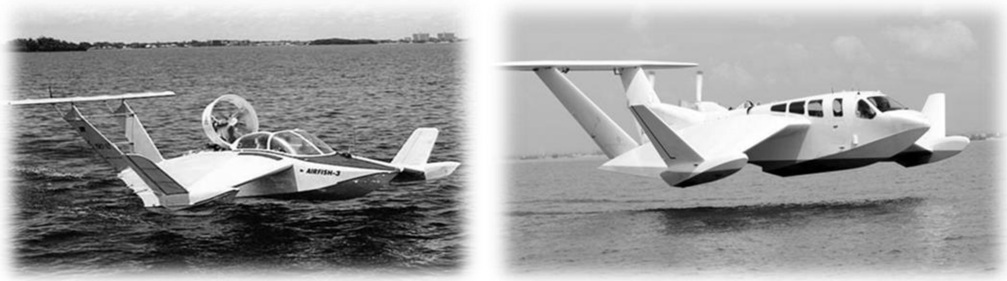

Figure 2.11: Air Fisch 3 and Air Fisch 8 develop by Hanno Fischer

American

From 1060s to late 1969s, American carry out a number of configurations of ground effect machines under defense development programed with a goal of developing a fast marine vehicle. However, the development focus remained with high-speed SES subsequently with hovercraft for amphibious assault. In early 1970s, American chooses to develop large high-speed SES rather than other concepts. This programed was cut short after by the mid-east fuel crisis and their intention was switch to other programed such as nuclear-powered submarine.

In 1990s, a conceptual design known as Hoverplane which is a combination of existing WIG and conventional technologies were developed by a company named Wingship Inc. Hoverplane main body is design as shallow catamaran, which is then sealed with semi rigid skirts at front and rear. It operates by pumping air into the chamber, so that the main body would be able to maneuver on the water like SES [28].

Korea

A five-seater wig craft [56] Aron-7 was developed by Korean company namely Aron Flying Ship Ltd as shown in Figure 2.12. It has a length of 10.8 meter and a wingspan of 12 meter. Aron-7 is equipped with Lycoming 540 engine and produces about 300 bhp. The takeoff speed is 100 km/h and cruising speed of 180 km/h. Aron 7 were intended for marine tourism, rescue and military applications [54].

Figure 2.12: Five-seater Aron-7 wig craft.

China

Started at late 1960s, Joint venture between the Russian and China, together they have developed a WIG craft called CYG-11 (see Figure 2.13) by a company called Hainan England WIG Manufacturing Co, Ltd. The appearance and technical characteristic similar to the Russian Wig craft called Ivolga. It can reach a cruising speed of 250 km/h and mileage of 1500km. CYG-11 capacity is 12 passengers and the maximum weight is 1200kg [57].

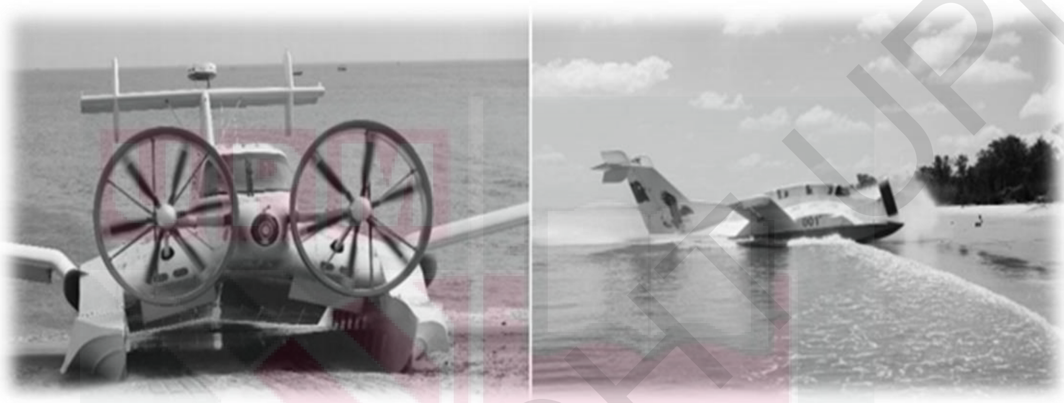

Figure 2.13: CYG-11, joint venture development between China and Russian

Iran

In 2010, Iran announced that Bavar 2, a fixed-wing WIG craft producing a low radar signature capable of flying undetected while carrying out patrolling mission are to be given the Iranian Navy. Eleven of these WIG crafts were delivered to the navy fleet on the same day. There is close resemblance between Bavar 2 and Eska-1. The craft has a seating capacity of one to two. Videos footages of assembly process and the craft flying are widely available on Internet. These craft are suggested to be aerodynamically stable based on the video footages. Figure 2.14 shows Iranian Bavar 2 loading on a carrier [54].

Figure 2.14: Bavar 2 loading on a carrier

Small Individual Initiatives

During the last ten years, separately to the large commercial venture initiatives, a number of enthusiasts started to construct WIG craft for their own personal reason. The first successful design was done by a pioneer in ACV, Bob Windt [28]. Other enthusiast was the Weber brothers which have also designed their own WIG craft embedded with tandem wing configurations. Another enthusiast was Rudy Heeman from New Zealand which we will further discuss in the next chapter.

UH18-SPW and UH19 XRW

In tourism, recreational Hoverwing [58] can be used as substitute for boat and ships. It is also a much faster recreational transportation compare to boats and ships. It will also provide a new attraction for tourists since the vehicle is flying rather than going on river and sea. Design and develop by Universal Hovercraft, a leading for innovative, high-speed hovercraft and solution worldwide. The development of UH18-SPW hoverwing were introduces by combining two technologies, hovercraft and ground effect creating a hovercraft that can fly called Hoverwing [59]. Later on, Universal Hovercraft developed UH19 XRW as the upgrade version of previous one. UH18-SPW specification were not written in any published journal and article making its aerodynamic performance remain unknown although it has been successfully to hover, fly, easy maneuverability and achieved sufficient stability during flight test. Figure 2.15 and Figure 2.16 shows the UH 18 SPW and UH 19 XRW respectively [53].

Figure 2.15: UH 18 SPW by Universal Hovercraft [53].

Figure 2.16: UH19XRW by Universal Hovercraft [60].

New Zealand Rudy Heeman

A New Zealand mechanic and enthusiasts, Rudy Heeman developed a successfully tested hoverwing after spending 11 years of building it. His hoverwing can reach an optimum height of 1.5 meter above the water and a top speed of 98 km/h. The hoverwing is powered by a modified Subaru engine and the body was made mostly from fiber glass. Figure 2.17 shows the Rudy Heeman hoverwing [61].

Figure 2.17: Hoverwing developed by New Zealand Mechanic, RudyHeeman [61].

New Generation and Conceptual Future WIG Craft

Over the last years, inspired by the monster craft during the cold war [49], Russian has started to develop a new generation of WIG craft [62]. The new Orlan craft will be a descendant of the so-called 'Caspian Sea Monster,' a now inoperative vehicle that flew across the sea at speeds of up to 400 mph. According to Russian Deputy Prime Minister Yuri Borisov, the Orlan which currently under develop will be ready by 2027. It is part of armament program for 2018-2027 and carrying missile armament. The Orlan craft is currently under development by the Alekseyev Central Hydrofoil Design Bureau, based in Nizhniy Novgorod, Russia. A conceptual design of the New Orlan by Russian is shown in Figure 2.18.

Figure 2.18: The conceptual Design of New Orlan.

2.1.3 Operational Challenges in WIG Craft Development

Up until now WIG craft are not yet commercially operated. The reason lies on its operational challenges in development. Yun Et Al stated that WIG craft disadvantage can be classified into “technical” and “operational” factor. We will first need to discuss about technical factor before getting to operational factor. For a technical factor, the takeoff speed of a WIG craft is high due to hydrodynamic drag [63] before takeoff also getting higher. This indicates that the WIG craft need to begin takeoff at lower speed. In order to overcome it a ‘lift enhancement’ capability need to be applied into the craft. Technologies on par to those elements are surface effect ships and hovercraft. The transversal and longitudinal stability of WIG craft will also be affected when wind gust or waves occur during high cruise speed. This means that the WIG craft will have maneuverability problem and need a manual handling from pilot. As such a commercial automated system for WIG craft is still not available [53]. Another technical factor worth mentioning is the trade-off between aerodynamic efficiency and lift force during take-off. It is dependent on the aspect ratio (AR) of the wing. A high AR will increase aerodynamic efficiency but decreases lift force. For operational factor, WIG craft require terminal similar to hover port. The hover port must be located near coastal cities and a suitable water runway with a length of 500m to 2000m and width of 500m is needed. Since WIG craft is not yet commercialize, there is no training available for pilot. A Boeing pilot and a ship captain may have a little experience in operating WIG craft. Other operational factor would be the noise produced by the WIG craft. It is comparative to a small turboprop airplane flying closer to water surface [53]. This will affect the acceptance level of tourist and communities nearby the terminal. Public reaction and acceptance will also influence the development of WIG craft since it is a new type of transportation compares to establish airplane and other marine transportation. Lastly, economical profitability will be the last key factor. WIG craft as transportation is more suitable for a short-range route of less than 400km. Aircraft transport is less efficient due to repeated landing operations. Yun Et Al said that competing with aircraft transport in their speed range is difficult due to the competing of low-cost airline.

2.2 Performance Analysis of WIG craft

This thesis is about estimating various type of aerodynamic parameters and verify aerodynamic and stability of patent claim. Therefore, it is consequential to include Computer Fluid Dynamic (CFD) into the investigation process.

2.2.1 Simulation Analysis

CFD mainly deals with the numerical analysis of fluid dynamics problems, which used the differential calculus. The Navier Stokes is the main equation involve in fluid dynamics. Until today, solutions to Navier–Stokes equations have not been explicitly found except for some cases such as Poiseuille flow, Couette flow, and Stokes flow with certain assumptions [64]. Because of that, engineers and scientists have spent their live times conceiving methods to solve these differential equations [65] so as to give a meaningful solution for a particular set of geometry and initial conditions. Thus, CFD is the process of converting the partial differential equations of fluid dynamics into simple algebraic equations and then solving them numerically to obtain some meaningful result.

Figure 2.19: The computational fluid dynamics process [64].

As shown in Figure 2.19, the entire CFD process consists of three stages: pre-processing, solving, and post-processing. All three processes are interdependent and 90% of effort is used in the meshing (preprocessing) stage. The next stage is to solve the governing equations of flow. An error embedded in the mesh will also generate in the solving stage as well. The last stage is post-processing. There, the results of input and solved are obtained and colorful pictures showing contours are interpreted for further development, or optimization. Experimental data are compared with result for validation. If there is any absent in experimental data, the grid convergence study better judges the authenticity of the results. For such a case, the mesh is refined two or three times, each time solving and getting results, until a never-changing result (asymptotically converged solution) is obtained. CFD used the Navier Stokes as its governing equations. These equations have been discovered 150 years ago by the French engineer Claude Navier and the Irish mathematician George Stokes. In principle, the mass, momentum and energy parameter must be conserved.

A) Conservation of mass or the continuity equation is written as; [64].

$$\frac{\partial p}{\partial t} + \nabla \cdot (\rho U) = 0 \qquad \vec{U} = [u, v, w]$$

Where

(2.1)

B) Conservation of momentum is based on Newton Second Law of motion F=Ma, where fluid particle is the mass, M and acceleration is a. When applied to a fluid particle under pressure, viscous and body forces compose a set of momentum equations in the x-direction written as;

$$\frac{\partial pu}{\partial t}+\frac{\partial puu}{\partial x}+\frac{\partial puv}{\partial y}+\frac{\partial puw}{\partial z}=-\frac{\partial p}{\partial x}+\mu\frac{\partial}{\partial x}\left(\frac{\partial u}{\partial x}+\frac{\partial u}{\partial y}+\frac{\partial u}{\partial z}\right)+\rho fx \tag{2.2}$$

in the y-direction is written as;

$$\frac{\partial pv}{\partial t}+\frac{\partial pvu}{\partial x}+\frac{\partial pvv}{\partial y}+\frac{\partial puw}{\partial z}=-\frac{\partial p}{\partial y}+\mu\frac{\partial}{\partial y}\left(\frac{\partial v}{\partial x}+\frac{\partial v}{\partial y}+\frac{\partial v}{\partial z}\right)+\rho fy \tag{2.3}$$

and in the z-direction is written as;

$$\frac{\partial pw}{\partial t}+\frac{\partial pwu}{\partial x}+\frac{\partial pwv}{\partial y}+\frac{\partial pww}{\partial z}=-\frac{\partial p}{\partial z}+\mu\frac{\partial}{\partial z}\left(\frac{\partial w}{\partial x}+\frac{\partial w}{\partial y}+\frac{\partial w}{\partial z}\right)+\rho fz \tag{2.4}$$

Stokes obtained a relation for the shear stress of Newtonian fluids with some modification in the viscosity terms; these equations are in xyz-direction written as;

$$\tau_{xx}=\lambda\left(\nabla\cdot\vec{U}\right)+2\mu\frac{\partial u}{\partial x} \tag{2.5}$$

$$\tau_{yy}=\lambda\left(\nabla\cdot\vec{U}\right)+2\mu\frac{\partial v}{\partial y}$$

(2.6)

$$\tau_{zz} = \lambda(\nabla \cdot \vec{U}) + 2\mu\frac{\partial w}{\partial z}$$

(2.7)

Asymmetric stress tensors are written as: [64]

$$\tau_{xy} = \tau_{yx} = \mu\left(\frac{\partial v}{\partial x} + \frac{\partial u}{\partial y}\right)$$

(2.8)

$$\tau_{yz} = \tau_{zy} = \mu\left(\frac{\partial v}{\partial z} + \frac{\partial w}{\partial y}\right)$$

(2.9)

$$\tau_{zx} = \tau_{xz} = \mu\left(\frac{\partial w}{\partial x} + \frac{\partial u}{\partial y}\right)$$

(2.10)

Where μ is the dynamics viscosity and ƛ is the kinematic viscosity coefficient, given by Stokes as:

$$\lambda = -\frac{2}{3}\mu$$

(2.11)

C) The energy equation, also called the First Law of Thermodynamics is based on the principle that energy is conserved. In general, the equation is written as;

$$\frac{\partial(pE)}{\partial t} + \nabla \cdot (\rho E \vec{U}) = \rho \dot{q} + \frac{\partial}{\partial x}\left(k\frac{\partial T}{\partial x}\right) + \frac{\partial}{\partial y}\left(k\frac{\partial T}{\partial y}\right) + \frac{\partial}{\partial z}\left(k\frac{\partial T}{\partial z}\right) - \rho \nabla \cdot \vec{U} + \lambda(\nabla \cdot \vec{U})^2 + \mu\left[2\left(\frac{\partial u}{\partial x}\right)^2 + 2\left(\frac{\partial v}{\partial y}\right)^2 + \left(\frac{\partial w}{\partial z}\right)^2 + \left(\frac{\partial v}{\partial y} + \frac{\partial v}{\partial x}\right)^2 + \left(\frac{\partial v}{\partial z} + \frac{\partial w}{\partial y}\right)^2 + \left(\frac{\partial w}{\partial x} + \frac{\partial u}{\partial z}\right)^2\right] \quad (2.12)$$

These equations are important in CFD. One should memorize these equations in order to understand the method of CFD. In CFD these equations are discretized along with points in space and then solved algebraically. To solve these equations, there are various approaches available, such as the finite difference method (FDM), finite volume method (FVM), and finite element method (FEA). These equations can be modified for compressible, or incompressible, inviscid and steady or unsteady fluid flow [64].

Reynolds Number

The transition from laminar to turbulent flow does not occur suddenly [66]. It occurs over some region in which the flow fluctuates between laminar and turbulent flows before it becomes fully turbulent. Among other things, it depends on the geometry, surface roughness, flow velocity, surface temperature, and type of fluid. Most flows encountered in practice are turbulent. Reynolds number [67] for a given airfoil can be expressed as;

$$Re = \nu C / \lambda$$

(2.13)

Where v is take-off velocity

C is root chord

λ is kinematic viscosity

Computational Domain

As shown in Figure 2.20, a computational domain is the region in space in which the equations of motion are solved by Computational Fluid Dynamic (CFD). The domain is divided into many small elements called cells. A cell is a small subset of the computational domain. Boundary conditions are specified on each edge and faces of the computational domain. The quality of a CFD solution is highly dependent on the quality of the grid. Therefore, it is important to make sure that the grid is of high quality before proceeding any further [69].

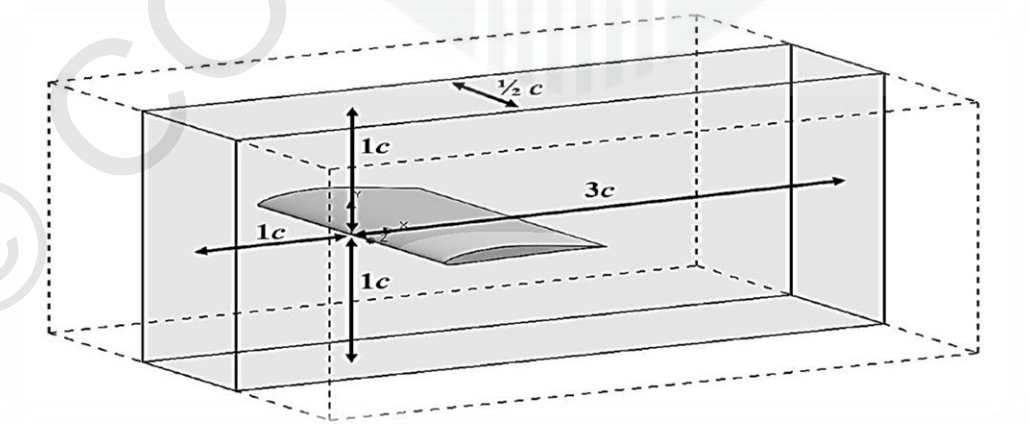

Figure 2.20: Initial computational domain size [68].

Properly defining the computational domain, including geometry, boundary conditions, and grid resolution, is essential for obtaining accurate and meaningful results in CFD simulations. Engineers and scientists must carefully analyze the problem requirements to create an appropriate computational domain that balances computational efficiency with result accuracy.

Y+ Calculation

Turbulent flows are an omnipresent phenomenon in CFD (Computational Fluid Dynamics). It is significantly affected by the presence of walls, where the viscosity-affected regions have large gradients in the solution variables. An accurate representation of the near wall region determines a successful prediction of wall bounded turbulent flows. Wall functions are equations empirically derived and used to satisfy the physics in the near wall region. It is used to bridge the inner region between the wall and the turbulence fully developed region. The first cell center needs to be placed in the log-law region to ensure the accuracy of the results. When using the wall functions approach, there is no need to resolve the boundary layer causing a significant reduction of the mesh size and the computational domain. A Y+ of 1 is considered good enough to resolve the boundary layer down to the sub viscous layer. This can be substituted into equation below alongside the friction velocity to obtain the distance the first node of the mesh must be from the model's wall.

$$y+=\frac{\mathrm{yu\tau}}{\nu}$$

(2.14)

uт is the so-called friction velocity

y is the absolute distance from the wall

v is the kinematic viscosity

Mesh Designs

As shown in Figure 2.21, mesh generation is started by dividing the rectangular computational domain into a set of rectangular cells formed by intersection of planes parallel to the axes of coordinate system. The mesh [70] can be refined by splitting each cuboid cell into 8 geometrically-similar cuboids using various adaptation criteria that can be defined for each solid body such as curvature, narrow channels, small features, and automatically according to gradients in the solution.

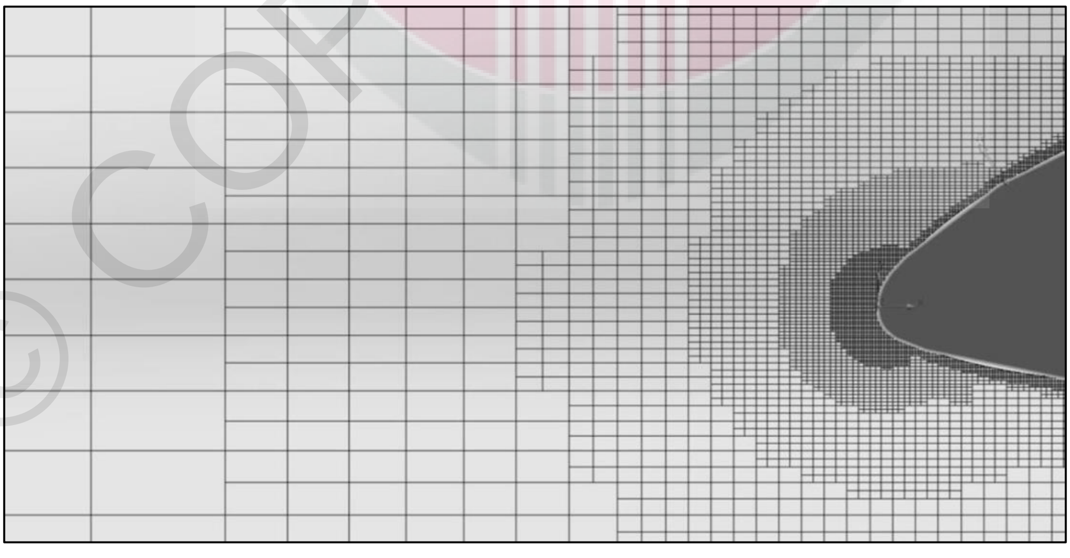

Figure 2.21: Mesh refinement with a level 5 global domain parameter on an E387 leading edge [68].

Published Aerodynamic Parameters from Simulation and Wind Tunnel Experiment

There are various types of CFD software to analyze aerodynamic flow or complex fluid dynamic problem however CFD software that was specifically design to investigate ground effect is limited. Husman Mahmood in his study used XLFR5 to investigate the comparative differences between an NACA 2415 airfoil and a NASA Sc-0714 supercritical airfoil in Ground Effect conditions. Also A. Nebylov in his study used Comsol Multiphysics CFD package to obtain a software model of a WIG craft near a flat surface. Hussain H. Al-Kayiem, [71] and Aananthan M [72] used Ansys Fluent in their study. Surjatin Wiriadidjaja in his paper conducted a wind tunnel test on 1:6 scaled models of WIG craft to study its longitudinal stability [73]. Also, Tom McLaughlin and his team, from US Airforce Academy created and tested a small-scale hoverwing models in the subsonic wind tunnel to determine its aerodynamic characteristics [74]. Even the author attempted to investigate Bixel USA PATENT #5105898 aerodynamic performance by conducting a simulation using XFLR5 [78]. Ultimately one should take carefully consideration of what he or she need the CFD software to provide given that each have their own pro and cons.

Cambered Airfoil

The first understanding in flight aerodynamic is the elements of flight. There are four forces that makes it up which is lift, weight, drag and thrust. These four forces also counteract against each other. For an aircraft in a steady flight, the aerodynamic force can be measured equally by an observer on the ground and the observer in the aircraft. Hence in frame of reference motion, the aircraft is stationary and the air moves at a velocity **-V**. This simplifies prediction of aerodynamic force since it can be measured in wind tunnel or computed by a numerical solution. [76]

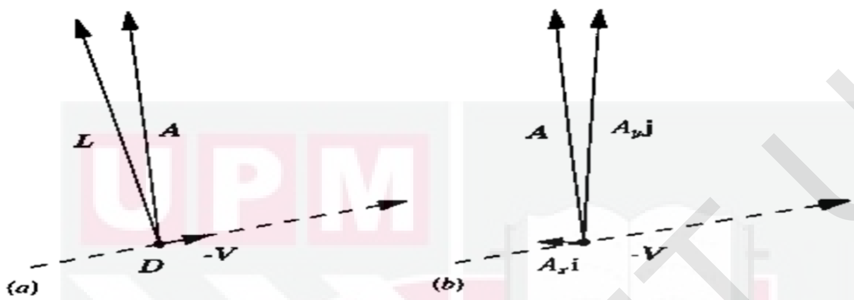

Figure 2.22: Lift and Drag as Cartesian Component [76]

Figure 2.22 shows a lift **L** and drag **D** component in cartesian mode. Aerodynamic force **A** can be resolved into a perpendicular component force such as;

$$\boldsymbol{A = L + D} \textit{ and,}$$

$$\boldsymbol{A = Ax\, i + Ay\, j} \tag{2.15}$$

Where $L = \frac{1}{2}\rho V^2 A\, CL$ (2.16)

$D = \frac{1}{2}\rho V^2 A\, CD$ (2.17)

The ***D*** *is* opposed to the direction of motion or parallel to the direction of the airstream relative to the aircraft **-V**.

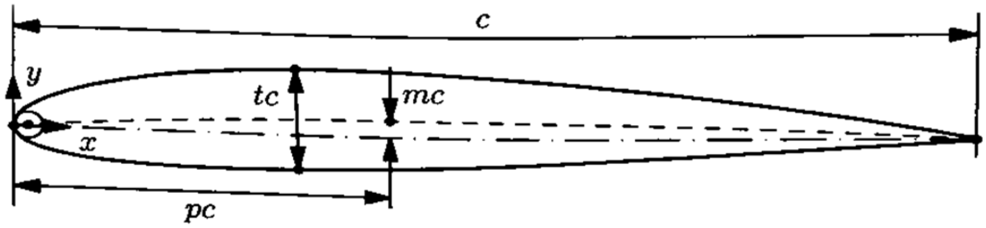

Figure 2.23: Naca2412 wing section. [76]

Figure 2.23 shows a Naca 2412 wing section as exemplary airfoil. Wing section can be characterized by;

a. Chord.

   Has a direction, position and length. Chord described the aerodynamic properties of a profile and therefore should be precisely defined [77].

b. Camber.

   Maximum distance from the chord. Usually denote from camber line between upper and lower chord surfaces.

c. Chord length, c

d. Maximum thickness ratio, t

e. Maximum camber ratio, m

f. Chord wise location of maximum camber, p

Another important element in aerodynamic flight is **Aspect Ratio**. It is described as the ratio of overall wing span to the average chord. [78] The formula for wing geometry aspect ratio is;

$$\text{Aspect Ratio} = \frac{Span}{Mean\ Chord} = \frac{Span^2}{Area} \qquad (2.18)$$

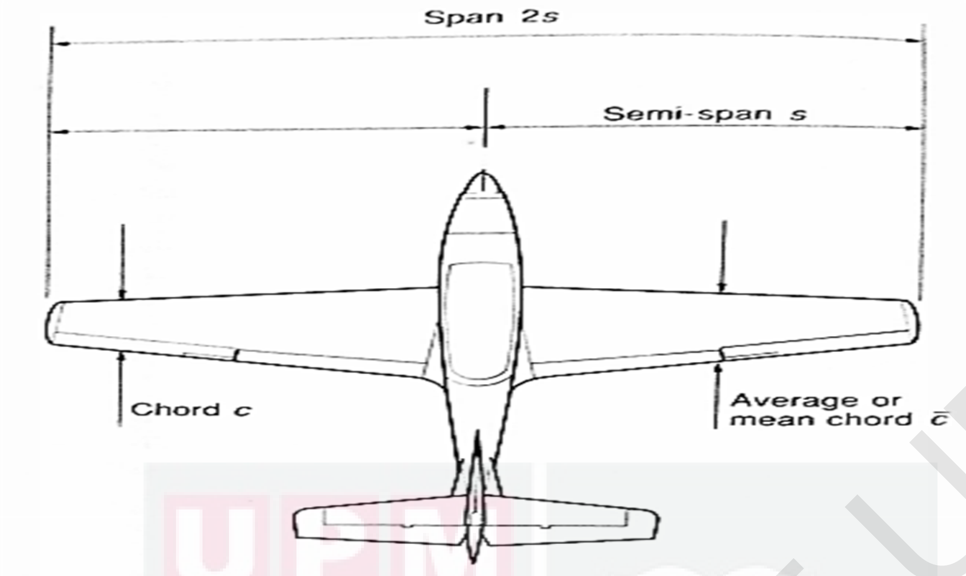

Figure 2.24: Wing Geometry

Many of previous studies of wing section have been limited to rigid wings [79]. For a rigid wing section, lift is typically achieved due to Newton third law of motion principle and coanda effect. According to Newton third law of motion, for every action force there is an equal force and opposite direction. Based on this law, lift is generated when wings are tilted upward, pushing air downwards so the wings get pushed upwards. For coanda effect, lift generated when an air particle that approached airfoil surface were force downward due to higher pressure at the top of the air particle [80]. This phenomenal makes the air particle to always attach to airfoil surfaces on a steady flight. According to Bernoulli equal time argument, wing is none other than a half of ventury tube hence assuming that the air moving over the rigid wing section moved faster than air below the wing to meet aft at the same time resulting in low pressure above and high pressure below the wing thus generating lift. This has become an argument and many oppose Bernoulli claimed such as Prof. Holger Babinsky from University of Cambridge and

Nasa Scientists. H. H. Al-Kayiem and AK Kartigesh in their study employed CFD simulation using Ansys and validated it by experiment of low-speed subsonic wind tunnel. The wind tunnel test section is 300 mm x 300 mm cross section and the flow velocity is varied up to 60 m/s. The 2-D wing model selection is NACA4412 airfoil section with 105 mm chord length and 300 mm. For each test, the fan speed was set to provide velocity corresponding to the desired Reynolds number, Re. The airfoil was adjusted first to -4o AOA and a height correspond to H/C = 0.1. All the aerodynamic parameters were measured over the range of AOA up to 20º. For the boundary condition, the flow field surrounding the airfoil was select as 9C in the flow direction times 5C in the transverse direction. The inflow was selected as 3C, the outflow as 5C and the far flow above the model as 4C and the underneath as 1C. All of this setting is to stabilize the prediction of the forces and moment. By taking the first point of leading-edge nose circle as the origin (0, 0). The resulting computational domain is as shown in Figure 2.25 [71].

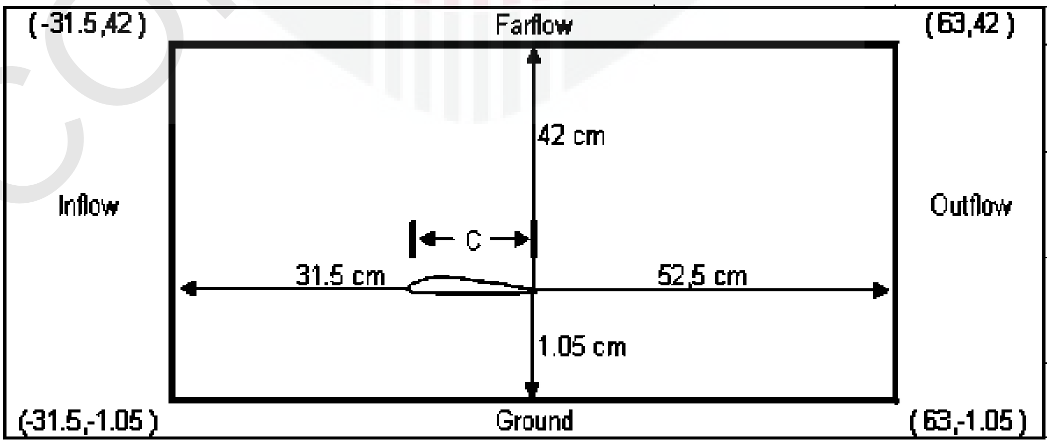

Figure 2.25: The Model Setup and the Boundary Conditions Adopted for the CFD Simulation at AOA = 0º [71].

For the grid generation, the field was meshed using the volume meshing tool. The selected elements were QUAD 8-node which is quadrilateral elements with mid edge nodes and the mesh were refined gradually to prove the grid independency. A total number of elements were 7,115. In Figure 2.26, the result has shown a significantly higher lift with low value of height to chord, h/c at AOA of 4 degrees. The lift effect decreases as the value of h/c increased.

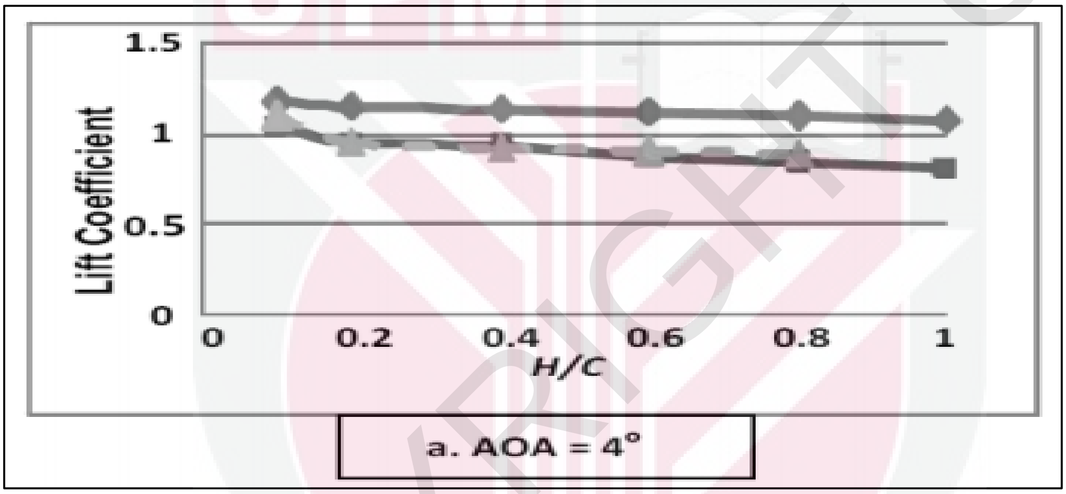

Figure 2.26: Variation of the Lift Coefficient with the Wing-Ground Distance at Re = 4×10^6 [71].

2.2.2 Experimental Analysis

Flat Plate

The air flow passing through a flat plate [81] held at an angle of inclination as shown in Figure 2.27 is considered to be the pioneer fundamental knowledge in aerodynamic study. According to Newton third law of motion, upward lift on the plate would be equal to downward momentum produce in downward deflection of flow or a downwash [82].The vertical velocity component at the plate trailing edge is equal to incoming air velocity times sine the angle of downwash. However, at this point Newton's interest was solely on how lift is generated hence the interference between flat plate and ground surface was discovered many decades later.

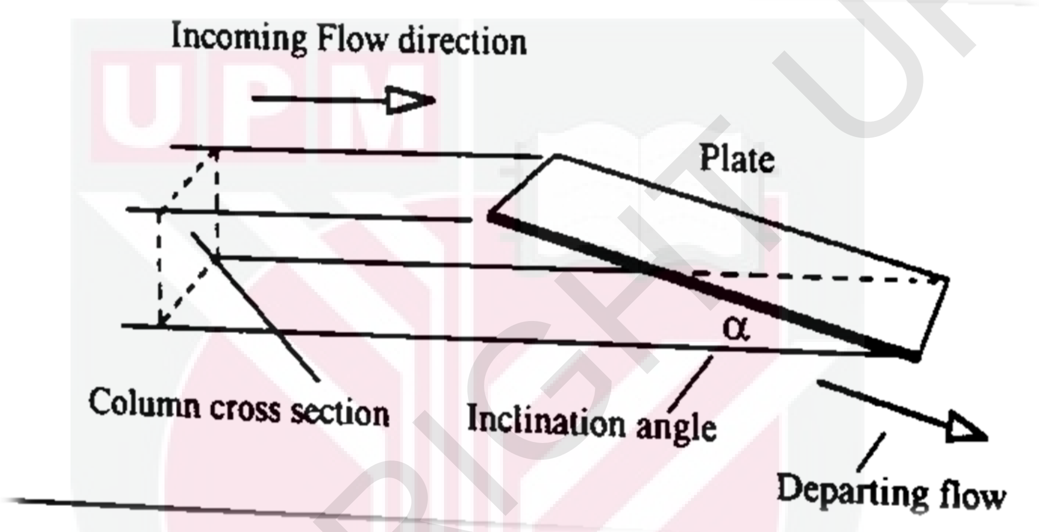

Figure 2.27: Newton Flat Plate [82]

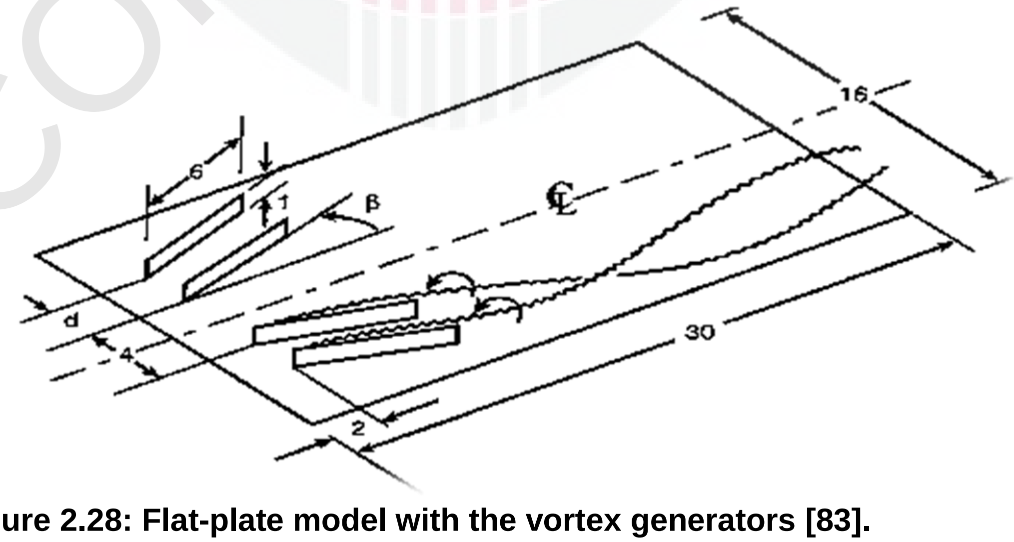

Figure 2.28: Flat-plate model with the vortex generators [83].

Today the studies involving flat plate aerodynamics on free stream are widely published in many sites. Unfortunately, the publication studies of flat plate on ground effect conditions are still limited. Still there are few attempted to study on the flat plate ground effect such as Darwin L. Garcia and Joseph Katz. Joseph and Darwin in their study attempted to find out the effects of vortices trapped between a flat plate and a ground plane in a wind-tunnel experiment. Their intention was to study the flow behavior when a vortex generator (VG) was embedded on the vehicle floor on a ground surface near collusion as shown in Figure 2.28. As a result, the VG created more aerodynamic load and it is clearly showed in the data that the larger VG incidence resulted in stronger vortices and more lift, which effect in general, increases with reduced ground clearance. As shown in Figure 2.29, the initially high lift force decreases as the height to chord, h/c value increased.

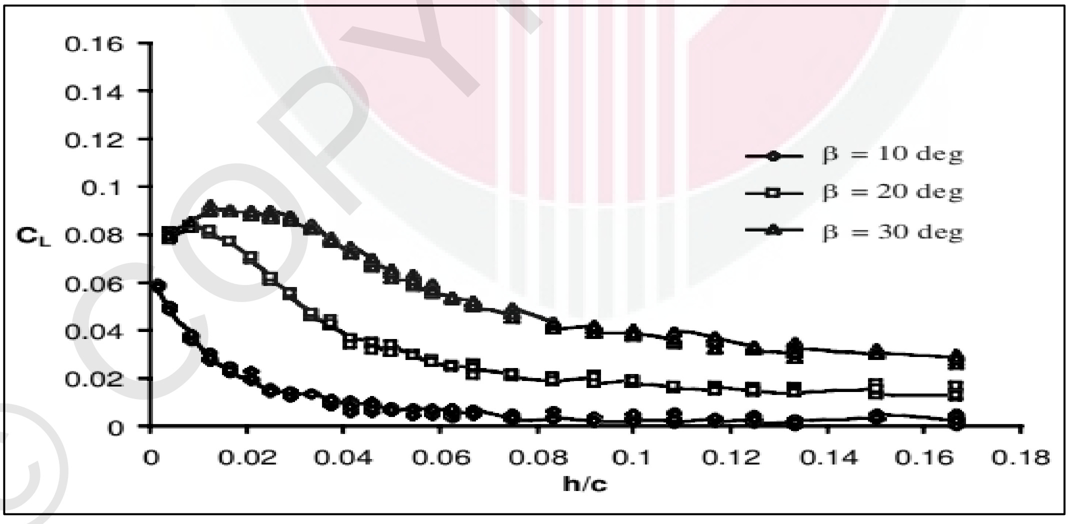

Figure 2.29: Effect of VG yaw angle on the flat-plate lift [83].

Membrane Wing

Figure 2.30 shows a micro light equipped with fabric wing. Fabric wing [84] or membrane wing has been an application in many engineering fields including parachute, hang glider [85] , and micro light [86]. It is known to be flexible and impervious [87]. Membrane wing elasticity property plays a significant part in its aerodynamic performance. Theoretically membrane wing operates by adjusting the shape of its wing in accordance to the flow environment [87]. Some study the modeling of hang glider in attempt to determine the twist dependency and camber shape [88] . Membrane wing [89] operates at low Reynold number and has unsteadiness due to flow separation at high incident. Manipulating the membrane wing adaptability is known to improve the aircraft performance [90]. Unfortunately, the aerodynamic of membrane wing is still largely unknown and the publishing studies on it are limited.

Figure 2.30: Micro light flying with membrane wing [91]

UH18-SPW with NACA 4412 Airfoil

In 2008, Steven Morris and his team from U.S. Air Force Academy conducted research to determine aerodynamic data on a hoverwing model similar to a commercially available vehicle (UH18-SPW). The experiment was conducted by placing the hoverwing model in the wind tunnel with ground plane that can be adjusted to different heights to simulate IGE and OGE. As shown in Figure 2.31, when comparing to the freestream flow without a ground plane, the craft experienced an 18% increase in lift coefficient at an angle of attack of 14 degrees for a height-to-chord ratio of 0. 303.

Figure 2.31: Experimental Test Setup for Hoverwing [60].

In Figure 2.32, when comparing to the freestream flow without a ground plane, the same ground plane height showed a 26% increase in lift-to-drag ratio at an angle of attack of 4 degrees. Pitching moment coefficient was not affected by varying ground plane height in common flight angles of attack (see Figure 2.34). Figure 2.31 shows the experimental test setup for hoverwing. The project's specific goals were to collect and analyze wind tunnel data to determine the aerodynamic characteristics of a hoverwing, including drag polar, lift curve, lift, drag, and moment coefficients, stability and control coefficients, and the effects of rolling the vehicle at varying angles of attack. The results of these testing will help to further the development of hoverwing vehicles.

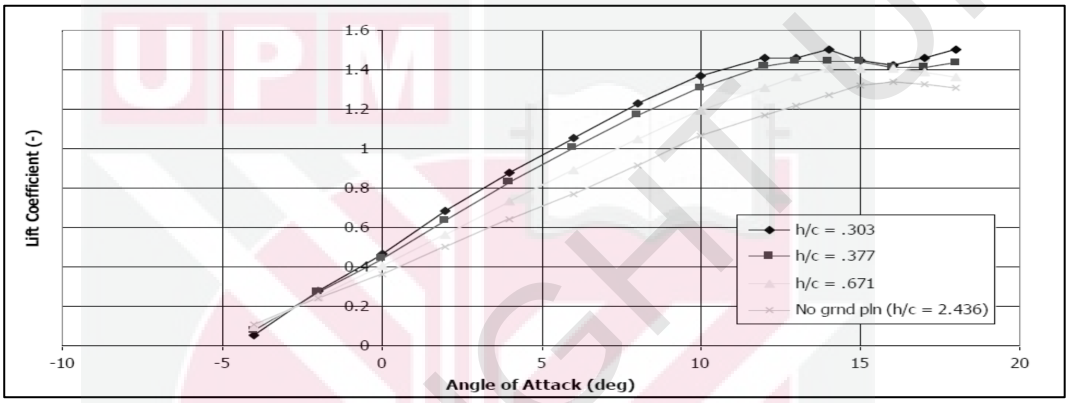

Figure 2.32: Lift Coefficient vs. Angle of Attack for Varying Ground Plane Heights [60].

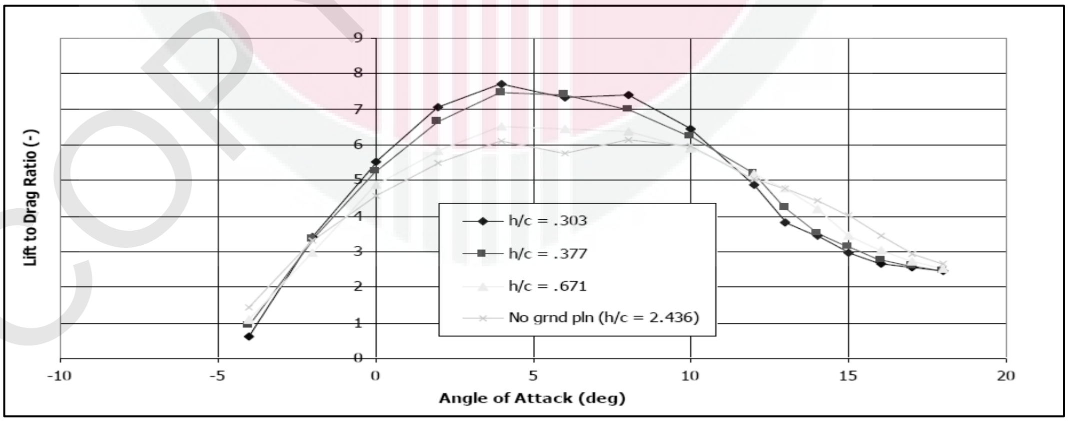

Figure 2.33: Lift/Drag vs. Angle of Attack for Varying Ground Plane Heights [60] .

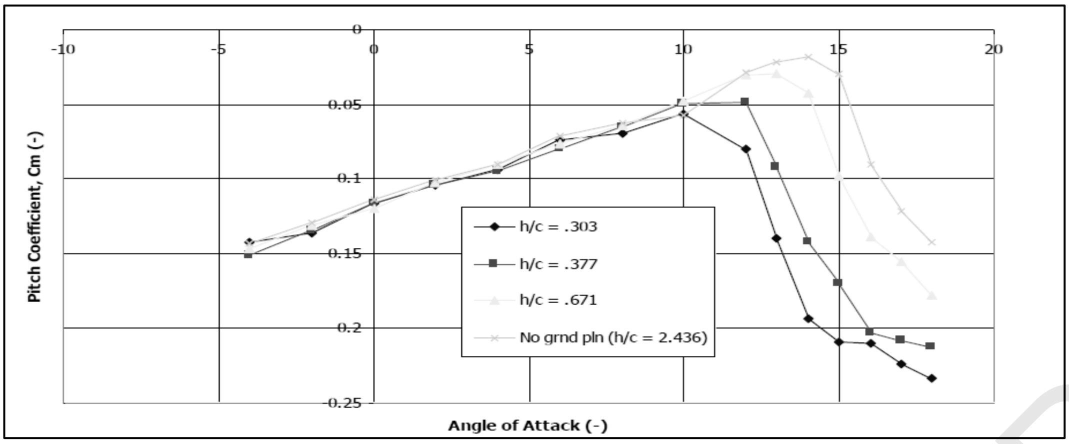

Figure 2.34: Pitching Moment Coefficient vs Angle of Attack for Varying Ground Plane Heights [60].

WIG Craft—NEW1 Model

In 2016, a research and development program creating the first prototype of 2-seat WIG craft called NEW1 [12] was established by the Royal Thai Navy. This research also performed an aerodynamic experiment on a small model of NEW1. The objectives of the experiment are to simulate the ground effect flow of the NEW1 model in a wind tunnel and collect the aerodynamic data for various flight attitudes and ground proximity conditions, and to determine the effects of ground proximity to the aerodynamic characteristics of the NEW1 model. The test results were expected to help in understanding the aerodynamic aspect of wing in ground effect and be useful for further design of a WIG craft. As shown in Figure 2.35. It was found that, when OGE, the center of pressure is located at 34% C, and when the WIG craft IGE the center of pressure moves towards trailing edge, and it is located at 41.5% C when H/C = 0.4.

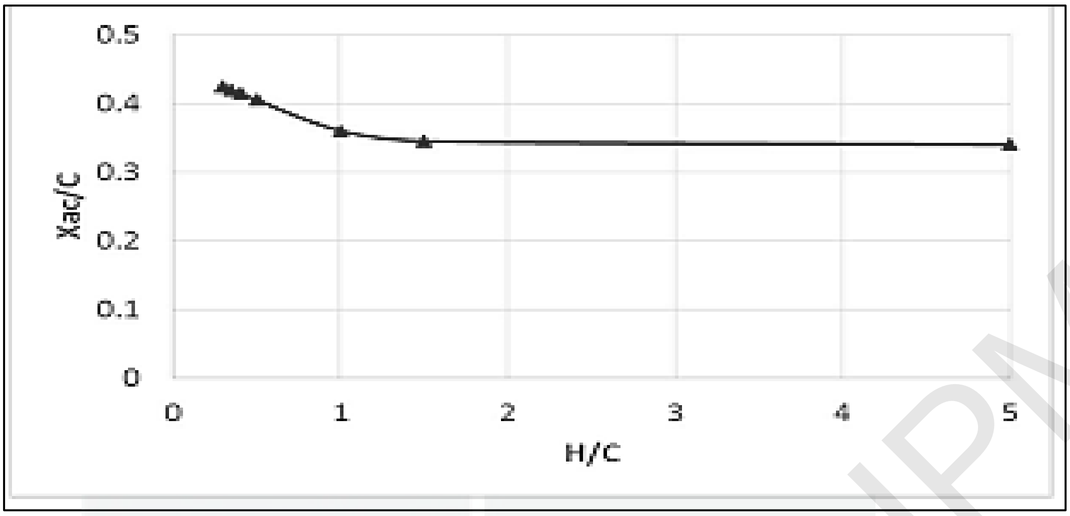

Figure 2.35: Effect of H/C to the Center of Pressure location.

2.2.3 Center of Pressure Migration Analysis

Generally, an aerodynamic performance includes the lift (Cl) and drag (Cd) capability of a WIG craft. Where these capabilities commonly be measured with wing airfoil angle of incident or angle of attack (AOA) such as Cl vs AOA and Cd vs AOA. A satisfy aerodynamic performance is achieve by having the number of Cl as high as possible and a low number of Cd. Another aerodynamic performance that needs to be highlighted is its stability [92]. It is defined as the ability of an aircraft to correct its position for conditions that act on it. There are two types of aircraft stability and they are static and dynamic. For each stability there is a positive, neutral and negative stability respectively. For a positive static stability, it is described as the aircraft tendencies to return to its original position when it's disturbed. For neutral static stability, it is described as the aircraft tendencies to maintain its new position when it is disturbed. For negative static stability, it is described as the aircraft tendencies to continue moving away from its original position when it is being disturbed.

Center of Moment

As shown in Figure 2.36, to have a static longitudinal stability the aircraft pitching moment must have a negative slope (see Airplane 1).

Which is; ɖCm/ ɖα

(2.19)

In addition to having a negative slop, one must also have a positive intercept to trim at positive angle of attack in which;

Cm0 > 0

(2.20)

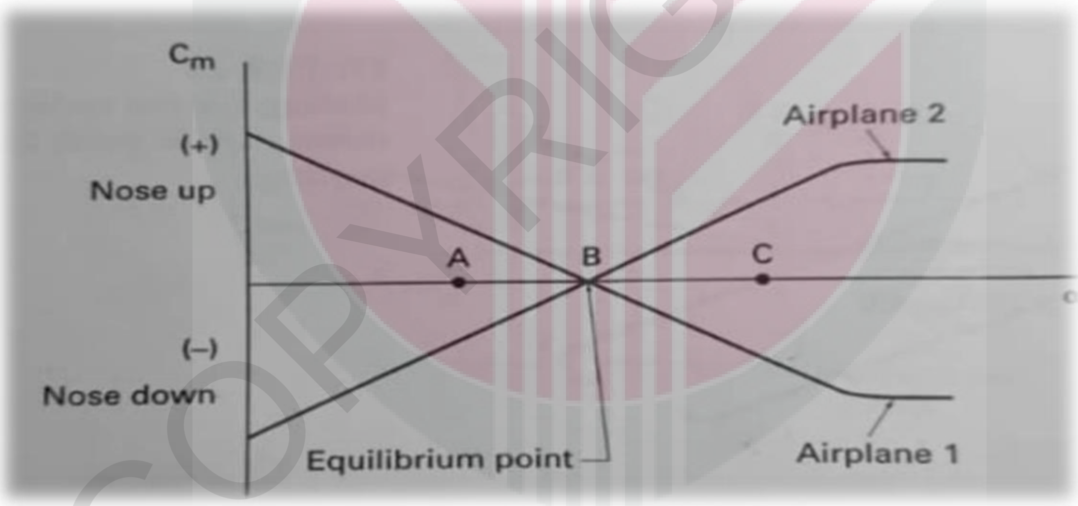

Figure 2.36: Moment center acting on airfoil [93].

This concluded that variables involving products of the drag coefficient and either vertical displacement of the WIG craft center of gravity (CG) can be ignored when analyzing longitudinal stability. Hence as shown below, the pitching moment about the center of gravity can written as;

$$C_{mcg} = C_{m0_\omega} + C_{L_\omega}\left(\frac{x_{cg}}{\bar{c}} - \frac{x_{ac}}{\bar{c}}\right) - \eta\frac{s_t}{S}C_{L_t}\left[\frac{L_t}{\bar{c}} - \left(\frac{x_{cg}}{\bar{c}} - \frac{x_{ac}}{\bar{c}}\right)\right] + C_{mcf}$$

(2.21)

The tail is usually symmetrical so we assume that Cm0t = 0.

Center of Pressure

Center of Pressure (COP) also have a significant contribution to WIG craft stability. COP is the single point of drag and lift force acting on aircraft wing. As shown in Figure 2.37, this awkward situation can easily occur in practice, so the center of pressure is rarely used in aerodynamics work. It forms a pitching moment when its location does not vary with the aircraft center of gravity. COP location does not move with angle of attack. Instead, its location migrates based on the pressure distribution over the wing surfaces. Theoretically when one considered an airfoil at angle of attack, the pressure variation around the airfoils can be determined and the aerodynamic force and center of pressure can be calculated.

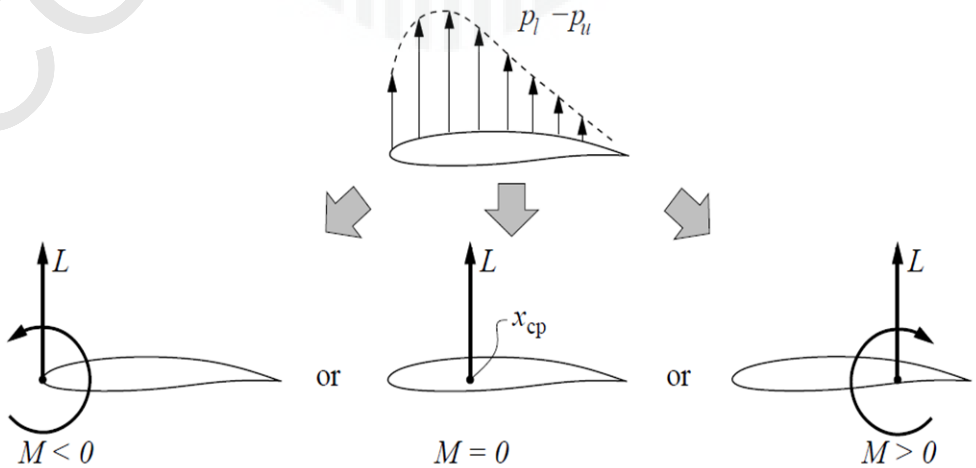

Figure 2.37: Center of Pressure acting on airfoil [94].

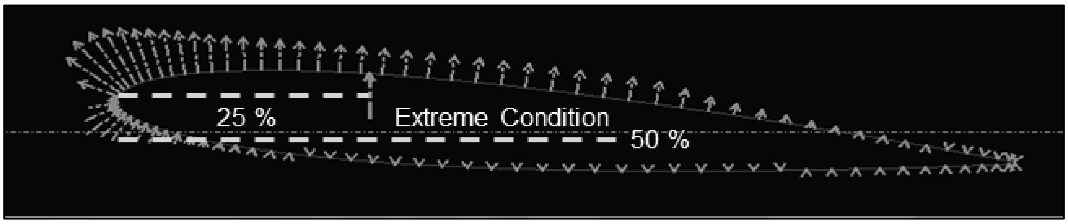

Figure 2.38: Pressure unevenly distributed around Naca0012

In general, as shown in Figure 2.38, COP is defined as a point representing an unevenly distributed pressure generated around lifting surfaces. These pressures can be replaced as a single resultant force. During true flight or out of ground effect (OGE), the approximate location of COP is about 25 % of chord [94]. The COP migrates aft in chord position as the lifting surfaces transit to in ground effect (IGE) zone. In an extreme ground effect condition, the COP can be shifted to up to 50% of the chords position [95]. Published research regarding COP migration around lifting surfaces in ground effect condition is very limited thus an actual description of how much COP migrates is difficult to explain. In theory, The Centre of pressure (COP) is determined by integrating pressure times the airfoil surfaces area over the lifting body. Figure 2.39 and equation 2.22 shows an example of pressure distribution graph and governing equation behind it in two dimensional conditions respectively. Generally, the final lifting value is the difference between the lower surface pressure and the upper surface pressure [96]. As shown in Equation 2.22, Fℓ is the Lift force, c is the chord length, P£, Pû is the lower and upper pressure respectively. The surface pressure represented a viscous turbulent flow of Navier stock equation for Newtonian fluid [64] , therefore an actual solution to calculate turbulent flow around lifting surfaces is still remained unsolved until today. However, Computational Fluid Dynamic

Analysis or (CFD) has been able to estimate the pressure variation using numerical analysis.

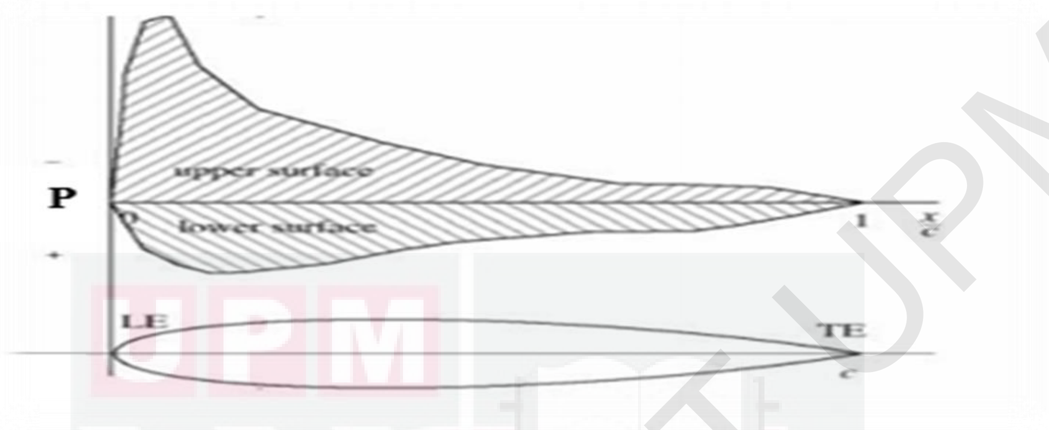

Figure 2.39: Example of Pressure distribution graph [96].

$$F\ell = \frac{1}{c}\int_{LE}^{TE} \mathrm{P£} - \frac{1}{c}\int_{LE}^{TE} \mathrm{P\hat{u}}\, dx = \frac{1}{c}\int_{LE}^{TE} (\mathrm{P£} - \mathrm{P\hat{u}})\, dx \qquad (2.22)$$

Governing equation of Lift force in 2D

A WIG craft uses ground effect phenomenon caused by the presence of a ground boundary below the surface of the wing. The boundary alters the flow of the air around the wing, causing an increase in wing lift and reduction in the induced drag. The overall effect is an increase of the lift to drag ratio. This ratio is a measure for the efficiency of an aircraft that can be expressed as the amount of thrust that is required to propel an aircraft on a certain weight. When a wing operating in ground effect zone, the wing tip vortices will reduce the downwash velocity and the wing tip vortex-induced velocity reduced the induced drag [1].

The WIG craft flies closer to the ground and the lift generated by the wing increases with the drag decreasing as the tip vortices are suppressed and the craft becomes more efficient in flying closer to water and ground surfaces. Owing to the flow blockage between the wing underside and the ground, the pressure on the lower surface of the wing increases, hence increases the lift. COP locations were influence by the pressure surrounding the surfaces. Therefore, its location migrates further from its original position when flying outside ground effect zone. This phenomenon disturbed the pilot handling capability and may require special control system or specific type of wing to solve this problem. For a WIG craft, being able to fly outside of ground effect zone is crucial in order to avoid sea wave and high obstacle in a long travel.

Ground effect-enhanced lift

An aircraft will produce a usable lift force from a pressure imbalance when its three-dimensional wing profile immersed in an appropriate flow [97]. Because of this phenomenal, the wing will have low pressure above and high pressure below wing surfaces [98].

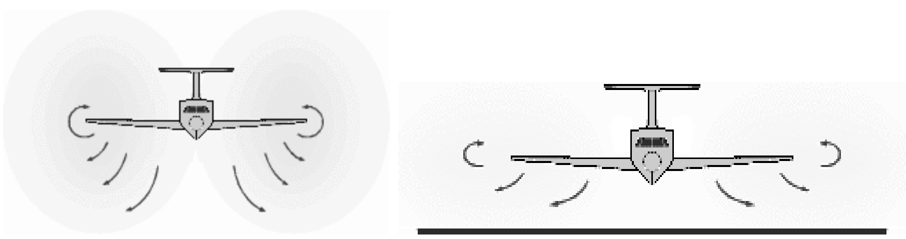

Figure 2.40: An air flow around aircraft on free flow flight (left) [1] and Tip Vortices Drag Reduction (right)

As shown in the left picture of Figure 2.40, due to the pressure equalization the air will flow around the wing tip thus creating air vortices [99]. These spinning air vortices [100] created an energy loss and this yields no useful advantages. Therefore, it must be reduced to stimulate the aircraft efficiency. As shown in Figure 2.40, the right picture showed the energy wasted by wing tip vortices is reduced by the surface interference with the lateral air flow hence reducing the induced drag. This Effect is commonly referred to as Span Dominated Surface Effect because the effect or benefit is proportional to span [101]. Figure 2.41 contour shows the air being disturbed or drag. It also shows when the airfoil gets closer to the ground, the pressure underneath it increases significantly. The location of the maximum suction is represented by the green area over the wing surface and the location of the maximum pressure is represented by the red area on the lower surface of the wing. Atmospheric pressure is represented by the yellow area while none yellow areas appear to be centered nearer to the leading edge of the wing which normally would be around 25% of chord. This is also typically referred to the center of pressure force or COP.

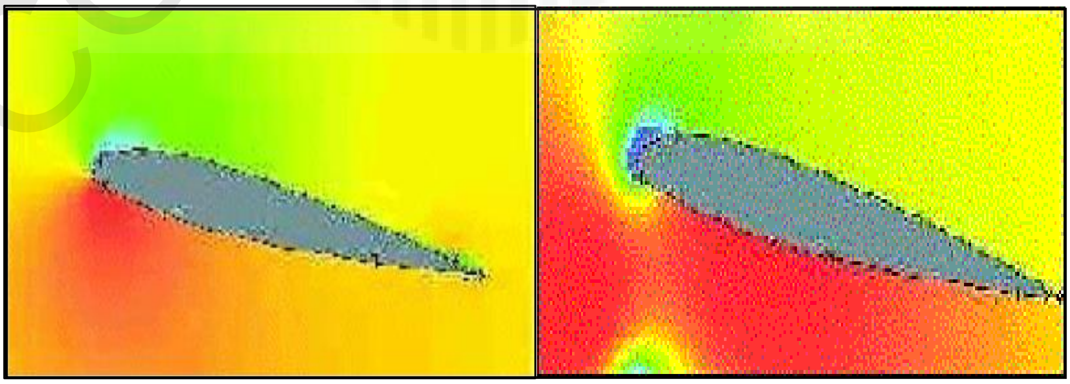

Figure 2.41: Two dimensional depiction of a Pressure Distribution around a Wing moving through free air (left) and in ground effect (right) [1]

Bixel Hoverwing Patent

Patented by Charles G. Bixel in 1989, it is defined as combination of flying hovercraft and ground effect vehicle design. This craft is a flat double wing design for small, medium and large cargo that allows travel from low to medium to high speed on land and water. It is a low AR capable of traveling at a speed of 150 to 200 knots in ground effect zone at a safe distance above the water [31]. Bixel claimed that a vehicle of this design is 250% more efficient than modern aircraft, 15 times faster than cargo ships, and capable of going into true flight to fly over land masses for ocean-to-ocean and Inland Lake or river access or any terrain. The patent Bixel drawing is as shown in Figure 2.42.

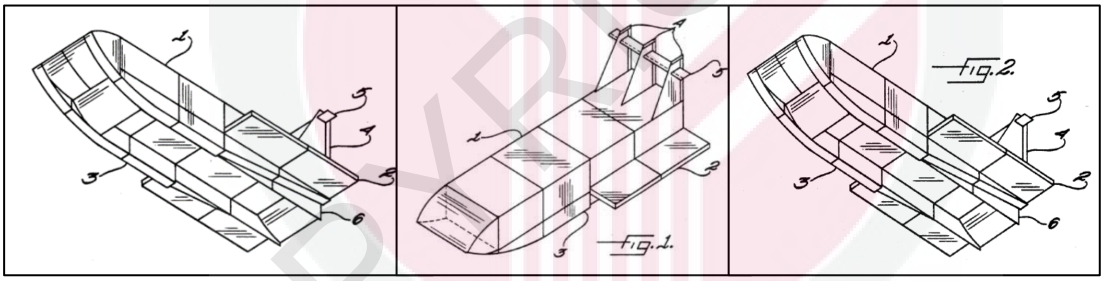

Figure 2.42: Patented Bixel craft.

The flat wing with low aspect ratio allows this craft to fly in the ground effect zone at a height four times greater than at which conventional planes can fly in the ground effect zone. Another reason claimed by Bixel is that Flat or symmetrical airfoil have almost none COP migration and have no pitch up tendencies when OGE. It is the intentions of this thesis to verify these claimed since there is no publication or information pertaining to this patent available yet. Figure 2.43 shows the prototype of Bixel craft by Charles Bixel.

Figure 2.43: Prototype of Bixel craft by Charles Bixel [5] .

2.3 Design Process

All design methodology shares the common goal of developing effective solutions that meet user needs and achieve the desired outcomes. It refers to the systematic approach or process used to develop a product, service, or system. It encompasses a set of strategies, methods, and tools that designers employ to guide their work from problem identification to solution implementation. Design methodology provides a structured framework for approaching design challenges as shown in Figure 2.44.

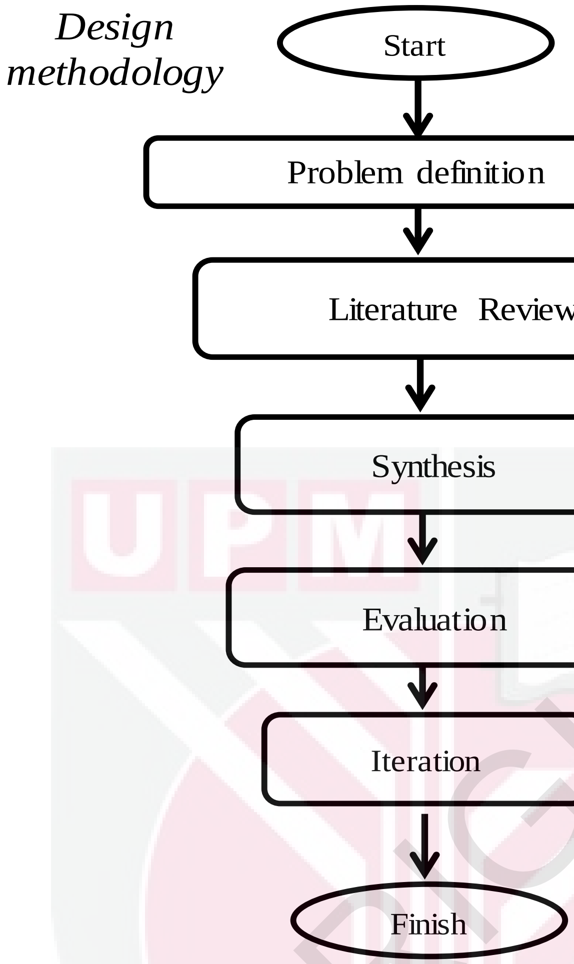

Figure 2.44: Design Methodology

2.3.1 Available Design Methodology

Engineering design, a multifaceted process involving problem-solving, innovation, and implementation, requires a structured approach to ensure efficiency and effectiveness. Various methodologies have emerged over time to cater to different project requirements and team dynamics. There are several available design methodologies such as the Waterfall, Agile, Lean Startup, Design Sprint, and Concierge Testing methodologies and their applicability to engineering design.

The Waterfall methodology, a traditional sequential approach, is characterized by its rigid phases, including requirements gathering, design, development, testing, and deployment. While it offers a clear structure and timeline, it can be inflexible, making it challenging to accommodate changes or address unforeseen challenges. In contrast, Agile methodologies, such as Scrum and Kanban, emphasize iterative development and flexibility. They involve breaking down projects into smaller, manageable increments, allowing for continuous feedback and adaptation. Agile methods are well-suited for projects with evolving requirements or uncertain outcomes. The Lean Startup approach, rooted in business development, focuses on minimizing waste and maximizing learning. It encourages rapid experimentation and pivoting as needed, ensuring that efforts are aligned with customer needs. This methodology is particularly valuable for engineering projects with uncertain market demand or technological feasibility. The Design Sprint methodology, a five-day process for rapid prototyping and testing, is designed to accelerate innovation. It involves defining a challenge, ideating solutions, prototyping, testing, and sharing insights. Design Sprints are effective for generating new ideas and validating assumptions quickly. Concierge Testing, a form of usability testing, involves providing personalized assistance to users as they interact with a product or system. It offers valuable insights into user behavior and pain points, helping engineers refine designs and improve user experience. While each methodology has its strengths and weaknesses, they are not mutually exclusive. In practice, a hybrid approach combining elements from different methodologies can often yield the best results. For example, an engineering team might use Agile for iterative development, Lean Startup for customer-centric innovation, and Design Sprints for rapid prototyping.

2.3.2 Available Design Techniques

To effectively tackle the challenges of engineering design, various techniques can be employed. Some of the most commonly used design techniques are brainstorming which is a technique that involves generating a large number of ideas in a short period of time. It encourages creative thinking and helps to identify potential solutions to design problems. A visual tool that helps to organize thoughts and ideas such as mind mapping involves creating a central concept and branching out related ideas, making it easy to see connections and relationships.

An effective way to visualize ideas such as sketching can help to communicate concepts, explore different design options, and identify potential issues. A technique that involves breaking down a complex system into smaller, more manageable components called functional decomposition can help to simplify the design process and make it easier to identify potential problems. Other than that, is design for Six Sigma. It is a quality improvement methodology that focuses on reducing defects and improving process efficiency. Design for Six Sigma can help to ensure that products meet customer expectations and are reliable. The most commonly used method is Computational Fluid Dynamics (CFD) and Finite Element Analysis (FEA). It is a simulation technique that can be used to analyze fluid flow and heat transfer and a simulation technique that can be used to analyze the structural behavior of a product. CFD can help to optimize designs, reduce costs, and improve product performance while FEA can help to identify potential failures, optimize designs, and improve product safety.

While each design technique has its own strengths and weaknesses, they are not mutually exclusive. In practice, a combination of techniques can often yield the best results. By carefully selecting and applying the appropriate design techniques, engineers can create innovative, efficient, and sustainable products.

2.2 Summary

Throughout history, advancements in technology have driven faster transportation. Hovercrafts and WIG crafts offer exciting alternatives to ferries and boats, overcoming limitations caused by water drag. In tourism, WIG crafts could revolutionize travel while also serving as test-beds for future aircraft and military technology. From the literature research of previous WIG craft design, the research and development of WIG craft only focusing on designing a suitable craft particularly on lift and drag performances that can operate efficiently in ground effect condition. To the author understanding, if this was only the case by now the world would already have a commercial WIG craft that can operate and function safely as conventional aircraft. Many of the experimental WIG craft previously made was met with accident either by flipping to the back or dive into water at high speed such as KM, Orlyonok, and X-114 [102] which indicates that WIG craft having a stability issue. Hence this thesis focuses on exploring alternative design solutions and perspectives to address the challenge of center of pressure (COP) migration during transitions between in-ground-effect and out-of-ground-effect conditions for Wing-In-Ground (WIG) craft. While existing experimental research, such as the New1 WIG craft by the Royal Thai Navy and the Bixel craft, offer valuable insights, they fall short of providing a comprehensive solution. However, these projects serve as a strong foundation for further development. By analyzing and building upon their designs, this thesis aims to contribute to overcoming the COP migration issue and advancing WIG technology.

CHAPTER 3

RESEARCH METHODOLOGY

The flow chart methodology is a diagram that visually represents the steps involved in the research process. It provides a clear and concise overview of the research process, making it easier to understand and follow. In objective one, the methodology flow starts from verifying CFD simulation by XFLR5 with existing experimental published paper. After that, conduct simulation on various airfoil profiles to obtain result of COP migration and behavior. Based on the result of COP migration from objective one, a lifting surface for two-seater hoverwing for objective two is produce. In the final objective, perform verification of solidwork flow simulation with published wind tunnel experiment paper. Next is to conduct aerodynamic simulation on the new lifting surface two-seater hoverwing with solidwork flow simulation to obtain preliminary performance result such as lift and drag and longitudinal stability. The thesis culminates in a comparison of the newly proposed two-seater WIG craft's conceptual design with existing WIG craft designs. This comparison will serve as the final evaluation and highlight the potential advancements offered by the new concept. Figure 3.1 shows the flow chart representing the whole methodology procedure.

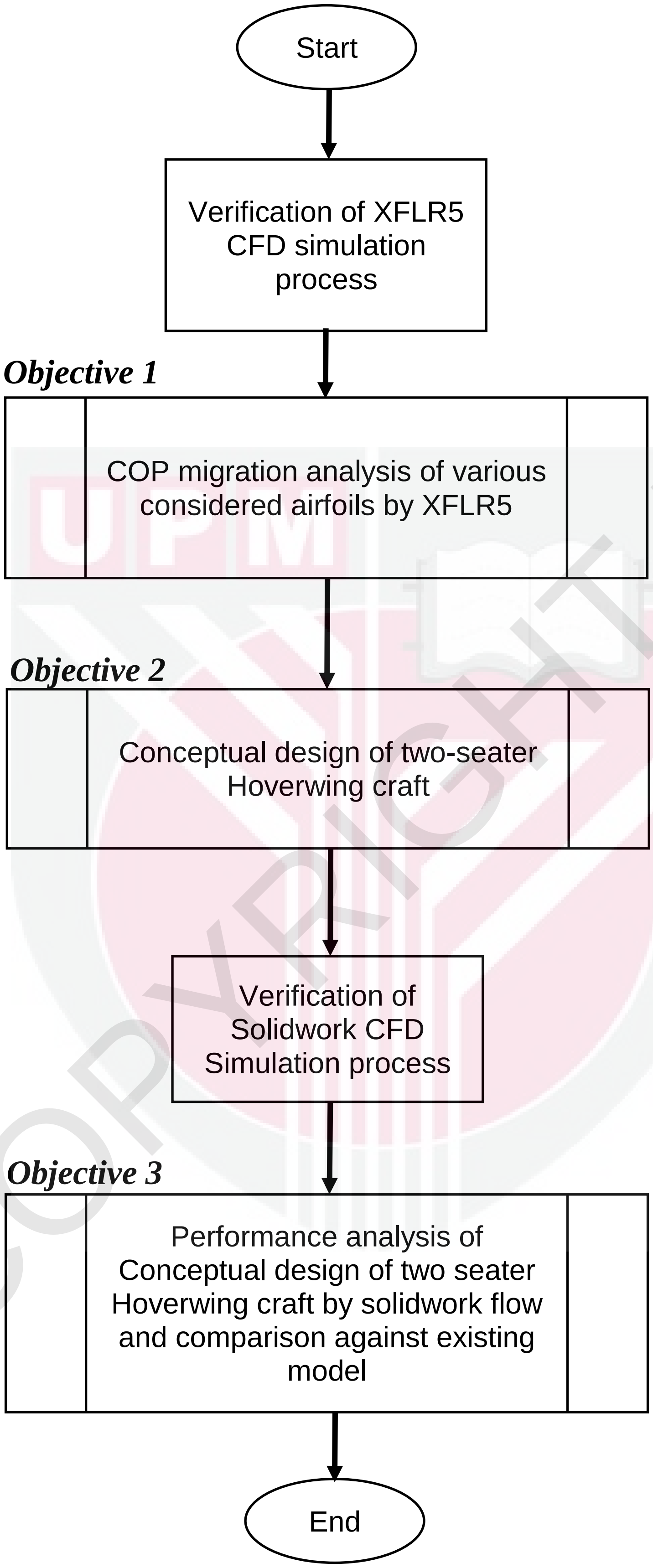

Figure 3.1: Flow Chart Methodology

3.1 Introduction to XFLR5

The XFLR5 is the chosen software to analyze and produce preliminary COP result on airfoils. XFLR5 is a free analysis tool for airfoils, wings and planes. It's used Reynold Average Navier (RAN) solver to calculate viscosity model and able to predict boundary layer thickness around airfoil in 2D [103].

3.1.1 Analysis Workflow

The XFLR5 analysis process can be summarized in the following steps:

1. **Define polar type:** The first step is to define the type of polar needed for analysis. There are fixed speed, fixed lift, fixed AOA and fixed beta range. The chosen polar type for this study is fixed speed at 15 m/s as shown in Figure 3.2.

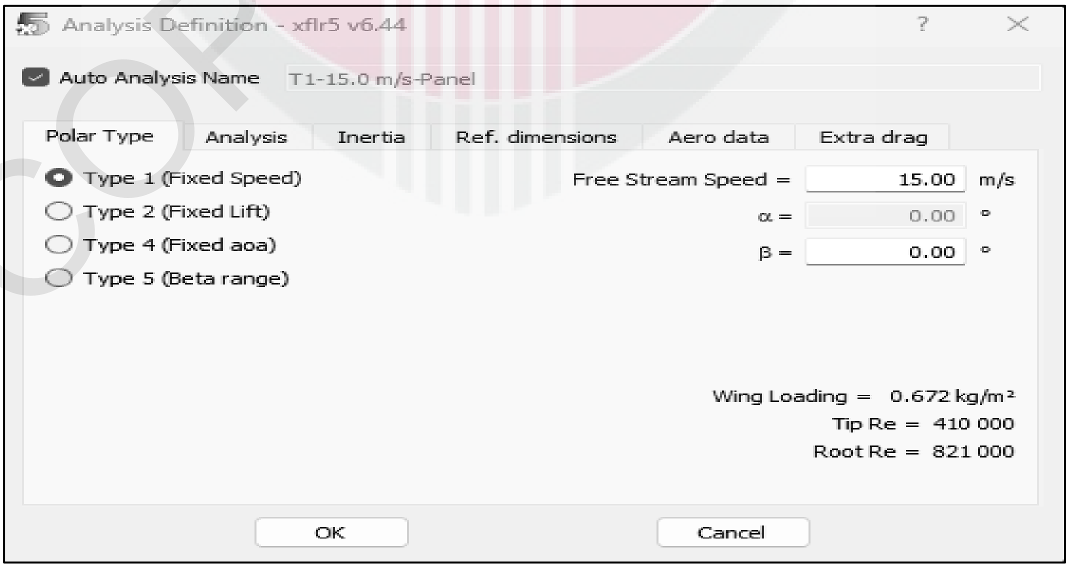

Figure 3.2: XFLR5 polar type definition

2. **Set the analysis method:** Once the polar type has been defined, the next step is to set the analysis method. These methods are lifting line theory, wing horseshoe vortex (VLM1), ring vortex (VLM) and 3D panel. The chosen method was VLM due to its simplicity in method of solution and highly versatile output result compared to the LLT and Panel as shown in Figure 3.3.

Figure3.3: XFLR5 analysis type definition

3. **Define aerodynamic data:** The final step is to define the aerodynamic data. This can be done by setting up the air data (Figure 3.4) such as density and kinematic viscosity. The ground height from chord also being the input in this step. After that, XFLR5 will then calculate the aerodynamic performance of the geometry, including the lift, drag, and moment coefficients.

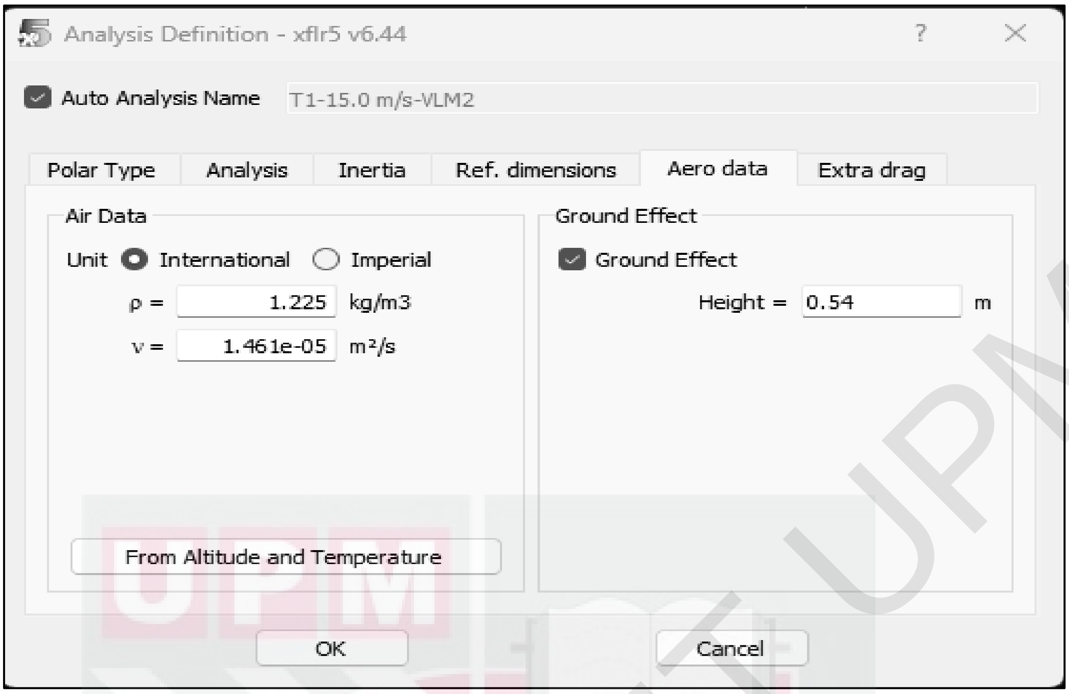

Figure 3.4: XFLR5 aerodynamic data type definition

3.1.2 Re number independent study

As shown in Figure 3.5, a study of Re number against COP behavior similar to grid independence study is an essential part of computational fluid dynamics (CFD) simulations. It is a process of systematically refining the Re number value and analyzing the effect on the solution to ensure that the results are not significantly affected by the discretization of the computational domain. As shown in Figure 3.6, the value of Re number changed insignificantly as Re number value increased. Therefore, COP behavior has less affection in relation to Re number increments. The chosen velocity for this study is 15m/s due to this is the normal speed for remote control aircraft flight.

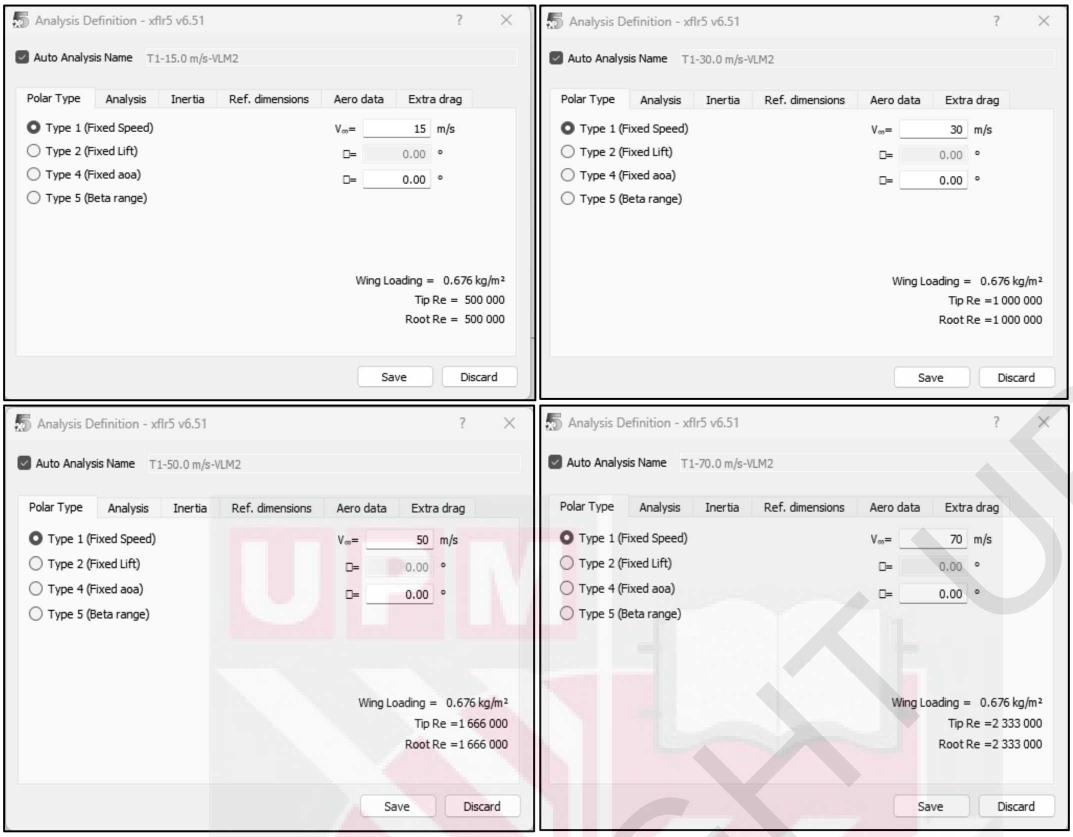

Figure 3.5: Various Re number and its respective air velocity

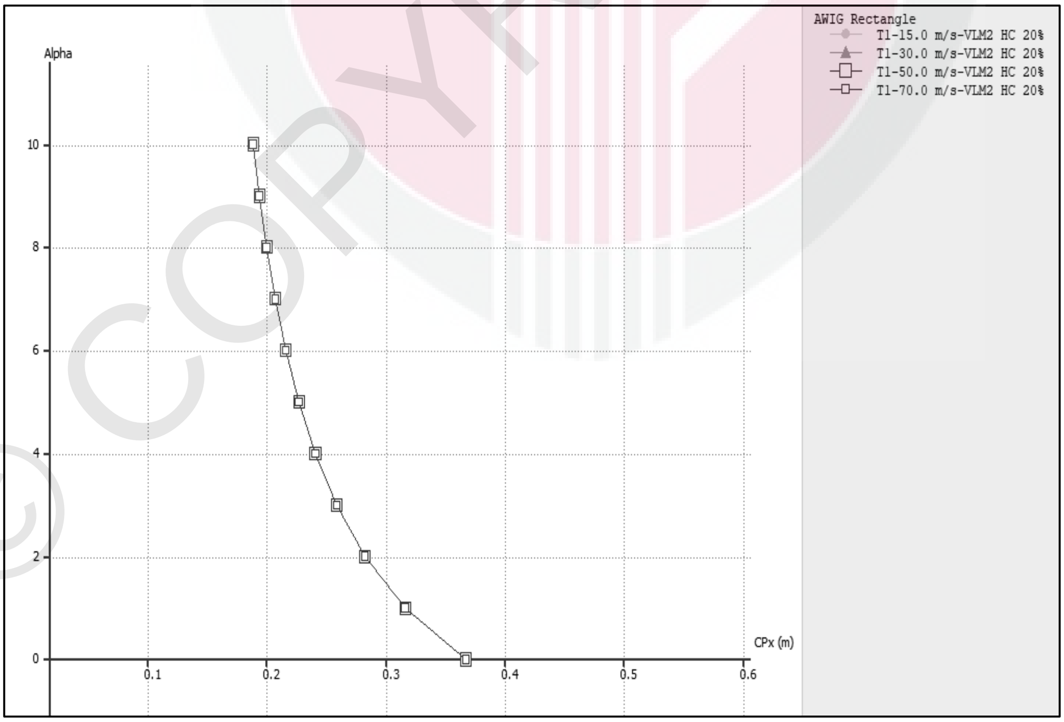

Figure 3.6: Angle of attack against COP distribution migration at various Re number

3.1.3 Aerodynamic analysis via XFLR5 software application

XFLR5 includes XFoil's direct and inverse analysis capabilities as well as wing design and analysis capabilities based on the lifting line theory, on the vortex lattice method, and on a 3D panel method. The analysis uses the Vortex lattice method (VLM) because of its simplicity in method of solution and highly versatile output result compared to the LLT and Panel method as shown in Figure 3.7. XFLR5 also able to calculated pressure distribution on lifting surfaces on every chord direction and displayed COP location acting on wing, vertical and horizontal stabilizer. Figure 3.8 shows an example of COP location on Naca 4412 inverse delta wing and Figure 3.9 shows the pressure distribution of root and tip chord.

3D	Elementary solutions	Boundary Condition
Lifting Line Theory (LLT)	Vortices	Neumann
Vortex Lattice Method (VLM)	Vortices	Neumann
Panel	Source/sink and doublet sheets	Dirichlet and/or Neumann

Figure 3.7: Laplace's equation solution method for 3D representation in XFLR5 [103].

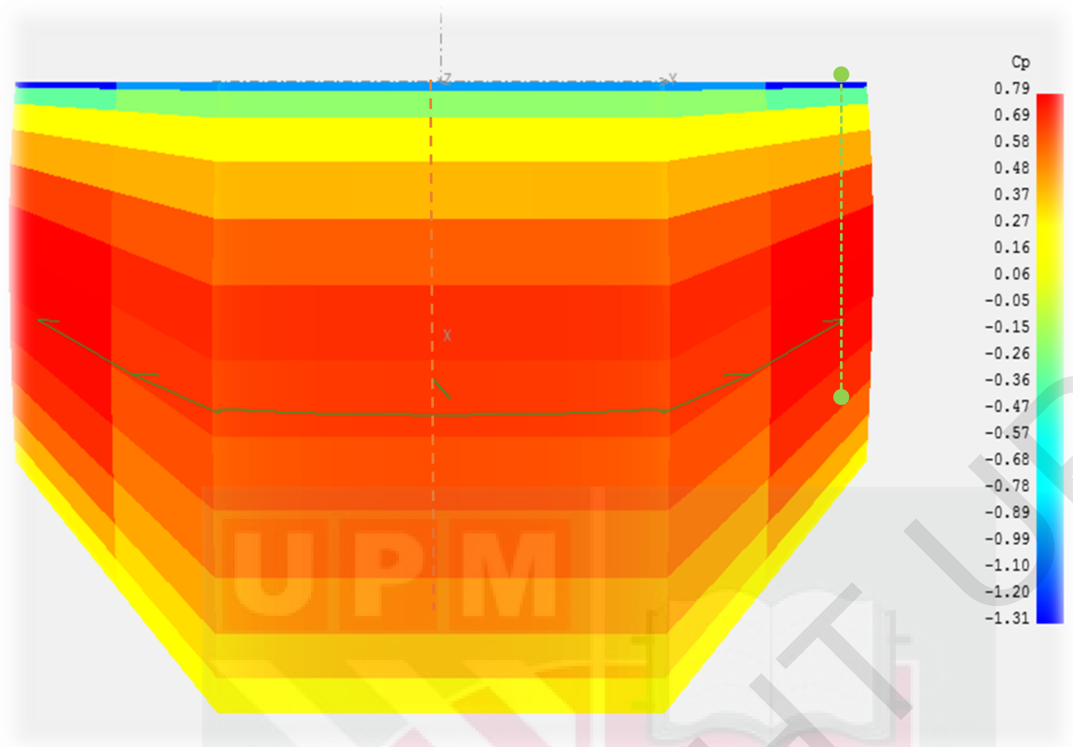

Figure 3.8: COP location (green line and point) on Naca 4412 inverse delta wing in XFLR5

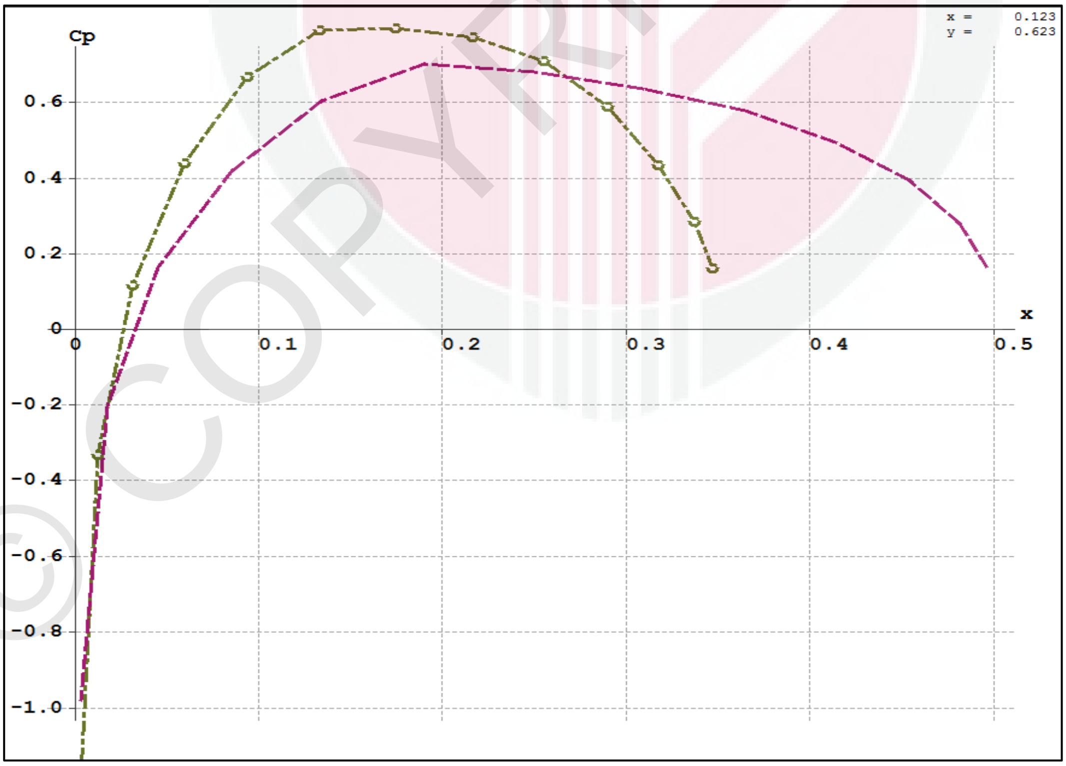

Figure 3.9: pressure distribution of root (dash line) and tip chord (dotted line) on Naca 4412 inverse delta wing in XFLR5

3.2 XFLR5 Simulations verification

A simulation of COP migration investigation was done to the New1 model to measure the accuracy of XFLR5. As a result, when comparing COP migration of the New1 model wind tunnel experiment and XFLR5 simulation (New1x) the result was differentiated by 8% to 10% at 0 angle of attack (AOA). Both New1 and New1x show a similar trend of decreasing COP with increasing H/C. This means that as the ground height increases relative to the chord length, the center of pressure movement percentage decreases. This is a well-known phenomenon in aerodynamics and is due to the influence of the ground on the airflow around the airfoil. In terms of differences, there are some noticeable discrepancies between the two data sets. New1x (based on XFLR5 software) shows a consistently higher XCOP than New1 (based on wind tunnel experiments) for all H/C values. This difference could be due to a number of factors, including modeling assumptions by XFLR5 software that make simplifying assumptions about the airflow around the airfoil that are not present in a wind tunnel experiment. These assumptions could lead to an over prediction of XCOP. Another factor would be experimental errors. Wind tunnel experiments can be susceptible to errors due to factors such as turbulence in the wind tunnel flow or imperfections in the model. These errors could lead to an under prediction of XCOP. There are also some key differences between the two datasets. New1x (based on XFLR5 software) shows a steeper decrease in XCOP compared to New1 (wind tunnel data) at lower H/C values.

In conclusion, the graph shows both similarities and differences between the XCOP data obtained from wind tunnel experiments (New1) and CFD simulations (New1x). The overall trends are similar, but the XFLR5 software may be over predicting the ground effect at low H/C values. These differences could be due to limitations of both wind tunnel experiments and CFD simulations. This suggests that the XFLR5 software may be over predicting the ground effect. At higher H/C values, the two datasets converge and show similar trends. This indication will be beneficial later to measure the accuracy of other simulations. Figure 3.10 and Figure 3.11 shows the NEW1x model by XFLR5 and the COP migration result at 0º angle of attack.

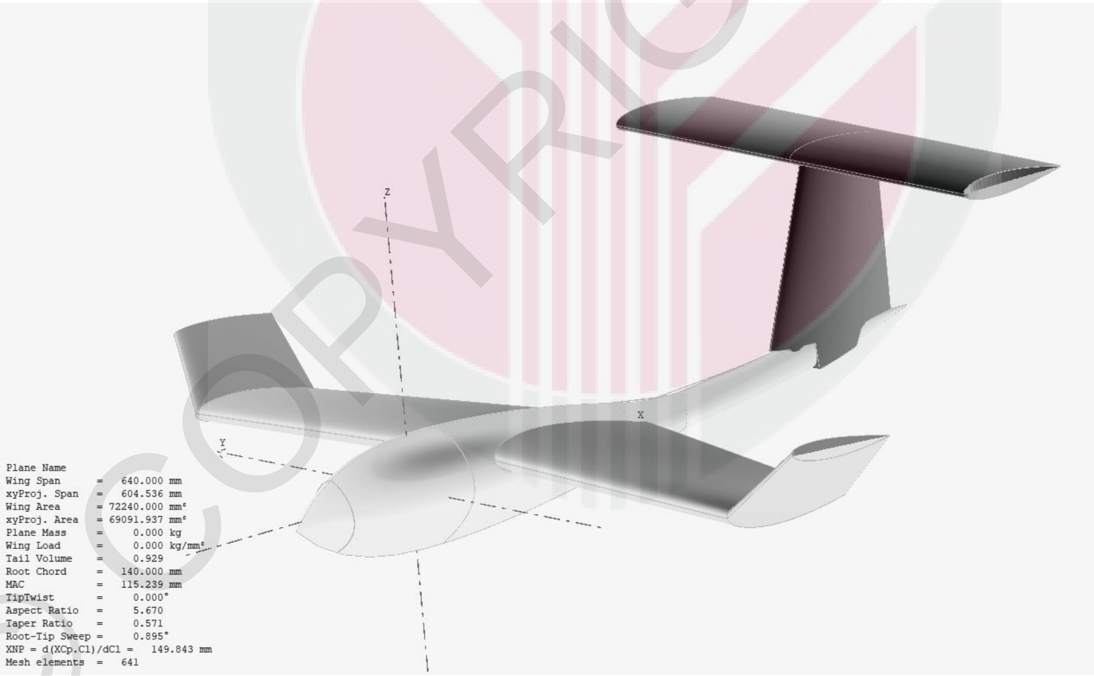

Figure 3.10: Simulation of NEW1x model in XFLR5

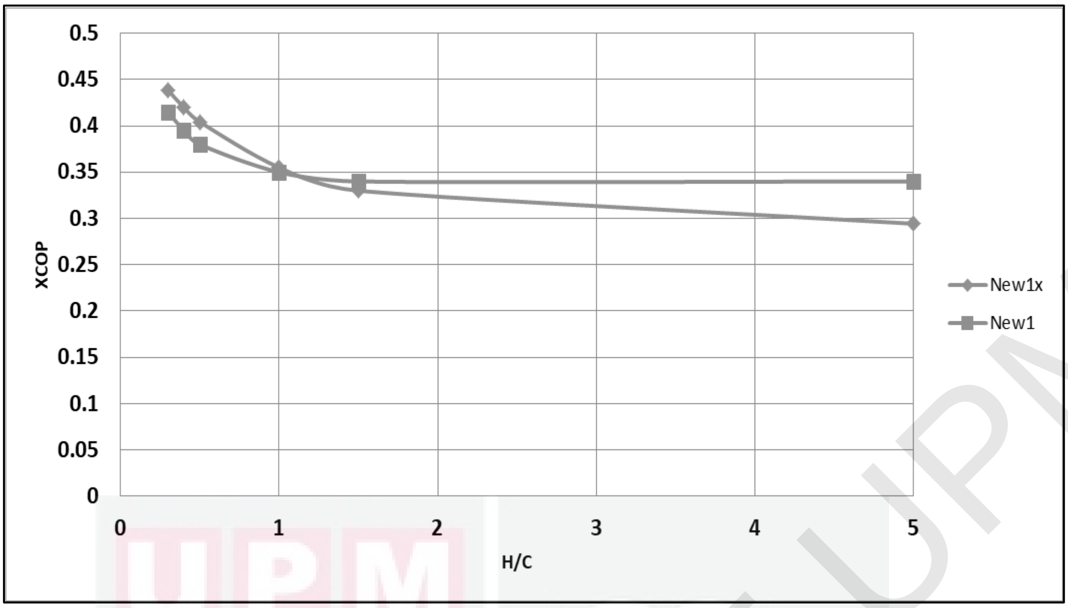

Figure 3.11: Result of New1 (Experimental) & New1x (XFLR5) model COP migration at 0⁰ AOA

3.3 Center of Pressure Migration Simulation of Six Types of Airfoils by XFLR5

This study highlighted the center of pressure migration which in essence is caused by pressure distribution caused by the flow around the airfoil. Thus, the author intention was to investigate the migration and behavior of center of pressure (COP) on various types of lifting surfaces. The chosen airfoils and wing configurations are Naca0012, Naca4412, Clark Y, DHMTU, AWIG and Flat surfaces.

3.3.1 Analysis Work Flow

The process of investigating COP migration behavior is done by computational work of XFLR5 software. As shown in Figure 3.12, it starts from verifying CFD simulation by XFLR5 with existing experimental published paper. After that, conduct simulation on rectangle configuration with airfoil profiles of Naca 0012, Flat surface, Naca 4412, Clark Y, AWIG and DHMTU to obtain result of COP migration and behavior. The next task is to conduct similar analysis setting on Inverse delta configuration six types of airfoils. After that similar analysis with six types of airfoils will be done to UH18 planform and NEW1 WIG Craft by the Royal Thai Navy. the control parameter is root chord length and lifting surface area.

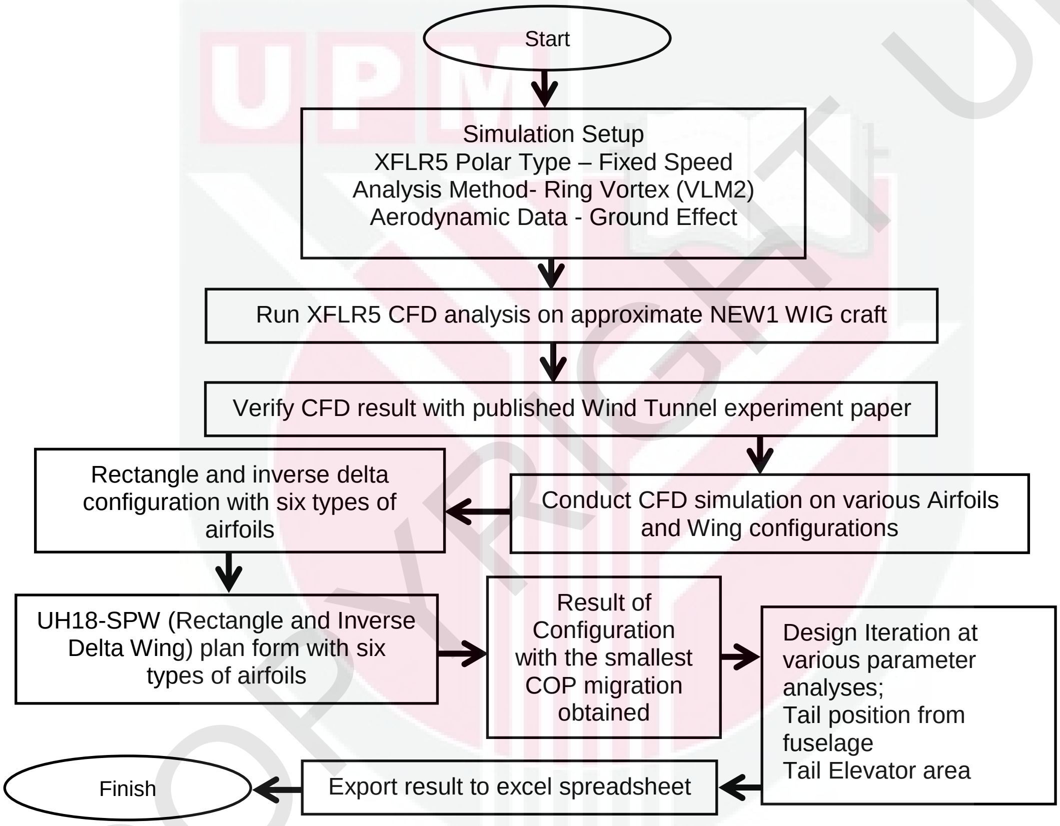

Figure 3.12: Analysis Workflow Chart

Naca 0012 & Flat Surfaces

In the simulation, flat profile is being refined to a thin symmetrical flat surface on both top and bottom surfaces with round edges at the leading and trailing edges. This is due to the difficulty of simulating an actual thin rectangular flat surface in CFD software. Naca0012 is chosen because of its similarity to flat surfaces in term of symmetrical curve on both top and bottom surfaces. Theoretically, Naca0012 and flat surfaces will have about the same COP migration compared to the rest of profiles. Figure 3.13, 3.14, and 3.15 shows the respected airfoils profiles and wing shape.

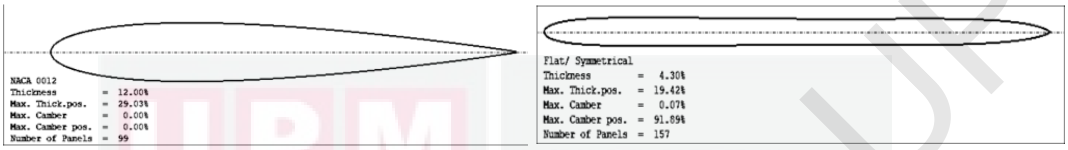

Figure 3.13: Naca0012 Flat and Surface profile profile in XFLR5 [105].

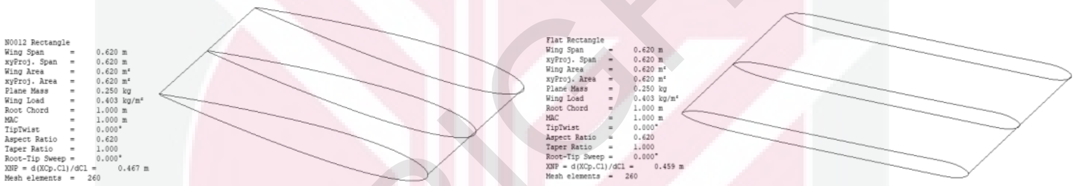

Figure 3.14: Naca0012 and Flat Surface rectangular wing configuration in XFLR5.

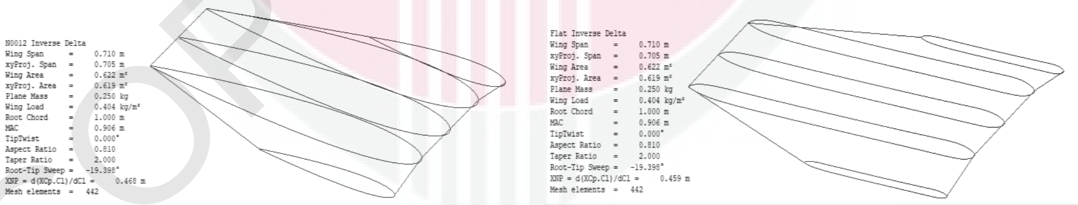

Figure 3.15: Naca0012 and Flat Surface inverse delta wing configuration in XFLR5.

Naca 4412 & Clark Y

The reason for choosing Naca4412 and Clark Y profiles is because of both having a high aerodynamic efficiency in extreme ground effect condition [106] and unsymmetrical curve on both top and bottom surfaces. As the first assumption, Naca4412, and Clark Y will be able to demonstrate a different COP migration and behavior in comparison with both Naca0012 and flat surface profile. Figure 3.16 to 3.18 shows the Naca 4412 and Clark Y Rectangle and inverse delta wing.

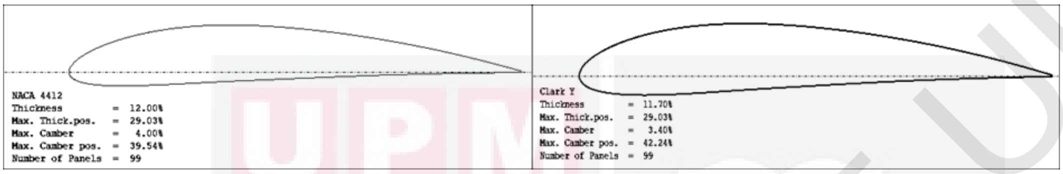

Figure 3.16: NACA 4412 and Clark Y profile in XFLR5.

Figure 3.17: NACA 4412 and Clark Y rectangular wing in XFLR5.

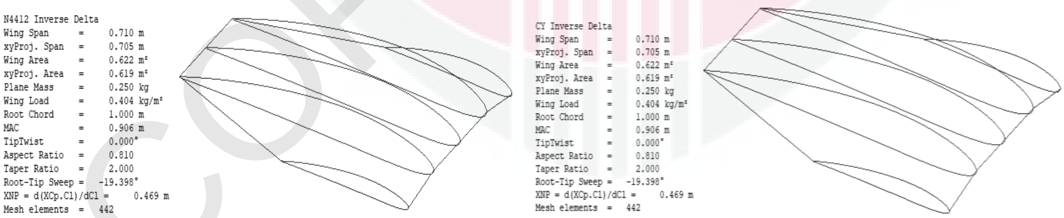

Figure 3.18: NACA 4412 and Clark Y inverse delta wing in XFLR5.

AWIG & DHMTU

As for Department of Hydromechanics of the Marine Technical University (DHMTU) and AWIG profiles, both profiles were designed specifically to be aerodynamically efficient in ground effect condition. Individually, all profile will be simulated in 2D and rectangular shape afterwards. After finishing with the rectangular shape, the next task is to incorporate inverse delta wing configurations to each profile. This is to find out how the COP will migrate and behave with the current most efficient wing configuration condition [28]. Figure 3.19 to 3.21 shows the Naca 4412 and Clark Y Rectangle and inverse delta wing.

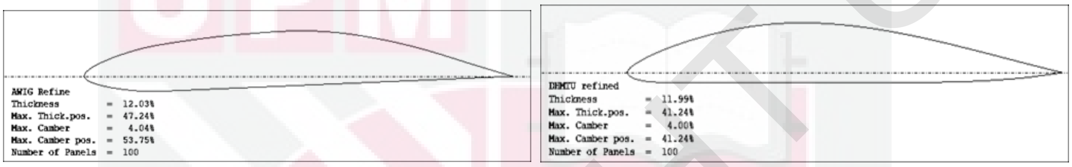

Figure 3.19: AWIG and DHMTU profile [98] in XFLR5.

Figure 3.20: AWIG and DHMTU rectangular wing in XFLR5.

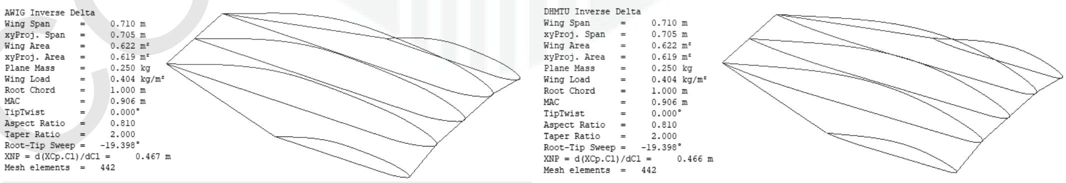

Figure 3.21: AWIG and DHMTU inverse delta wing in XFLR5.

3.4 Center of Pressure Migration Simulation of Six Airfoils With UH18-SPW Planform Area

It is by the author observation on UH18-SPW, Rude Heeman Hoverwing and Bixel craft, that its lifting capability is generated by their respective wing area which then further being enhanced by its fuselage area hence the planform area. The reason is due to these types of WIG craft has a nose up tendency when it's in flying mode (see Figure 2.15, 2.16, and 2.17). This capability is similar to Bixel craft which utilised a double wing design to generate more lift while having a shorter wing for easy turning (roll and yaw).

With that being said, the initial task of this topic is to determine center of pressure (COP) migration and behavior of various airfoil profiles such as Naca0012, Naca4412, Clark Y, DHMTU, AWIG and Flat surfaces based on UH18-SPW planform area. As shown in Figure 3.25, the UH18-SPW real scale planform area [60] has been scale down in order to make sure that simulation process time are reduce. It is also important to conduct the simulation on a small-scale model so that in future the result can be validated through wind tunnel test.

Naca 0012 & Flat Surface

Simulating a perfectly flat, rectangular object in CFD software can be challenging. To address this, the simulation uses a very thin, symmetrical airfoil with rounded leading and trailing edges. NACA 0012 airfoil is closely resembles a flat plate due to its symmetrical top and bottom curves. In theory, both NACA 0012 and a true flat surface should experience similar Center of Pressure (COP) movement compared to other. Figure 3.22 shows the NACA 0012 and Flat surface with UH18-SPW planform.

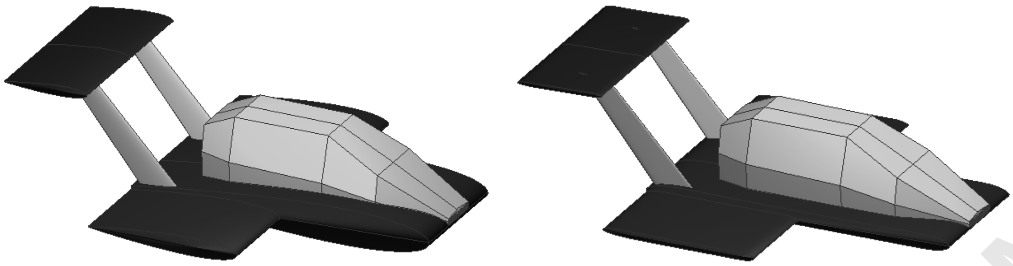

Figure 3.22: NACA 0012 and Flat surface with UH18-SPW planform.

Naca 4412 & Clark Y

The NACA 4412 and Clark Y airfoils were chosen due to their exceptional aerodynamic efficiency when operating close to the ground effect condition [106] and their unique asymmetrical shapes on both the upper and lower surfaces. We hypothesize that these characteristics will lead to distinct center of pressure (COP) movement and behavior compared to the NACA 0012 airfoil and a flat plate. Figure 3.23 shows the NACA 4412 and Clark Y with UH18-SPW planform.

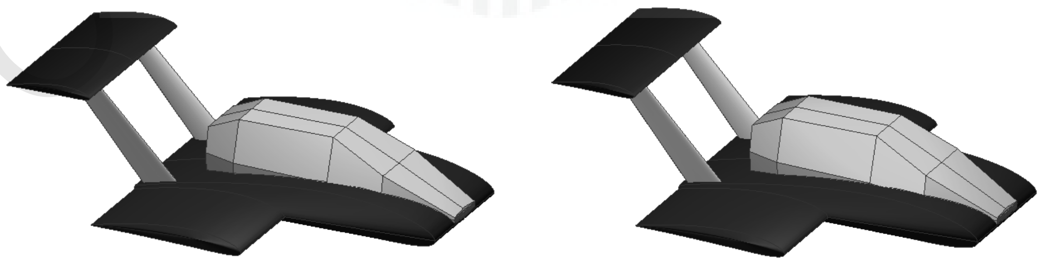

Figure 3.23: NACA 4412 and Clark Y with UH18-SPW planform.

AWIG & DHMTU

The Department of Hydromechanics of the Marine Technical University (DHMTU) and AWIG designed two airfoils specifically for ground effect aerodynamics. These airfoils will be initially simulated in a two-dimensional rectangular shape. Once complete, the simulations will be modified to incorporate an inverse delta wing configuration for each profile. This is to find out how the COP will migrate and behave with the current most efficient wing configuration condition [28]. Figure 3.24 shows the AWIG and DHMTU with UH18-SPW planform.

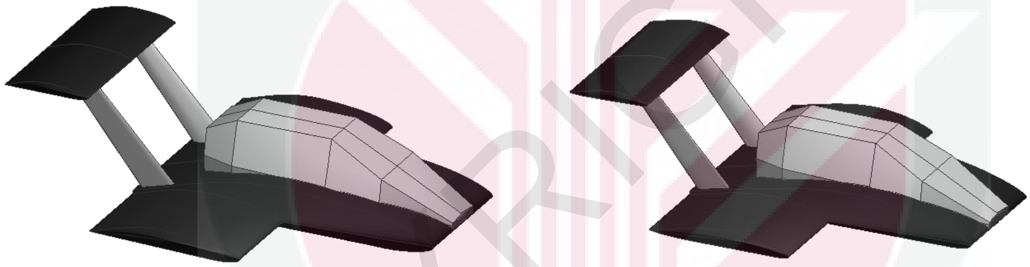

Figure 3.24: AWIG and DHMTU with UH18-SPW planform.

Approximate New1 Royal Navy Thai

The approximate model of NEW1 Wig Craft was done in order to analyze its COP migration behavior. In this analysis various conditions such as height from ground level, and angle of attack position to determine its COP migration value. The result obtained from this simulation will be further compare with the wind tunnel experimental publication. Figure 3.25 shows the approximate Configuration of NEW1 Royal Navy Thai.

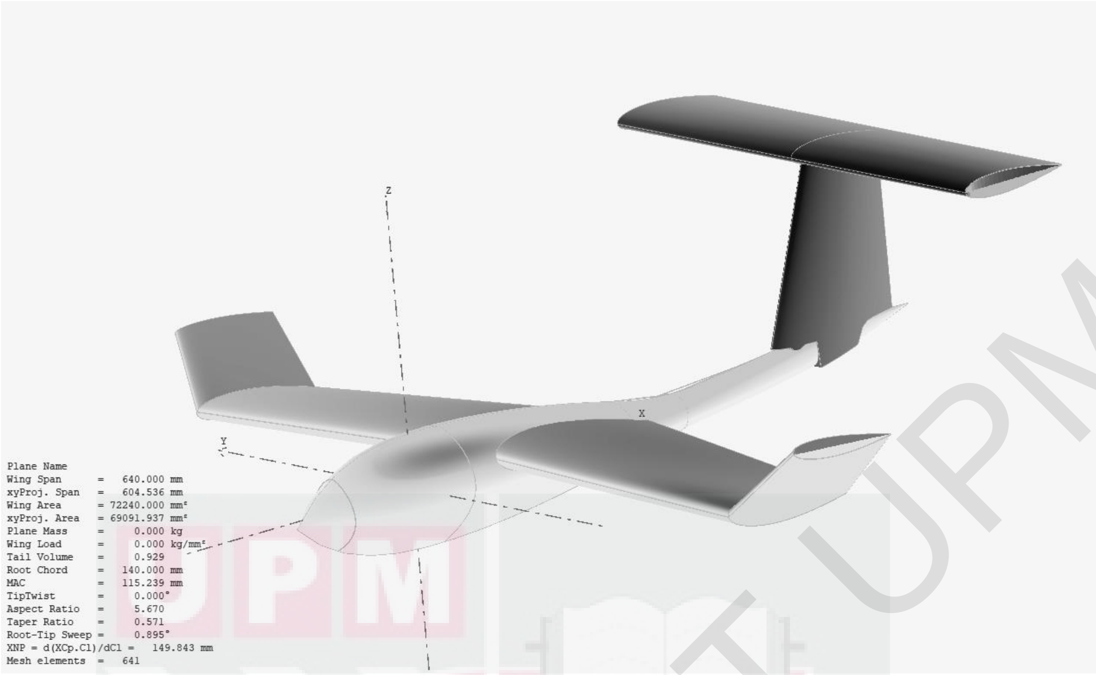

Figure 3.25: Approximate Configuration of NEW1 Royal Navy Thai

3.5 Center of Pressure Migration Simulation of UHID Hoverwing configuration with Six types of Airfoils

After done with rectangle, inverse delta and UH18 COP migration simulation, the author realizes that UH18-SPW utilizes rectangle shape wing and the COP behavior becomes significantly better afterwards. Hence the author decided to incorporate inverse delta wing to UH18 planform. The next task to do is to perform similar investigation of COP migration with six types of airfoils and compare all result of all configurations to determine the best result which is the lowest COP migration. Figure 3.26 to 3.28 shows the UH18 and inverse delta wing (UHID) with six types of airfoils.

Naca 0012 & Flat Surface

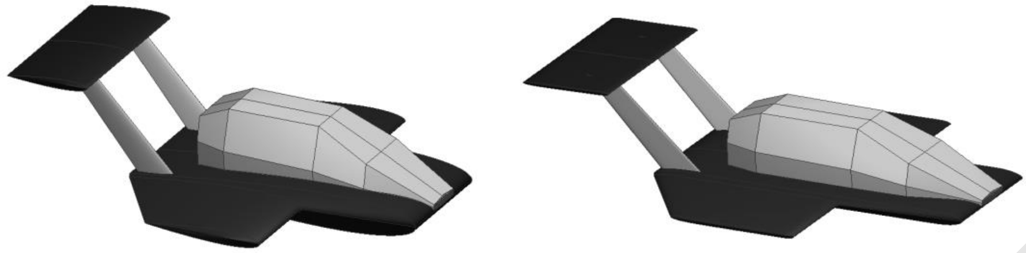

Figure 3.26: Final Iteration with NACA 0012 and Flat surface.

Naca 4412 & Clark Y

Figure 3.27: Final Iteration with NACA 4412 and Clark Y

AWIG & DHMTU

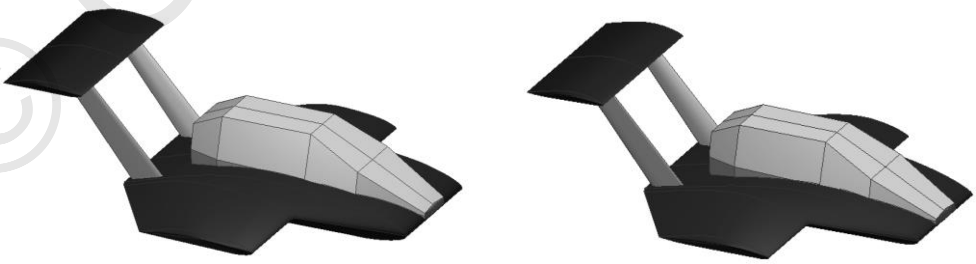

Figure 3.28: Final Iteration with AWIG and DHMTU

After that, the author realizes that the COP behavior is closely affected by the WIG craft configurations. The final analysis task performed afterwards is parameter design iteration where the chosen parameter is the tail elevator area and distance from fuselage.

3.6 Design of Two-Seater Hoverwing (WIG) Craft

In this chapter, the process of designing two seats hoverwing was explained. Six design solutions were made using morph matrix criterion and final decision on design solution was decided using PUGH matrix. After that based on UH18-SPW CAD model from SolidWorks workbench, three iterations were proposed at the end of the process. The whole design process of two seat Hoverwing was discussed with an expert in the design process of product development from industry namely Ir.Adruin Shazaen Bin Mohd Mustaffa. Ir.Adruin is a Professional Engineer certified by Board of Engineering Malaysia, a Naval Architect, chief executive officer (CEO) at Acnetic Naval Consultancy and Principle Naval Architect at Citranaval Asia Sdn Bhd. He is also a Chartered Engineer certified by the Engineering Council UK, a fellow member of Royal Institution of Naval Architects and corporate member of the institution of Engineering Malaysia. Currently Ir. Adruin is collaborating with SEA STRIDER SDN BHD for the development of the Hoverwing technology demonstrator. Figure 3.29 shows the discussion on new Hoverwing concept design process took place in Bukit Jelutong, Shah Alam, Selangor Darul Ehsan.

Figure 3.29: Discussion on new Hoverwing concept design process with Ir.Adruin Shazaen

3.6.1 Conceptual Design Process Flow Chart

In this chapter, the process of design methodology is discussed in the next paragraph. It is start from the four Ws, affinity and tree diagram to determine the functional and quality requirements that are needed to form the quality functional deployment matrix. The next task is to identify the morphological matrix and design solution which then solve by using PUBH matrix solution. Figure 3.30 shows the flow chart design of two-seater hoverwing lifting surface.

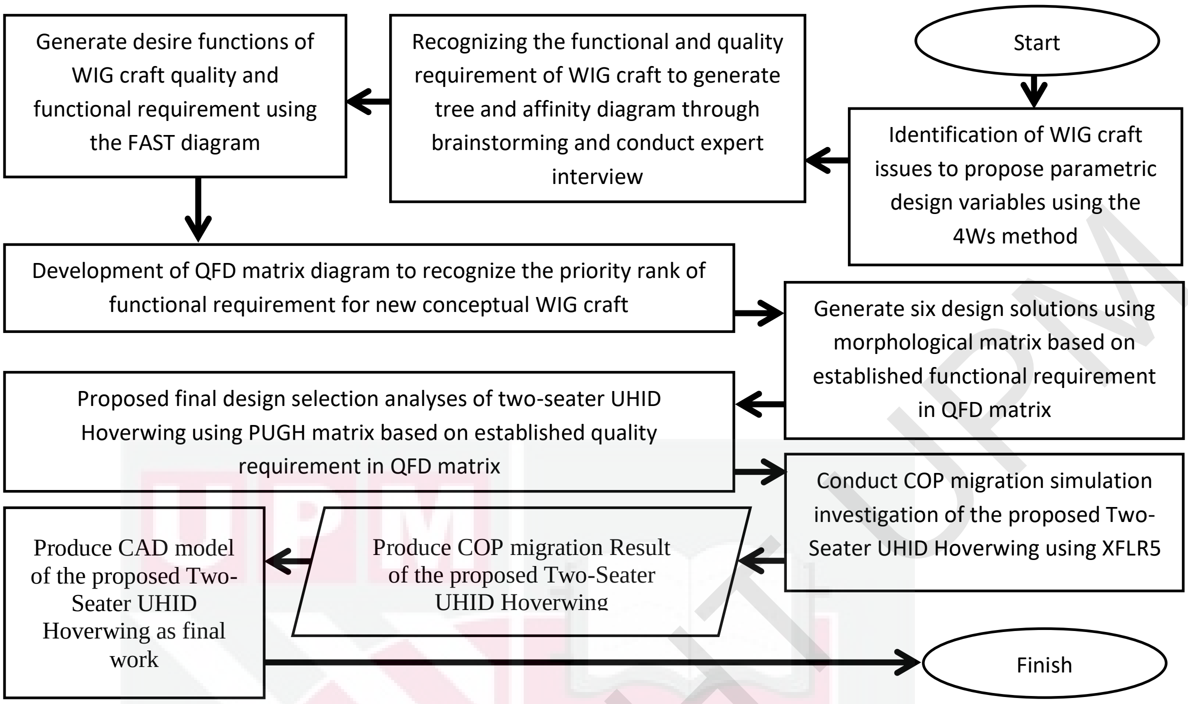

Figure 3.30: Flow Chart Design of two-seater hoverwing lifting surface (Objective 2)

3.6.2 Design Methodology

This chapter presents the conceptual design of a new two-seater Hoverwing WIG craft, developed to fulfill a range of mission profiles, including personal recreation, coastal transport, and serving as a training platform for aspiring WIG pilots. The design process is firmly rooted in the systems engineering methodology, ensuring that every aspect of the craft's development from initial requirements to testing and validation follows a structured approach. This methodology includes defining customer needs, developing functional and performance requirements, and systematically validating each design decision against mission objectives. Key performance parameters for the Hoverwing include an estimated weight of 500-600 kg, an operating speed of

120-150 km/h, a range of approximately 250-300 km, and an endurance of 3-4 hours at cruising speed. These specifications make the craft suitable for medium-range coastal transport missions, while also providing enough operational flexibility to support comprehensive WIG pilot training. The design process follows the systems engineering V-model, beginning with the identification of stakeholder needs and requirements, and moving through design synthesis, analysis, and verification. Tools such as the 4Ws, Affinity Diagrams, Tree Diagrams, and Quality Function Deployment (QFD) were employed to define the craft's functional and performance requirements. After the initial requirements were established, a Morphological Matrix was used to generate six potential design solutions. These designs were evaluated through a Pugh Matrix analysis, and the final configuration was selected based on its minimal center of pressure migration, verified through aerodynamic simulations in XFLR5. These systems engineering process ensures that the two-seater Hoverwing meets the diverse needs of its mission profile. It is optimized for both efficiency and stability in ground-effect conditions, serving as a highly functional vessel for recreational use, coastal transport, and, importantly, as a trainer craft for WIG pilots.

The craft's stable and intuitive handling characteristics make it an ideal platform for training new pilots, supporting the broader development of WIG technology. Figure 3.31 shows the four W (who, what, where and why) to established the fundamental issue of WIG craft. Graham Taylor's 2003 study highlighted the significant hydrodynamic challenges faced by WIG craft during takeoff, leading to decreased efficiency and increased power consumption. This, in turn, impacted investment and maintenance costs. In 2020, Rattapol Sakornsin emphasized the importance of addressing the longitudinal stability issues of WIG craft to enhance safety and pave the way for the development of a new aerospace-marine industry specializing in aircraft designed to operate both in and out of ground effect.

WHO is affected by the problem?	WHAT is the problem and how did It arise?	WHERE is it worth saving the problem?	WHY is it worth solving the problem?
Pilot and passanger	No Commercial Transport like conventional Aircraft	High lift by maximising the WIG craft payload to accommodate larger amount of seater (Graham K Taylor, 2002)	New aerospace industry segment for special aircraft which is uniquely designed to operate in the ground effect environment
Company owner and Investor	High Power to take off due to Hydrodynamic drag which affects investment and maintenance cost (Graham Taylor, 2003)	Reduced drag by minimizing the operational power requirement of current WIG Craft configuration (Wei Yang, 2011)	Reduce investment and operational Cost
Engineering Development Team	Instability of the WIG craft due to high pressure in ground effect (IGE), when transiting from IGE to OGE which cause the WIG craft to back flip and crash	Solve the longitudinal stability issue of WIG Craft (Rattapol Sakornsin, 2020)	Increase safety

Figure 3.31: The Four Ws method of two seats Hoverwing Craft

The affinity diagram in Figure 3.32 shows the relationship between the customer requirements and the functional requirements. The customer requirements are the features and capabilities that the customer wants the Hoverwing craft to have. The functional requirements are the technical specifications that the Hoverwing craft must meet in order to meet the customer requirements. The customer requirements are divided into four categories which are efficiency, safety, and performance. The functional requirements are divided into three categories which is high payload, levitation, and high flight. The customer would want the Hoverwing craft to have good performance in terms of fuel consumption, space utilization and product safety. The functional requirements that meet this customer requirement include low drag, high lift, decent speed, personalization vehicle, and stable pitch.

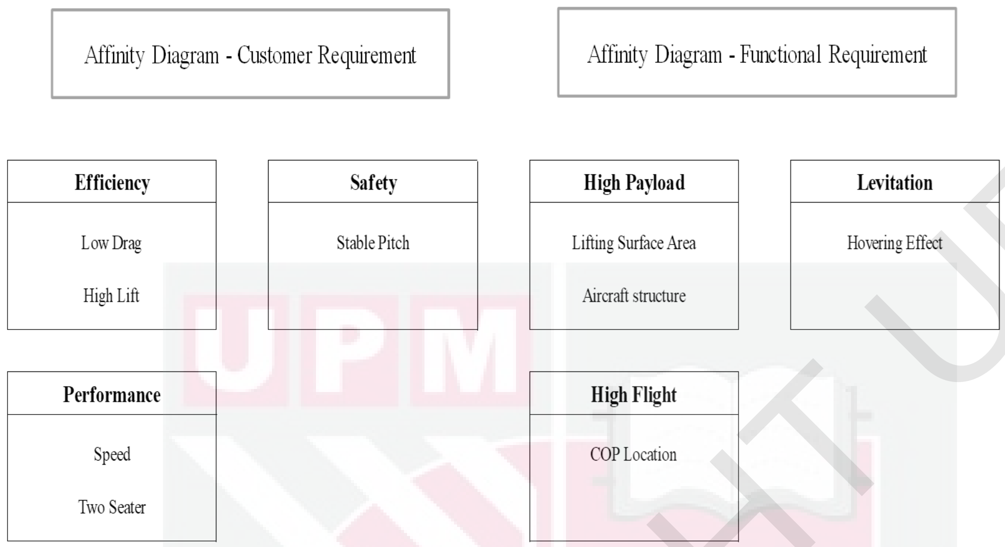

Figure 3.32: The Affinity Diagram method of two seats Hoverwing Craft

Furthermore, the customer wants the Hoverwing craft to be safe to operate. The functional requirements that meet this customer requirement are stable pitch. Other than that, the customer wants the Hoverwing craft to have a high payload capacity. The functional requirements that meet this customer requirement include aircraft structure types and lifting surface area.

Tree Diagram Method

The Tree diagram in Figure 3.33 shows the functional requirements and the customer requirements for a new Hoverwing craft. Functional requirements are the specific capabilities that the Hoverwing craft must have. In this case, the functional requirements are the Hoverwing craft must have enough lifting surface area to generate enough lift to take off and fly. Furthermore, the

Hoverwing craft must be able to carry a high payload, or weight. The Hoverwing craft must be efficient in its use of fuel and the Hoverwing craft must have an airfoil profile that is designed to generate high lift. Other than that, the Hoverwing craft must be able to hover in the air. In term of safety, the Hoverwing craft must be safe to operate. This can be achieved by having a stable pitch, or low angle of attack. It also must be able to fly at a decent speed. Lastly, the Hoverwing craft must have control surfaces to allow it to be maneuvered.

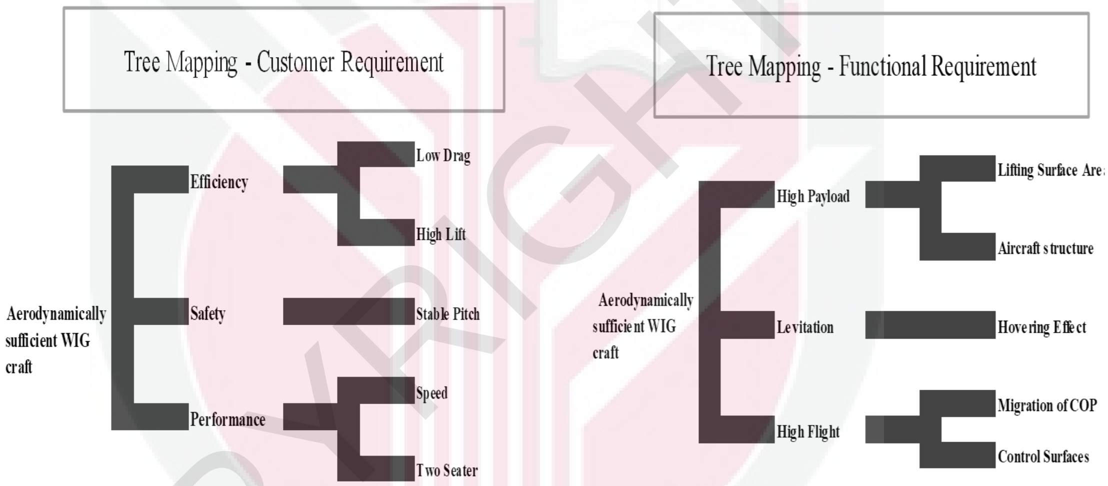

Figure 3.33: The tree diagram method of Hoverwing Craft

The customer requirements are low drag, high lift, High flight, and performance. The Hoverwing craft should have low drag to reduce fuel consumption. It also should have high lift to generate enough lift to take off and fly and should be able to hop at high altitude to avoid obstacle. Finally, the Hoverwing craft should have a decent speed to operate and have two-seater requirements for personal vessel.

Functional Analysis System Technique (FAST Diagram)

The FAST diagram of the new hoverwing craft in Figure 3.34 shows how the different components of the craft work together to achieve its desired functions. The diagram is divided into two main sections which are "HOW" and "WHY". In WHY section for wingtip, double wing, power increment, and large stabilizer, the reason is due to it’s the requirement of a lifting surface area. Lifting surface area and aircraft structure that is lightweight are the reason why the need of high payload.

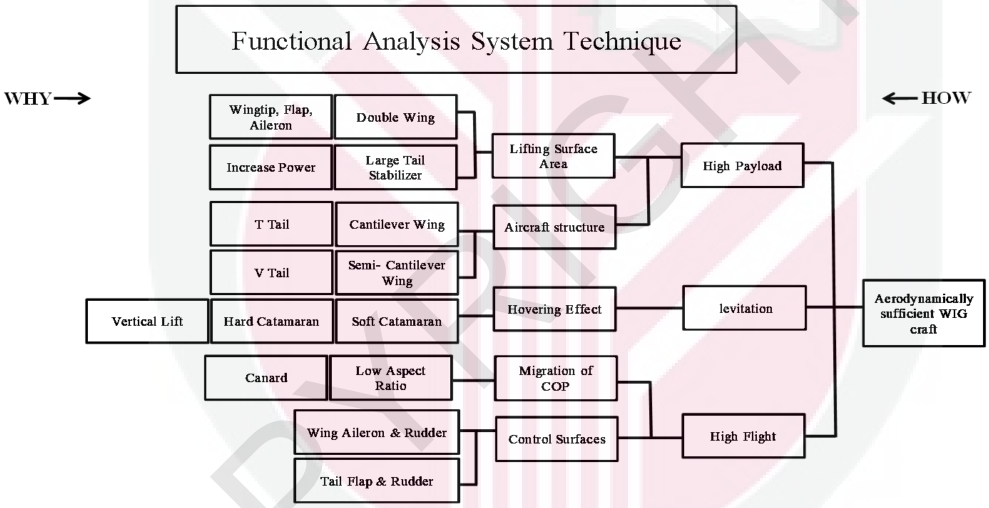

Figure 3.34: The Functional Analysis System Technique of Hoverwing Craft

This leads to high payload become a reason for an aerodynamically efficient WIG craft. In HOW section, an aerodynamically efficient WIG craft are achieved by having a high flight. To achieve high flight, the investigation of COP migration and control surface is required. These lead to canard, and Low Aspect Ratio lifting surfaces become a requirement of investigating the COP migration.

Quality Function Deployment Method

The Quality Function Deployment matrix in Figure 3.35 shows the priority ranks of the various customer requirements for a new type of WIG craft called a hoverwing craft. The priority ranks are based on the weighted importance score of each requirement, which is calculated by multiplying the customer importance rating by the technical importance rating.

The number of weightages is defined as 9, 3 and 1 which indicated strong, moderate and weak relationship towards each other. The relationship between low drag and lifting surface area in aerodynamics is strong 9 due to while a large wing area is necessary for lift, it also inherently increases drag. This is why there is a strong relationship between low drag and lifting surface area. Reducing the size of the wing will definitely decrease drag, but it will also come at the cost of reduced lift. The relationship between high lift and lifting surface area in aerodynamics is strong 9 because of a direct and positive correlation exists between lifting surface area and lift generation. A bigger wing surface area provides more "real estate" for air to interact with, translating to significantly higher lift. The relationship between stable pitch and lifting surface area in aerodynamics is strong 9 due to wing area also plays a main role, it's one of main factor among many that influence pitch stability. However, simply having a large wing area doesn't guarantee good pitch stability. The placement of that wing area relative to the center of gravity is more critical. Even a smaller wing can be designed for good stability if the center of lift is positioned correctly. The relationship between aircraft speed and lifting surface area in aerodynamics is weak 1 due to although wing area does influence airspeed for generating lift, but it's not a perfectly proportional relationship. While a larger wing area inherently generates more lift, it also creates more drag. To achieve a specific amount of lift at a desired cruise speed, an aircraft with a larger wing area might not need to fly as fast as an aircraft with a smaller wing area. The relationship between a two-seater aircraft and lifting surface area in aerodynamics is weak 1 because of passenger capacity is a secondary factor. The number of seats only indirectly influences the weight. A two-seater aircraft can be light enough to fly efficiently with a proportionally smaller wing area compared to a larger passenger airplane. There are also many two-seater aircraft designed for heavier occupants or additional cargo, which would necessitate a larger wing area.

In term of the relationships between aircraft structure and low drag, the relationship is moderate 3. This is because aircraft structure plays a less role in determining how much drag an aircraft wing produces. The relationship between aircraft structure and high lift in aerodynamics is strong 9. This is because the specific aircraft structure directly influences how much weight capacity it can generate. Therefore, with lightweight structure the lift capability will also increase. The relationship between aircraft structure and stable pitch in aerodynamics is strong 9 due to the influence of Center of gravity (COG) location. For good pitch stability, the entire aerodynamic layout correspondence to the aircraft COG needs to be considered. The relationship between aircraft structure and speed in aerodynamics is strong 9 due to the aircraft structure plays significant part of the role in influencing an aircraft's speed capability. The interplay between light structure, types, and structure materials determines the optimal cruising speed for a particular aircraft. The relationship between aircraft structure and a two-seater requirement in aerodynamics is weak 1. This is because the aircraft structure does not necessarily determine by the weight and desired performance of the aircraft, or simply by the fact that it has two seats. The number of seats is a general classification and doesn't directly translate to a specific aircraft lift capacity. The relationship between hovering effect towards the low drag, high lift, stable pitch, height from ground level, speed and two-seater requirements varies depending on the specific factor. The first comparison (hovering effect and low drag) is strong 9.

Hovering inherently requires constant power to maintain lift, which creates drag. Low drag isn't a primary concern for hovering. The second comparison (hovering effect and high lift) is moderate 3. Hovering requires significant lift to counteract gravity and stay airborne. The airfoil profile and flight controls are specifically designed to generate high lift at low airspeeds. The third comparison (hovering effect and stable pitch) is weak 1. While some level of pitch stability is desirable, it's not the most critical factor for hovering. Precise control inputs from the pilot are more important for maintaining a stable hover. The fourth comparison (hovering effect and speed) is weak 1. Hovering by definition requires minimal forward airspeed. Speed control is crucial for maintaining a stable hover. The final comparison (hovering effect and two-seater requirement) is moderate 3. The ability to hover is independent of the number of seats. Both single-seat and multi-seat VTOL aircraft can achieve hovering flight.

The relationship between migration of Center of Pressure (COP) towards the low drag, high lift, stable pitch, height from ground level, speed and two-seater requirements varies depending on specific context. The first comparison (COP and low drag) is strong 9. Drag is primarily influenced by the overall aircraft design and airspeed. While COP shift can affect control forces, it also has a direct impact on drag such as induced drag. This drag is inherent to generating lift. As an airfoil creates lift, it also creates swirling airflow at the wingtips, which contributes to drag. Minimizing induced drag is a key goal in airfoil design and induced drag is reduced as aircraft transient into in ground effect zone. The second comparison (COP and high lift) is also strong 9. COP migration can directly affect lift. For example, high lift is generated by the design of lifting surface to create more lift than their typical counterparts at a specific angle of attack and this has a significant impact on the migration of COP. This is crucial during takeoff, landing, and maneuvers. The third comparison (COP and stable pitch) is strong 9. This is a key relationship. An aircraft's stability relies on a predictable relationship between the COP location and the center of gravity (CG). If the COP migrates significantly relative to the CG, it can lead to pitching moments that require pilot input or control system adjustments to maintain stable flight. The fourth comparison (COP and speed) is moderate 3. Airflow characteristics can influence COP location. At higher speeds, the COP tends to move slightly forward compared to slower speeds. However, wing design and angle of attack play a more significant role in COP location than airspeed itself. The final comparison (COP and two-seater requirement) is weak 1. The number of seats doesn't directly affect COP migration. The aircraft's overall weight distribution is the primary factor.

A two-seater aircraft can be well-balanced with a minimal COP shift, and a larger multi-seater aircraft might experience more prominent COP migration depending on loading configuration. The relationship between migration of control surfaces towards the low drag, high lift, stable pitch, height from ground level, speed and two-seater requirements varies depending on specific factors. The first relationship (control surfaces and low drag) is moderate 3. Control surfaces like ailerons can be used for drag control to an extent. By adjusting the angle of ailerons slightly, pilots can induce a small amount of asymmetry in lift, which can be used to counter inherent drag caused by other factors like the fuselage or tail design. However, minimizing drag is more about the overall aircraft shape and wing profile. The second relationship (control surfaces and high lift) is strong 9. Control surfaces like flaps and slats are specifically designed to increase lift. By deploying these high-lift devices, the curvature of the wing is effectively increased, allowing for more lift generation at lower airspeeds, particularly during takeoff and landing. The third relationship (control surfaces and stable pitch) is strong 9. Control surfaces like elevators are crucial for maintaining pitch stability. By adjusting the elevator pitch, pilots can modify the angle of attack of the horizontal stabilizer, which generates a balancing moment to counteract pitching tendencies caused by wind gusts or maneuvers. The fourth relationship (control surfaces and speed) is moderate 3. While not the primary function, control surfaces can influence airspeed indirectly. Ailerons can be used for slight speed adjustments by inducing drag. Similarly, trimming the aircraft with elevators can affect overall drag, which can have a secondary effect on airspeed. The final relationship (control surfaces and Two-Seater Requirement) is weak 1. The number of seats on an aircraft doesn't influence the control surfaces themselves. The control surfaces are designed based on the overall aerodynamic properties of the aircraft, including its weight, wing design, and center of gravity location. A two-seater aircraft and a larger aircraft would likely have different sized control surfaces due to their varying weight and aerodynamic needs, but the basic principles of how the control surface function remain the same. Based on exploration of various aerodynamic concepts, it can be concluded that understanding the relationships between an aircraft's design and its flight characteristics is crucial. The top three priorities are low drag, high lift, and stable pitch. These priorities reflect the importance of these factors in ensuring the efficiency, performance, and safety of the crafts. Low drag is essential for the crafts to achieve high speeds and efficiency. Hoverwing crafts operate on the ground effect, which reduces drag, but they still face aerodynamic resistance. By designing the crafts with low drag features, such as a streamlined shape and efficient hovering system, fuel consumption can be reduced and aircraft performance can be improved. High lift is also essential for Hoverwing crafts to take off and maintain flight. The crafts operate on the ground effect, which provides additional lift, but they still need to generate enough lift to fly. By designing the crafts with high lift features, such as large wing area and efficient airfoils, required takeoff speed can be reduced and aircraft payload capacity can be increased. Stable pitch is essential for the Hoverwing crafts to maintain safe and controlled flight. The crafts can experience pitch instability due to the ground effect, which can lead to loss of control and crashes. By designing the crafts with stable pitch characteristics, the risk of pitch instability can be minimized and overall safety can be improved.

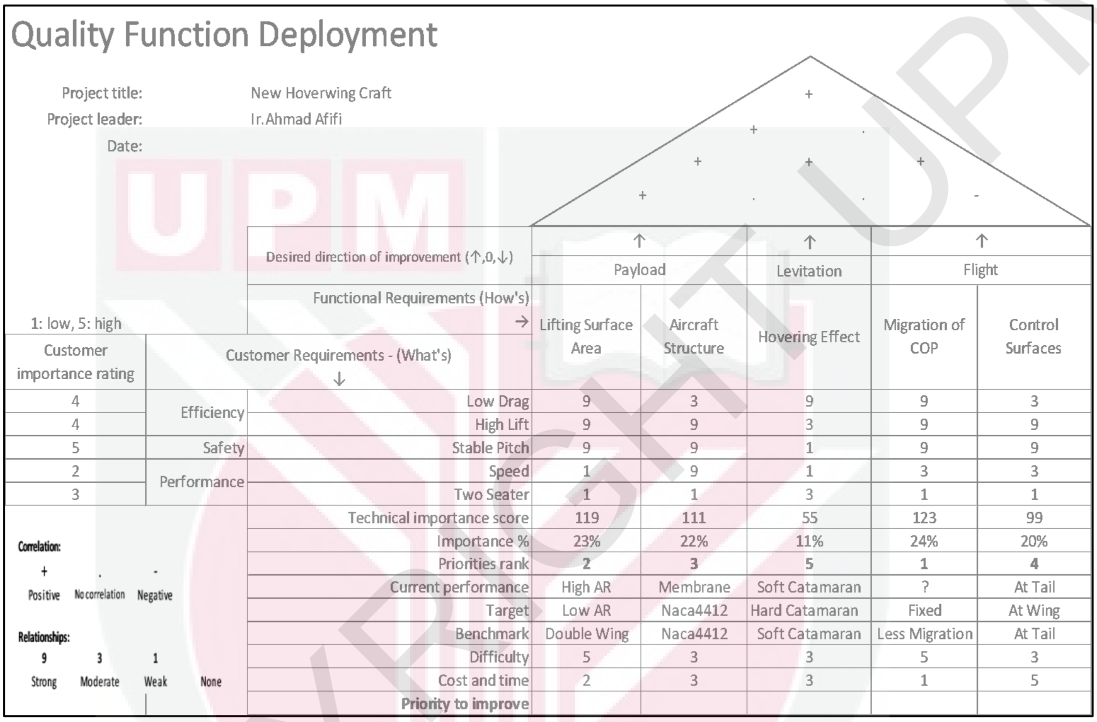

Quality Function Deployment

Project title: New Hoverwing Craft
Project leader: Ir.Ahmad Afifi
Date:

Customer importance rating (1: low, 5: high)		Customer Requirements - (What's) / Functional Requirements (How's)	Lifting Surface Area	Aircraft Structure	Hovering Effect	Migration of COP	Control Surfaces
		Desired direction of improvement (↑,0,↓)	↑		↑	↑	
			Payload		Levitation	Flight	
4	Efficiency	Low Drag	9	3	9	9	3
4		High Lift	9	9	3	9	9
5	Safety	Stable Pitch	9	9	1	9	9
2	Performance	Speed	1	9	1	3	3
3		Two Seater	1	1	3	1	1
		Technical importance score	119	111	55	123	99
		Importance %	23%	22%	11%	24%	20%
		Priorities rank	2	3	5	1	4
		Current performance	High AR	Membrane	Soft Catamaran	?	At Tail
		Target	Low AR	Naca4412	Hard Catamaran	Fixed	At Wing
		Benchmark	Double Wing	Naca4412	Soft Catamaran	Less Migration	At Tail
		Difficulty	5	3	3	5	3
		Cost and time	2	3	3	1	5
		Priority to improve					

Figure 3.35: The Quality Function Deployment method of Hoverwing Craft

The other customer requirements, such as two-seater and speed, are also important, but they are not as critical as the top three priorities. This is because two-seater accommodation and speed can be improved to some extent through design optimization, but low drag, high lift, and stable pitch are fundamental requirements that must be met for WIG crafts to be successful.

Morphological Matrix Method

The Morphological chart shows in Figure 3.36 indicates the various design solutions for a new type of Hoverwing craft. The design solution one focuses on maximizing hovering effect and reducing COP migration. The vertical lift design provides a strong ground effect, which allows the Hoverwing craft to fly at very low altitudes, without stalling. The tail, flaps and rudder help to keep the Hoverwing craft stable in pitch. The canard helps to reduce COP migration. The cantilever wing structure helps to achieve lower WIG craft gross weight.

SOLUTIONS -> ˅ FUNCTIONS	SOLUTION 1	SOLUTION 2	SOLUTION 3	SOLUTION 4
LIFTING SURFACE AREA	DOUBLE WING	LARGE TAIL STABILIZER	INCREASE POWER	WINGTIP, FLAP, AILERON
AIRCRAFT STRUCTURE	CANTILEVER WING	SEMI-CANTILEVER WING	T TAIL	V TAIL
HOVERING EFFECT	SOFT CATAMARAN	HARD CATAMARAN	VERTICAL LIFT	
MIGRATION OF COP	LOW ASPECT RATIO	CANARD		
CONTROL SURFACES	WING AILERON & RUDDER	TAIL FLAP & RUDDER		

FUNCTION ->	LIFTING SURFACE AREA	LIGHT WEIGHT STRUCTURE	HOVERING EFFECT	MIGRATION OF COP	CONTROL SURFACES
DESIGN SOLUTION 1	INCREASE POWER	CANTILEVER WING	VERTICAL LIFT	CANARD	TAIL FLAP & RUDDER
DESIGN SOLUTION 2	LARGE TAIL STABILIZER	SEMI-CANTILEVER WING	SOFT CATAMARAN	CANARD	TAIL FLAP & RUDDER
DESIGN SOLUTION 3	DOUBLE WING	T TAIL	HARD CATAMARAN	LOW ASPECT RATIO	WING AILERON & RUDDER
DESIGN SOLUTION 4	WINGTIP, FLAP, AILERON	CANTILEVER WING	VERTICAL LIFT	LOW ASPECT RATIO	TAIL FLAP & RUDDER
DESIGN SOLUTION 5	DOUBLE WING	V TAIL	SOFT CATAMARAN	CANARD	TAIL FLAP & RUDDER
DESIGN SOLUTION 6	INCREASE POWER	T TAIL	HARD CATAMARAN	LOW ASPECT RATIO	WING AILERON & RUDDER

Figure 3.36: The Morphological chart method of Hoverwing Craft

The design solution two focuses on reducing wing area and improving efficiency. The soft catamaran hull is lightweight and flexible, which reduces drag. The high aspect ratio wing provides a large lift coefficient, which allows the Hoverwing craft to carry a heavier payload. The flap and aileron controls help to improve maneuverability. Design solution three is similar to Design Solution two, but with a hard catamaran hull. The hard catamaran hull is more structurally rigid, which makes it better suited for rough seas. The design solution four focuses on improved maneuverability. The low aspect ratio wing reduces drag and increase speed at low speed. The increased power allows the Hoverwing craft to fly at higher speeds. The flap and aileron controls also assist to improve maneuverability. The design five solution is similar to Design Solution two, but with a lower wing aspect ratio. The lower wing aspect ratio reduces CP migration and improves longitudinal stability. The design solution six focuses on reducing structure weight. The hard catamaran hull is lighter than a soft catamaran hull. The reduced structure weight improves performance and efficiency. The best design solution for a new Hoverwing craft will depend on the specific requirements of the application. For example, if the Hoverwing craft is designed for passenger transport, then Design Solution 1 or Design Solution two may be the best choice. If the Hoverwing craft is designed for cargo transport, then Design Solution three or Design Solution four may be the best choice. If the Hoverwing craft is designed for maritime patrol, then Design Solution five or Design Solution six may be the best choice. Figure 3.37 shows the design solution conceptual design.

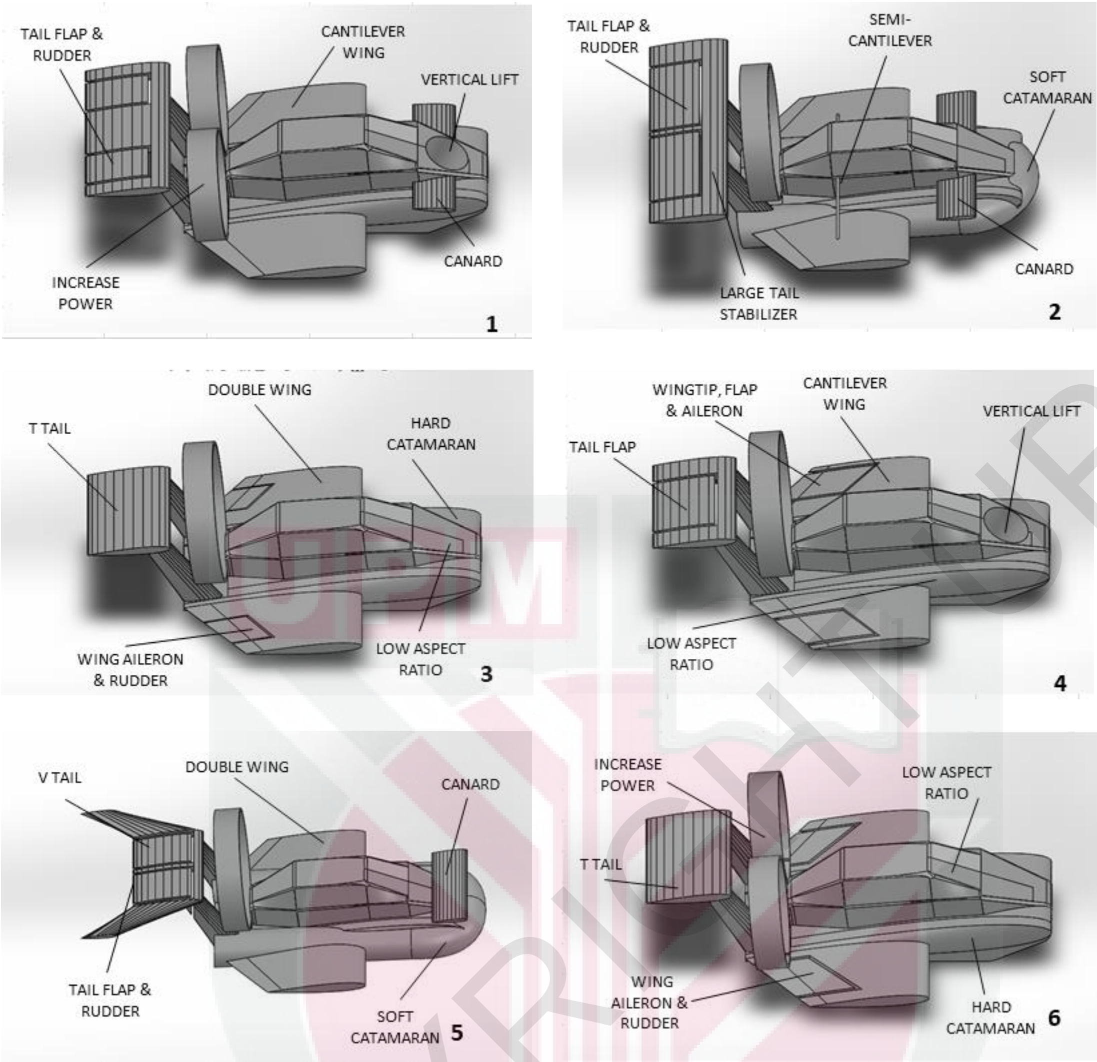

Figure 3.37: The six design solution concept of Hoverwing Craft derived from morph matrix

PUGH Matrix Method

Based on the total score in the Pugh analysis matrix shown in Figure 3.38, the design solution 3 is ranks as the best option. It has the highest total score of 32, followed by Solution 4 (28), Solution 1 (22), Solution 6 (20), Solution 2 (16), and Solution 5 (14). The design solution three has a good score in all of the evaluation criteria, except for speed. It has the highest score in terms of low drag, high lift, stable pitch, and two-seater requirements. Design solution four also has a good score overall, but it is lesser in term of performance than the design solution three.

Pugh Matrix Hoverwing							
Critical Quality	***Weight*** *(1 being least important, 10 being most important)*	Design Solution 1	Design Solution 2	Design Solution 3	Design Solution 4	Design Solution 5	Design Solution 6
Low Drag	8	1	1	1	0	0	0
High Lift	8	1	-1	1	1	1	1
Stable Pitch	10	0	1	1	1	0	1
Two Seater	6	1	1	1	1	1	1
Speed	4	0	0	0	1	0	-1

Summary Table						
Total "1s"	3	3	4	4	2	3
Total "0s"	2	1	1	1	3	1
Total "-1s"	0	1	0	0	0	1
Total	22	16	32	28	14	20

Figure 3.38: The PUGH Matrix of Hoverwing Craft

It also has a lower score in terms of high lift requirements. Solution one has a good score in terms of low drag, high lift, and two-seater, but it has a lower score in terms of stable pitch and speed. Design solution six has a good score in terms of two-seater, high lift, and stable pitch, but it has a lower score in terms of speed and low drag requirements. Design solution two has a good score in terms of low drag, stable pitch, and two-seater requirement, but it has a lower score in terms of speed and lift capability. Solution five has the lowest total score of 14. It has a lower score in all of the evaluation criteria, except for high lift and two-seater. Overall, the design solution three is the best option based on the Pugh analysis. It has a good score in all of the evaluation criteria, and it is the most well performance option.

3.6.3 Finalize Design

Figure 3.39 illustrates the final design selected using the established design methodology. The design solution 3 with NACA 0012 airfoil emerged as the preferred choice for the Hoverwing wig craft design. The wing span is 0.880, wing area is 0.622m, chord length is 1m, mean aerodynamic chord is 0.792m, aspect ratio is 1.245m, take off velocity is 25m/s, CL is 0.318 and CD is 0.024. Its superior stability and control characteristics, demonstrated by minimal COP migration across the tested AOA range, significantly contribute to the overall safety and performance of the aircraft. This selection aligns with the design objectives of ensuring reliable and predictable flight behavior, especially in challenging operating conditions. While other configurations offered potential advantages in certain areas, the NACA 0012's balanced performance and robust stability made it the most suitable option for this application.

DESIGN SOLUTION 3	DOUBLE WING	T TAIL	HARD CATAMARAN	LOW ASPECT RATIO	WING AILERON & RUDDER

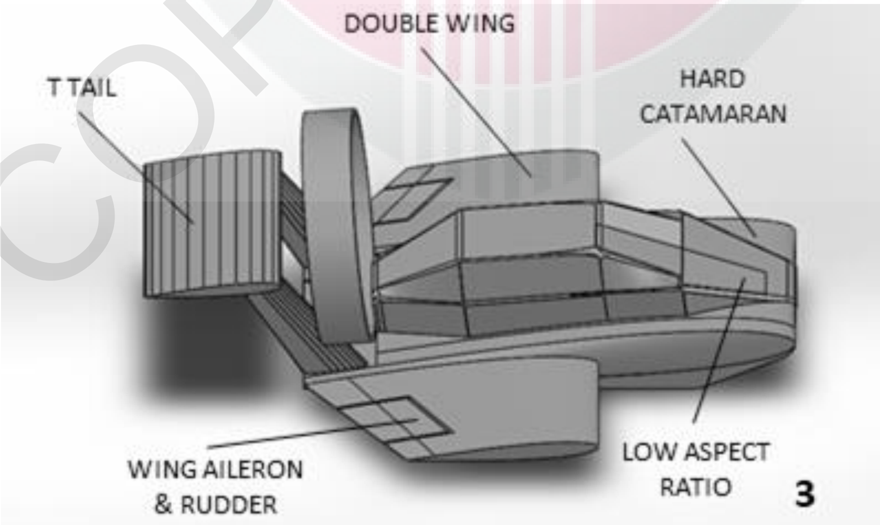

Figure 3.39 the final design selected using the established design methodology

3.7 Solidwork Flow Simulation Software

Solidworks Flow Simulation is the chosen software to produce preliminary aerodynamic result which is lift, drag and moments acting on the Dragonfly DF2 lifting surfaces. Solidworks Flow solves the Navier-Stokes equations in fluid region which are formulations of mass, momentum and energy conservation laws as stated below [104];

3.7.1 Analysis Procedure

$$\frac{\partial (pu_i)}{\partial \mathrm{t}} + \frac{\partial}{\partial x_j}(pu_i u_j) + \frac{\partial P}{\partial x_i} = \frac{\partial}{\partial x_j}(\tau_{ij} + \tau_{ij}^R) + S_i$$

$$\frac{\partial p\mathrm{H}}{\partial \mathrm{t}} + \frac{\partial pu_i H}{\partial x_i} = \frac{\partial}{\partial x_i}(u_j(\tau_{ij} + \tau_{ij}^R) + q_i) + \frac{\partial p}{\partial \mathrm{t}} - \tau_{ij}^R \frac{\partial u_i}{\partial x_j} + p_\varepsilon + S_i u_i + Q_H$$

$$\mathrm{H} = \mathrm{h} + \frac{u^2}{2}$$

(3.1)

For calculation of high-speed compressible flows, the following energy equation is used [104];

$$\frac{\partial pE}{\partial t} + \frac{\partial pu_i\left(E + \frac{P}{p}\right)}{\partial x_i} = \frac{\partial}{\partial x_i}\ (u_j(\tau_{ij} + \tau_{ij}^R) - \ \tau_{ij}^R \frac{\partial u_i}{\partial x_j} + p_\varepsilon + S_i u_i + Q_H$$

$$\mathrm{E} = \mathrm{e} + \frac{u^2}{2}$$

(3.2)

Both laminar and turbulent flows can be considered in Solidworks Flow simulation. Laminar flows are defined as the product of representative scales of velocity and length divided by the kinematic viscosity and it occurred at low values of the Reynolds number. The flow transitions smoothly to turbulent when the Reynolds number exceeds a critical value. To predict turbulent flows, the Favre-averaged Navier-Stokes equations are used, where time-averaged effects of the flow turbulence on the flow parameters are considered, whereas the large-scale, time-dependent phenomena are taken into account directly. Extra terms called as Reynolds stresses occur in the equations as a result of this approach, which requiring further information. To close this system of equations, Transport equations are used in SOLIDWORKS FLOW Simulation for the turbulent kinetic energy and its dissipation rate, using the k-ε model. The modified k-ε turbulence model with damping functions proposed by Lam and Bremhorst (1981) describes laminar, turbulent, and transitional flows of homogeneous fluids consisting of the following turbulence conservation laws [104];

$$\frac{\partial pk}{\partial t}+\frac{\partial p\mathrm{k}u_i}{\partial x_i}=\frac{\partial}{\partial x_i}\left(\left(\mu+\frac{\mu_t}{\sigma_\varepsilon}\right)\frac{\partial k}{\partial x}\right)+\tau_{ij}^{R}\frac{\partial u_i}{\partial x_j}-p_\varepsilon+u_tP_B,$$

$$\frac{\partial p_\varepsilon}{\partial t}+\frac{\partial p_\varepsilon u_i}{\partial x_i}=\frac{\partial}{\partial x_i}\left(\left(\mu+\frac{\mu_t}{\sigma_\varepsilon}\right)\frac{\partial \varepsilon}{\partial x_i}\right)+C_{\varepsilon l}\frac{\varepsilon}{k}\left(f_i\,\tau_{ij}^{R}\frac{\partial u_i}{\partial x_j}+C_Bu_tP_B\right)-f_2C_{\varepsilon 2}\frac{p\varepsilon^2}{k}$$

$$\tau_{ij}=\mu S_{ij},\tau_{ij}^{R}=\mu S_{ij}-\frac{2}{3}pk\delta_{ij},\ S_{ij}=\frac{\partial u_i}{\partial x_j}+\frac{\partial u_j}{\partial x_i}-\frac{2}{3}\delta_{ij}\ \frac{\partial u_k}{\partial x_k}$$

$$P_B=-\frac{g_i}{\sigma_B}\frac{1}{p}\frac{\partial p}{\partial x_i},$$

(3.3)

3.7.2 Grid independent study

A grid independence study is conducted to ensure that the results of the CFD simulation are not significantly affected by the mesh size based on Figure 3.40 and 3.41. This is done by running the simulation with a series of different mesh sizes and comparing the results. The series of mesh is 3823, 159296, 388651, and 806912. The comparison graph is CL against angle of attack at different mesh level. Figure 3.42 shows a graph of CL against mesh element at 0° angle of attack. The chosen mesh level is around 388651 due to the value stabilize until 806912.

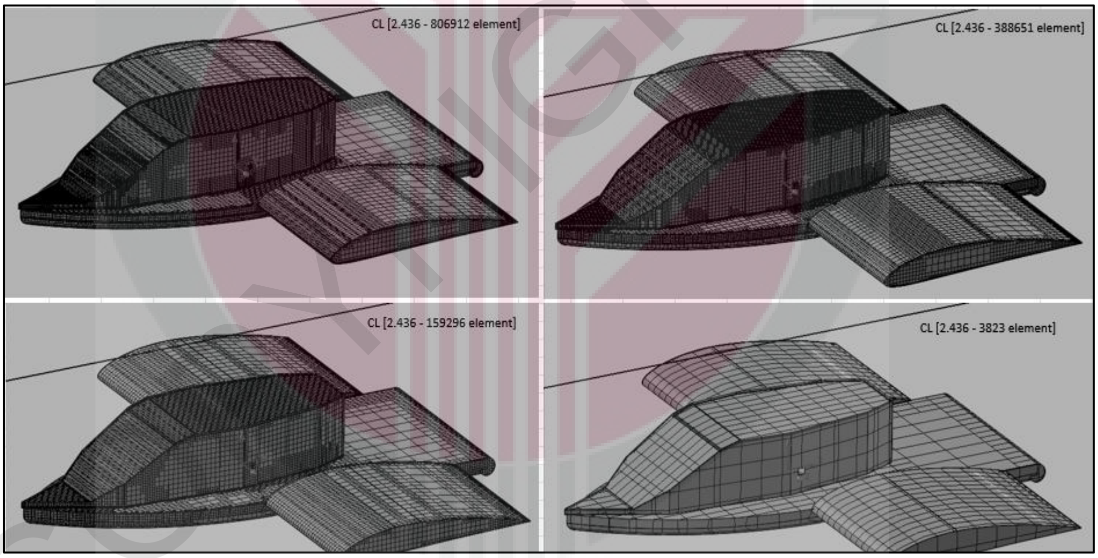

Figure 3.40: Grid independent study on UH18-SPW with Naca4412 at various meshing level

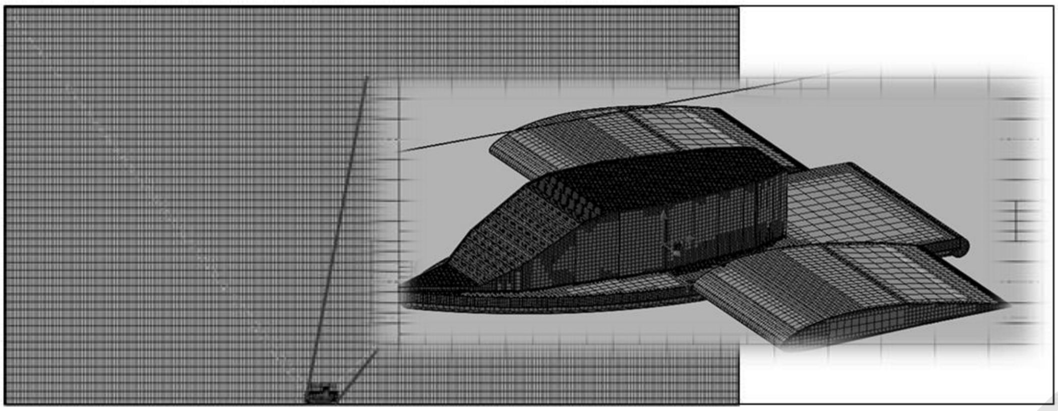

Figure 3.41: Mesh set up in SOLIDWORK Flow in ground effect condition

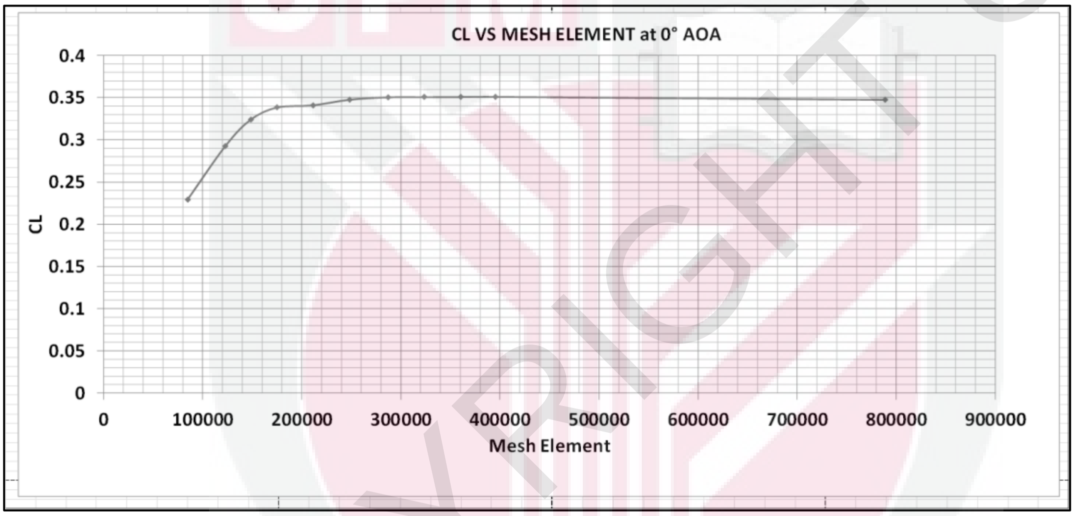

Figure 3.42: Grid independent study of CL VS MESH ELEMENT at 0° AOA

3.8 Aerodynamic Performance and Stability of UH18-SPW with Naca4412

The CFD analysis for UH18-SPW model was done by using Solidwork flow analysis. The preliminary performance result obtained from the Solidworks Flow Simulations is then verified by using UH18-SPW wind tunnel test analysis data produce by Steven Morris, 2008 to verify the software capability. The comparison of between performance result of conceptual two-seater hoverwing and existing WIG craft model was presented as final conclusion. The main values of interest are preliminary data of lift, drag and moments acting on the two-seater hoverwing. Figure 3.43 shows the flow chart of conceptual design of two-seater hoverwing performance analysis.

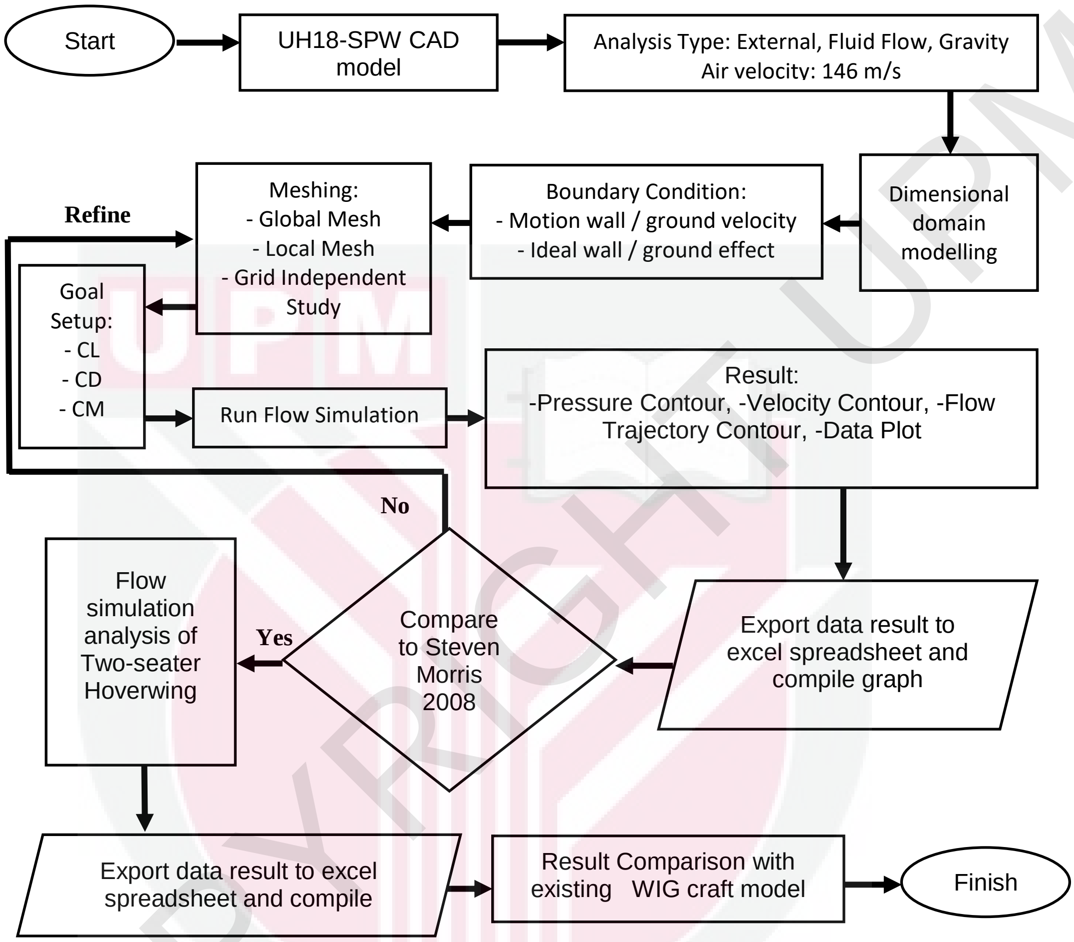

Figure 3.43: Flow chart of conceptual two-seater hoverwing performance analysis

3.8.1 Flow parameter calculation

The turbulence models used in the study are k-ε turbulence model since this model works better for far field boundary condition. The models are run on its default settings. Figure 3.44 to 3.46 shows the settings used in setting up the solver in Solidworks Flow Simulation. Solidworks Flow Simulation includes a variety of analysis types to simulate different flow phenomena. The most common types of analysis include external flow analysis. This type of analysis is used to simulate the flow of fluids around an object, such as an airplane wing, car body, or building. The first step is to choose external type for analysis, then exclude cavities without flow conditions as well as internal space. After that choose air as fluid property and set up the thermodynamic and velocity parameter.

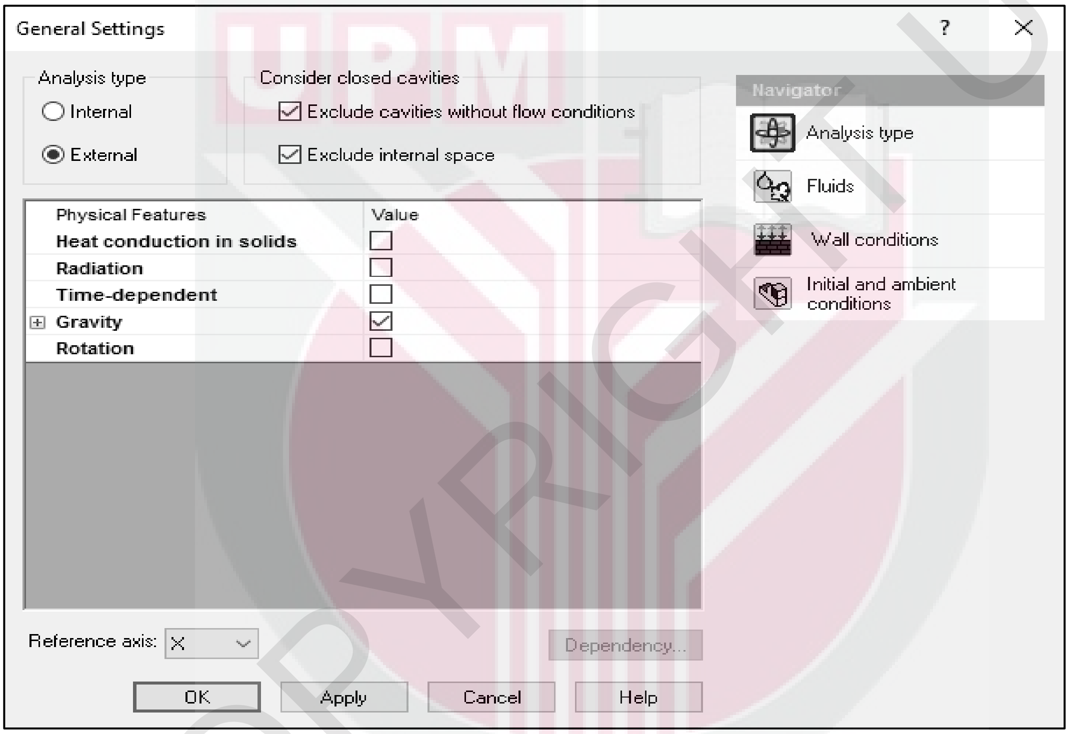

Figure 3.44: Analysis Type setting of Solidwork Flow Simulation

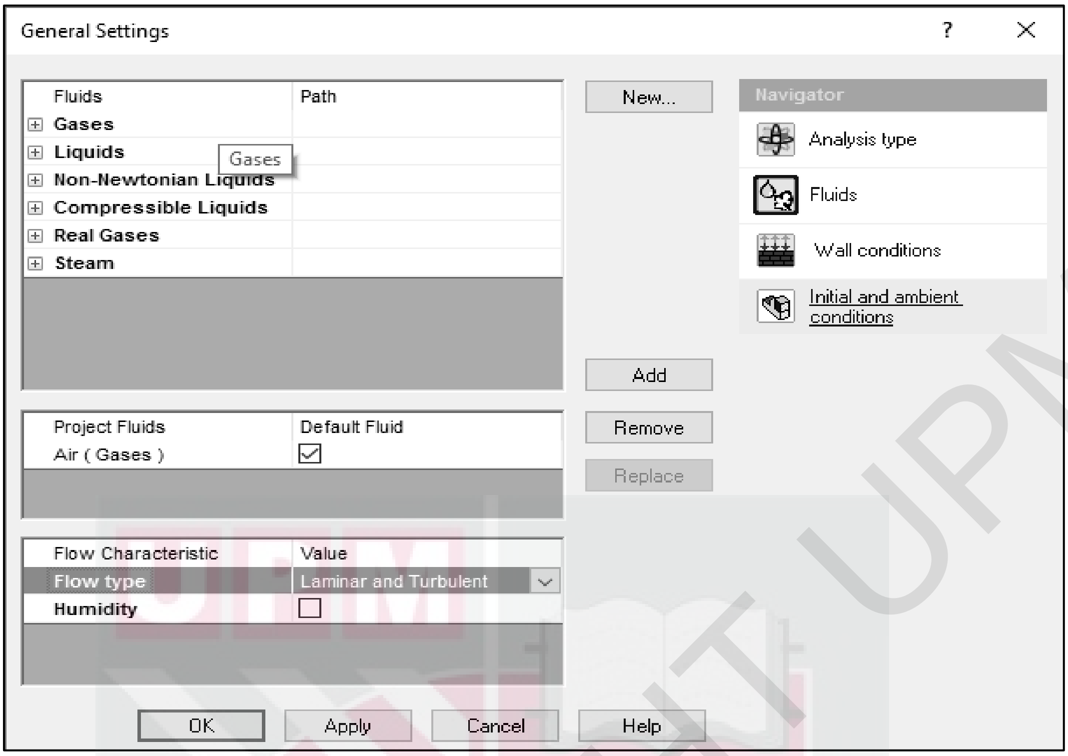

Figure 3.45: Fluid setting of Solidwork Flow Simulation

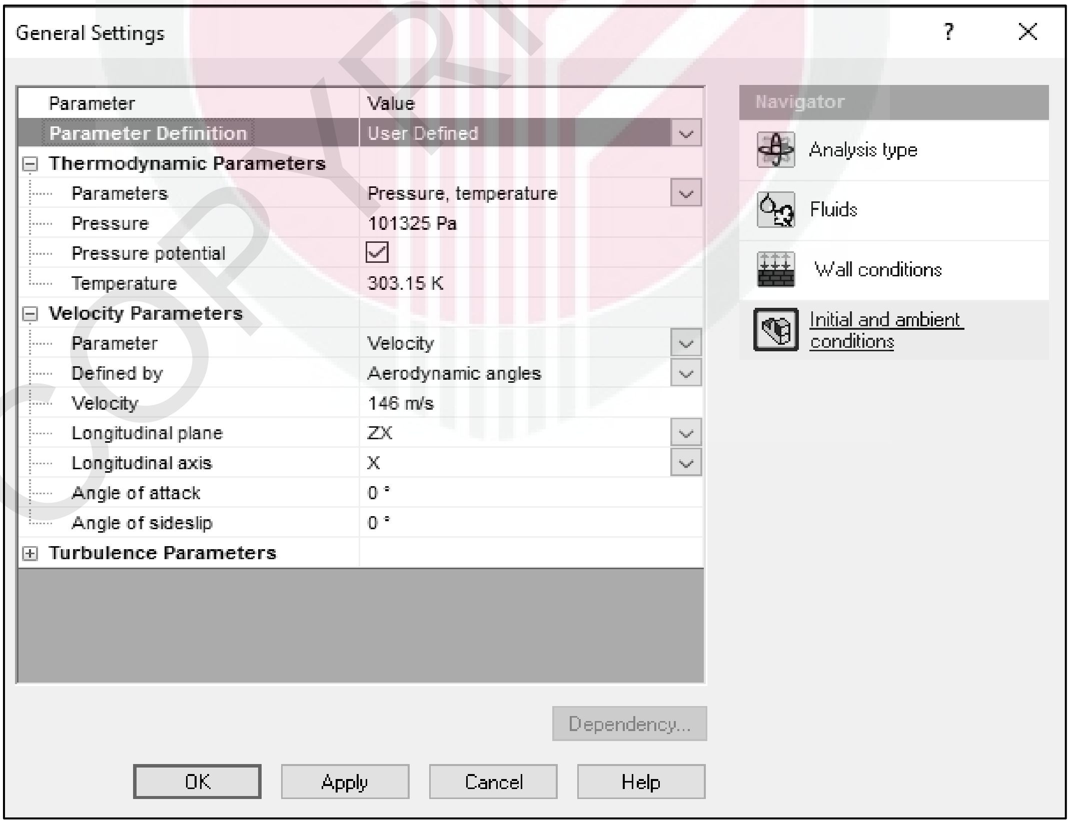

Figure 3.46: Flow parameter setting of Solidwork Flow Simulation

Dimensional Domain

The dimensional domain refers to the spatial extent of the computational domain, which is the region of space within which the flow simulation is performed. The dimensional domain is defined by specifying the length, width, and height of the computational domain. The choice of dimensional domain is important because it affects the accuracy of the flow simulation. A too-small dimensional domain will not capture the full extent of the flow field, while a too-large dimensional domain will unnecessarily increase the computational cost of the simulation. In general, the dimensional domain should be chosen to be slightly larger than the physical domain of the problem being simulated. This will ensure that the flow field is fully captured and that boundary effects are minimized. Figure 3.47 shows the dimensional domain set up in Solidwork Flow in ground effect condition.

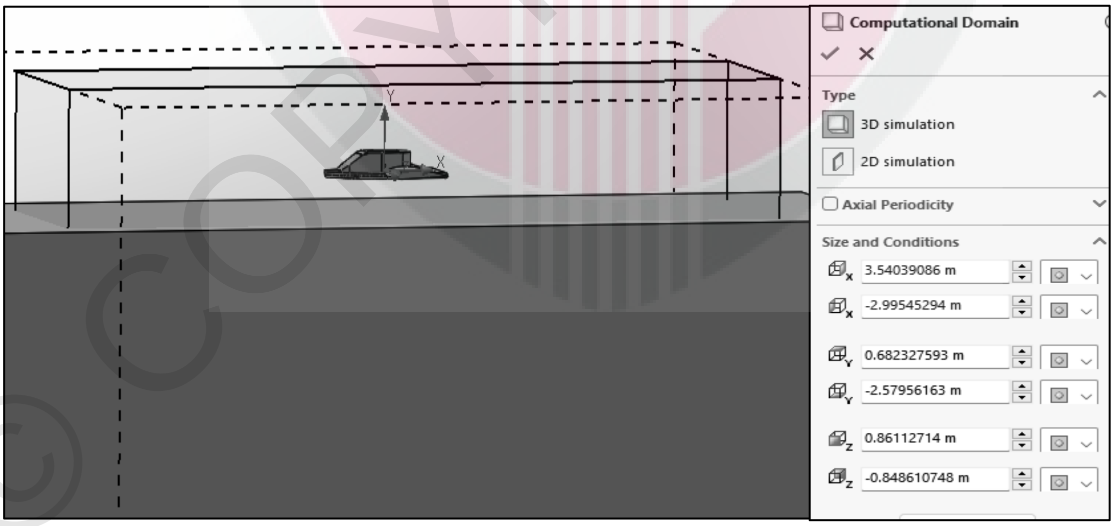

Figure 3.47: Dimensional domain set up in Solidwork Flow in ground effect condition

Boundary Condition

The choice of boundary conditions is important because it affects the accuracy of the flow simulation. Incorrect boundary conditions can lead to inaccurate results, such as unrealistic flow patterns or incorrect pressure and velocity distributions. In general, it is a good idea to use as realistic boundary conditions as possible. This will help to ensure that the flow simulation accurately represents the real-world problem. In this process, wall boundary conditions are utilized to represent a moving ground or ground effect conditions. It specifies the behavior of the fluid on the walls of the computational domain. wall boundary conditions can be defined by specifying the no-slip condition, the slip condition, or the heat flux condition. Figure 3.48 shows boundary condition set up in SolidWorks Flow in ground effect condition

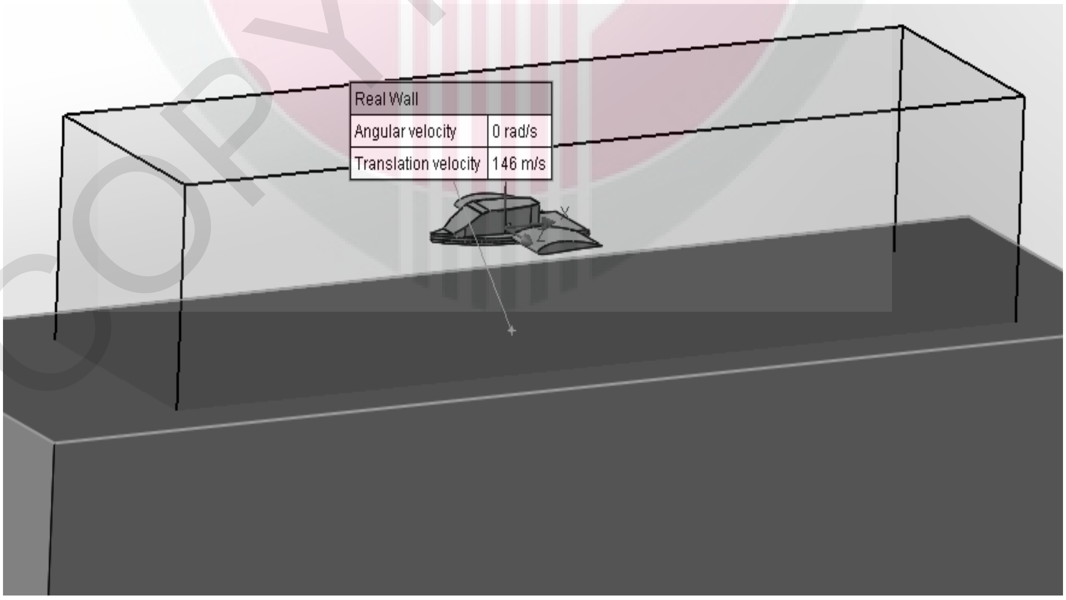

Figure 3.48: Boundary condition set up in Solidwork Flow in ground effect condition

Meshing

Meshing is a critical step in any CFD simulation. The type of mesh used, the quality of the mesh, and the mesh size can all affect the accuracy and efficiency of the simulation. It is important to choose the right meshing parameters for the specific problem being simulated.

Y+ calculation

A Y+ of 1 is considered good enough to resolve the boundary layer down to the sub viscous layer. This can be substituted into equation below alongside the friction velocity to obtain the distance the first node of the mesh must be from the model's wall. The Y+ calculation is as follow and the final value was replaced in local mesh input setting in solid work flow mesh set up as shown in Figure 3.49:

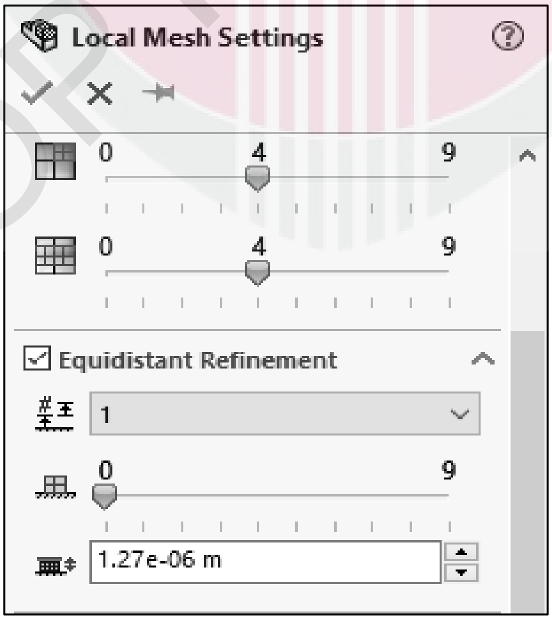

Figure 3.49: SOLIDWORK Flow Local mesh setting in ground effect condition

$$Cf = [2 \log 10 (Re) - 6.5]^{-2 \bullet 3} = 0.00996$$

(Skin Friction Calculation Ahmed, 2008)) (3.4)

$$Tw = ½ \, x \, Cf \, x \, p \, x \, u^2 = 0.5 \, x \, 0.00996 \, x \, 1.225 \, x \, 146^2 = 130.08$$

(Wall Shear Stress Calculation (Ahmed, 2008))

(3.5)

$$\text{Ut} = \sqrt{\frac{\text{TW}}{\text{p}}} \quad = 10.305 \text{ m/s}$$

(Friction Velocity Calculation (Ahmed, 2008)) (3.6)

$$\text{y1} = \frac{y + x \, u}{\text{p} \; x \; Ut} \quad = 1.27 \; x \; 10^{-6} \text{ m}$$

(First Mesh Node Distance (Ahmed, 2008)) (3.7)

Reynolds number

The flow Reynolds number [107] is calculated. Taking into consideration that the take-off velocity for UH18-SPW is 90 km/h and the root chord length is 5.85m. The Re calculation is as stated below:

$$Re = \nu \, C \, / \lambda$$

(2.13)

$$Re = 25 \frac{m}{s} \; x \; 5.85m \; / 1.608x10^{-5}$$

$$Re = 90.95\text{x}10^5$$

Where ν is take-off velocity

C is root chord

λ is kinematic viscosity

Taking into consideration that scale model root chord is 1m. Hence the velocity calculation for simulation is as stated below.

$$\nu = \mathrm{Re}\lambda\ /\mathrm{C} = 90.95\mathrm{x}10^{5}\ \mathrm{x}\ 1.608\mathrm{x}10^{-5}\ /\ 1 = 146.25\ \mathrm{m/s} \sim 146\ \mathrm{m/s}$$

Goal Set Up

In Solidworks Flow Simulation, goals are used to define specific parameters that intended to measure or monitor during the simulation. Goals can be used to assess the performance of a design or to compare different design options. They can be used to identify areas of improvement in a design or to compare different design options. The chosen goal is CL, CD and CM value along with fluid density, force x, y direction, actual lift and drag result. Figure 3.50 show the goal set up in solidwork flow simulation.

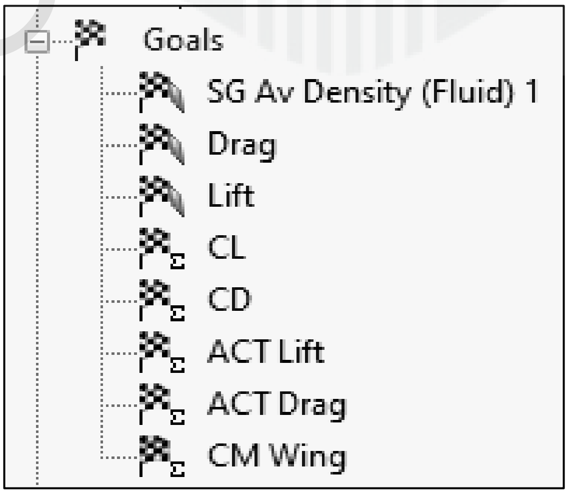

Figure 3.50: goal set up in solidwork flow simulation.

Pitching Moment

To have a static longitudinal stability, the hoverwing pitching moment curve must have a negative slope. Furthermore, in addition to having a static stability the curve must also have a positive intercept. The Free body diagram of pitching moment for UH18-SPW model is illustrated in Figure 3.51. The further calculation is as follow;

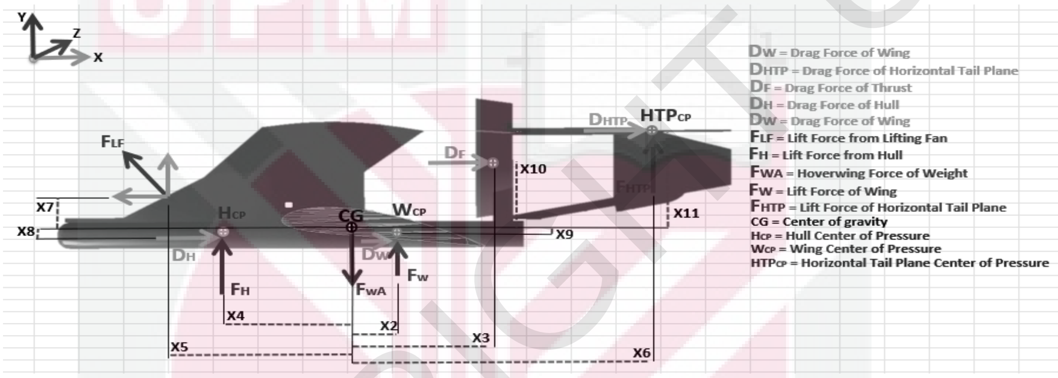

Figure 3.51: Free body diagram of pitching moment for UH18-SPW model

Taking a moment about HTP COP as shown in Figure 3.51, in an assumption that the downwash angle being neglected;

$+\uparrow \mathcal{E} F_y = 0;$

$0 = F_H + F_W + F_{HTP} + F_{LF} \cos \Theta$

$+\rightarrow \mathcal{E} F_X = 0;$

$0 = D_F + D_{HTP} + D_W + D_H - F_{LF} \sin \Theta$

$\mathcal{E} M_{CG} = 0 (Clockwise +);$

$0 = - F_{LF} \sin \Theta (X7) - D_H (X8) - D_W (X9) + D_F (X10) + D_{HTP} (X11)$

$+ F_{LF} \cos \Theta (X5) + F_H (X4) - F_W (X2) - F_{HTP} (X6)$

(3.8)

3.9 Conceptual Design of Two-Seater Dragonfly DF2 stability and Performances Setup

After confirming simulation method in previous chapter, the same set up was used to simulate the CL, CD, CM and COP migration of two seats UHID Hoverwing.

3.9.1 XFLR5 simulation Set Up

In XFLR5 simulation as shown in Figure 3.52, the simulation was done to investigate COP migration is done from OGE to IGE zone. The wing span is 0.882 m, mass is 0.25 kg, mean aerodynamic chord is 0.792 m and the mesh element is 914. The several tests were simulated for variation in vertical height (H) as percentage of chord (C) which is 20% HC (0.2 m), 40% HC (0.4 m), 60% HC (0.6 m), 80% HC (0.8 m), and >100% HC (>1 m). The applied velocity is 15 m/s as this is a suitable take off speed for low-speed aircraft. The wing area is 0.622 m² and the analysis uses the Vortex lattice method (VLM). The maximum height above the applied surface is 1 m.

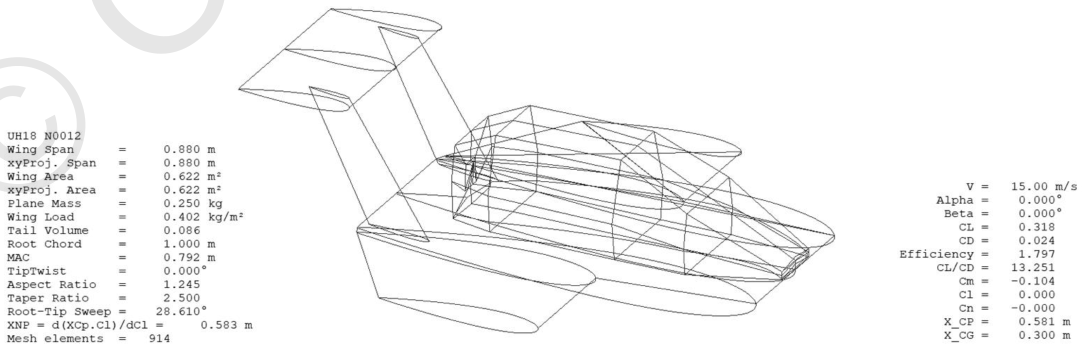

Figure 3.52: COP investigation simulation of UHID Hoverwing in XFLR5.

3.9.2 Solidwork flow simulation Set Up

In Solidwork flow simulation as shown in Figure 3.53, the simulation was done to produce aerodynamic performance of the final design from OGE to IGE zone. The several tests were simulated for variation in vertical height (H) to chord ratio (C) which is 0.303 HC, 0.371 HC, 0.671 HC, and 2.436 HC. The applied velocity is 146 m/s as this is a converted take off speed for scale down model based on matching Re number. The mesh level is 388651 and the analysis uses the k-ε model and transport equations for the turbulent kinetic energy and its dissipation rate. The maximum height ratio above the applied surface is 2.436.

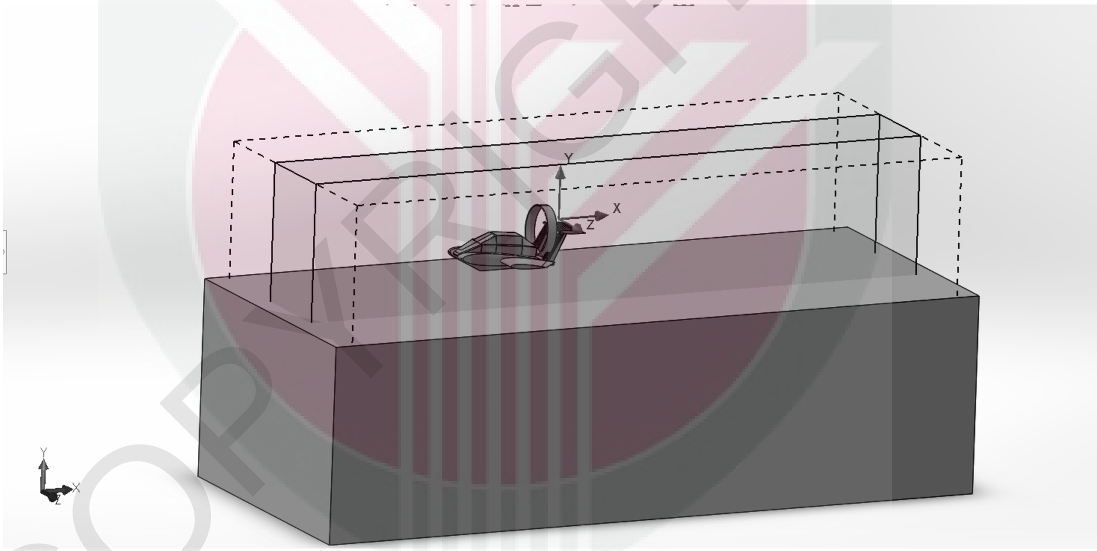

Figure 3.53: External Flow simulation of Conceptual UHID Hoverwing in SolidWorks Flow.

3.10 Finalized Work

The methodology outlined in chapter three is a step-by-step process for designing and developing a new hoverwing craft. It begins with the selection of a CFD software program, which are XFLR5 and SOLIDWORKS Flow Simulation. XFLR5 is used to simulate the center of pressure migration of various types of airfoils, rectangle and inverse delta wings. This is important because the center of pressure migration affects the stability of the hoverwing. The next step is to design a two-seat hoverwing using the SOLIDWORK workbench and later simulate the aerodynamic performance and stability of the hoverwing by using SOLIDWORK flow simulation. In this task, the design process was determined to select a suitable design solution for the new hoverwing. This includes designing the airfoils, rectangle and inverse delta, and planform area. The design process is iterative, meaning that it is repeated until the desired performance and stability characteristics are achieved. After done with the design process, process of design iteration was concluded with iterations with the lowest achievable COP migration. The next step is to determine the performance of individual iteration in term of lift, drag and moment coefficient. Final selections were going to be decided by comparison of all iteration along with UH18-SPW Naca 4412 aerodynamic performances.

CHAPTER 4

RESULT AND DISCUSSION

Chapter three dives into the heart of the research. It outlines all the objectives of the study and presents the methods used to achieve them, following the exact order in which they were implemented. The analysis of the results and their interpretation are presented in Chapter four. After numerical simulation for each configuration was done, the location of each configurations COP is determined and the result was plotted in Excel spreadsheet form for better visualization.

4.1 Center Of Pressure Migration Result In & Out of Ground Effect for Rectangle and Inverse Delta of six types of airfoils

From the result, it was observed that the migration of COP behaves differently as stated below;

1. The COP migrates as the ground envelope and Angle of Attack (AOA) increase or decrease.
2. Negative value indicates that the COP shifted towards Trailing Edge as HC increases.
3. The Chord % Vs. HC % graph is divided into three region which is green, yellow and red. Green indicates Pitch stable, yellow indicates Neutrally Stable Pitch and red indicates Unstable Pitch region.

The following Figures show the result for each wing configurations. HC is height to chord percentage and XCp is the center of pressure (COP) migration on wing chord in meter. The maximum Angle of Attack (AOA) is limited to 10º due to currently this is the preliminary research parameter. It is a given to conclude that to avoid instability in longitudinal direction, the COG must not migrate to any region of neutrally stable and unstable region. This is due to the hoverwing stability is too sensitive to any sudden force in yellow region.

4.1.1 Naca 0012 & Flat Surface

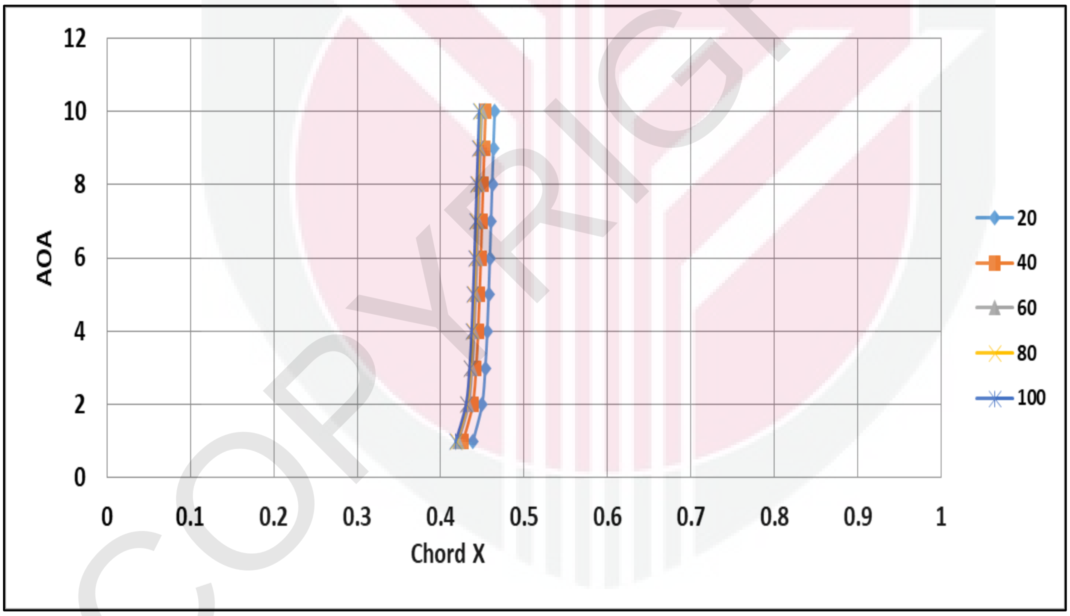

Figure 4.0: Naca0012 rectangular wing configuration COP migration

Table 1: Naca0012 rectangular wing configuration COP migration

HC %/AOA	0	1	2	3	4	5	6	7	8	9	10
20		0.438726	0.449781	0.453744	0.456033	0.457736	0.459214	0.460623	0.462041	0.463512	0.465062
40		0.426361	0.438159	0.442362	0.444764	0.446525	0.448033	0.449453	0.450869	0.452329	0.45386
60		0.421487	0.433531	0.437813	0.440251	0.44203	0.443546	0.444969	0.446384	0.447838	0.449361
80		0.419347	0.431504	0.435822	0.438277	0.440065	0.441586	0.44301	0.444425	0.445878	0.447398
100		0.418316	0.430532	0.43487	0.437334	0.439127	0.44065	0.442076	0.443492	0.444944	0.446464

Figure 4.0 and Table 1 shows how Naca0012 rectangular shape COP migrated as HC changes at different AOA. The COP values is positive indicated that it has migrated toward leading edge in longitudinal position as HC increases from 20% to 100%(OGE). At 0◦ of AOA, COP remains constant on the leading-edge position. This is due to no pressure acted on the location hence it could not be calculated. The COP location migrated from 0.438726 m to 0.469062 m in chord direction as the AOA changed from 1◦ to 10◦. The maximum and minimum increment as the HC rise is about 0.418316% and 0.4464638% of its original position. It was also observed that the COP migrated as much as -0.77381% towards only leading edge from 0◦ to 10°.

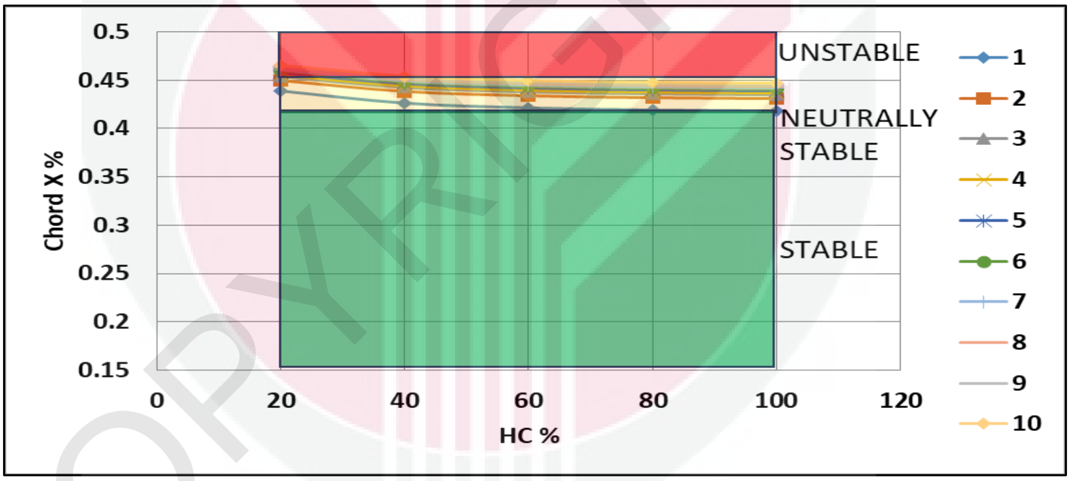

Figure 4.1: Naca0012 rectangular wing configuration COP migration percentage increment from 20% HC to 100% HC° at various AOA

Table 2: Naca0012 rectangular wing configuration COP migration percentage increment from 20% HC to 100% HC° at various AOA

HC %/AOA	0	1	2	3	4	5	6	7	8	9	10
20	0	0.438726	0.449781	0.453744	0.456033	0.457736	0.459214	0.460623	0.462041	0.463512	0.465062
40	0	0.426361	0.438159	0.442362	0.444764	0.446525	0.448033	0.449453	0.450869	0.452329	0.45386
60	0	0.421487	0.433531	0.437813	0.440251	0.44203	0.443546	0.444969	0.446384	0.447838	0.449361
80	0	0.419347	0.431504	0.435822	0.438277	0.440065	0.441586	0.44301	0.444425	0.445878	0.447398
100	0	0.418316	0.430532	0.43487	0.437334	0.439127	0.44065	0.442076	0.443492	0.444944	0.446464

Figure 4.1 and Table 2 shows Naca0012 COP migration on every AOA increment. It was found that, when CG enters or moves inside the green region, it indicates that it is stable longitudinally. The yellow to red region indicates that it will unstable when CG enters these regions. The location of COP is located at 44.64% Chord when it is OGE, and when the it flies closer to the ground (IGE) the location of COP move towards Trailing Edge (TE), and it is located at 43.87% Chord when H/C = 0.2.

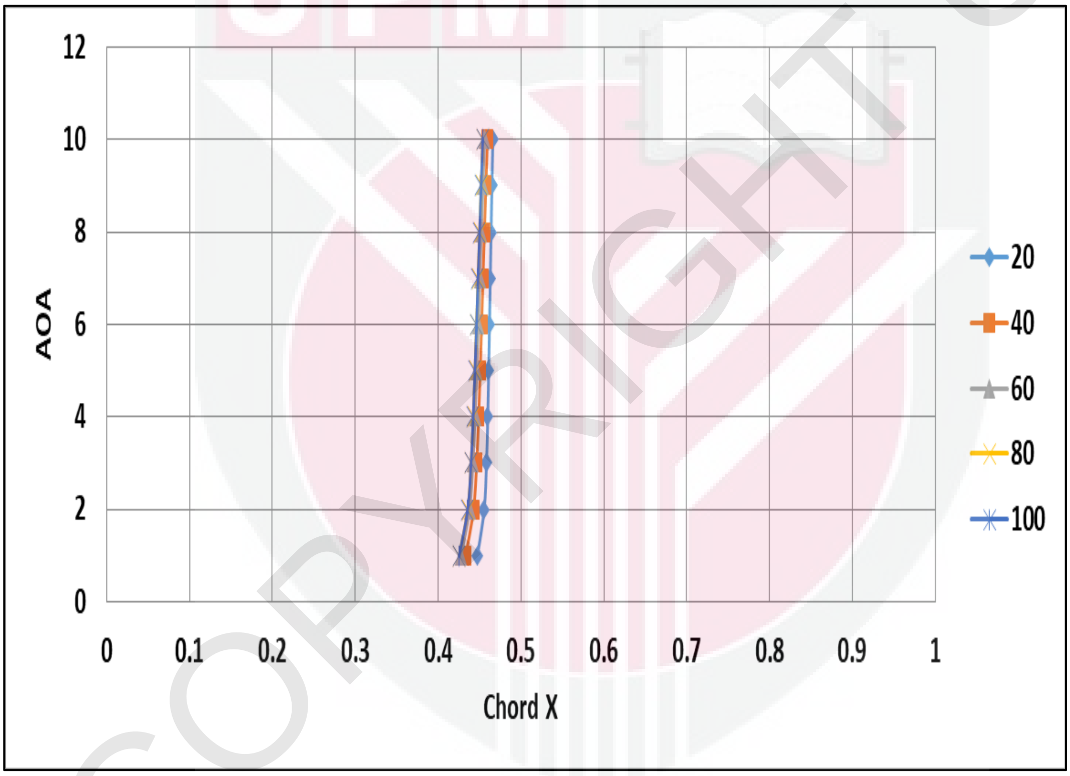

Figure 4.2: Naca0012 Inverse Delta wing configuration COP migration

Table 3: Naca0012 Inverse Delta wing configuration COP migration

HC %/AOA	0	1	2	3	4	5	6	7	8	9	10
20		0.447275	0.455445	0.458228	0.459759	0.460868	0.461832	0.462771	0.463744	0.464785	0.465913
40		0.433077	0.442813	0.446589	0.448969	0.450869	0.452594	0.454276	0.455981	0.457747	0.459595
60		0.427942	0.438071	0.442049	0.444584	0.446619	0.44847	0.450272	0.452093	0.453973	0.455934
80		0.425825	0.436106	0.440154	0.442737	0.444813	0.4467	0.448536	0.45039	0.452301	0.454292
100		0.424844	0.435197	0.439276	0.44188	0.443971	0.445872	0.447721	0.449588	0.451511	0.453513

Figure 4.2 and Table 3 shows Naca0012 Inverse Delta shape COP migration as HC changes at different AOA. The COP values is positive indicating that it has migrated toward leading edge in longitudinal position as HC increases from 20% to 100% (OGE). At 0◦ of AOA, COP remains constant on the leading-edge position. This is due to no pressure acted on the location hence it could not be calculated. The COP location migrates from 0 m to 0.4659126 m in chord direction as the AOA changed from 0◦ to 10◦. The maximum and minimum increment as the HC rise is about 2.24319% and 1.23993% of its original position. It was also observed that the COP migrated as much as -0.62379% towards only leading edge from 0◦ to 10°.

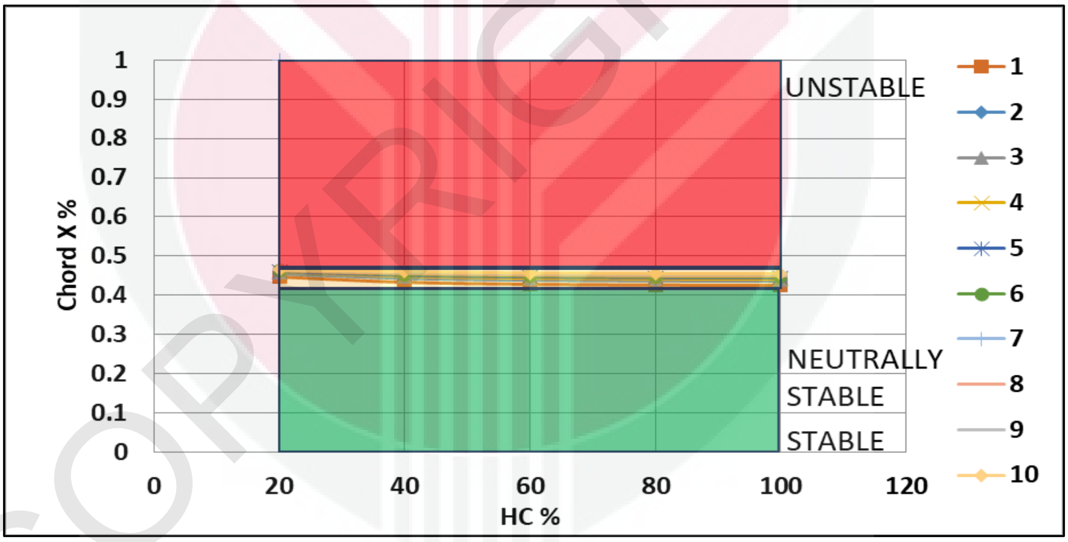

Figure 4.3: Naca0012 Inverse Delta wing configuration COP migration percentage increment from 20% HC to 100% HC° at various AOA

Table 4: Naca0012 Inverse Delta wing configuration COP migration percentage increment from 20% HC to 100% HC° at various AOA

HC %/AOA	0	1	2	3	4	5	6	7	8	9	10
20	0	0.447275	0.455445	0.458228	0.459759	0.460868	0.461832	0.462771	0.463744	0.464785	0.465913
40	0	0.433077	0.442813	0.446589	0.448969	0.450869	0.452594	0.454276	0.455981	0.457747	0.459595
60	0	0.427942	0.438071	0.442049	0.444584	0.446619	0.44847	0.450272	0.452093	0.453973	0.455934
80	0	0.425825	0.436106	0.440154	0.442737	0.444813	0.4467	0.448536	0.45039	0.452301	0.454292
100	0	0.424844	0.435197	0.439276	0.44188	0.443971	0.445872	0.447721	0.449588	0.451511	0.453513

Figure 4.3 and Table 4 shows Naca0012 Inverse Delta shape COP migration on every AOA increment. It was found that, when CG enters or moves inside the green region, it indicates that it is stable longitudinally. The yellow to red region indicates that it will unstable when CG enters these regions. The location of COP is located at 44.72% Chord when it is OGE, and when the it flies closer to the ground (IGE) the location of COP move towards Trailing Edge (TE), and it is located at 45.35% Chord when H/C = 0.2.

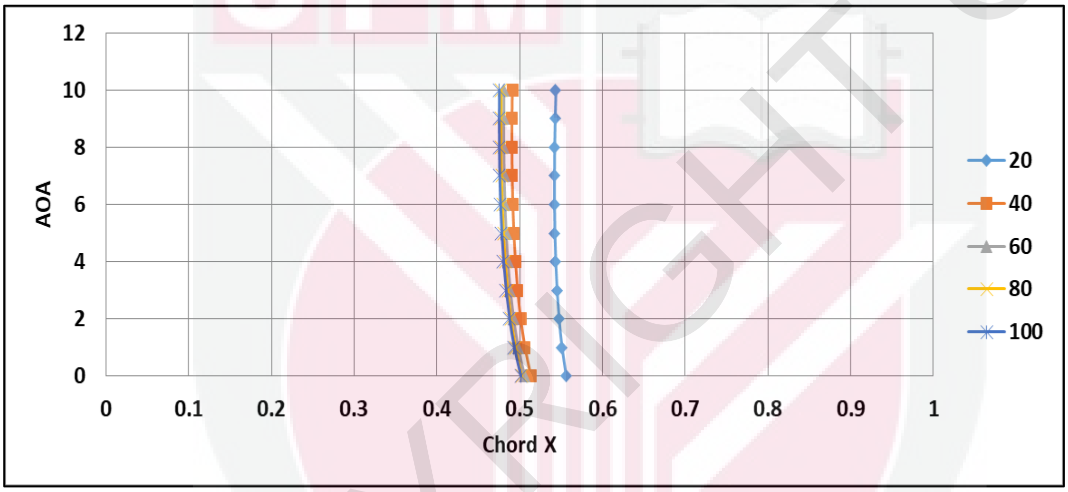

Figure 4.4: Flat rectangular wing configuration COP migration

Table 5: Flat rectangular wing configuration COP migration

HC %/AOA	0	1	2	3	4	5	6	7	8	9	10
20	0.555697	0.550692	0.54724	0.54486	0.54327	0.542291	0.541803	0.541728	0.542007	0.542598	0.543472
40	0.513568	0.506382	0.501264	0.497567	0.4949	0.49302	0.491763	0.491016	0.490699	0.490756	0.491141
60	0.50572	0.498079	0.492612	0.488636	0.485741	0.483668	0.482244	0.481351	0.480903	0.48084	0.481115
80	0.503137	0.495346	0.489765	0.485697	0.482727	0.48059	0.479112	0.478171	0.47768	0.477578	0.477817
100	0.500968	0.493025	0.487329	0.483172	0.480129	0.477932	0.476403	0.475419	0.474891	0.474755	0.474965

Figure 4.4 and Table 5 shows how flat surfaces rectangular shape COP migrated as HC changes at different AOA. The COP is a mix of negative and positive value which indicated that the COP has migrated toward trailing

edge from 0◦ to 1◦ and migrated back towards leading edge from 2◦ to 10◦ of AOA in longitudinal position as HC increases from 20% to 100 %(OGE). The COP location migrated from 0.5556973 m to 0.474965 m in chord direction as the AOA changed from 0◦ to 10◦. The maximum and minimum increment as the HC rise is about 5.47% and 6.85% of its original position. It was also observed that the COP migrated as much as 8.07% towards only leading edge from 0◦ to 10°.◦.

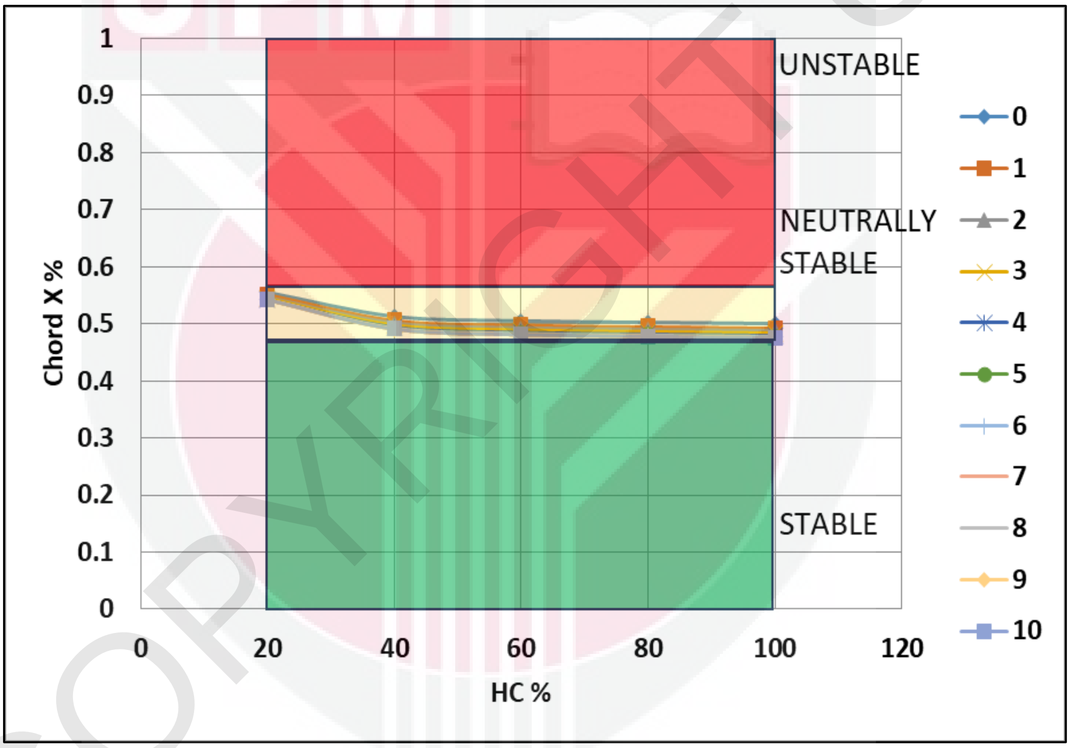

Figure 4.5: Flat rectangular wing configuration COP migration percentage increment from 20% HC to 100% HC° at various AOA

Table 6: Flat rectangular wing configuration COP migration percentage increment from 20% HC to 100% HC° at various AOA

HC %/AOA	0	1	2	3	4	5	6	7	8	9	10
20	0.555697	0.550692	0.54724	0.54486	0.54327	0.542291	0.541803	0.541728	0.542007	0.542598	0.543472
40	0.513568	0.506382	0.501264	0.497567	0.4949	0.49302	0.491763	0.491016	0.490699	0.490756	0.491141
60	0.50572	0.498079	0.492612	0.488636	0.485741	0.483668	0.482244	0.481351	0.480903	0.48084	0.481115
80	0.503137	0.495346	0.489765	0.485697	0.482727	0.48059	0.479112	0.478171	0.47768	0.477578	0.477817
100	0.500968	0.493025	0.487329	0.483172	0.480129	0.477932	0.476403	0.475419	0.474891	0.474755	0.474965

Figure 4.5 and Table 6 shows Flat surfaces COP migration on every AOA increment. It was found that, when CG enters or moves inside the green region, it indicates that it is stable longitudinally. The yellow to red region indicates that it will unstable when CG enters these regions. The location of COP is located at 47.49% Chord when it is OGE, and when the it flies closer to the ground (IGE) the location of COP move towards Leading Edge (LE), and it is located at 55.57% Chord when H/C = 0.2.

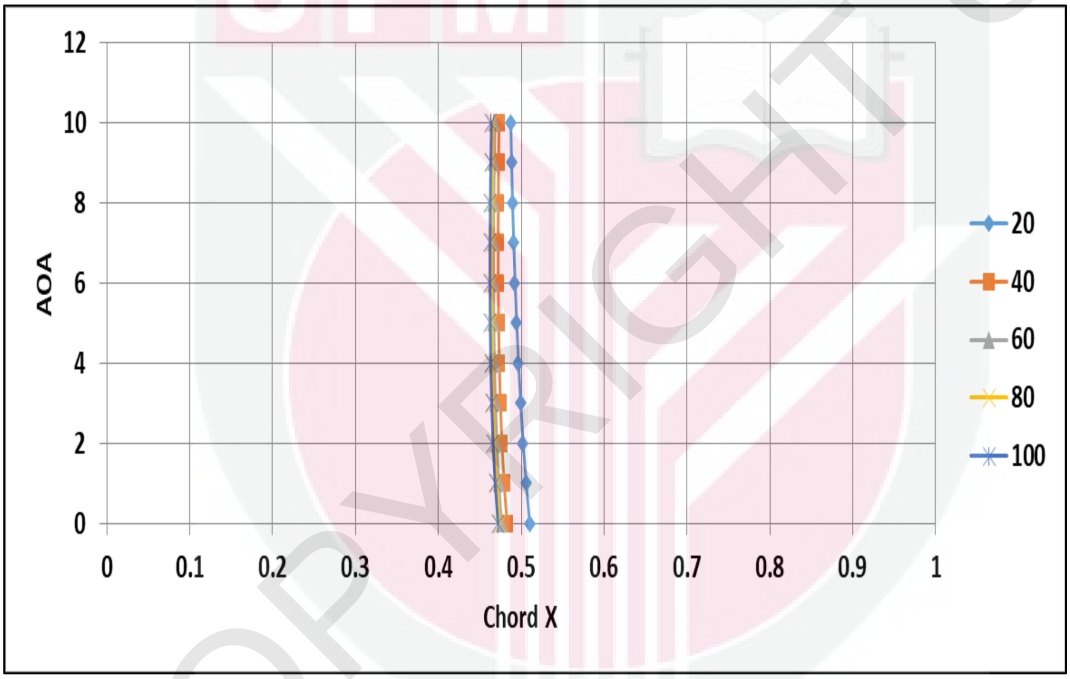

Figure 4.6: Flat Inverse Delta wing configuration COP migration

Table 7: Flat Inverse Delta wing configuration COP migration

HC %/AOA	0	1	2	3	4	5	6	7	8	9	10
20	0.509838	0.505462	0.501886	0.498885	0.496329	0.494135	0.49225	0.490636	0.489266	0.488122	0.487189
40	0.482975	0.479288	0.476698	0.474871	0.473614	0.472803	0.472359	0.472227	0.472368	0.472753	0.473363
60	0.4764	0.472667	0.470097	0.468336	0.467175	0.466483	0.466173	0.466187	0.466482	0.46703	0.467808
80	0.474103	0.470337	0.467757	0.466	0.464853	0.464183	0.4639	0.463945	0.464275	0.464859	0.465675
100	0.472102	0.468287	0.465683	0.463917	0.462772	0.462111	0.461844	0.461909	0.462263	0.462875	0.463722

Figure 4.6 and Table 7 shows a Flat Inverse Delta shape COP migration as HC changes at different AOA. The COP is a mix of negative and positive value which indicated that its COP migrated toward trailing edge from 0◦ to 1◦ and migrated back towards leading edge from 2◦ to 10◦ of AOA in longitudinal position as HC increases from 20% to 100% (OGE). The COP location migrated from 0.5098382 m to 0.4637219m in chord direction as the AOA changed from 0◦ to 10◦. The maximum and minimum increment as the HC rise is about 3.77364% and 4.046086207% of its original position. It was also observed that the COP migrated as much as 3.64756% towards only leading edge from 0◦ to 10°.

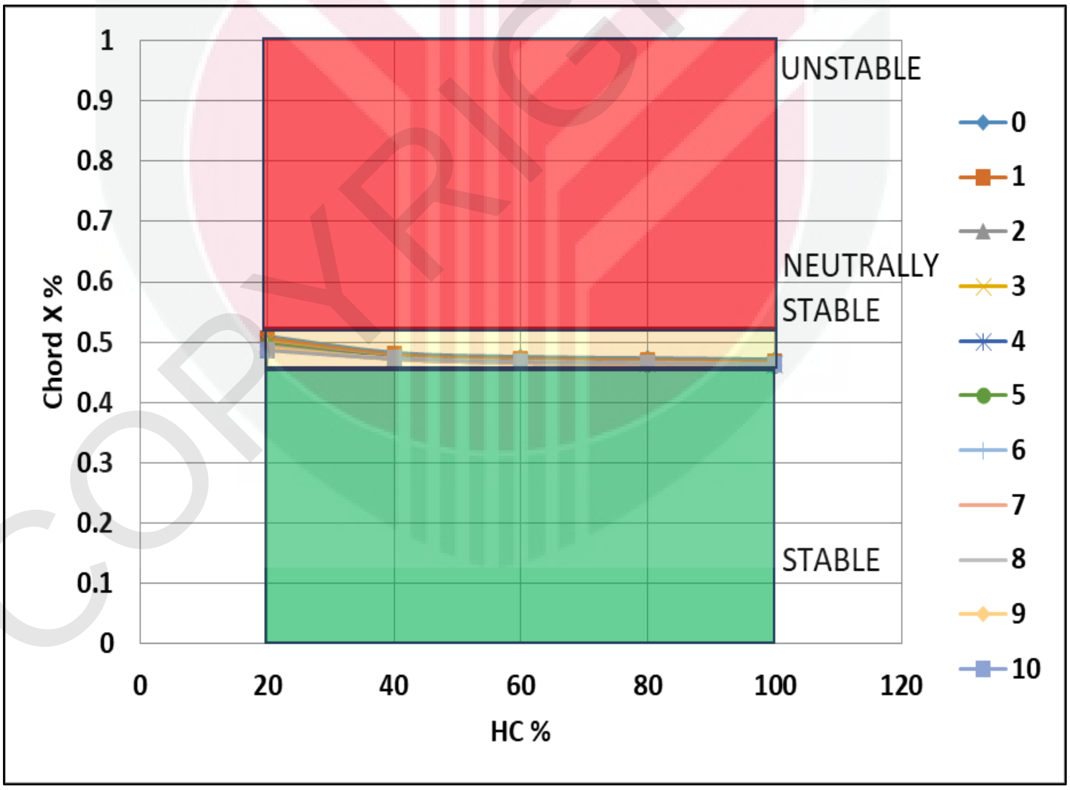

Figure 4.7: Flat Inverse Delta wing configuration COP migration percentage increment from 20% HC to 100% HC° at various AOA

Table 8: Flat Inverse Delta wing configuration COP migration percentage increment from 20% HC to 100% HC° at various AOA

HC%/AOA	0	1	2	3	4	5	6	7	8	9	10
20	0.509838	0.505462	0.501886	0.498885	0.496329	0.494135	0.49225	0.490636	0.489266	0.488122	0.487189
40	0.482975	0.479288	0.476698	0.474871	0.473614	0.472803	0.472359	0.472227	0.472368	0.472753	0.473363
60	0.4764	0.472667	0.470097	0.468336	0.467175	0.466483	0.466173	0.466187	0.466482	0.46703	0.467808
80	0.474103	0.470337	0.467757	0.466	0.464853	0.464183	0.4639	0.463945	0.464275	0.464859	0.465675
100	0.472102	0.468287	0.465683	0.463917	0.462772	0.462111	0.461844	0.461909	0.462263	0.462875	0.463722

Figure 4.7 and Table 8 shows a Flat Inverse Delta shape COP migration on every AOA increment. It was found that, when CG enters or moves inside the green region, it indicates that it is stable longitudinally. The yellow to red region indicates that it will unstable when CG enters these regions. The location of COP is located at 46.38% Chord when it is OGE, and when the it flies closer to the ground (IGE) the location of COP move towards Leading Edge (LE), and it is located at 50.98% Chord when H/C = 0.2.

***See Appendix B**

4.1.2 Naca 4412 & Clark Y

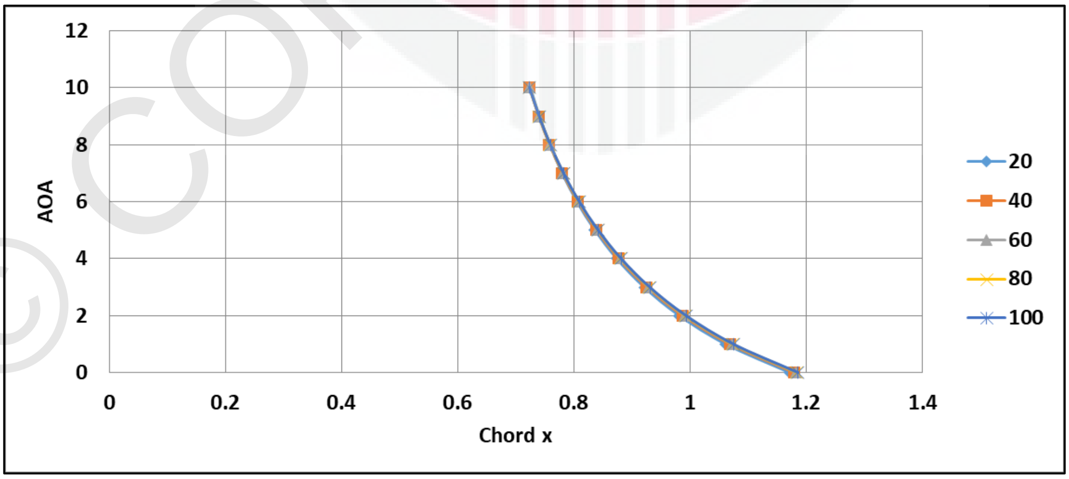

Figure 4.8: Naca4412 rectangular wing configuration COP migration

Table 9: Naca4412 rectangular wing configuration COP migration

HC %/AOA	0	1	2	3	4	5	6	7	8	9	10
20	1.171874	1.061608	0.981583	0.921002	0.873679	0.835816	0.804952	0.779421	0.758059	0.740022	0.724689
40	1.179597	1.068646	0.987489	0.925684	0.877176	0.838214	0.806346	0.779905	0.757716	0.738931	0.722916
60	1.183015	1.071998	0.990531	0.928339	0.879434	0.840089	0.807863	0.781093	0.758602	0.73954	0.723271
80	1.184866	1.073806	0.992193	0.929824	0.880738	0.841219	0.808833	0.781913	0.759287	0.7401	0.723718
100	1.185976	1.074873	0.993174	0.930707	0.881524	0.841915	0.809444	0.782448	0.759752	0.740502	0.724062

Figure 4.8 and Table 9 shows how Naca4412 rectangular shape COP migrated as HC changes at different AOA. The COP values is negative indicated that it has migrated toward trailing edge in longitudinal position as HC increases from 20% to 100%(OGE). The COP location migrated from 1.171874 m to 0.7240619 m in chord direction as the AOA changed from 0◦ to 10◦. The maximum and minimum increment as the HC rise is about -1.4102 % and 0.0627% of its original position. It was also observed that the COP migrated as much as 44.78121% towards only leading edge from 0◦ to 10°.

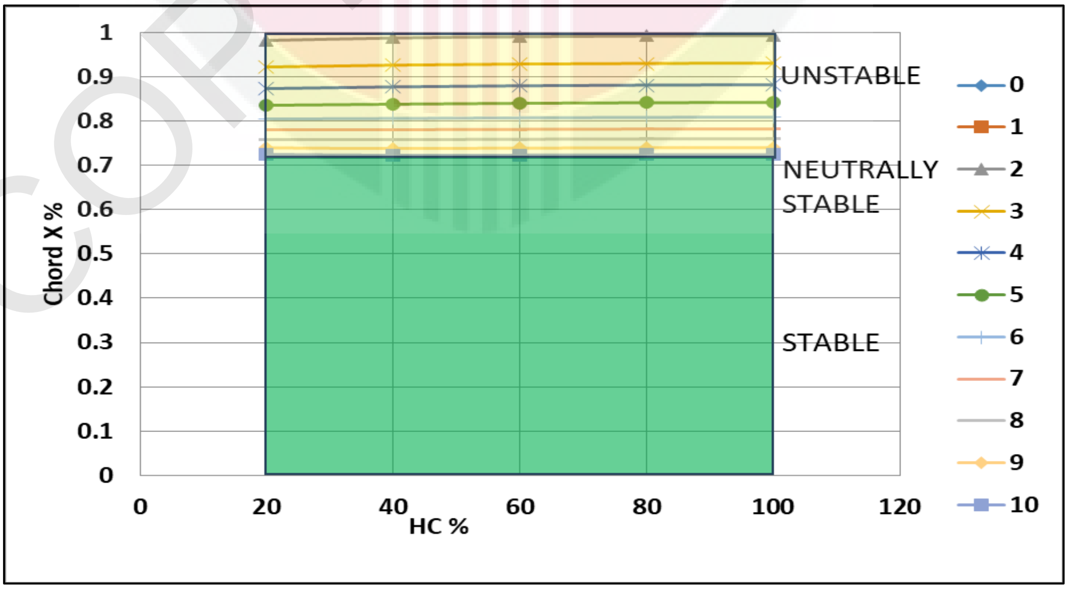

Figure 4.9: Naca4412 rectangular wing configuration COP migration percentage increment from 20% HC to 100% HC° at various AOA

Table 10: Naca4412 rectangular wing configuration COP migration percentage increment from 20% HC to 100% HC° at various AOA

HC %/AOA	0	1	2	3	4	5	6	7	8	9	10
20	1.171874	1.061608	0.981583	0.921002	0.873679	0.835816	0.804952	0.779421	0.758059	0.740022	0.724689
40	1.179597	1.068646	0.987489	0.925684	0.877176	0.838214	0.806346	0.779905	0.757716	0.738931	0.722916
60	1.183015	1.071998	0.990531	0.928339	0.879434	0.840089	0.807863	0.781093	0.758602	0.73954	0.723271
80	1.184866	1.073806	0.992193	0.929824	0.880738	0.841219	0.808833	0.781913	0.759287	0.7401	0.723718
100	1.185976	1.074873	0.993174	0.930707	0.881524	0.841915	0.809444	0.782448	0.759752	0.740502	0.724062

Figure 4.9 and Table 10 shows Naca4412 COP migration on every AOA increment. It was found that, when CG enters or moves inside the green region, it indicates that it is stable longitudinally. The yellow to red region indicates that it will unstable when CG enters these regions. The location of COP is located at 72.4% Chord when it is OGE, and when the it flies closer to the ground (IGE) the location of COP move towards Leading Edge (LE), and it is located at 117% Chord when H/C = 0.2.

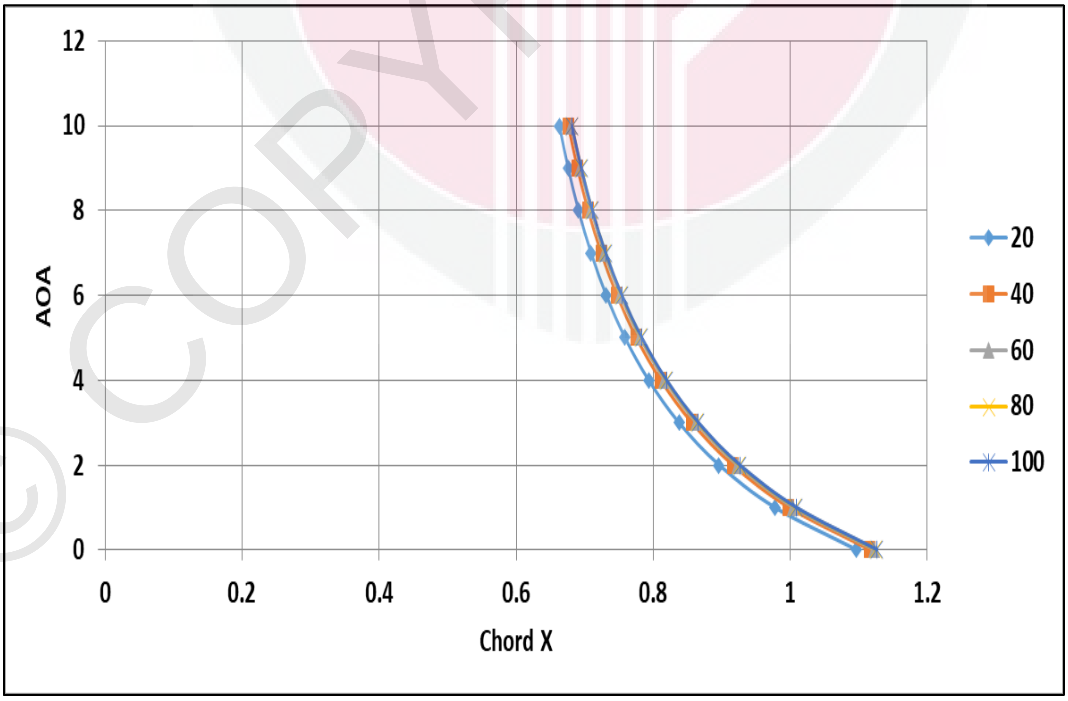

Figure 4.10: Naca4412 Inverse Delta wing configuration COP migration

Table 11: Naca4412 Inverse Delta wing configuration COP migration

HC %/AOA	0	1	2	3	4	5	6	7	8	9	10
20	1.096223	0.977076	0.896019	0.837451	0.793291	0.758934	0.731561	0.709355	0.691087	0.6759	0.663175
40	1.115714	0.997846	0.916197	0.856506	0.811153	0.775694	0.747364	0.724352	0.705424	0.689708	0.676571
60	1.121912	1.00432	0.922389	0.862249	0.81642	0.78051	0.751771	0.728397	0.70915	0.693156	0.679777
80	1.124811	1.007231	0.925123	0.864757	0.818702	0.782581	0.753653	0.73011	0.710714	0.694588	0.681094
100	1.126415	1.008788	0.926565	0.866071	0.819893	0.783661	0.754634	0.731003	0.71153	0.695337	0.681783

Figure 4.10 and Table 11 shows Naca4412 Inverse Delta shape COP migration as HC changes at different AOA. The COP values is negative indicating that it has migrated toward trailing edge in longitudinal position as HC increases from 20% to 100% (OGE). The COP location migrated from 1.096223 m to 0.6817831 m in chord direction as the AOA changed from 0◦ to 10◦. The maximum and minimum increment as the HC rise is about -3.0192% and -3.208362069% of its original position. It was also observed that the COP migrated as much as 41.96521% towards only leading edge from 0◦ to 10°.

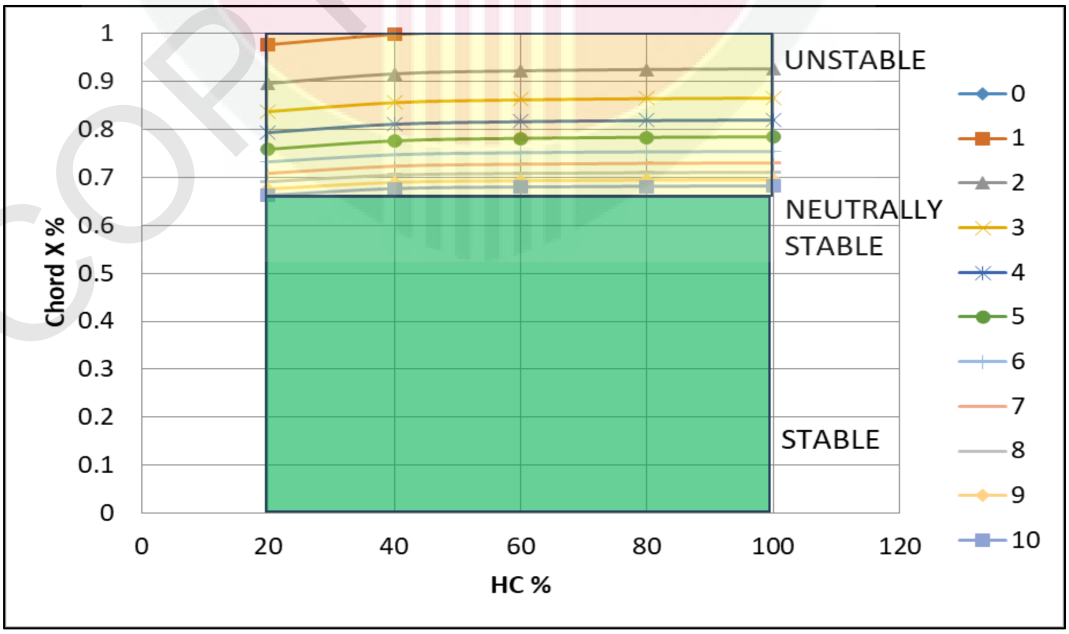

Figure 4.11: Naca4412 Inverse Delta wing configuration COP migration percentage increment from 20% HC to 100% HC° at various AOA

Table 12: Naca4412 Inverse Delta wing configuration COP migration percentage increment from 20% HC to 100% HC° at various AOA

HC %/AOA	0	1	2	3	4	5	6	7	8	9	10
20	1.096223	0.977076	0.896019	0.837451	0.793291	0.758934	0.731561	0.709355	0.691087	0.6759	0.663175
40	1.115714	0.997846	0.916197	0.856506	0.811153	0.775694	0.747364	0.724352	0.705424	0.689708	0.676571
60	1.121912	1.00432	0.922389	0.862249	0.81642	0.78051	0.751771	0.728397	0.70915	0.693156	0.679777
80	1.124811	1.007231	0.925123	0.864757	0.818702	0.782581	0.753653	0.73011	0.710714	0.694588	0.681094
100	1.126415	1.008788	0.926565	0.866071	0.819893	0.783661	0.754634	0.731003	0.71153	0.695337	0.681783

Figure 4.11 and Table 12 shows Naca4412 Inverse Delta shape COP migration on every AOA increment. It was found that, when CG enters or moves inside the green region, it indicates that it is stable longitudinally. The yellow to red region indicates that it will unstable when CG enters these regions. The location of COP is located at 68.17% Chord when it is OGE, and when the it flies closer to the ground (IGE) the location of COP move towards Leading Edge (LE), and it is located at 109% Chord when H/C = 0.2.

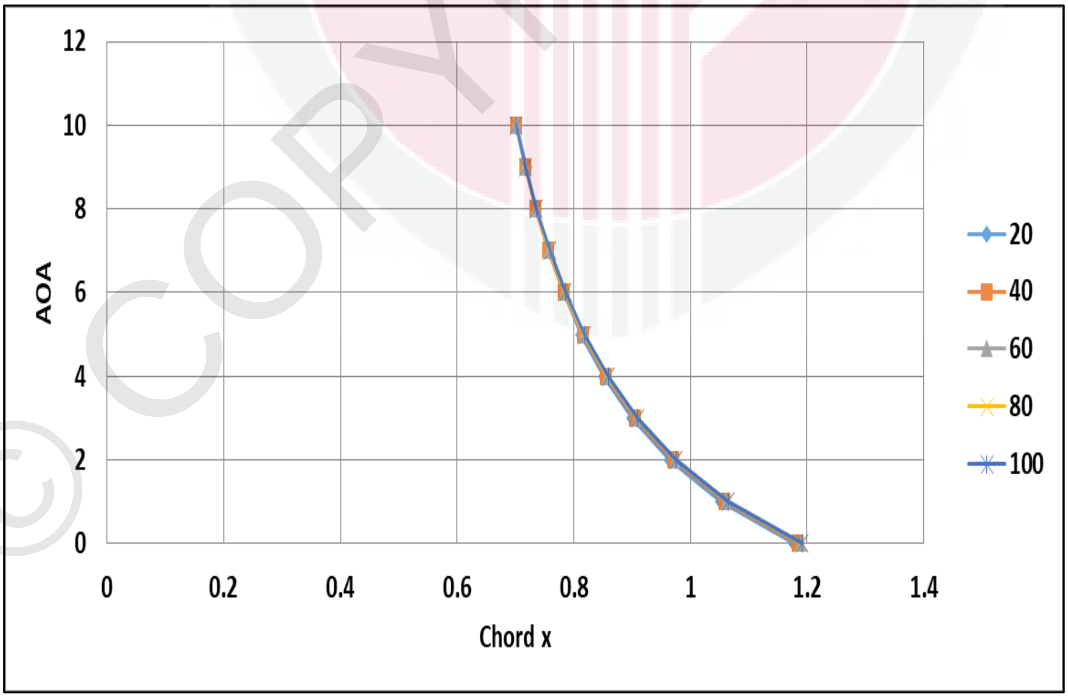

Figure 4.12: Clark Y rectangular wing configuration COP migration

Table 13: Clark Y rectangular wing configuration COP migration

HC %/AOA	0	1	2	3	4	5	6	7	8	9	10
20	1.176741	1.051853	0.964689	0.900553	0.851527	0.812966	0.781968	0.756624	0.735628	0.718057	0.703239
40	1.184377	1.058857	0.970465	0.905	0.854705	0.814983	0.782939	0.756657	0.73482	0.716493	0.700992
60	1.187796	1.062208	0.973449	0.907538	0.856796	0.816654	0.784225	0.757595	0.735442	0.716828	0.701067
80	1.189656	1.064014	0.975078	0.908959	0.858011	0.817677	0.785073	0.758284	0.735988	0.717245	0.701366
100	1.190774	1.065078	0.976037	0.909804	0.858746	0.818312	0.785617	0.758746	0.736376	0.717567	0.701629

Figure 4.12 and Table 13 shows how Clark Y rectangular shape COP migrated as HC changes at different AOA. The COP values is negative indicated that it has migrated toward trailing edge in longitudinal position as HC increases from 20% to 100% (OGE). The COP location migrates from 1.176741 m to 0.7016291 m in chord direction as the AOA changed from 0◦ to 10◦. The maximum and minimum increment as the HC rise is about -1.4033% and 0.16101% of its original position. It could also be observed that the COP migrated as much as 47.51119% towards only leading edge from 0◦ to 10°.

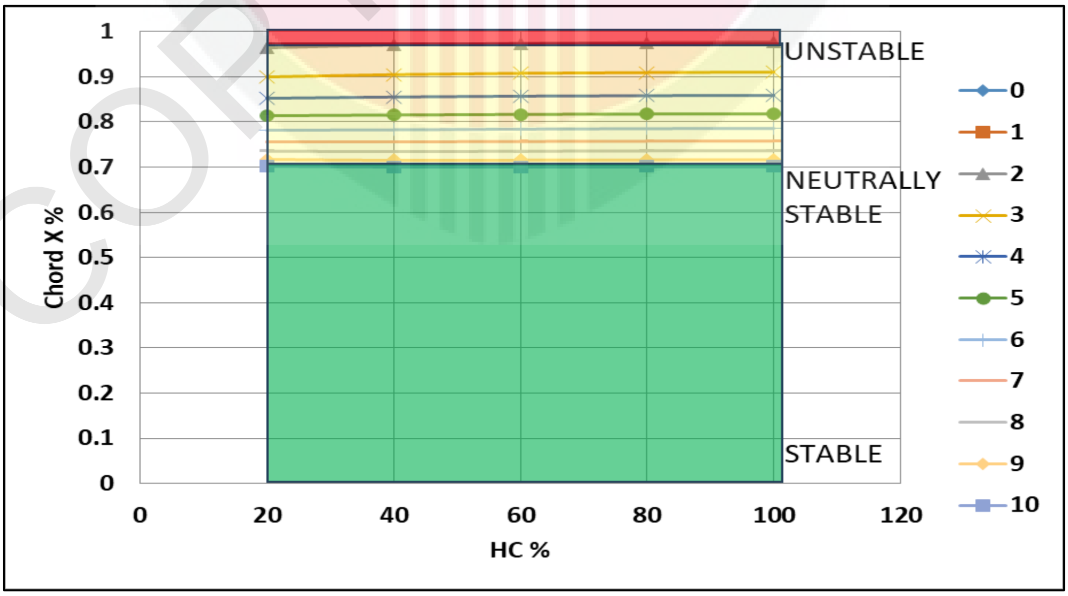

Figure 4.13: Clark Y rectangular wing configuration COP migration percentage increment from 20% HC to 100% HC° at various AOA

Table 14: Clark Y rectangular wing configuration COP migration percentage increment from 20% HC to 100% HC° at various AOA

HC %/AOA	0	1	2	3	4	5	6	7	8	9	10
20	1.176741	1.051853	0.964689	0.900553	0.851527	0.812966	0.781968	0.756624	0.735628	0.718057	0.703239
40	1.184377	1.058857	0.970465	0.905	0.854705	0.814983	0.782939	0.756657	0.73482	0.716493	0.700992
60	1.187796	1.062208	0.973449	0.907538	0.856796	0.816654	0.784225	0.757595	0.735442	0.716828	0.701067
80	1.189656	1.064014	0.975078	0.908959	0.858011	0.817677	0.785073	0.758284	0.735988	0.717245	0.701366
100	1.190774	1.065078	0.976037	0.909804	0.858746	0.818312	0.785617	0.758746	0.736376	0.717567	0.701629

Figure 4.13 and Table 14 shows Clark Y COP migration on every AOA increment. It was found that, when CG enters or moves inside the green region, it indicates that it is stable longitudinally. The yellow to red region indicates that it will unstable when CG enters these regions. The location of COP is located at 70.16% Chord when it is OGE, and when the it flies closer to the ground (IGE) the location of COP move towards Leading Edge (LE), and it is located at 117% Chord when H/C = 0.2.

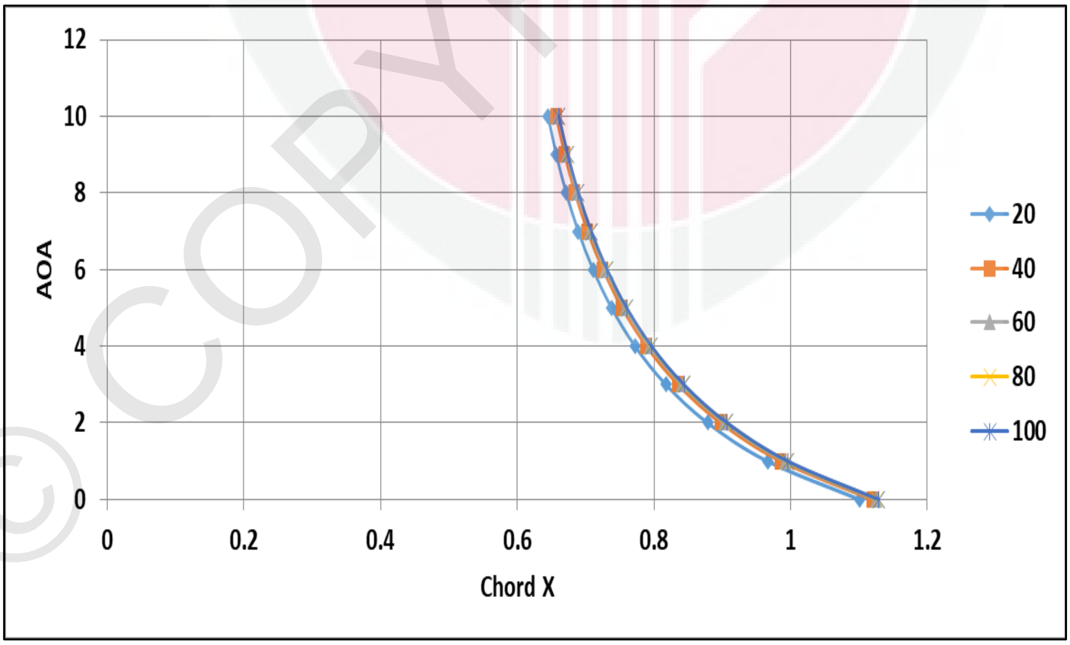

Figure 4.14: Clark Y Inverse Delta wing configuration COP migration

Table 15: Clark Y Inverse Delta wing configuration COP migration

HC %/AOA	0	1	2	3	4	5	6	7	8	9	10
20	1.101211	0.966398	0.878926	0.817737	0.772674	0.738238	0.711192	0.689505	0.67184	0.657281	0.645178
40	1.119087	0.985873	0.89766	0.83517	0.788784	0.753167	0.725122	0.702617	0.684299	0.669231	0.656745
60	1.125003	0.992097	0.903516	0.840493	0.793569	0.757458	0.728978	0.706095	0.68745	0.672102	0.659376
80	1.127827	0.994923	0.906122	0.842835	0.795655	0.759314	0.730631	0.707572	0.688774	0.673292	0.660451
100	1.129406	0.996442	0.907501	0.844066	0.79675	0.760288	0.7315	0.708349	0.689472	0.673922	0.66102

Figure 4.14 and Table 15 shows Clark Y Inverse Delta shape COP migration as HC changes at different AOA. The COP values is negative indicating that it has migrated toward trailing edge in longitudinal position as HC increases from 20% to 100% (OGE). The COP location migrated from 1.101211 m to 0.66102 m in chord direction as the AOA changed from 0◦ to 10◦. The maximum and minimum increment as the HC rise is about -2.8195% and -2.731396552% of its original position. It was also observed that the COP migrated as much as 44.4466% towards only leading edge from 0◦ to 10°.

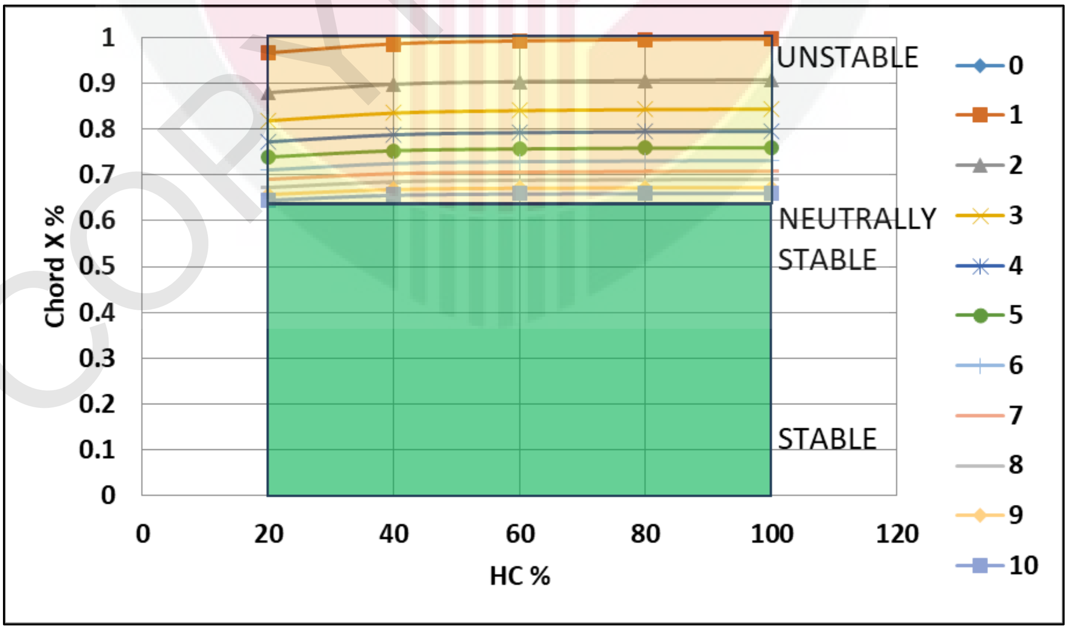

Figure 4.15: Clark Y Inverse Delta wing configuration COP migration percentage increment from 20% HC to 100% HC° at various AOA

Table 16: Clark Y Inverse Delta wing configuration COP migration percentage increment from 20% HC to 100% HC° at various AOA

HC %/AOA	0	1	2	3	4	5	6	7	8	9	10
20	1.101211	0.966398	0.878926	0.817737	0.772674	0.738238	0.711192	0.689505	0.67184	0.657281	0.645178
40	1.119087	0.985873	0.89766	0.83517	0.788784	0.753167	0.725122	0.702617	0.684299	0.669231	0.656745
60	1.125003	0.992097	0.903516	0.840493	0.793569	0.757458	0.728978	0.706095	0.68745	0.672102	0.659376
80	1.127827	0.994923	0.906122	0.842835	0.795655	0.759314	0.730631	0.707572	0.688774	0.673292	0.660451
100	1.129406	0.996442	0.907501	0.844066	0.79675	0.760288	0.7315	0.708349	0.689472	0.673922	0.66102

Figure 4.15 and Table 16 shows Clark Y Inverse Delta shape COP migration on every AOA increment. It was found that, when CG enters or moves inside the green region, it indicates that it is stable longitudinally. The yellow to red region indicates that it will unstable when CG enters these regions. The location of COP is located at 66.1% Chord when it is OGE, and when the it flies closer to the ground (IGE) the location of COP move towards Leading Edge (LE), and it is located at 110% Chord when H/C = 0.2.

***See Appendix B**

4.1.3 AWIG & DHMTU

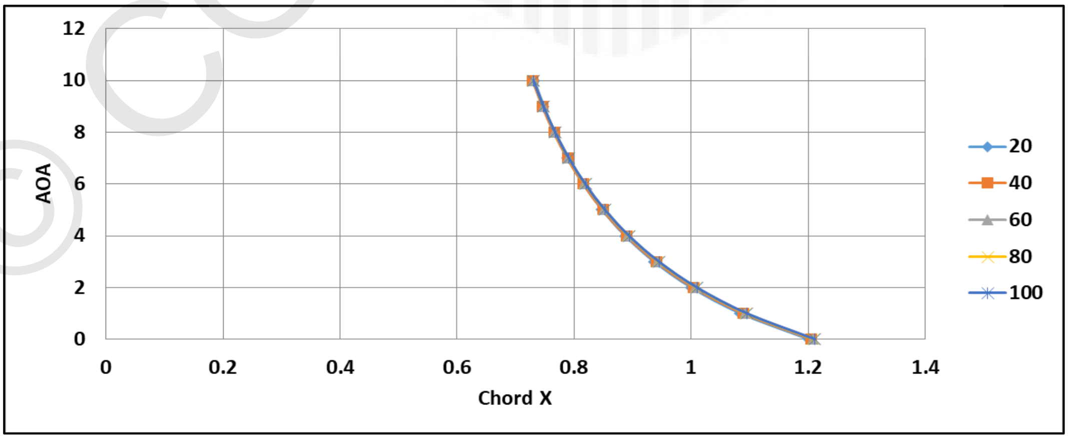

Figure 4.16: AWIG rectangular wing configuration COP migration

Table 17: AWIG rectangular wing configuration COP migration

HC %/AOA	0	1	2	3	4	5	6	7	8	9	10
20	1.200056	1.083783	0.999729	0.936277	0.886814	0.847298	0.815122	0.788527	0.766282	0.747505	0.73154
40	1.205617	1.089326	1.004564	0.940181	0.889747	0.849295	0.816243	0.78884	0.765857	0.746403	0.729819
60	1.208633	1.092484	1.007531	0.942834	0.892048	0.851244	0.817857	0.79014	0.766866	0.747143	0.730312
80	1.2104	1.094277	1.009215	0.944361	0.893406	0.852436	0.818892	0.79103	0.767621	0.747775	0.73083
100	1.211495	1.095355	1.010219	0.945274	0.894226	0.853167	0.81954	0.791601	0.768123	0.748213	0.73121

Figure 4.16 and Table 17 shows how AWIG rectangular shape COP migrated as HC changes at different AOA. The COP values is negative which indicates that it has migrated toward trailing edge in longitudinal position as HC increases from 20% to 100% (OGE). The COP location migrated from 1.200056 m to 0.7312104 m in chord direction as the AOA changed from 0◦ to 10◦. The maximum and minimum increment as the HC rise is about -1.1439 % and 0.03296 % of its original position. It was also observed that the COP migrated as much as 46.88456 % towards only leading edge from 0◦ to 10°.

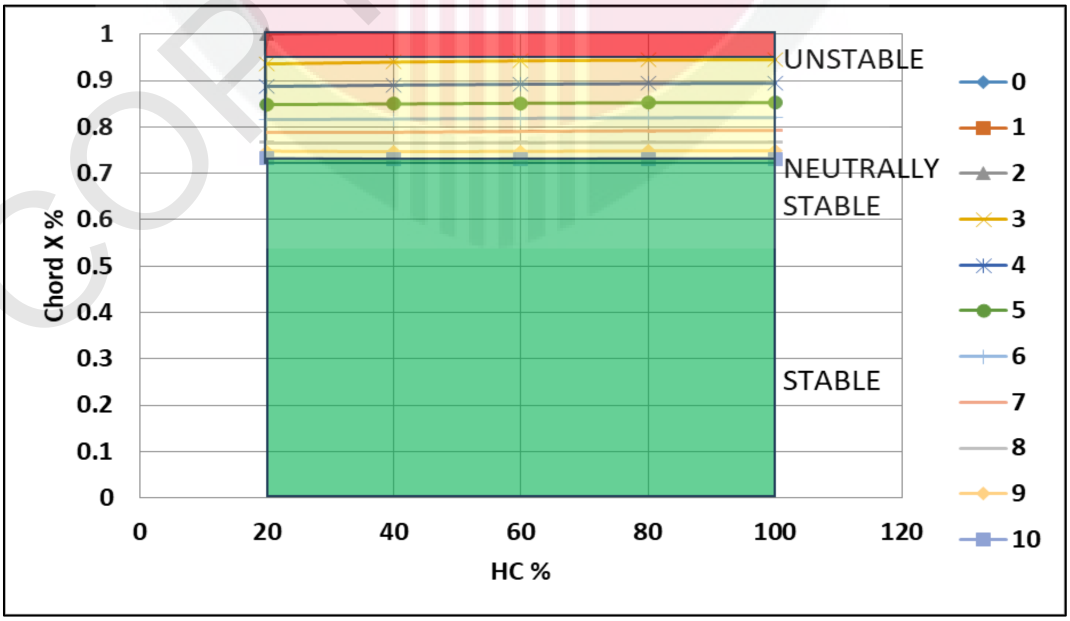

Figure 4.17: AWIG rectangular wing configuration COP migration percentage increment from 20% HC to 100% HC° at various AOA

Table 18: AWIG rectangular wing configuration COP migration percentage increment from 20% HC to 100% HC° at various AOA

HC %/AOA	0	1	2	3	4	5	6	7	8	9	10
20	1.200056	1.083783	0.999729	0.936277	0.886814	0.847298	0.815122	0.788527	0.766282	0.747505	0.73154
40	1.205617	1.089326	1.004564	0.940181	0.889747	0.849295	0.816243	0.78884	0.765857	0.746403	0.729819
60	1.208633	1.092484	1.007531	0.942834	0.892048	0.851244	0.817857	0.79014	0.766866	0.747143	0.730312
80	1.2104	1.094277	1.009215	0.944361	0.893406	0.852436	0.818892	0.79103	0.767621	0.747775	0.73083
100	1.211495	1.095355	1.010219	0.945274	0.894226	0.853167	0.81954	0.791601	0.768123	0.748213	0.73121

Figure 4.17 and Table 18 shows AWIG COP migration on every AOA increment. It was found that, when CG enters or moves inside the green region, it indicates that it is stable longitudinally. The yellow to red region indicates that it will unstable when CG enters these regions. The location of COP is located at 73.12% Chord when it is OGE, and when the it flies closer to the ground (IGE) the location of COP move towards Leading Edge (LE), and it is located at 120% Chord when H/C = 0.2.

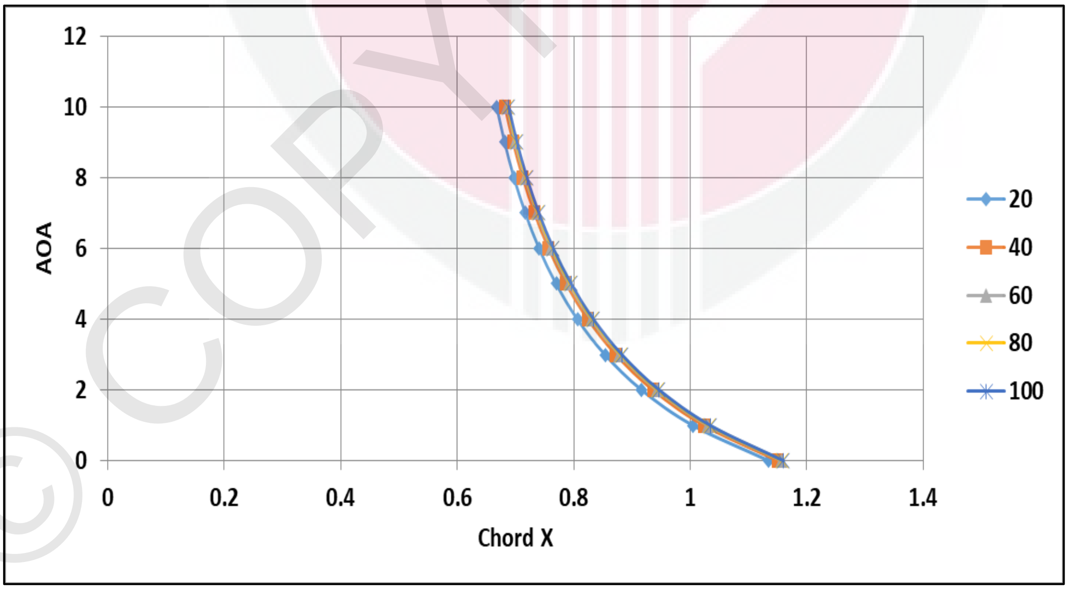

Figure 4.18: AWIG Inverse Delta wing configuration COP migration

Table 19: AWIG Inverse Delta wing configuration COP migration

HC %/AOA	0	1	2	3	4	5	6	7	8	9	10
20	1.134557	1.004387	0.916723	0.853812	0.806602	0.769996	0.740901	0.717334	0.697963	0.681863	0.668368
40	1.150644	1.023658	0.936319	0.872776	0.824657	0.78712	0.757176	0.732873	0.712887	0.696288	0.682402
60	1.156295	1.030004	0.942577	0.878682	0.830138	0.792178	0.761839	0.737179	0.716877	0.7	0.685869
80	1.159091	1.032935	0.945386	0.881291	0.832531	0.794366	0.763837	0.739008	0.718556	0.701545	0.687296
100	1.160682	1.034524	0.946877	0.882661	0.833782	0.795505	0.764877	0.739959	0.719428	0.702348	0.688038

Figure 4.18 and Table 19 shows AWIG Inverse Delta shape COP migration as HC changes at different AOA. The COP values is negative indicating that it has migrated toward trailing edge in longitudinal position as HC increases from 20% to 100% (OGE). The COP location migrated from 1.134557 m to 0.6880383 m in chord direction as the AOA changed from 0◦ to 10◦. The maximum and minimum increment as the HC rise is about -2.6125% and -3.391448276% of its original position. It was also observed that the COP migrated as much as 45.21554% towards only leading edge from 0◦ to 10°.

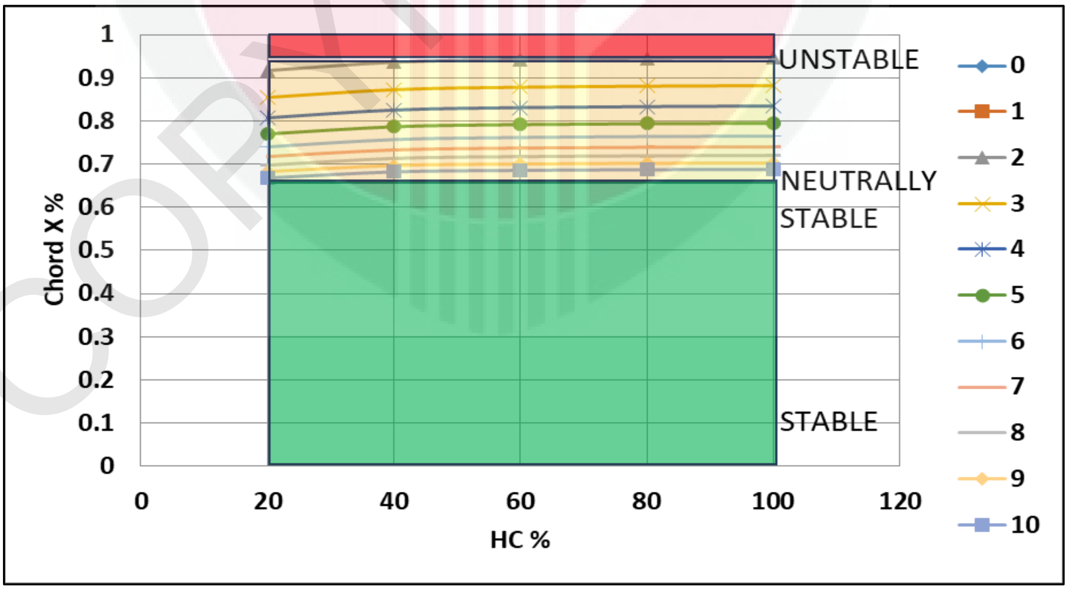

Figure 4.19: AWIG Inverse Delta wing configuration COP migration percentage increment from 20% HC to 100% HC° at various AOA

Table 20: AWIG Inverse Delta wing configuration COP migration percentage increment from 20% HC to 100% HC° at various AOA

HC %/AOA	0	1	2	3	4	5	6	7	8	9	10
20	1.134557	1.004387	0.916723	0.853812	0.806602	0.769996	0.740901	0.717334	0.697963	0.681863	0.668368
40	1.150644	1.023658	0.936319	0.872776	0.824657	0.78712	0.757176	0.732873	0.712887	0.696288	0.682402
60	1.156295	1.030004	0.942577	0.878682	0.830138	0.792178	0.761839	0.737179	0.716877	0.7	0.685869
80	1.159091	1.032935	0.945386	0.881291	0.832531	0.794366	0.763837	0.739008	0.718556	0.701545	0.687296
100	1.160682	1.034524	0.946877	0.882661	0.833782	0.795505	0.764877	0.739959	0.719428	0.702348	0.688038

Figure 4.19 and Table 20 AWIG Inverse Delta shape COP migration on every AOA increment. It was found that, when CG enters or moves inside the green region, it indicates that it is stable longitudinally. The yellow to red region indicates that it will unstable when CG enters these regions. The location of COP is located at 68.8% Chord when it is OGE, and when the it flies closer to the ground (IGE) the location of COP move towards Leading Edge (LE), and it is located at 113% Chord when H/C = 0.2.

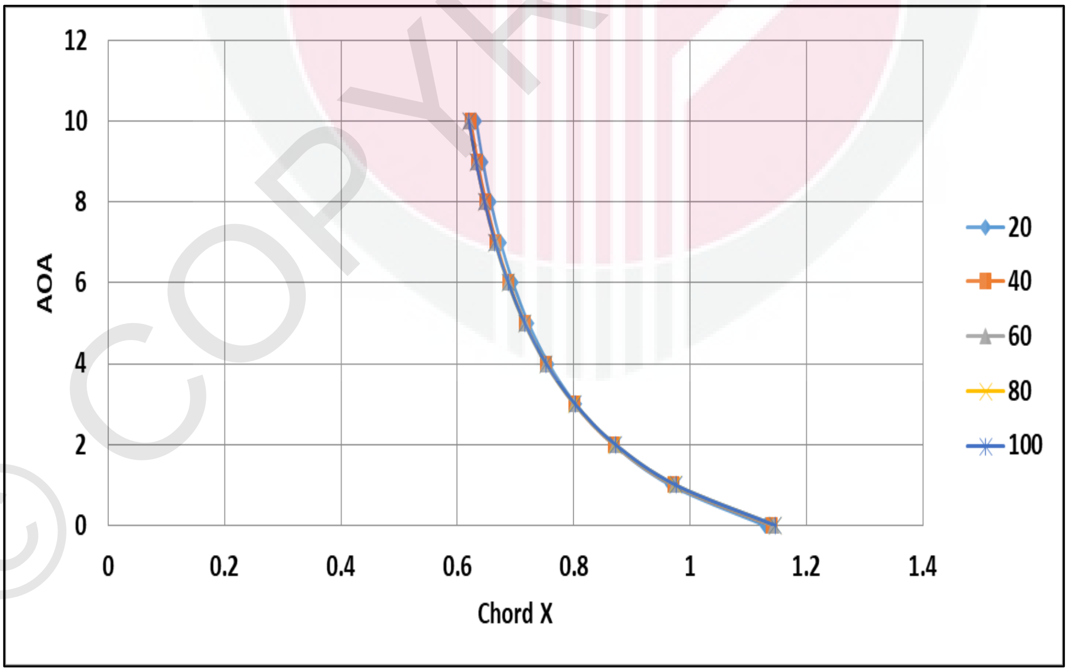

Figure 4.20: DHMTU rectangular wing configuration COP migration

Table 21: DHMTU rectangular wing configuration COP migration

HC %/AOA	0	1	2	3	4	5	6	7	8	9	10
20	1.129506	0.967107	0.869046	0.803595	0.756976	0.72224	0.695501	0.674419	0.657498	0.64374	0.632449
40	1.140012	0.970901	0.868858	0.800769	0.75227	0.716122	0.688283	0.666315	0.648663	0.634288	0.622469
60	1.14391	0.973385	0.870249	0.801325	0.752176	0.715511	0.687249	0.664931	0.646982	0.632352	0.620311
80	1.145856	0.974859	0.871284	0.802001	0.752561	0.715659	0.687202	0.664719	0.64663	0.63188	0.619734
100	1.146983	0.975757	0.871961	0.802493	0.752904	0.71588	0.687321	0.664753	0.646592	0.631779	0.619578

Figure 4.20 and Table 21 shows how DHMTU rectangular shape COP migrated as HC changes at different AOA. The COP values is a mix of negative and positive value which indicated that the COP has migrated toward trailing edge from 0◦ to 5◦ and migrated back towards leading edge from 6◦ to 10◦ of AOA in longitudinal position as HC increases from 20% to 100% (OGE). The COP location migrated from 1.129506 m to 0.6195784 m in chord direction as the AOA changed from 0◦ to 10◦. The maximum and minimum increment as the HC rise is about -1.7477% and 1.2871% of its original position. It was also observed that the COP migrated as much as 50.99276% towards only leading edge from 0◦ to 10°.

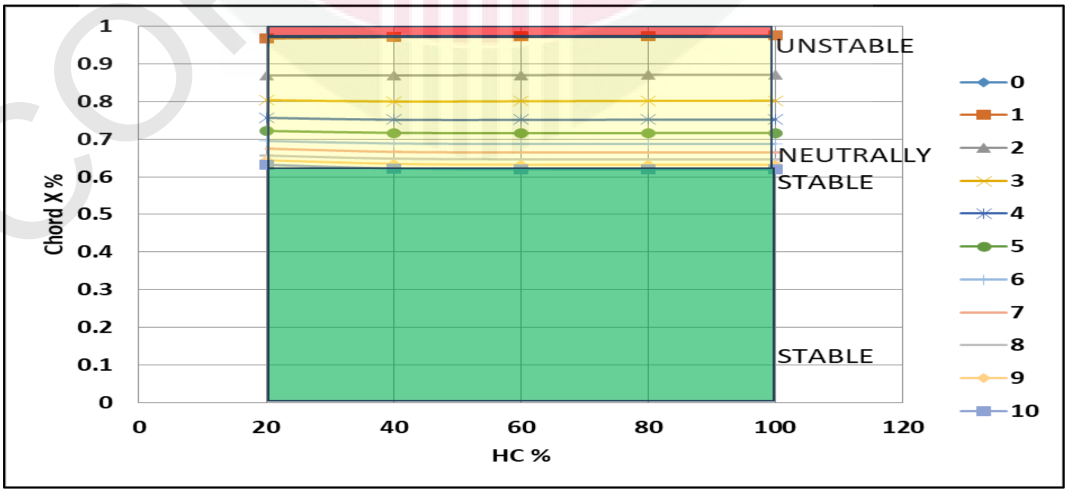

Figure 4.21: DHMTU rectangular wing configuration COP migration percentage increment from 20% HC to 100% HC° at various AOA

Table 22: DHMTU rectangular wing configuration COP migration percentage increment from 20% HC to 100% HC° at various AOA

HC %/AOA	0	1	2	3	4	5	6	7	8	9	10
20	1.129506	0.967107	0.869046	0.803595	0.756976	0.72224	0.695501	0.674419	0.657498	0.64374	0.632449
40	1.140012	0.970901	0.868858	0.800769	0.75227	0.716122	0.688283	0.666315	0.648663	0.634288	0.622469
60	1.14391	0.973385	0.870249	0.801325	0.752176	0.715511	0.687249	0.664931	0.646982	0.632352	0.620311
80	1.145856	0.974859	0.871284	0.802001	0.752561	0.715659	0.687202	0.664719	0.64663	0.63188	0.619734
100	1.146983	0.975757	0.871961	0.802493	0.752904	0.71588	0.687321	0.664753	0.646592	0.631779	0.619578

Figure 4.21 and Table 22 shows DHMTU COP migration on every AOA increment. It was found that, when CG enters or moves inside the green region, it indicates that it is stable longitudinally. The yellow to red region indicates that it will unstable when CG enters these regions. The location of COP is located at 61.95% Chord when it is OGE, and when the it flies closer to the ground (IGE) the location of COP move towards Leading Edge (LE), and it is located at 113% Chord when H/C = 0.2.

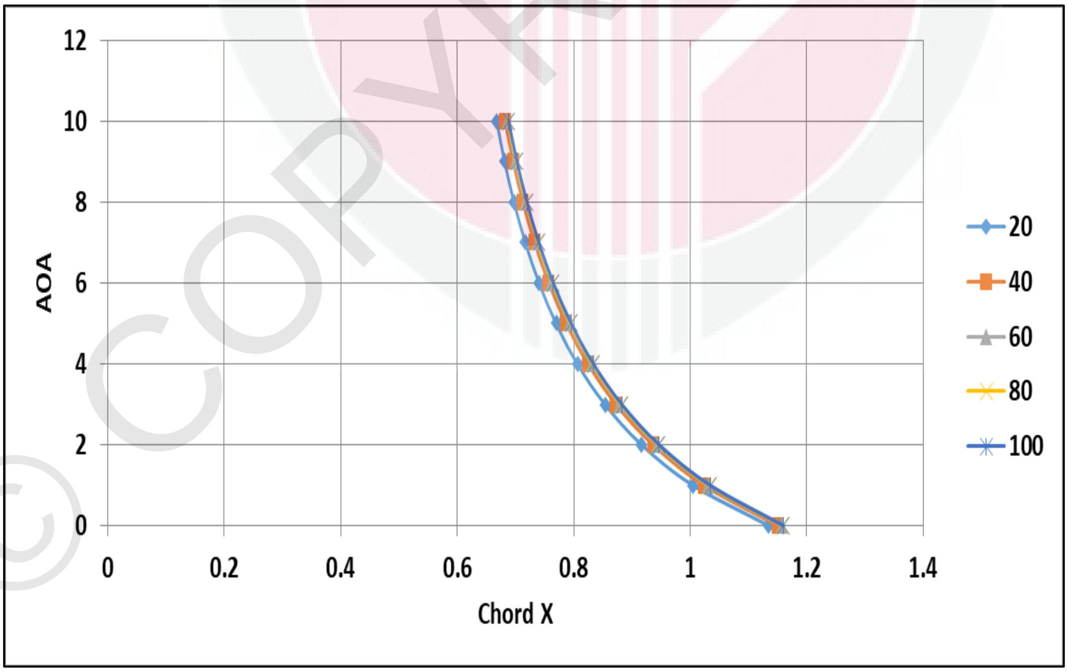

Figure 4.22: DHMTU Inverse Delta wing configuration COP migration

Table 23: DHMTU Inverse Delta wing configuration COP migration

HC %/AOA	0	1	2	3	4	5	6	7	8	9	10
20	1.134557	1.004387	0.916723	0.853812	0.806602	0.769996	0.740901	0.717334	0.697963	0.681863	0.668368
40	1.150644	1.023658	0.936319	0.872776	0.824657	0.78712	0.757176	0.732873	0.712887	0.696288	0.682402
60	1.156295	1.030004	0.942577	0.878682	0.830138	0.792178	0.761839	0.737179	0.716877	0.7	0.685869
80	1.159091	1.032935	0.945386	0.881291	0.832531	0.794366	0.763837	0.739008	0.718556	0.701545	0.687296
100	1.160682	1.034524	0.946877	0.882661	0.833782	0.795505	0.764877	0.739959	0.719428	0.702348	0.688038

Figure 4.22 and Table 23 shows DHMTU Inverse Delta shape COP migration as HC changes at different AOA. The COP values is negative indicated that it has migrated toward trailing edge in longitudinal position as HC increases from 20% to 100% (OGE). The COP location migrated from 1.134557 m to 0.6880383 m in chord direction as the AOA changed from 0◦ to 10◦. The maximum and minimum increment as the HC rise is about -2.6125% and -3.391448276% of its original position. It was also observed that the COP migrated as much as 45.21554% towards only leading edge from 0◦ to 10°.

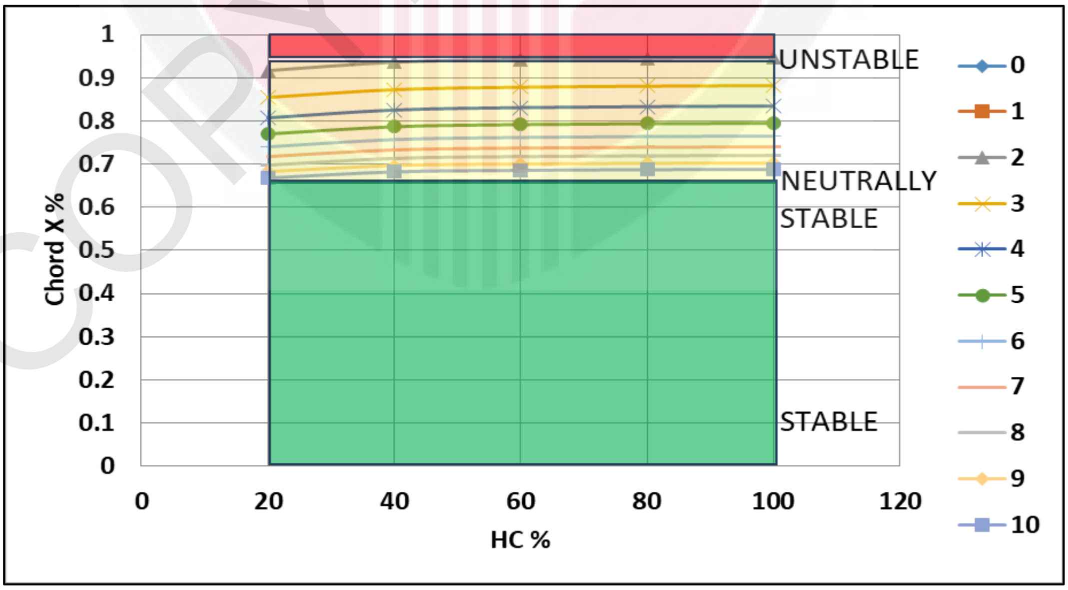

Figure 4.23: DHMTU Inverse Delta wing configuration COP migration percentage increment from 20% HC to 100% HC° at various AOA

Table 24: DHMTU Inverse Delta wing configuration COP migration percentage increment from 20% HC to 100% HC° at various AOA

HC %/AOA	0	1	2	3	4	5	6	7	8	9	10
20	1.134557	1.004387	0.916723	0.853812	0.806602	0.769996	0.740901	0.717334	0.697963	0.681863	0.668368
40	1.150644	1.023658	0.936319	0.872776	0.824657	0.78712	0.757176	0.732873	0.712887	0.696288	0.682402
60	1.156295	1.030004	0.942577	0.878682	0.830138	0.792178	0.761839	0.737179	0.716877	0.7	0.685869
80	1.159091	1.032935	0.945386	0.881291	0.832531	0.794366	0.763837	0.739008	0.718556	0.701545	0.687296
100	1.160682	1.034524	0.946877	0.882661	0.833782	0.795505	0.764877	0.739959	0.719428	0.702348	0.688038

Figure 4.23 and Table 24 shows DHMTU Inverse Delta shape COP migration on every AOA increment. It was found that, when CG enters or moves inside the green region, it indicates that it is stable longitudinally. The yellow to red region indicates that it will unstable when CG enters these regions. The location of COP is located at 68.8% Chord when it is OGE, and when the it flies closer to the ground (IGE) the location of COP move towards Leading Edge (LE), and it is located at 113% Chord when H/C = 0.2.

***See Appendix B**

BIXEL Patent

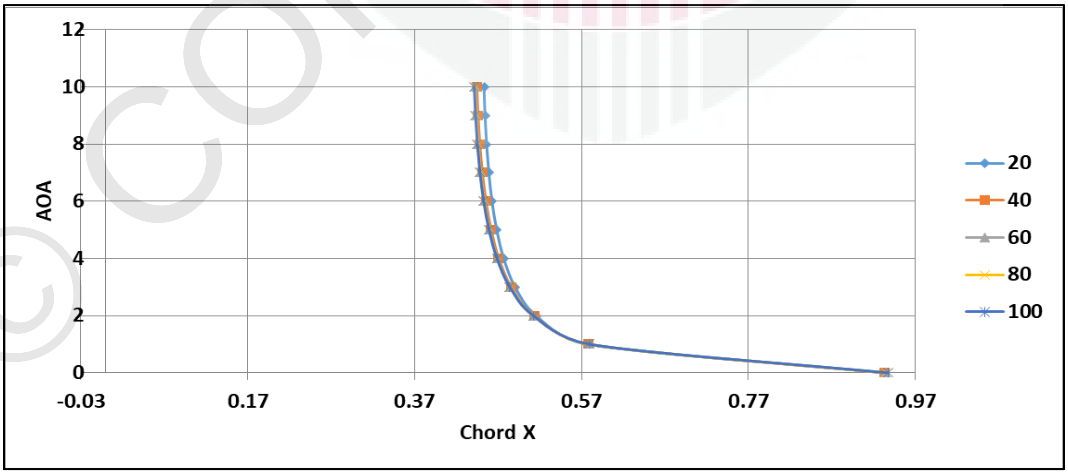

Figure 4.24: Bixel 0.25 AR double wing configuration COP migration

Table 25: Bixel 0.25 AR double wing configuration COP migration

HC %/AOA	0	1	2	3	4	5	6	7	8	9	10
20	0.933356	0.577118	0.515843	0.490532	0.476831	0.468376	0.462771	0.458914	0.456224	0.45437	0.453147
40	0.933112	0.578582	0.513225	0.485832	0.4709	0.461639	0.455467	0.45119	0.448178	0.446068	0.444636
60	0.934644	0.578964	0.512629	0.484754	0.469541	0.460096	0.453796	0.449424	0.446339	0.444172	0.442693
80	0.935633	0.579188	0.512466	0.484406	0.469086	0.459573	0.453225	0.448818	0.445706	0.443517	0.442022
100	0.937618	0.579704	0.512512	0.484237	0.468795	0.459204	0.452803	0.448358	0.445218	0.443009	0.441497
%	-0.43938	-0.26658	0.343474	0.64899	0.828454	0.945588	1.02768	1.088216	1.134629	1.17132	1.201052

Figure 4.24 and Table 25 shows a Bixel 0.25 AR Double wing configuration COP migration as HC changes at different AOA. The COP values is a mix of negative and positive value which indicated that its COP migrated toward trailing edge from 0◦ to 2◦ and migrated back towards leading edge from 3◦ to 10◦ of AOA in longitudinal position as HC increases from 20% to 100% (OGE). The COP location migrated to 0.933356 m to 0.441497 m in chord direction as the AOA changed from 0◦ to 10◦. The maximum and minimum increment as the HC rise is about 1.201052% and 0.26658% of its original position. It was also observed that the COP migrated as much as 50.38351% towards only leading edge from 0◦ to 10°.

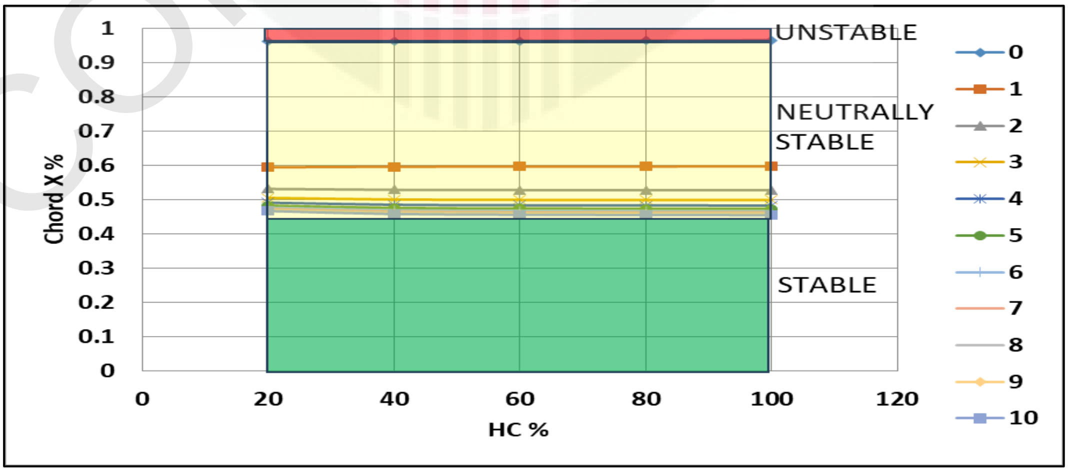

Figure 4.25: Bixel 0.25 AR double wing configuration COP migration percentage increment from 20% HC to 100% HC° at various AOA

Table 26: Bixel 0.25 AR double wing configuration COP migration percentage increment from 20% HC to 100% HC° at various AOA

HC %/AOA	0	1	2	3	4	5	6	7	8	9	10
20	0.962223	0.594967	0.531797	0.505703	0.491578	0.482862	0.477084	0.473107	0.470334	0.468423	0.467162
40	0.961971	0.596476	0.529098	0.500857	0.485464	0.475916	0.469554	0.465145	0.462039	0.459864	0.458388
60	0.96355	0.59687	0.528483	0.499746	0.484062	0.474326	0.467831	0.463324	0.460144	0.457909	0.456385
80	0.96457	0.597101	0.528315	0.499388	0.483594	0.473786	0.467242	0.462699	0.459491	0.457234	0.455693
100	0.966617	0.597632	0.528362	0.499213	0.483294	0.473406	0.466807	0.462225	0.458988	0.45671	0.455152

Figure 4.25 and Table 26 shows a Bixel 0.25 AR Double wing configuration COP migration on every AOA increment. It was found that, when CG enters or moves inside the green region, it indicates that it is stable longitudinally. The yellow to red region indicates that it will unstable when CG enters these regions. The location of COP is located at 96.67% Chord when it is OGE, and when the it flies closer to the ground (IGE) the location of COP move towards Leading Edge (LE), and it is located at 46.72% Chord when H/C = 0.2.

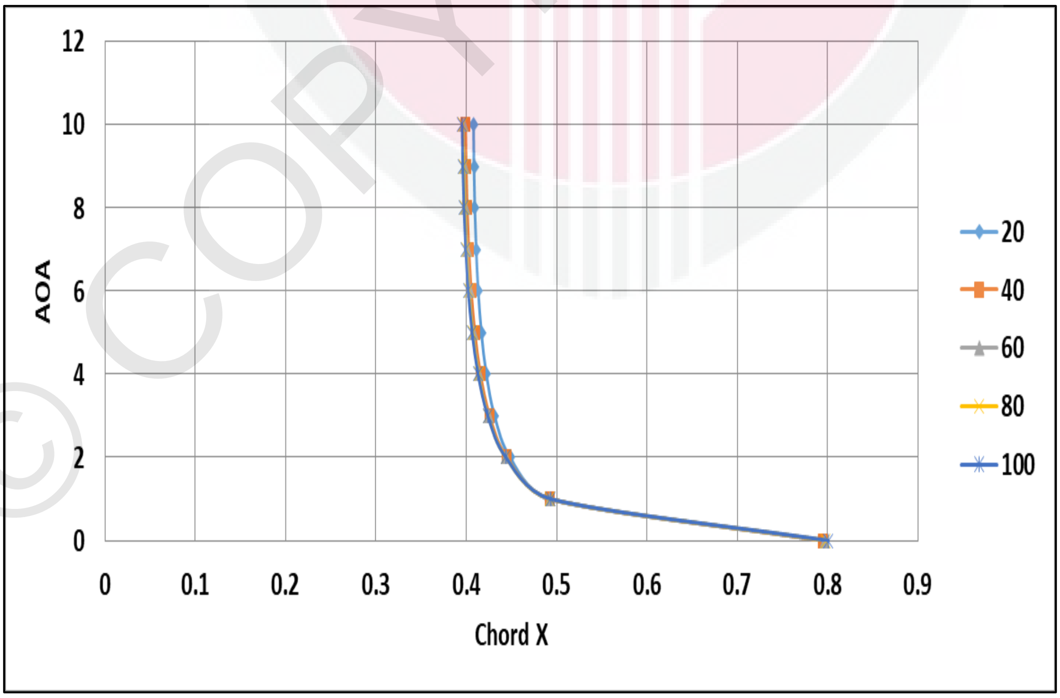

Figure 4.26: Bixel 0.33 AR double wing configuration COP migration

Table 27: Bixel 0.33 AR double wing configuration COP migration

HC %/AOA	0	1	2	3	4	5	6	7	8	9	10
20	0.79472	0.492001	0.448524	0.431275	0.422181	0.416717	0.413213	0.410912	0.409419	0.408508	0.408042
40	0.795004	0.492619	0.44513	0.425952	0.415736	0.409536	0.405511	0.402818	0.401018	0.399858	0.399183
60	0.796942	0.492822	0.444259	0.424579	0.414075	0.407688	0.403532	0.400742	0.398866	0.397645	0.396921
80	0.798228	0.492989	0.443975	0.424089	0.413468	0.407006	0.402797	0.399969	0.398063	0.39682	0.396077
100	0.800869	0.493504	0.44392	0.423784	0.413024	0.406474	0.402205	0.399334	0.397397	0.396131	0.39537
%	-0.73202	-0.17893	0.54819	0.891786	1.090155	1.219357	1.31044	1.378345	1.431131	1.473548	1.50856

Figure 4.26 and Table 27 shows a Bixel 0.33 AR Double wing configuration COP migration as HC changes at different AOA. The COP values is a mix of negative and positive value which indicated that its COP migrated toward trailing edge from 0◦ to 1◦ and migrated back towards leading edge from 2◦ to 10◦ of AOA in longitudinal position as HC increases from 20% to 100% (OGE). The COP location migrated from 0.79472 m to 0.39537 m in chord direction as the AOA changed from 0◦ to 10◦. The maximum increment as the HC rise is about 0.73202% and 1.50856% of its original position. It was also observed that the COP migrated as much as 47.08769% towards only leading edge from 0◦ to 10°.

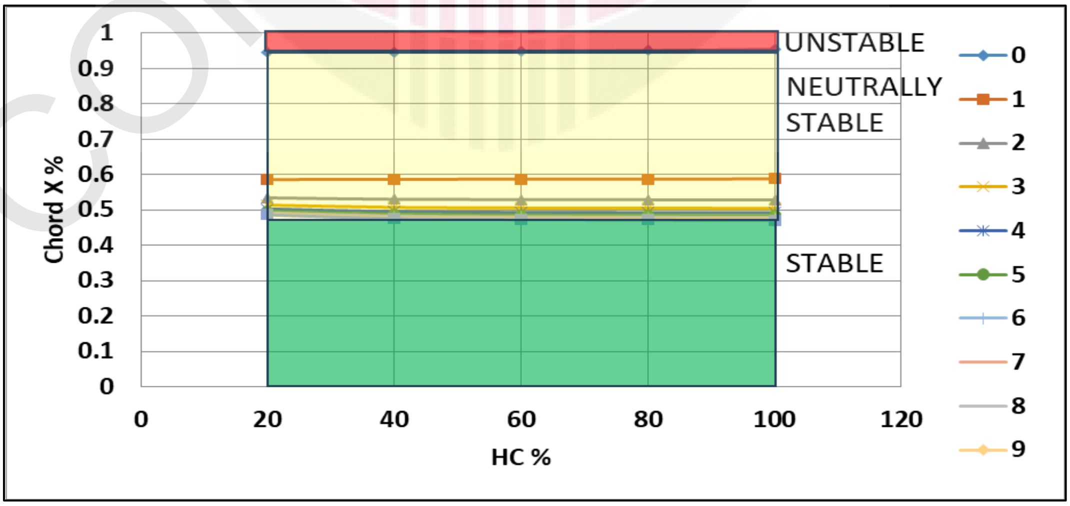

Figure 4.27: Bixel 0.33 AR double wing configuration COP migration percentage increment from 20% HC to 100% HC° at various AOA

Table 28: Bixel 0.33 AR double wing configuration COP migration percentage increment from 20% HC to 100% HC° at various AOA

HC %/AOA	0	1	2	3	4	5	6	7	8	9	10
20	0.946095	0.585715	0.533958	0.513423	0.502596	0.496091	0.49192	0.489181	0.487403	0.486319	0.485765
40	0.946433	0.586451	0.529917	0.507086	0.494924	0.487543	0.482751	0.479545	0.477402	0.476021	0.475218
60	0.94874	0.586693	0.52888	0.505452	0.492947	0.485343	0.480395	0.477073	0.47484	0.473387	0.472525
80	0.950271	0.586892	0.528541	0.504868	0.492224	0.484531	0.479521	0.476153	0.473885	0.472405	0.47152
100	0.953415	0.587505	0.528476	0.504505	0.491695	0.483898	0.478816	0.475398	0.473092	0.471584	0.470679

Figure 4.27 and Table 28 shows a Bixel 0.33 AR Double wing configuration COP migration on every AOA increment. It was found that, when CG enters or moves inside the green region, it indicates that it is stable longitudinally. The yellow to red region indicates that it will unstable when CG enters these regions. The location of COP is located at 95.34% Chord when it is OGE, and when the it flies closer to the ground (IGE) the location of COP move towards Leading Edge (LE), and it is located at 48.57% Chord when H/C = 0.2.

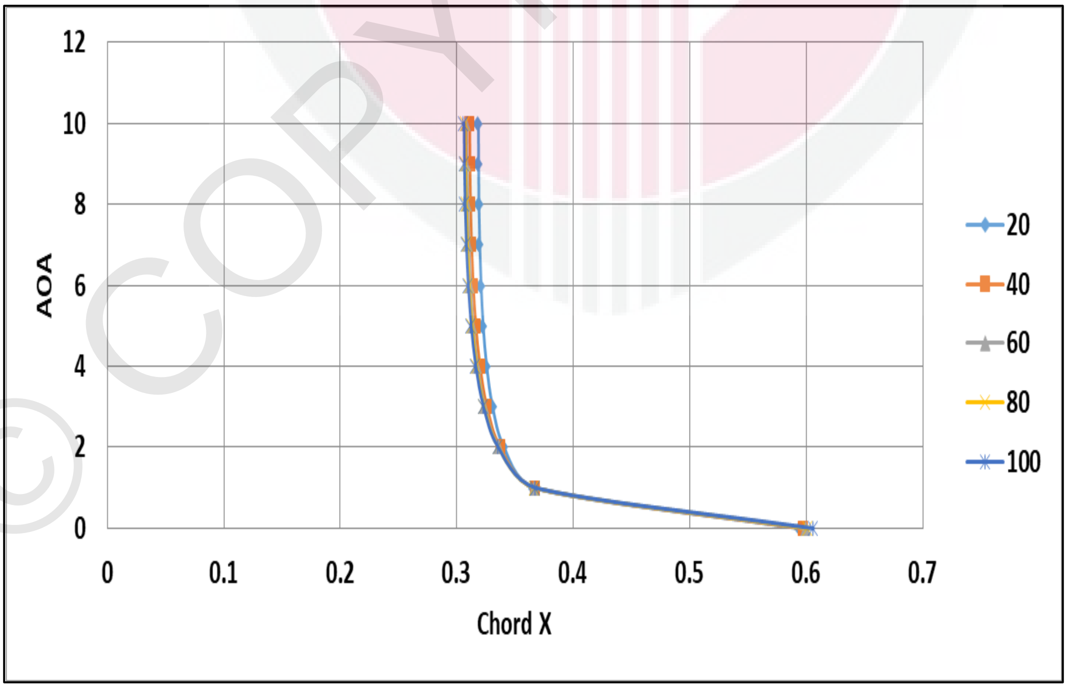

Figure 4.28: Bixel 0.50 AR double wing configuration COP migration

Table 29: Bixel 0.50 AR double wing configuration COP migration

HC %/AOA	0	1	2	3	4	5	6	7	8	9	10
20	0.594886	0.366603	0.340592	0.330695	0.325612	0.322639	0.3208	0.319657	0.318983	0.318651	0.318582
40	0.596792	0.367124	0.337437	0.325898	0.319893	0.31633	0.31408	0.312634	0.311728	0.311212	0.310994
60	0.599837	0.367251	0.336288	0.32419	0.317872	0.31411	0.311723	0.310177	0.309196	0.308621	0.308356
80	0.601909	0.367389	0.335839	0.323488	0.31703	0.313179	0.310732	0.309143	0.308129	0.30753	0.307245
100	0.606172	0.367981	0.335647	0.322969	0.316333	0.312373	0.309852	0.308212	0.307162	0.306537	0.306234
%	-1.65972	-0.20256	0.727103	1.136206	1.364574	1.509809	1.61	1.683015	1.738368	1.7815	1.815853

Figure 4.28 and Table 29 shows the Bixel 0.5 AR Double wing configuration COP migration as HC changes at different AOA. The COP values is a mix of negative and positive value which indicated that its COP migrated toward trailing edge from 0◦ to 1◦ and migrated back towards leading edge from 2◦ to 10◦ of AOA in longitudinal position as HC increases from 20% to 100% (OGE). The COP location migrates from 0.594886 m to 0.306234 m in chord direction as the AOA changed from 0◦ to 10◦. The maximum increment as the HC rise is about 1.815853% and 0.20256% of its original position. It was also observed that the COP migrated as much as 41.74878% towards only leading edge from 0◦ to 10°.

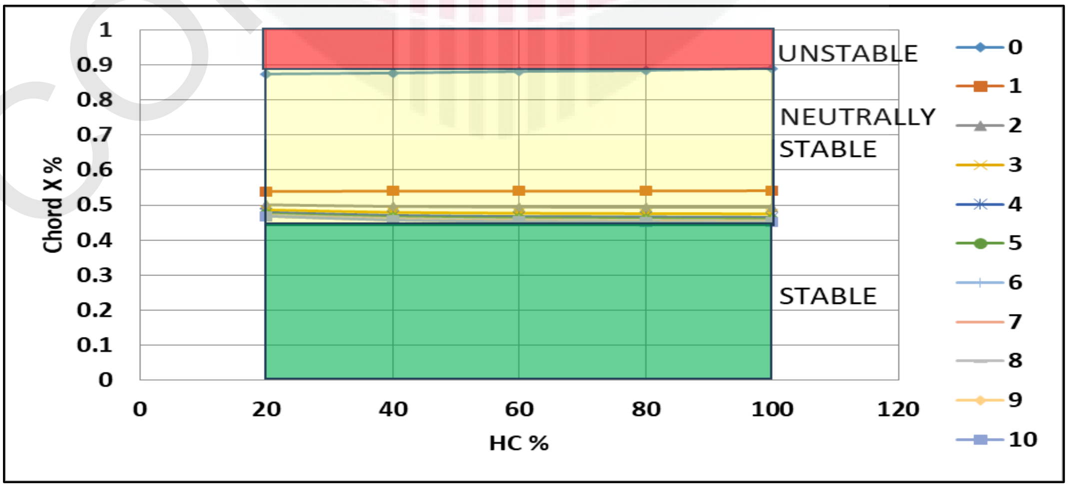

Figure 4.29: Bixel 0.50 AR double wing configuration COP migration percentage increment from 20% HC to 100% HC° at various AOA

Table 30: Bixel 0.50 AR double wing configuration COP migration percentage increment from 20% HC to 100% HC° at various AOA

HC %/AOA	0	1	2	3	4	5	6	7	8	9	10
20	0.874832	0.539122	0.50087	0.486316	0.478842	0.47447	0.471765	0.470083	0.469093	0.468604	0.468503
40	0.877635	0.539888	0.49623	0.479262	0.470431	0.465191	0.461882	0.459756	0.458424	0.457665	0.457345
60	0.882113	0.540075	0.494541	0.47675	0.467459	0.461926	0.458416	0.456143	0.4547	0.453855	0.453465
80	0.885161	0.540278	0.493881	0.475717	0.46622	0.460558	0.456959	0.454622	0.453131	0.452249	0.451831
100	0.89143	0.541148	0.493599	0.474954	0.465196	0.459371	0.455665	0.453253	0.451709	0.450789	0.450345

Figure 4.29 and Table 30 shows a Bixel 0.5 AR Double wing configuration COP migration on every AOA increment. It was found that, when CG enters or moves inside the green region, it indicates that it is stable longitudinally. The yellow to red region indicates that it will unstable when CG enters these regions. The location of COP is located at 89.14% Chord when it is OGE, and when the it flies closer to the ground (IGE) the location of COP move towards Leading Edge (LE), and it is located at 46.85% Chord when H/C = 0.2.

***See Appendix B**

4.2 Center of Pressure Migration Simulation Results for Six type of Airfoils with UH18-SPW Planform Area

4.2.1 Naca 0012 & Flat Surface

Figure 4.30 and Table 31 shows how Naca0012 with UH18-SPW planform area COP migrated as HC changes at different AOA. The COP values is negative indicated that it has migrated toward trailing edge (TE) in longitudinal position as HC increases from 20% to 100%(OGE).

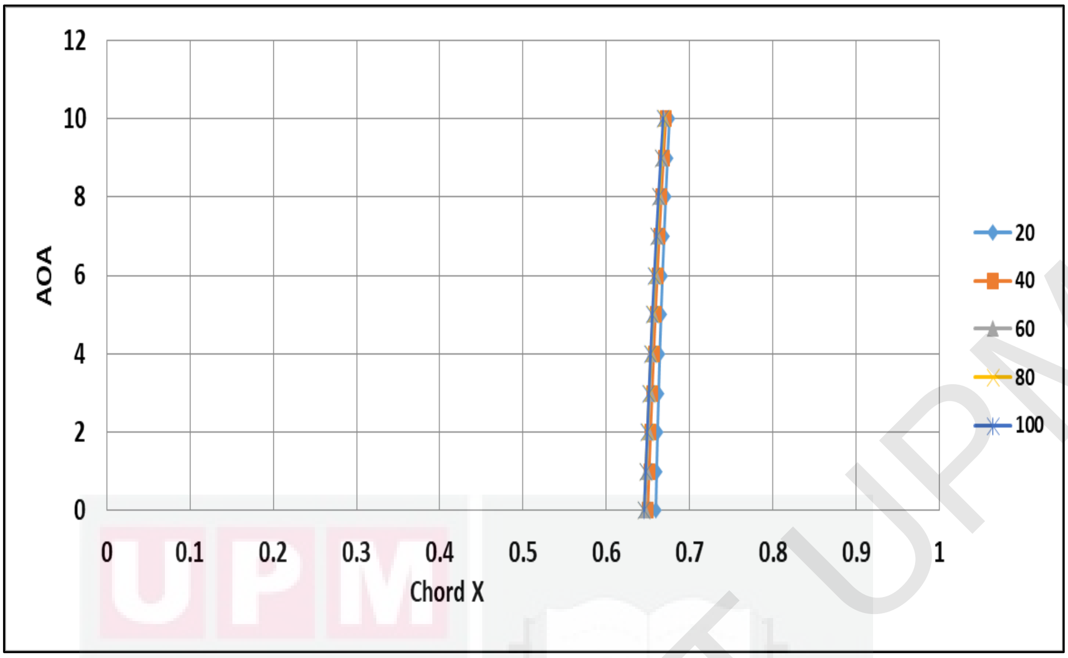

Figure 4.30: Naca0012 with UH18-SPW planform area COP migration

Table 31: Naca0012 with UH18-SPW planform area COP migration

HC %/AOA	0	1	2	3	4	5	6	7	8	9	10
20	0.659234	0.660203	0.661325	0.662602	0.664037	0.665631	0.667384	0.669296	0.671369	0.673603	0.675997
40	0.649881	0.651555	0.653283	0.655099	0.657026	0.659081	0.661273	0.66361	0.666099	0.668744	0.671549
60	0.646853	0.648673	0.65053	0.652465	0.654504	0.656666	0.658963	0.661405	0.663999	0.666749	0.669661
80	0.645687	0.647547	0.649442	0.651414	0.65349	0.655688	0.658021	0.6605	0.663132	0.665921	0.668874
100	0.645126	0.647001	0.648912	0.650899	0.65299	0.655204	0.657554	0.66005	0.662699	0.665508	0.66848

The COP location migrated from 0.6592341 m to 0.6684798m in chord direction as the HC rise from 20% to true flight (TF). The minimum and maximum increment as the HC rise is about 2.82172% and 0.75175% of its original position. It was also observed that the COP migrated as much as -0.82769% towards leading edge from 0◦ to 10°.

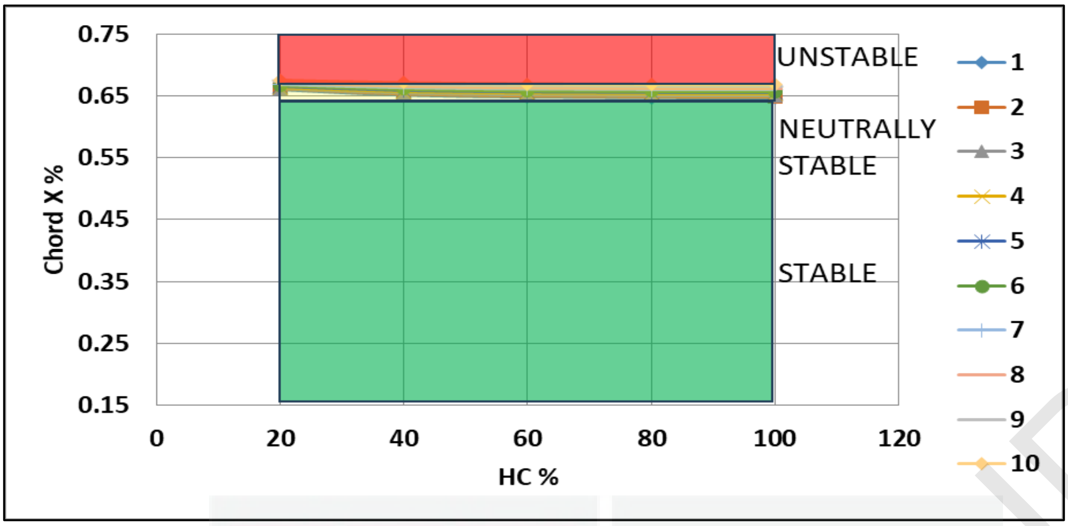

Figure 4.31: Naca0012 with UH18-SPW planform area COP migration percentage increment from 20% HC to 100% HC° at various AOA

Table 32: Naca0012 with UH18-SPW planform area COP migration percentage increment from 20% HC to 100% HC° at various AOA

HC %/AOA	0	1	2	3	4	5	6	7	8	9	10
20	0.659234	0.660203	0.661325	0.662602	0.664037	0.665631	0.667384	0.669296	0.671369	0.673603	0.675997
40	0.649881	0.651555	0.653283	0.655099	0.657026	0.659081	0.661273	0.66361	0.666099	0.668744	0.671549
60	0.646853	0.648673	0.65053	0.652465	0.654504	0.656666	0.658963	0.661405	0.663999	0.666749	0.669661
80	0.645687	0.647547	0.649442	0.651414	0.65349	0.655688	0.658021	0.6605	0.663132	0.665921	0.668874
100	0.645126	0.647001	0.648912	0.650899	0.65299	0.655204	0.657554	0.66005	0.662699	0.665508	0.66848

Figure 4.31 and Table 32 shows Naca0012 with UH18-SPW planform area COP migration on every AOA increment. It was found that, when CG enters or moves inside the green region, it indicates that it is stable longitudinally. The yellow to red region indicates that it will unstable when CG enters these regions. The location of COP is located at 66.84% Chord when it is OGE, and when the it flies closer to the ground (IGE) the location of COP move towards Leading Edge (LE), and it is located at 65.92% Chord when H/C = 0.2.

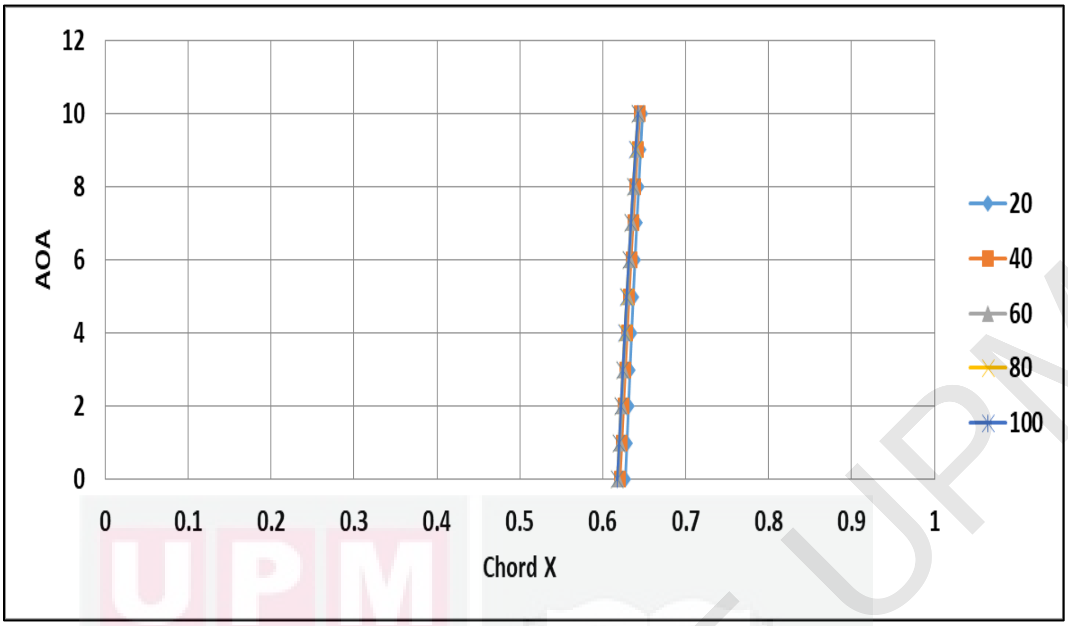

Figure 4.32: Flat Surface with UH18-SPW planform area COP migration

Table 33: Flat Surface with UH18-SPW planform area COP migration

HC %/AOA	0	1	2	3	4	5	6	7	8	9	10
20	0.627533	0.629442	0.631298	0.633163	0.635076	0.637063	0.639144	0.641331	0.643635	0.64594	0.648244
40	0.621028	0.623229	0.625371	0.627518	0.629713	0.631984	0.634353	0.636835	0.63944	0.642177	0.645054
60	0.618773	0.621014	0.623202	0.625401	0.627652	0.629985	0.632418	0.634968	0.637646	0.640461	0.643419
80	0.617834	0.620085	0.622288	0.624504	0.626775	0.62913	0.631588	0.634164	0.636871	0.639716	0.642707
100	0.617374	0.619628	0.621836	0.624059	0.626338	0.628703	0.631172	0.633761	0.636482	0.639342	0.642349

Figure 4.32 and Table 33 shows how Flat Surface with UH18-SPW planform area COP migrated as HC changes at different AOA. The COP values is positive indicated that it has migrated toward leading edge (TE) in longitudinal position when HC increases from 20 % to 100 %(OGE) and as AOA increased. The COP location migrated from 0.6275327 m to 0.6423492 m in chord direction as the HC rise from 20 % to true flight (TF). The minimum and maximum increment as the HC rise is about 1.01589 % and 0.5895 % of its original position. It was also observed that the COP migrated as much as -1.48165 % towards only trailing edge from 0◦ to 10°.

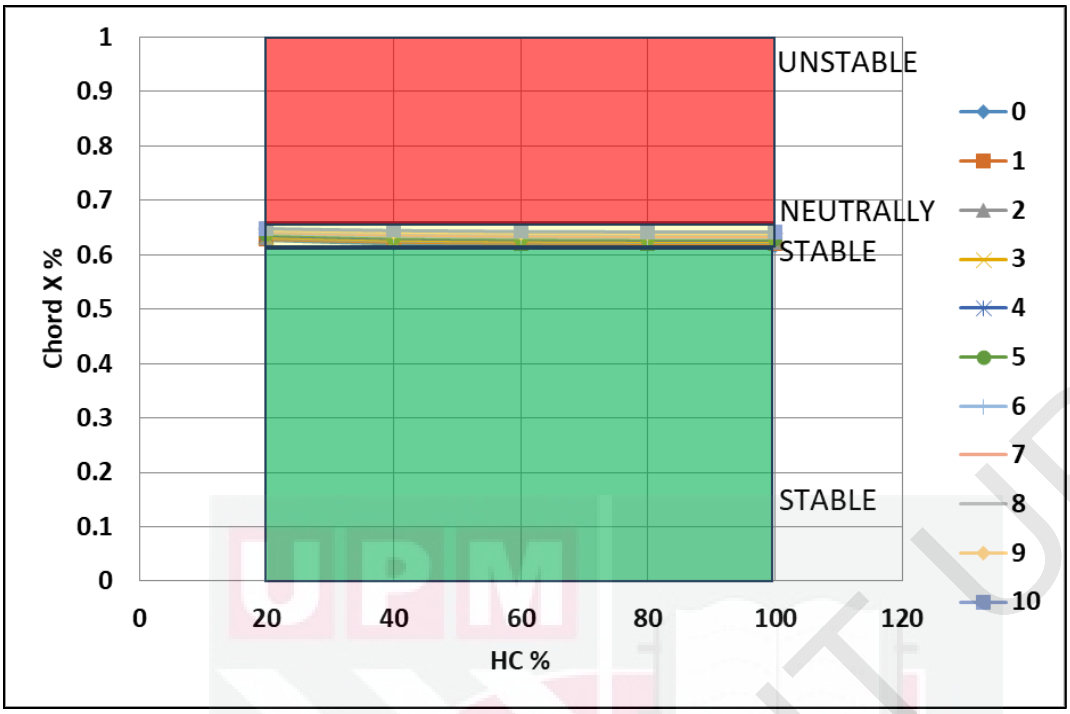

Figure 4.33: Flat Surface with UH18-SPW planform area COP migration percentage increment from 20% HC to 100% HC° at various AOA

Table 34: Flat Surface with UH18-SPW planform area COP migration percentage increment from 20% HC to 100% HC° at various AOA

HC %/AOA	0	1	2	3	4	5	6	7	8	9	10
20	0.627533	0.629442	0.631298	0.633163	0.635076	0.637063	0.639144	0.641331	0.643635	0.64594	0.648244
40	0.621028	0.623229	0.625371	0.627518	0.629713	0.631984	0.634353	0.636835	0.63944	0.642177	0.645054
60	0.618773	0.621014	0.623202	0.625401	0.627652	0.629985	0.632418	0.634968	0.637646	0.640461	0.643419
80	0.617834	0.620085	0.622288	0.624504	0.626775	0.62913	0.631588	0.634164	0.636871	0.639716	0.642707
100	0.617374	0.619628	0.621836	0.624059	0.626338	0.628703	0.631172	0.633761	0.636482	0.639342	0.642349

Figure 4.33 and Table 34 shows Flat Surface with UH18-SPW planform area COP migration on every AOA increment. It was found that, when CG enters or moves inside the green region, it indicates that it is stable longitudinally. The yellow to red region indicates that it will unstable when CG enters these regions. The location of COP is located at 64.23% Chord when it is OGE, and when the it flies closer to the ground (IGE) the location of COP move towards Trailing Edge (TE), and it is located at 62.73% Chord when H/C = 0.2.

4.2.2 Naca 4412 & Clark Y

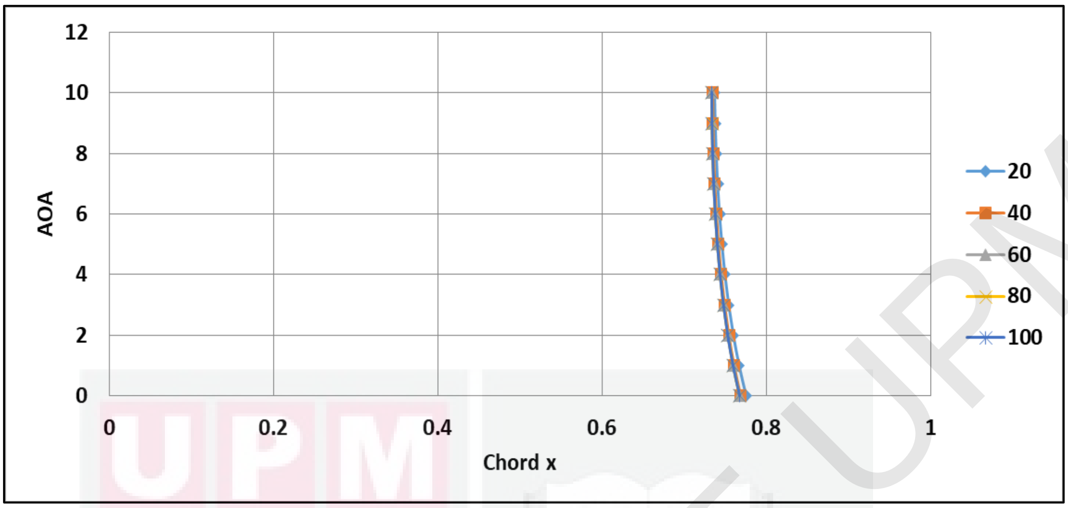

Figure 4.34: Naca4412 with UH18-SPW planform area COP migration

Table 35: Naca4412 with UH18-SPW planform area COP migration

HC %/AOA	0	1	2	3	4	5	6	7	8	9	10
20	0.775289	0.766853	0.760012	0.754454	0.749948	0.746323	0.743447	0.741215	0.739547	0.738377	0.737653
40	0.769288	0.761274	0.754797	0.749569	0.745377	0.742058	0.739488	0.737569	0.736222	0.735386	0.735009
60	0.767993	0.760017	0.753574	0.74838	0.744225	0.740948	0.738426	0.73656	0.735274	0.734505	0.734202
80	0.767717	0.759732	0.753284	0.748088	0.743935	0.740664	0.738151	0.736298	0.735029	0.734281	0.734003
100	0.767652	0.759655	0.753198	0.747996	0.743839	0.740567	0.738056	0.736207	0.734945	0.734205	0.733937

Figure 4.34 and Table 35 shows how Naca4412 with UH18-SPW planform area COP migrated as HC changes at different AOA. The COP values is negative indicated that it has migrated toward trailing edge (TE) in longitudinal position as HC increases from 20% to 100%(OGE). The COP location migrated from 0.7752893 m to 0.7339368 m in chord direction as the HC rise from 20% to true flight (TF). The minimum and maximum increment as the HC rise is about 0.76376% and 0.3716% of its original position. It was also observed that the COP migrated as much as 2.256% towards leading edge from 0◦ to 8° and migrated back to trailing edge from 9◦ to 10°.

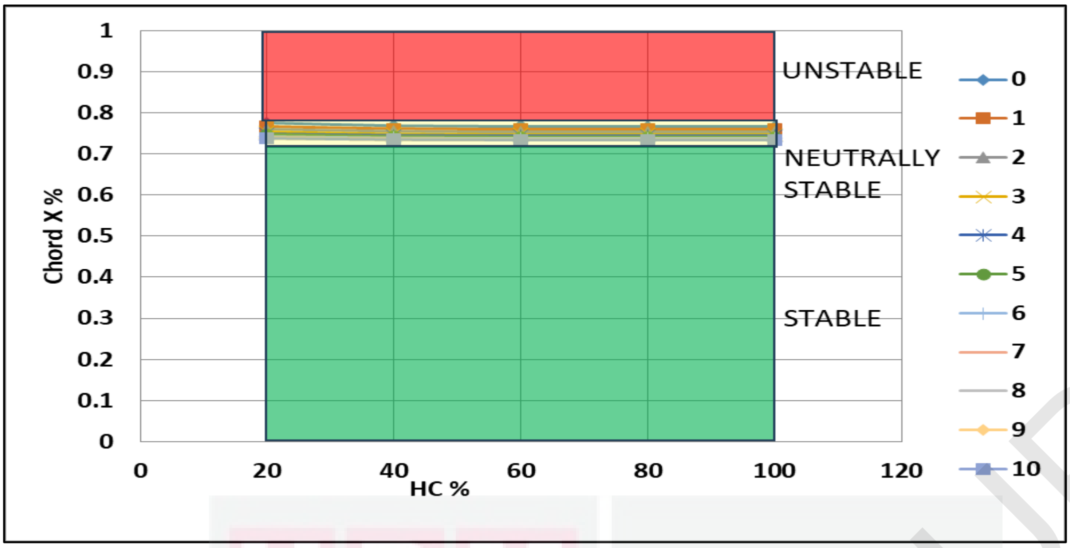

Figure 4.35: Naca4412 with UH18-SPW planform area COP migration percentage increment from 20% HC to 100% HC° at various AOA

Table 36: Naca4412 with UH18-SPW planform area COP migration percentage increment from 20% HC to 100% HC° at various AOA

HC %/AOA	0	1	2	3	4	5	6	7	8	9	10
20	0.775289	0.766853	0.760012	0.754454	0.749948	0.746323	0.743447	0.741215	0.739547	0.738377	0.737653
40	0.769288	0.761274	0.754797	0.749569	0.745377	0.742058	0.739488	0.737569	0.736222	0.735386	0.735009
60	0.767993	0.760017	0.753574	0.74838	0.744225	0.740948	0.738426	0.73656	0.735274	0.734505	0.734202
80	0.767717	0.759732	0.753284	0.748088	0.743935	0.740664	0.738151	0.736298	0.735029	0.734281	0.734003
100	0.767652	0.759655	0.753198	0.747996	0.743839	0.740567	0.738056	0.736207	0.734945	0.734205	0.733937

Figure 4.35 and Table 36 shows Naca4412 with UH18-SPW planform area COP migration on every AOA increment. It was found that, when CG enters or moves inside the green region, it indicates that it is stable longitudinally. The yellow to red region indicates that it will unstable when CG enters these regions. The location of COP is located at 73.39% Chord when it is OGE, and when the it flies closer to the ground (IGE) the location of COP move towards Leading Edge (LE), and it is located at 77.53% Chord when H/C = 0.2.

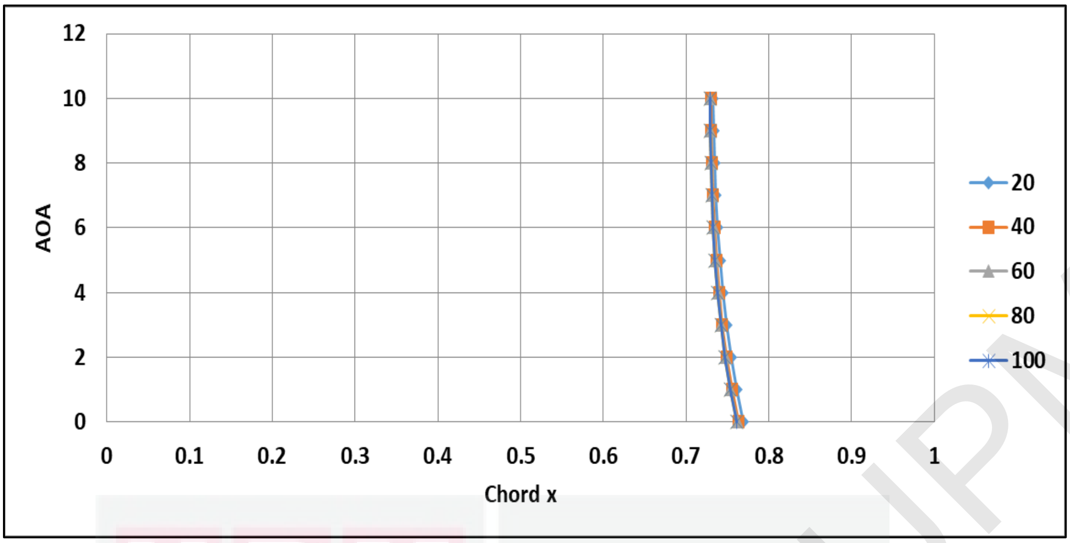

Figure 4.36: Clark Y with UH-18SPW planform area COP migration

Table 37: Clark Y with UH-18SPW planform area COP migration

HC %/AOA	0	1	2	3	4	5	6	7	8	9	10
20	0.769166	0.760793	0.754058	0.748628	0.74426	0.740775	0.738036	0.735938	0.734397	0.733348	0.732737
40	0.763172	0.755232	0.748866	0.743767	0.739712	0.736532	0.734098	0.732309	0.731087	0.730368	0.730101
60	0.761842	0.753939	0.747606	0.742541	0.738522	0.735382	0.732994	0.731258	0.730095	0.729442	0.729248
80	0.761545	0.753633	0.747293	0.742225	0.738207	0.735072	0.732692	0.730969	0.729823	0.72919	0.72902
100	0.761466	0.753541	0.747192	0.742117	0.738095	0.734959	0.73258	0.730861	0.72972	0.729096	0.728936

Figure 4.36 and Table 37 shows how Clark Y with UH18-SPW planform area COP migrated as HC changes at different AOA. The COP values is a mix of positive and negative indicated that it has migrated toward leading edge (LE) and returning migrated towards trailing edge (TE) in longitudinal position when HC increases from 20 % to 100 % (OGE) and as AOA increased. The COP location migrated from 0.7691661 m to 0.7289358 m in chord direction as the HC rise from 20 % to true flight (TF). The minimum and maximum increment as the HC rise is about 0.77001% and 0.38011% of its original position. It was also observed that the COP migrated as much as 4.02303% towards leading edge from 0◦ to 8° and migrated back to trailing edge from 9◦ to 10°.

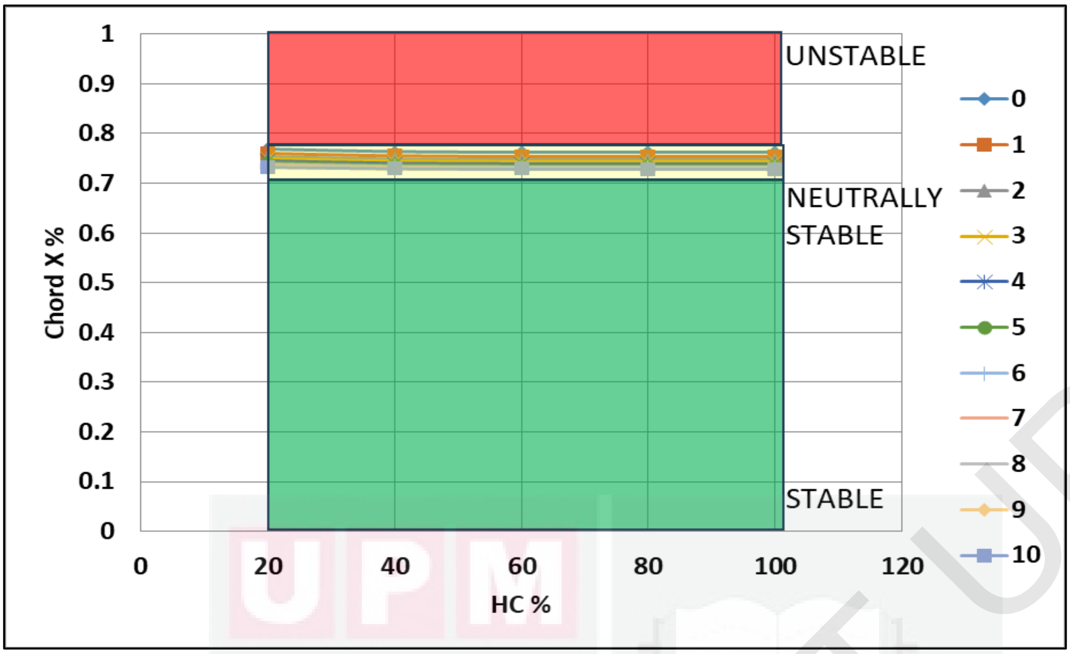

Figure 4.37: Clark Y with UH-18SPW planform area COP migration percentage increment from 20% HC to 100% HC° at various AOA

Table 38: Clark Y with UH-18SPW planform area COP migration percentage increment from 20% HC to 100% HC° at various AOA

HC %/AOA	0	1	2	3	4	5	6	7	8	9	10
20	0.769166	0.760793	0.754058	0.748628	0.74426	0.740775	0.738036	0.735938	0.734397	0.733348	0.732737
40	0.763172	0.755232	0.748866	0.743767	0.739712	0.736532	0.734098	0.732309	0.731087	0.730368	0.730101
60	0.761842	0.753939	0.747606	0.742541	0.738522	0.735382	0.732994	0.731258	0.730095	0.729442	0.729248
80	0.761545	0.753633	0.747293	0.742225	0.738207	0.735072	0.732692	0.730969	0.729823	0.72919	0.72902
100	0.761466	0.753541	0.747192	0.742117	0.738095	0.734959	0.73258	0.730861	0.72972	0.729096	0.728936

Figure 4.37 and Table 38 shows Naca4412 with UH18-SPW planform area COP migration on every AOA increment. It was found that, when CG enters or moves inside the green region, it indicates that it is stable longitudinally. The yellow to red region indicates that it will unstable when CG enters these regions. The location of COP is located at 72.89% Chord when it is OGE, and when the it flies closer to the ground (IGE) the location of COP move towards Leading Edge (LE), and it is located at 76.91% Chord when H/C = 0.2.

4.2.3 AWIG & DHMTU

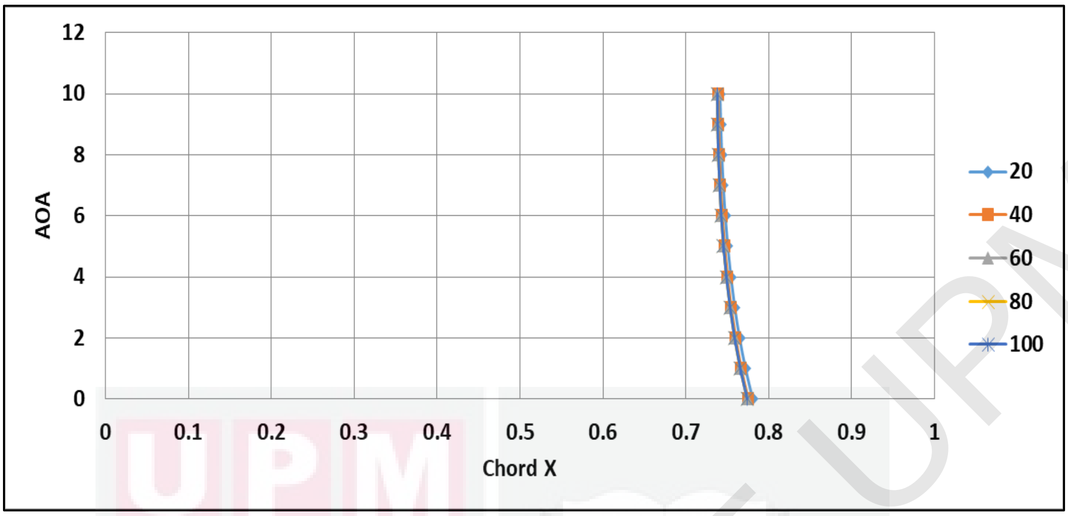

Figure 4.38: AWIG with UH18-SPW planform area COP migration

Table 39: AWIG with UH18-SPW planform area COP migration

HC %/AOA	0	1	2	3	4	5	6	7	8	9	10
20	0.781029	0.772178	0.764993	0.759146	0.754394	0.750557	0.747495	0.745101	0.74329	0.741993	0.741155
40	0.775152	0.766743	0.759936	0.754428	0.749996	0.746469	0.743718	0.741638	0.74015	0.739188	0.738697
60	0.773943	0.765574	0.758802	0.753329	0.748933	0.745448	0.742743	0.740717	0.739288	0.738392	0.737975
80	0.77371	0.765332	0.758554	0.753079	0.748684	0.745204	0.742508	0.740494	0.739082	0.738206	0.737813
100	0.773668	0.765278	0.758491	0.753008	0.74861	0.745128	0.742433	0.740423	0.739017	0.738149	0.737766

Figure 4.38 and Table 39 shows how AWIG with UH18-SPW planform area COP migrated as HC changes at different AOA. The COP values is negative indicated that it has migrated toward trailing edge (TE) in longitudinal position when HC increases from 20 % to 100 %(OGE) and as AOA increased. The COP location migrated from 0.7810287 m to 0.7377661 m in chord direction as the HC rise from 20 % to true flight (TF). The minimum and maximum increment as the HC rise is about 0.73609 % and 0.33892 % of its original position. It was also observed that the COP migrated as much as 4.32626 % towards only leading edge from 0◦ to 10°.

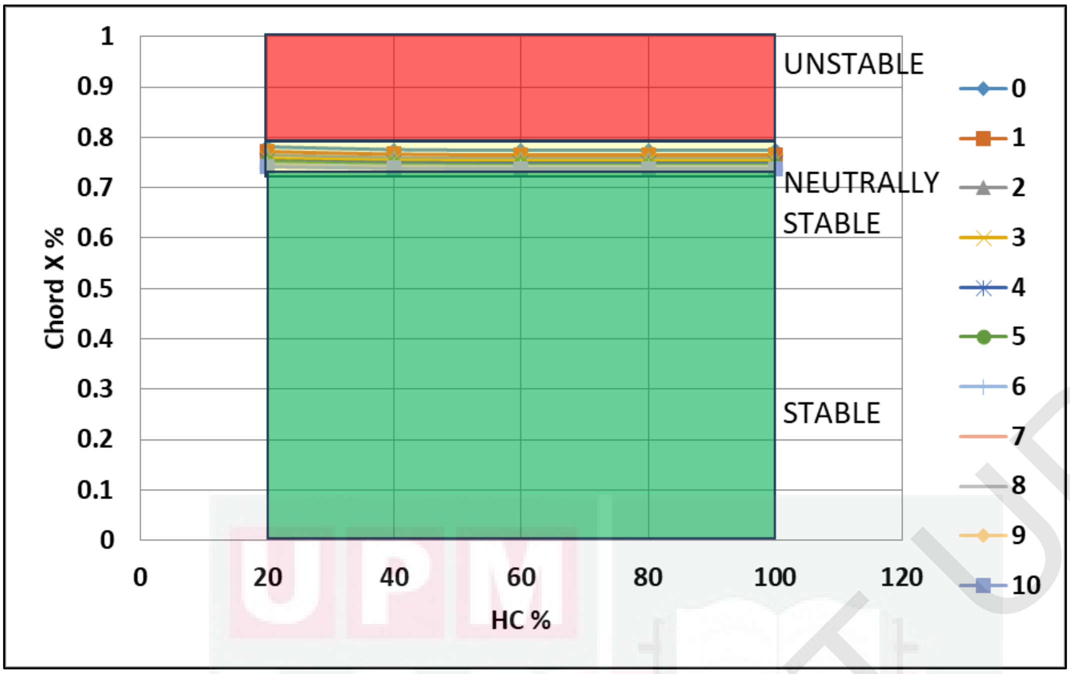

Figure 4.39: AWIG with UH18-SPW planform area COP migration percentage increment from 20% HC to 100% HC° at various AOA

Table 40: AWIG with UH18-SPW planform area COP migration percentage increment from 20% HC to 100% HC° at various AOA

HC %/AOA	0	1	2	3	4	5	6	7	8	9	10
20	0.781029	0.772178	0.764993	0.759146	0.754394	0.750557	0.747495	0.745101	0.74329	0.741993	0.741155
40	0.775152	0.766743	0.759936	0.754428	0.749996	0.746469	0.743718	0.741638	0.74015	0.739188	0.738697
60	0.773943	0.765574	0.758802	0.753329	0.748933	0.745448	0.742743	0.740717	0.739288	0.738392	0.737975
80	0.77371	0.765332	0.758554	0.753079	0.748684	0.745204	0.742508	0.740494	0.739082	0.738206	0.737813
100	0.773668	0.765278	0.758491	0.753008	0.74861	0.745128	0.742433	0.740423	0.739017	0.738149	0.737766

Figure 4.39 and Table 40 shows AWIG with UH18-SPW planform area COP migration on every AOA increment. It was found that, when CG enters or moves inside the green region, it indicates that it is stable longitudinally. The yellow to red region indicates that it will unstable when CG enters these regions. The location of COP is located at 73.77% Chord when it is OGE, and when the it flies closer to the ground (IGE) the location of COP move towards Leading Edge (LE), and it is located at 78.1% Chord when H/C = 0.2.

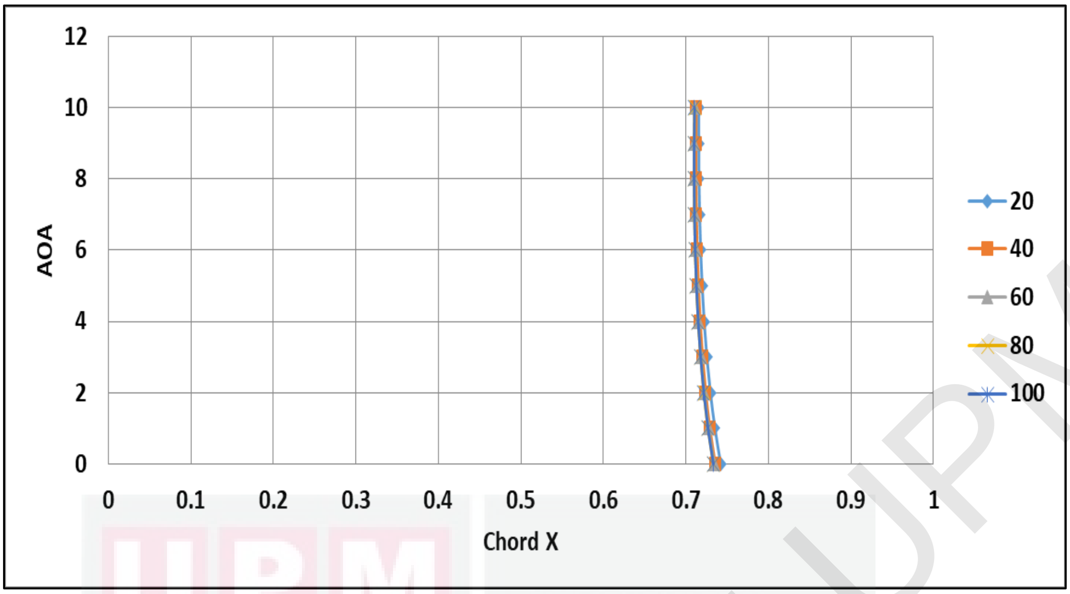

Figure 4.40: DHMTU with UH18-SPW planform area COP migration

Table 41: DHMTU with UH18-SPW planform area COP migration

HC %/AOA	0	1	2	3	4	5	6	7	8	9	10
20	0.741707	0.734752	0.72936	0.725179	0.721963	0.719534	0.717762	0.716551	0.715823	0.715521	0.715597
40	0.73549	0.728856	0.723736	0.719803	0.716827	0.714641	0.713119	0.712169	0.711716	0.711704	0.712088
60	0.733857	0.727241	0.72214	0.718228	0.715277	0.713123	0.71164	0.710736	0.710337	0.710386	0.710838
80	0.733389	0.726759	0.721646	0.717729	0.714777	0.712625	0.71115	0.710257	0.709873	0.709941	0.710416
100	0.73321	0.726565	0.721442	0.717516	0.71456	0.712407	0.710932	0.710043	0.709665	0.709741	0.710226

Figure 4.40 and Table 41 shows how DHMTU with UH18-SPW planform area COP migrated as HC changes at different AOA. The COP values is positive indicated that it has migrated toward leading edge (LE) in longitudinal position when HC increases from 20% to 100%(OGE) and as AOA increased. The COP location migrated from 0.7417068 m to 0.7102259 m in chord direction as the HC rise from 20% to true flight (TF). The minimum and maximum increment as the HC rise is about 0.84973 % and 0.53715 % of its original position. It was also observed that the COP migrated as much as 3.14809% towards leading edge from 0◦ to 6° and migrated back to trailing edge from 7◦ to 10°.

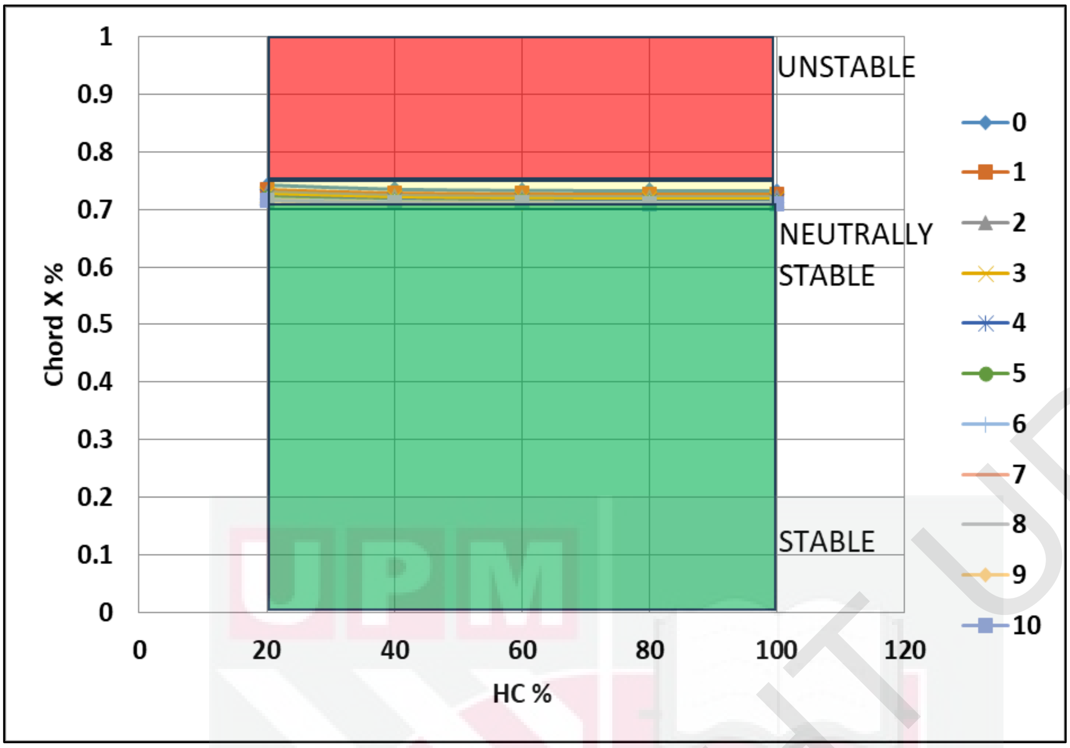

Figure 4.41: DHMTU with UH18-SPW planform area COP migration percentage increment from 20% HC to 100% HC° at various AOA

Table 42: DHMTU with UH18-SPW planform area COP migration percentage increment from 20% HC to 100% HC° at various AOA

HC %/AOA	0	1	2	3	4	5	6	7	8	9	10
20	0.741707	0.734752	0.72936	0.725179	0.721963	0.719534	0.717762	0.716551	0.715823	0.715521	0.715597
40	0.73549	0.728856	0.723736	0.719803	0.716827	0.714641	0.713119	0.712169	0.711716	0.711704	0.712088
60	0.733857	0.727241	0.72214	0.718228	0.715277	0.713123	0.71164	0.710736	0.710337	0.710386	0.710838
80	0.733389	0.726759	0.721646	0.717729	0.714777	0.712625	0.71115	0.710257	0.709873	0.709941	0.710416
100	0.73321	0.726565	0.721442	0.717516	0.71456	0.712407	0.710932	0.710043	0.709665	0.709741	0.710226

Figure 4.41 and Table 42 shows DHMTU with UH18-SPW planform area COP migration on every AOA increment. It was found that, when CG enters or moves inside the green region, it indicates that it is stable longitudinally. The yellow to red region indicates that it will unstable when CG enters these regions. The location of COP is located at 71% Chord when it is OGE, and

when the it flies closer to the ground (IGE) the location of COP move towards Leading Edge (LE), and it is located at 74.17% Chord when H/C = 0.2.

BIXEL Patent

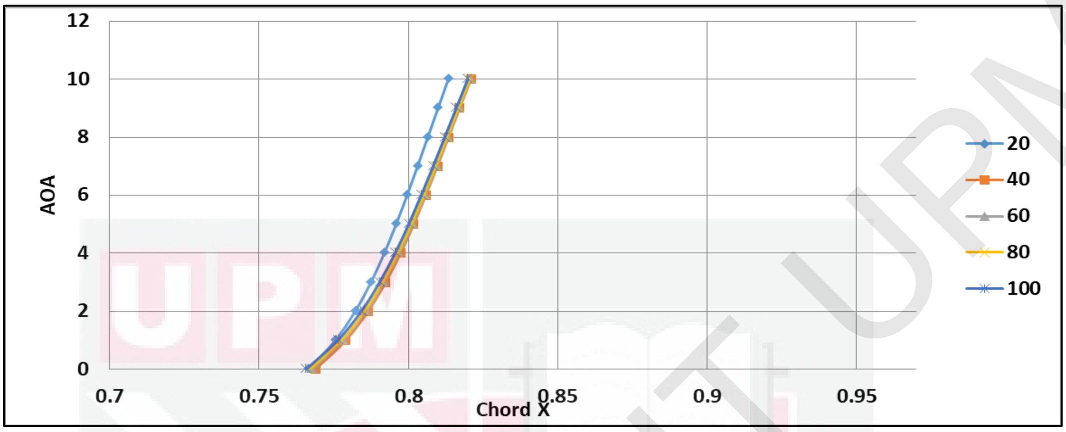

Figure 4.42: Bixel 0.25 AR double wing configuration COP migration

Table 43: Bixel 0.25 AR double wing configuration COP migration

HC %/AOA	0	1	2	3	4	5	6	7	8	9	10
20	0.766526	0.775529	0.782165	0.787444	0.79191	0.795879	0.799552	0.80306	0.806492	0.809912	0.813367
40	0.768832	0.778994	0.786455	0.792366	0.797344	0.801748	0.805803	0.809657	0.81341	0.817135	0.820883
60	0.767719	0.778132	0.785768	0.791811	0.796894	0.801386	0.805517	0.809439	0.813256	0.81704	0.820845
80	0.766952	0.777462	0.785168	0.791263	0.796386	0.800913	0.805074	0.809023	0.812865	0.816673	0.820501
100	0.765752	0.776385	0.784176	0.790337	0.795515	0.800087	0.804289	0.808276	0.812154	0.815996	0.819859
%	0.079711	0.088268	0.207361	0.298268	0.371701	0.433814	0.488351	0.537753	0.58366	0.627227	0.66932

Figure 4.42 and Table 43 shows how Bixel 0.25 AR with UH18-SPW planform area COP migrated as HC changes at different AOA. The COP values is positive indicated that it has migrated toward leading edge (TE) in longitudinal position when HC increases from 20 % to 100 % (OGE) and as AOA increased. The COP location migrated from 0.744684 m to 0.800527 m in chord direction as the HC rise from 20 % to true flight (TF). The minimum and maximum increment as the HC rise is about 0.007608 % and 0.414402

% of its original position. It was also observed that the COP migrated as much as 5.498 % towards only trailing edge from 0◦ to 10°.

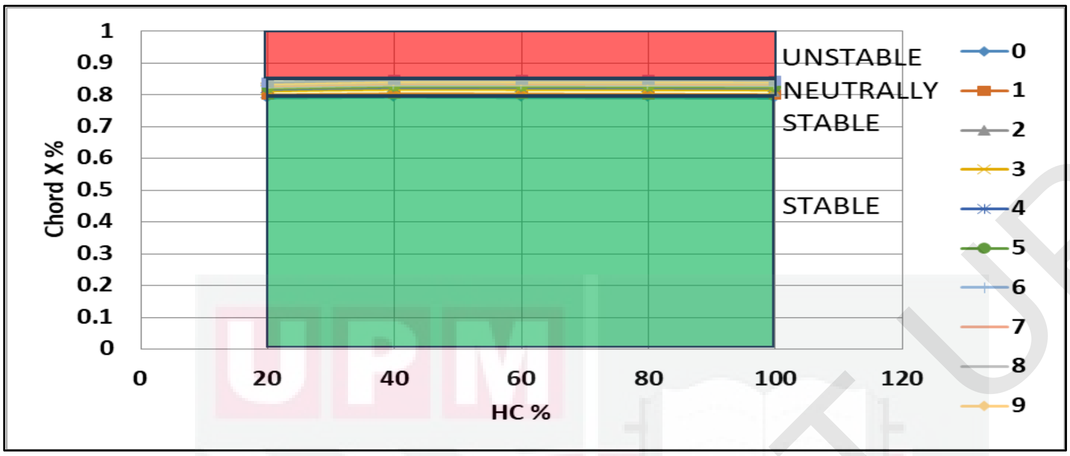

Figure 4.43: Bixel 0.25 AR double wing configuration COP migration percentage increment from 20% HC to 100% HC° at various AOA

Table 44: Bixel 0.25 AR double wing configuration COP migration percentage increment from 20% HC to 100% HC° at various AOA

HC %/AOA	0	1	2	3	4	5	6	7	8	9	10
20	0.790232	0.799514	0.806356	0.811798	0.816402	0.820494	0.824281	0.827897	0.831435	0.834961	0.838522
40	0.792611	0.803086	0.810778	0.816872	0.822004	0.826544	0.830724	0.834697	0.838567	0.842407	0.846271
60	0.791463	0.802197	0.81007	0.8163	0.82154	0.826171	0.83043	0.834473	0.838408	0.842309	0.846232
80	0.790672	0.801508	0.809451	0.815735	0.821017	0.825683	0.829973	0.834045	0.838005	0.841931	0.845878
100	0.789435	0.800397	0.808429	0.814781	0.820119	0.824832	0.829164	0.833274	0.837272	0.841233	0.845215

Figure 4.43 and Table 44 shows Bixel 0.25 AR with UH18-SPW planform area COP migration on every AOA increment. It was found that, when CG enters or moves inside the green region, it indicates that it is stable longitudinally. The yellow to red region indicates that it will unstable when CG enters these regions. The location of COP is located at 84.52% Chord when it is OGE, and when the it flies closer to the ground (IGE) the location of COP move towards Leading Edge (LE), and it is located at 79.02% Chord when H/C = 0.2.

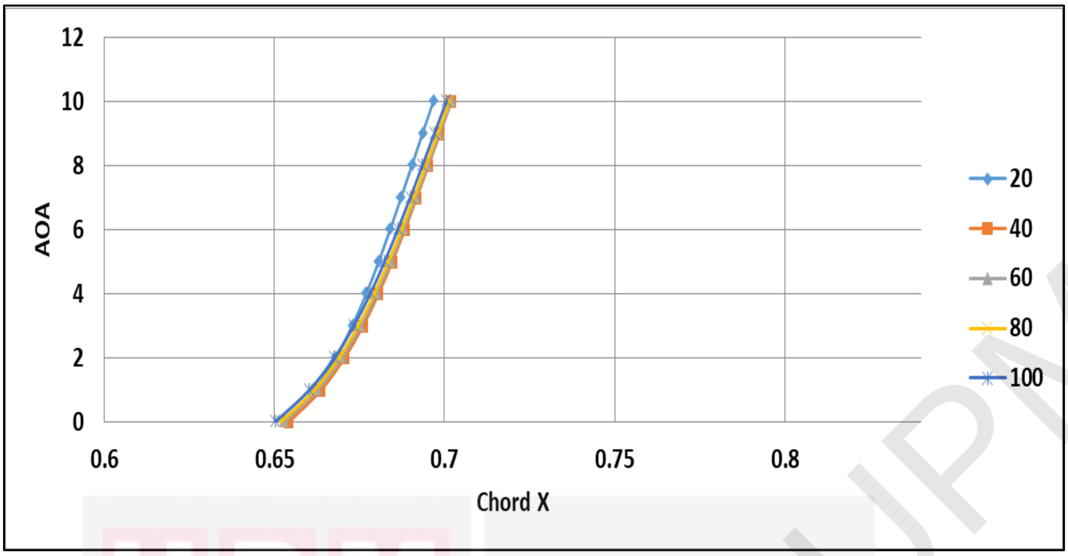

Figure 4.44: Bixel 0.33 AR double wing configuration COP migration

Table 45: Bixel 0.33 AR double wing configuration COP migration

HC %/AOA	0	1	2	3	4	5	6	7	8	9	10
20	0.653632	0.661917	0.668026	0.672884	0.676991	0.68064	0.684015	0.687237	0.690389	0.69353	0.696701
40	0.654275	0.663702	0.670602	0.676047	0.680614	0.684641	0.688339	0.691845	0.695256	0.698639	0.702043
60	0.652912	0.662634	0.669738	0.675335	0.680021	0.684145	0.687926	0.691506	0.694983	0.698429	0.701892
80	0.65194	0.661788	0.66898	0.674641	0.679379	0.683545	0.687362	0.690974	0.694482	0.697955	0.701445
100	0.650276	0.660291	0.667599	0.67335	0.678158	0.682385	0.686255	0.689915	0.693468	0.696984	0.700516
%	0.3995	0.193583	0.050821	-0.0554	-0.13894	-0.20773	-0.26664	-0.31885	-0.3665	-0.41112	-0.45413

Figure 4.44 and Table 45 shows how Bixel 0.33 AR with UH18-SPW planform area COP migrated as HC changes at different AOA. The COP values is positive indicated that it has migrated toward leading edge (TE) in longitudinal position when HC increases from 20 % to 100 %(OGE) and as AOA increased. The COP location migrated from 0.654745 m to 0.700516 m in chord direction as the HC rise from 20 % to true flight (TF). The minimum and maximum increment as the HC rise is about 0.01913 % and 0.532024 % of its original position. It was also observed that the COP migrated as much as 5.581 % towards only trailing edge from 0◦ to 10°.

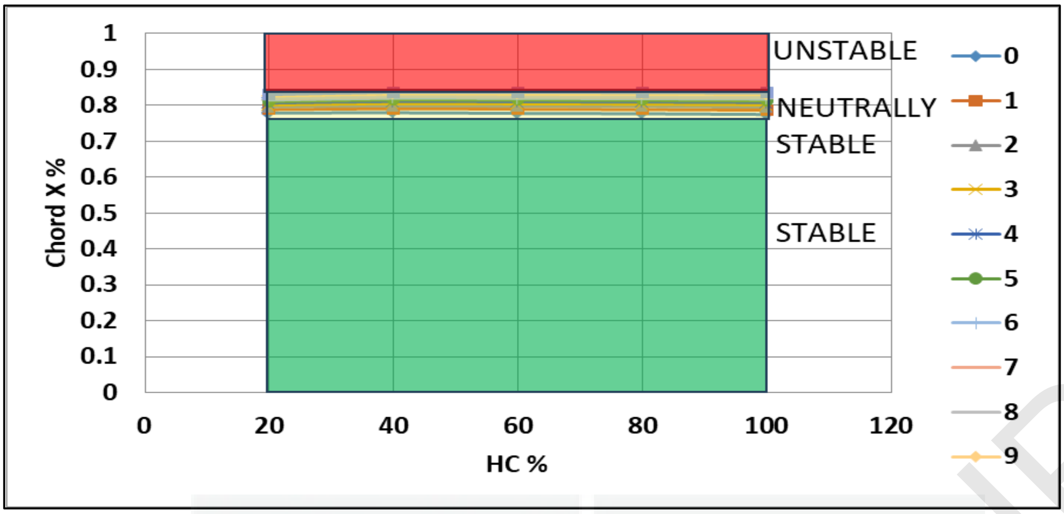

Figure 4.45: Bixel 0.33 AR double wing configuration COP migration percentage increment from 20% HC to 100% HC° at various AOA

Table 46: Bixel 0.33 AR double wing configuration COP migration percentage increment from 20% HC to 100% HC° at various AOA

HC %/AOA	0	1	2	3	4	5	6	7	8	9	10
20	0.778133	0.787996	0.795269	0.801053	0.805942	0.810286	0.814304	0.818139	0.821892	0.825631	0.829406
40	0.778899	0.790121	0.798335	0.804818	0.810255	0.815049	0.819451	0.823625	0.827686	0.831713	0.835765
60	0.777276	0.78885	0.797307	0.80397	0.809549	0.814458	0.818959	0.823221	0.827361	0.831463	0.835586
80	0.776119	0.787843	0.796404	0.803144	0.808784	0.813744	0.818288	0.822589	0.826764	0.830898	0.835054
100	0.774138	0.78606	0.794761	0.801607	0.807331	0.812363	0.81697	0.821328	0.825557	0.829742	0.833948

Figure 4.45 and Table 46 shows Bixel 0.33 AR with UH18-SPW planform area COP migration on every AOA increment. It was found that, when CG enters or moves inside the green region, it indicates that it is stable longitudinally. The yellow to red region indicates that it will unstable when CG enters these regions. The location of COP is located at 83.39% Chord when it is OGE, and when the it flies closer to the ground (IGE) the location of COP move towards Leading Edge (LE), and it is located at 77.81% Chord when H/C = 0.2.

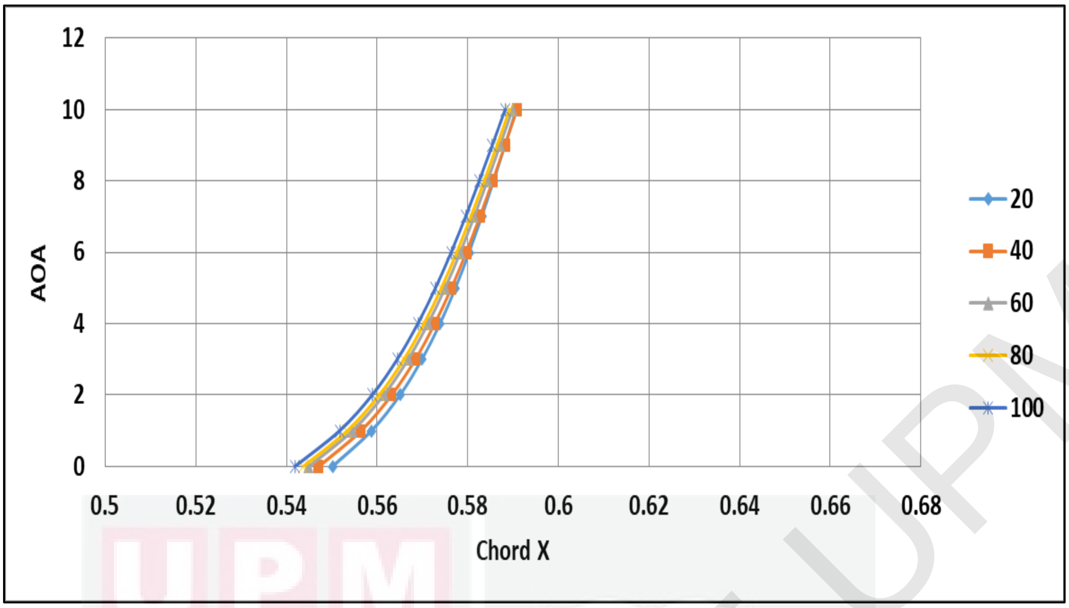

Figure 4.46: Bixel 0.50 AR double wing configuration COP migration

Table 47: Bixel 0.50 AR double wing configuration COP migration

HC %/AOA	0	1	2	3	4	5	6	7	8	9	10
20	0.550127	0.558766	0.565029	0.569889	0.573869	0.577279	0.580311	0.583093	0.585713	0.58823	0.590692
40	0.547118	0.556444	0.563198	0.568436	0.572726	0.576401	0.579671	0.582673	0.5855	0.588219	0.590878
60	0.544943	0.554519	0.561452	0.566826	0.571228	0.575	0.578357	0.581438	0.584341	0.587133	0.589865
80	0.543735	0.553436	0.560457	0.5659	0.570357	0.574177	0.577576	0.580697	0.583637	0.586466	0.589234
100	0.541836	0.551726	0.558883	0.564431	0.568975	0.57287	0.576337	0.579521	0.582522	0.58541	0.588237
%	1.219279	1.035221	0.903897	0.802647	0.719721	0.648353	0.584456	0.525338	0.469191	0.414706	0.361

Figure 4.46 and Table 47 shows how Bixel 0.50 AR with UH18-SPW planform area COP migrated as HC changes at different AOA. The COP values is positive indicated that it has migrated toward leading edge (TE) in longitudinal position when HC increases from 20 % to 100 %(OGE) and as AOA increased. The COP location migrated from 0.549197 m to 0.591458 m in chord direction as the HC rise from 20% to 100% (OGE). The minimum and maximum increment as the HC rise is about 0.473632 % and 1.082529 % of its original position. It was also observed that the COP migrated as much as 5.604 % towards only trailing edge from 0◦ to 10°.

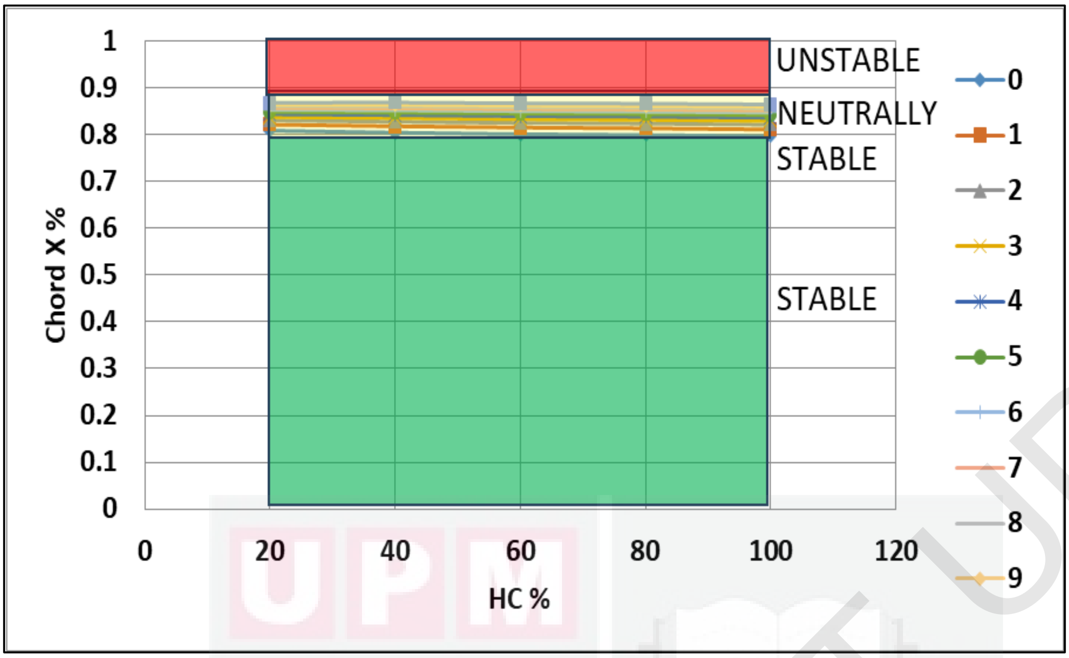

Figure 4.47: Bixel 0.50 AR double wing configuration COP migration percentage increment from 20% HC to 100% HC° at various AOA

Table 48: Bixel 0.50 AR double wing configuration COP migration percentage increment from 20% HC to 100% HC° at various AOA

HC %/AOA	0	1	2	3	4	5	6	7	8	9	10
20	0.80901	0.821714	0.830925	0.838072	0.843926	0.84894	0.853399	0.85749	0.861342	0.865045	0.868665
40	0.804585	0.818299	0.828232	0.835935	0.842244	0.847649	0.852458	0.856872	0.861029	0.865028	0.868939
60	0.801386	0.815469	0.825664	0.833568	0.840042	0.845589	0.850524	0.855056	0.859325	0.863431	0.867449
80	0.799611	0.813876	0.824201	0.832205	0.83876	0.844378	0.849376	0.853966	0.85829	0.86245	0.866521
100	0.796817	0.811362	0.821886	0.830046	0.836728	0.842456	0.847554	0.852237	0.85665	0.860898	0.865055

Figure 4.47 and Table 48 shows Bixel 0.50 AR with UH18-SPW planform area COP migration on every AOA increment. It was found that, when CG enters or moves inside the green region, it indicates that it is stable longitudinally. The yellow to red region indicates that it will unstable when CG enters these regions. The location of COP is located at 79.68% Chord, when it is OGE, and when the it flies closer to the ground (IGE) the location of COP move towards Trailing Edge (TE), and it is located at 86.87% Chord when H/C = 0.2.

NEW1 WIG Craft

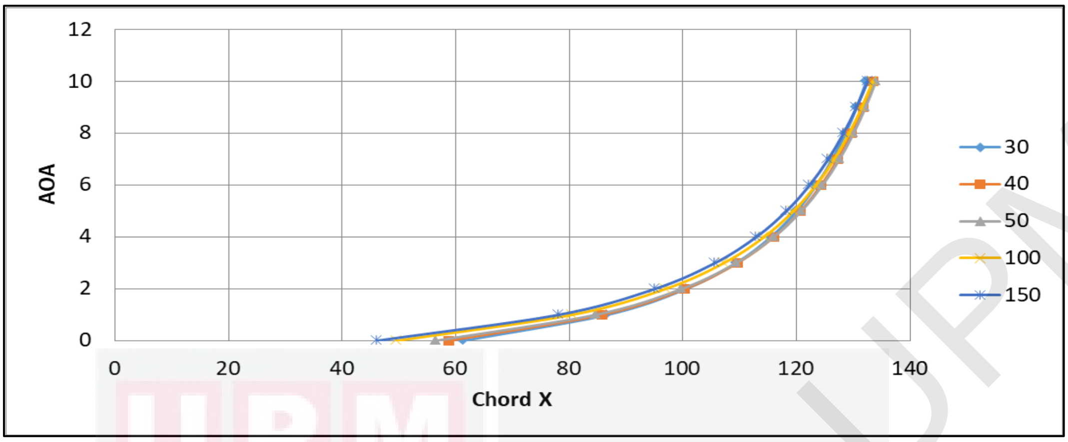

Figure 4.48: Approximate Model of NEW1 WIG configuration COP migration

Table 49: Approximate Model of NEW1 WIG configuration COP migration

HC %/AOA	0	1	2	3	4	5	6	7	8	9	10
1.5	0.330051	0.558181	0.679449	0.754941	0.806699	0.844615	0.873791	0.897125	0.916384	0.93270571	0.94685929
1	0.355114	0.575244	0.69279	0.766146	0.816514	0.853448	0.881884	0.904634	0.923414	0.93933071	0.95313214
0.5	0.404354	0.604866	0.71336	0.781564	0.828609	0.863211	0.889906	0.911292	0.928961	0.943945	0.95694071
0.4	0.419788	0.612206	0.716945	0.783012	0.828681	0.86232	0.8883	0.909129	0.926347	0.94095429	0.95362643
0.3	0.438519	0.619254	0.718517	0.781451	0.825099	0.857322	0.882251	0.902261	0.918819	0.932875	0.94507571

Figure 4.48 and Table 49 shows how Approximate Model of NEW1 WIG configuration COP migrated as HC changes at different AOA. The COP values is positive indicated that it has migrated toward leading edge (TE) in longitudinal position when HC increases from 30% to 150% and as AOA increased. The COP location migrated from 0.330051 m to 0.94686 m in chord direction as the HC rise from 20 % to true flight (TF). The minimum and maximum increment as the HC rise is about 2.374% and 17.925% of its original position. It was also observed that the COP migrated as much as 66.26% towards only trailing edge from 0◦ to 10°.

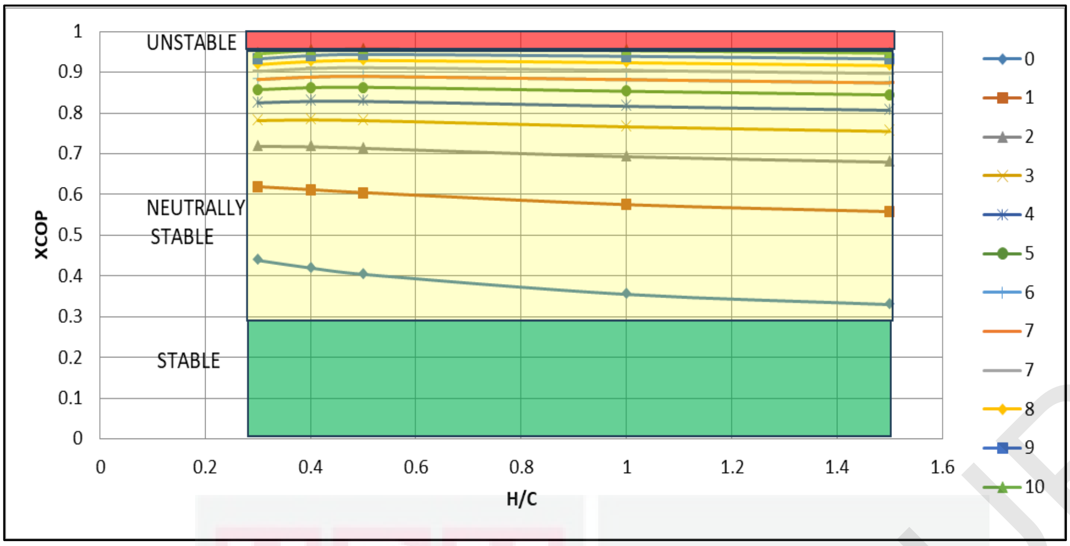

Figure 4.49: Approximate Model of NEW1 WIG COP migration percentage increment from 20% HC to 100% HC° at various AOA

Table 50: Approximate Model of NEW1 WIG COP migration percentage increment from 20% HC to 100% HC° at various AOA

HC %/AOA	0	1	2	3	4	5	6	7	8	9	10
150	46.20714	78.14533	95.12284	105.6918	112.9378	118.2461	122.3308	125.5975	128.2937	130.5788	132.5603
100	49.71598	80.53411	96.99059	107.2605	114.312	119.4827	123.4638	126.6488	129.2779	131.5063	133.4385
50	56.60949	84.68126	99.87037	109.419	116.0053	120.8495	124.5868	127.5809	130.0546	132.1523	133.9717
40	58.77036	85.70885	100.3723	109.6217	116.0154	120.7248	124.362	127.278	129.6886	131.7336	133.5077
30	61.39259	86.69558	100.5924	109.4032	115.5139	120.0251	123.5151	126.3165	128.6346	130.6025	132.3106

Figure 4.49 and Table 50 shows approximate Model of NEW1 WIG COP migration on every AOA increment. It was found that, when CG enters or moves inside the green region, it indicates that it is stable longitudinally. The yellow to red region indicates that it will unstable when CG enters these regions. The location of COP is located at 33% Chord when it is OGE, and when the it flies closer to the ground (IGE) the location of COP move towards Trailing Edge (TE), and it is located at 94.5% Chord when H/C = 0.2.

4.3 Center of Pressure Migration Simulation Results of New conceptual UHID Hoverwing configuration with Six types of Airfoils

4.3.1 Naca 0012 & Flat Surface

Figure 4.50 and Table 51 shows how Naca0012 with New conceptual UHID Hoverwing configuration COP migrated as HC changes at different AOA. The COP values is negative indicated that it has migrated toward trailing edge (TE) in longitudinal position as HC increases from 20% to 100%(OGE).

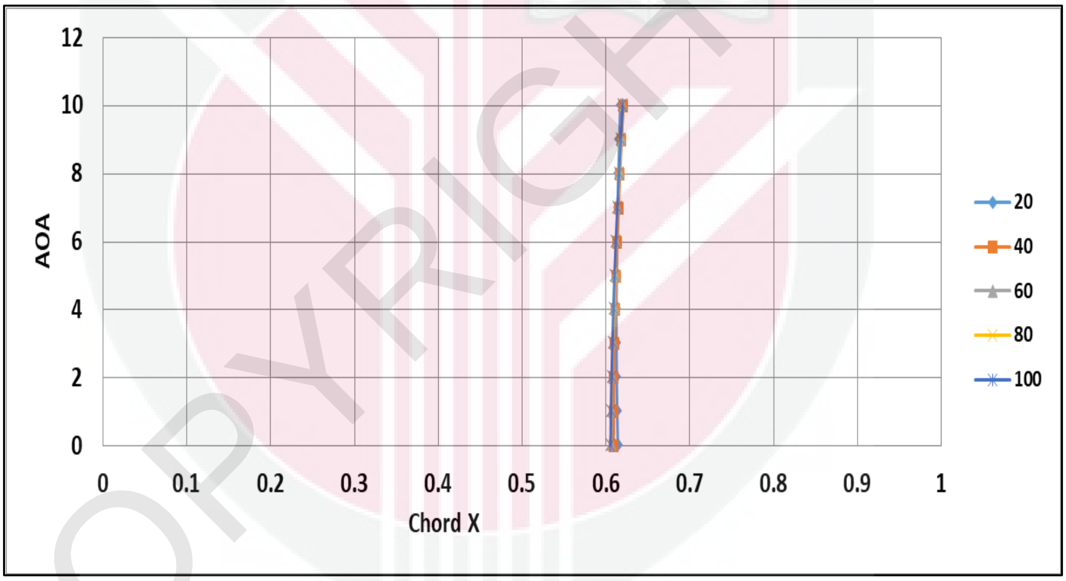

Figure 4.50: Naca0012 with UHID Hoverwing planform area COP migration

Table 51: Naca0012 with UHID Hoverwing configuration COP migration

HC %/AOA	0	1	2	3	4	5	6	7	8	9	10
20	0.61411	0.613213	0.612675	0.612437	0.612459	0.612714	0.613184	0.613856	0.614721	0.615771	0.617001
40	0.608886	0.609062	0.60951	0.610199	0.611108	0.612224	0.613536	0.615037	0.616724	0.618591	0.620636
60	0.606749	0.607129	0.60777	0.608644	0.609735	0.611029	0.61252	0.6142	0.616065	0.618114	0.620342
80	0.605871	0.606306	0.607001	0.607931	0.609076	0.610427	0.611975	0.613714	0.615639	0.617749	0.62004
100	0.605427	0.605882	0.606598	0.607548	0.608717	0.610091	0.611662	0.613426	0.615378	0.617515	0.619834

The COP location migrated from 0.61411 m to 0.619834 m in chord direction as the HC rise from 20% to true flight (TF). The minimum and maximum increment as the HC rise is about 0.6054271 % and 0.6198344 % of its original position. It was also observed that the COP migrated as much as -0.57241 % towards leading edge from 0◦ to 10°.

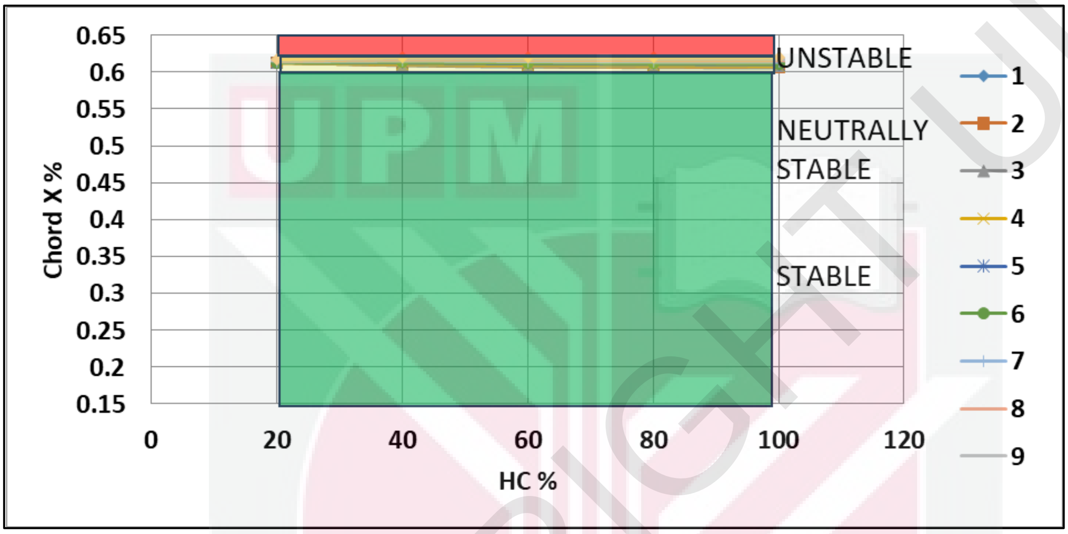

Figure 4.51: Naca0012 with UHID Hoverwing configuration COP migration percentage increment from 20% HC to 100% HC° at various AOA

Table 52: Naca0012 with UHID Hoverwing configuration COP migration percentage increment from 20% HC to 100% HC° at various AOA

HC %/AOA	0	1	2	3	4	5	6	7	8	9	10
20	0.61411	0.613213	0.612675	0.612437	0.612459	0.612714	0.613184	0.613856	0.614721	0.615771	0.617001
40	0.608886	0.609062	0.60951	0.610199	0.611108	0.612224	0.613536	0.615037	0.616724	0.618591	0.620636
60	0.606749	0.607129	0.60777	0.608644	0.609735	0.611029	0.61252	0.6142	0.616065	0.618114	0.620342
80	0.605871	0.606306	0.607001	0.607931	0.609076	0.610427	0.611975	0.613714	0.615639	0.617749	0.62004
100	0.605427	0.605882	0.606598	0.607548	0.608717	0.610091	0.611662	0.613426	0.615378	0.617515	0.619834

Figure 4.51 and Table 52 shows Naca0012 with New conceptual UHID Hoverwing configuration COP migration on every AOA increment. It was found that, when CG enters or moves inside the green region, it indicates that it is stable longitudinally. The yellow to red region indicates that it will

unstable when CG enters these regions. The location of COP is located at 61.19% Chord when it is OGE, and when the it flies closer to the ground (IGE) the location of COP move towards Leading Edge (LE), and it is located at 61.41% Chord when H/C = 0.2.

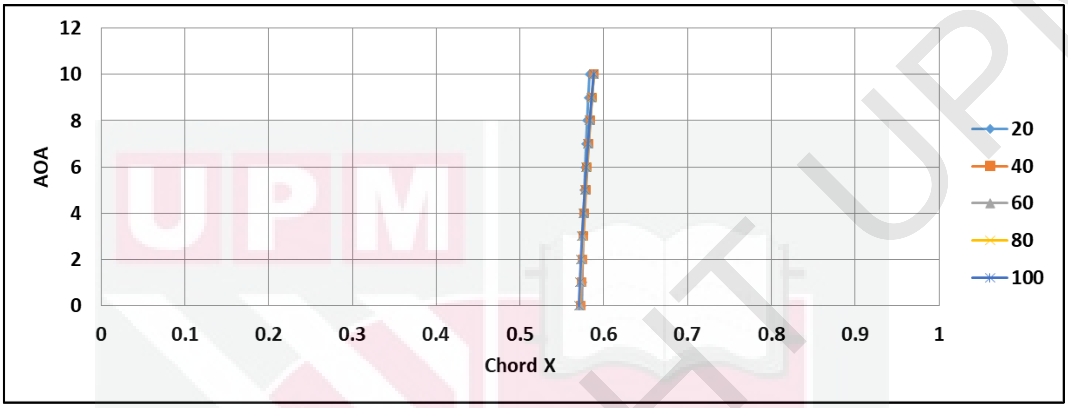

Figure 4.52: Flat Surface with UHID Hoverwing configuration COP migration

Table 53: Flat Surface with UHID Hoverwing configuration COP migration

HC %/AOA	0	1	2	3	4	5	6	7	8	9	10
20	0.573883	0.574284	0.574764	0.575342	0.576033	0.576845	0.577785	0.578857	0.580064	0.581409	0.582894
40	0.572453	0.573483	0.574603	0.57583	0.577178	0.578656	0.580269	0.582022	0.58392	0.585963	0.588156
60	0.57123	0.572354	0.573579	0.574921	0.57639	0.577996	0.579743	0.581636	0.583678	0.58587	0.588216
80	0.570606	0.571755	0.573009	0.574385	0.575894	0.577541	0.579333	0.581273	0.583364	0.585609	0.588009
100	0.57027	0.571425	0.57269	0.574079	0.575603	0.577267	0.579078	0.581038	0.583151	0.585419	0.587843

Figure 4.52 and Table 53 shows how Flat Surface with New conceptual UHID Hoverwing configuration COP migrated as HC changes at different AOA. The COP values is positive indicated that it has migrated toward leading edge (TE) in longitudinal position when HC increases from 20 % to 100 %(OGE) and as AOA increased. The COP location migrated from 0.5738833 m to 0.5878431 m in chord direction as the HC rise from 20 % to true flight (TF).

The minimum and maximum increment as the HC rise is about 0.36131 % and -0.49493 % of its original position. It was also observed that the COP migrated as much as -1.39598 % towards only trailing edge from 0◦ to 10°.

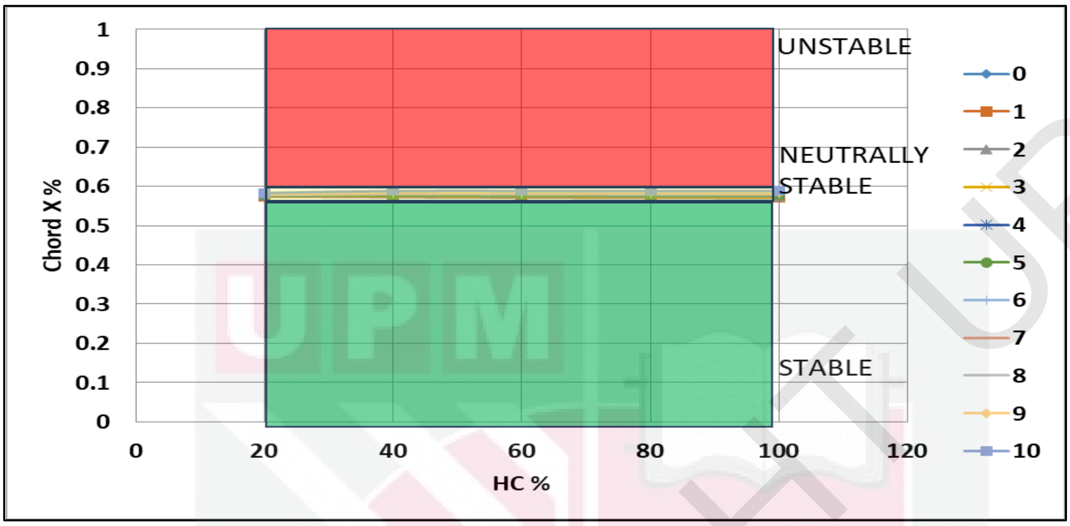

Figure 4.53: Flat Surface UHID Hoverwing configuration COP migration percentage increment from 20% HC to 100% HC° at various AOA

Table 54: Flat Surface with UHID Hoverwing configuration COP migration percentage increment from 20% HC to 100% HC° at various AOA

HC %/AOA	0	1	2	3	4	5	6	7	8	9	10
20	0.573883	0.574284	0.574764	0.575342	0.576033	0.576845	0.577785	0.578857	0.580064	0.581409	0.582894
40	0.572453	0.573483	0.574603	0.57583	0.577178	0.578656	0.580269	0.582022	0.58392	0.585963	0.588156
60	0.57123	0.572354	0.573579	0.574921	0.57639	0.577996	0.579743	0.581636	0.583678	0.58587	0.588216
80	0.570606	0.571755	0.573009	0.574385	0.575894	0.577541	0.579333	0.581273	0.583364	0.585609	0.588009
100	0.57027	0.571425	0.57269	0.574079	0.575603	0.577267	0.579078	0.581038	0.583151	0.585419	0.587843

Figure 4.53 and Table 54 shows Flat Surface with New conceptual UHID Hoverwing configuration COP migration on every AOA increment. It was found that, when CG enters or moves inside the green region, it indicates that it is stable longitudinally. The yellow to red region indicates that it will unstable when CG enters these regions. The location of COP is located at 58.78% Chord when it is OGE, and when the it flies closer to the ground

(IGE) the location of COP move towards Trailing Edge (TE), and it is located at 57.38% Chord when H/C = 0.2.

4.3.2 Naca 4412 & Clark Y

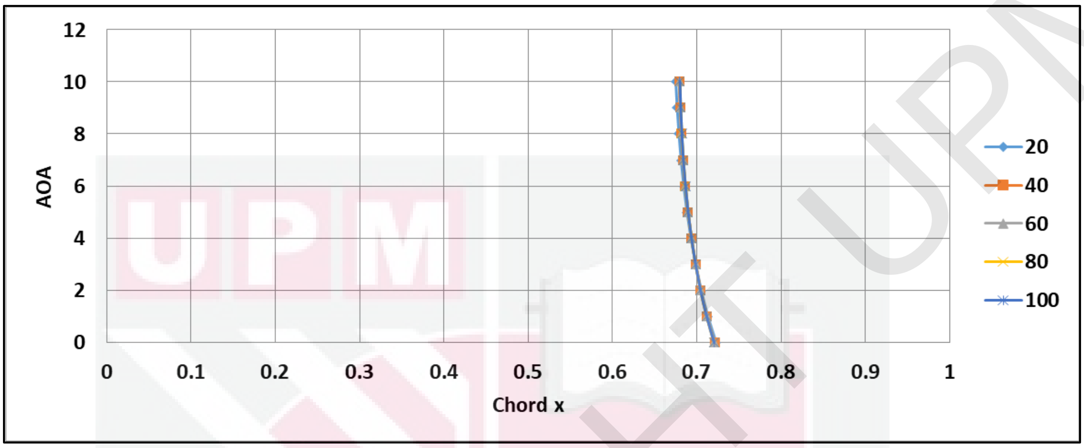

Figure 4.54: Naca4412 with UHID Hoverwing configuration COP migration

Table 55: Naca4412 with UHID Hoverwing configuration COP migration

HC %/AOA	0	1	2	3	4	5	6	7	8	9	10
20	0.723044	0.713328	0.705305	0.698638	0.693078	0.688442	0.684587	0.681403	0.678802	0.676716	0.675088
40	0.721137	0.712138	0.704764	0.698704	0.693727	0.68966	0.68637	0.68375	0.681718	0.680207	0.679163
60	0.720638	0.711741	0.704464	0.698498	0.693619	0.689652	0.686466	0.683956	0.682039	0.68065	0.679732
80	0.720599	0.711714	0.70445	0.698502	0.693642	0.689699	0.686539	0.68406	0.682177	0.680825	0.679948
100	0.720624	0.711735	0.704469	0.698521	0.693665	0.689727	0.686576	0.684107	0.682237	0.680899	0.680039

Figure 4.54 and Table 55 shows how Naca4412 with New conceptual UHID Hoverwing configuration COP migrated as HC changes at different AOA. The COP values is negative indicated that it has migrated toward trailing edge (TE) in longitudinal position as HC increases from 20% to 100%(OGE). The COP location migrated from 0.7230441 m to 0.6800391 m in chord direction as the HC rise from 20% to true flight (TF). The minimum and maximum increment as the HC rise is about 0.24198 % and -0.49511 % of its original

position. It was also observed that the COP migrated as much as 4.3005 % towards leading edge from 0◦ to 8° and migrated back to trailing edge from 9◦ to 10°.

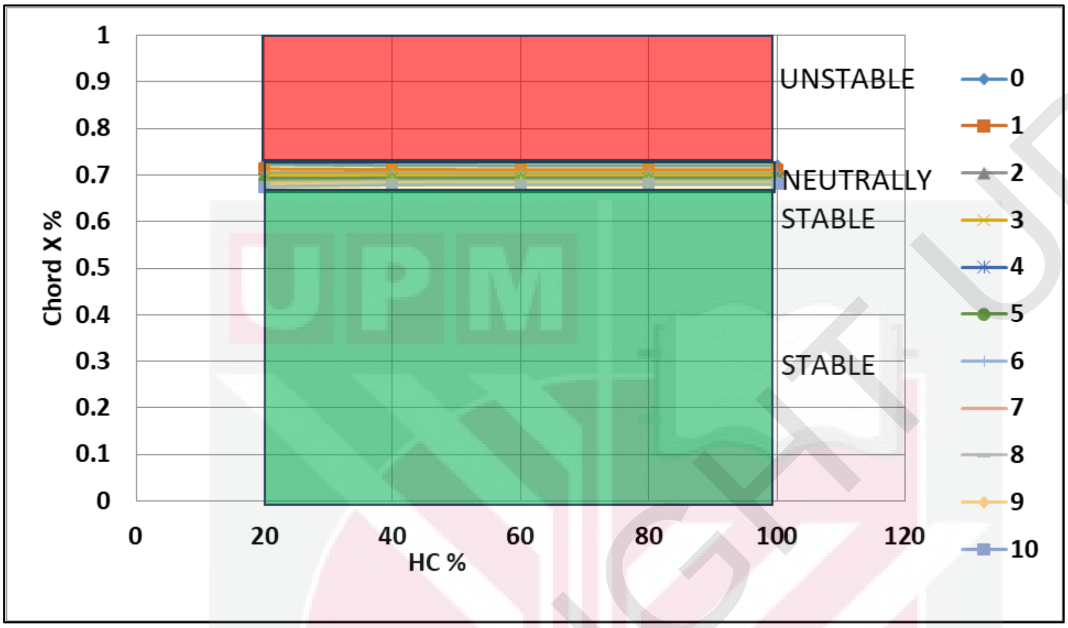

Figure 4.55: Naca4412 with UHID Hoverwing configuration COP migration percentage increment from 20% HC to 100% HC° at various AOA

Table 56: Naca4412 with New conceptual hoverwing configuration COP migration percentage increment from 20% HC to 100% HC° at various AOA

HC %/AOA	0	1	2	3	4	5	6	7	8	9	10
20	0.723044	0.713328	0.705305	0.698638	0.693078	0.688442	0.684587	0.681403	0.678802	0.676716	0.675088
40	0.721137	0.712138	0.704764	0.698704	0.693727	0.68966	0.68637	0.68375	0.681718	0.680207	0.679163
60	0.720638	0.711741	0.704464	0.698498	0.693619	0.689652	0.686466	0.683956	0.682039	0.68065	0.679732
80	0.720599	0.711714	0.70445	0.698502	0.693642	0.689699	0.686539	0.68406	0.682177	0.680825	0.679948
100	0.720624	0.711735	0.704469	0.698521	0.693665	0.689727	0.686576	0.684107	0.682237	0.680899	0.680039

Figure 4.55 and Table 56 shows Naca4412 with New conceptual UHID Hoverwing configuration COP migration on every AOA increment. It was found that, when CG enters or moves inside the green region, it indicates

that it is stable longitudinally. The yellow to red region indicates that it will unstable when CG enters these regions. The location of COP is located at 68% Chord when it is OGE, and when the it flies closer to the ground (IGE) the location of COP move towards Leading Edge (LE), and it is located at 72.3% Chord when H/C = 0.2.

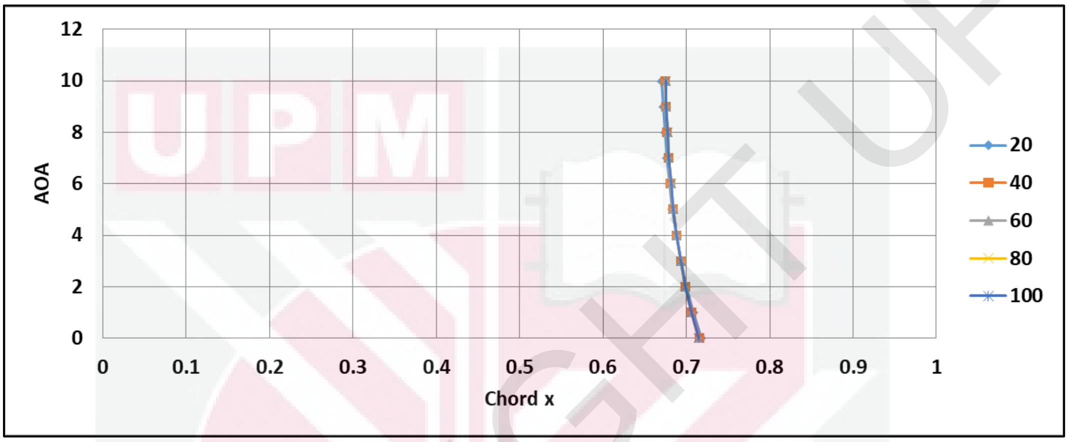

Figure 4.56: Clark Y with UHID Hoverwing configuration COP migration

Table 57: Clark Y with UHID Hoverwing configuration COP migration

HC %/AOA	0	1	2	3	4	5	6	7	8	9	10
20	0.717701	0.707983	0.700015	0.693434	0.687977	0.683451	0.679709	0.676636	0.674144	0.672162	0.670632
40	0.715663	0.706674	0.699359	0.693387	0.688513	0.684556	0.681376	0.678866	0.67694	0.675531	0.674582
60	0.715098	0.70621	0.698991	0.693112	0.688334	0.684475	0.681399	0.678997	0.677186	0.675896	0.675074
80	0.71503	0.706153	0.698946	0.693083	0.688323	0.684487	0.681437	0.679065	0.677287	0.676034	0.675252
100	0.715038	0.706156	0.698946	0.693083	0.688327	0.684496	0.681454	0.679092	0.677326	0.676087	0.675321

Figure 4.56 and Table 57 shows how Clark Y with New conceptual UHID Hoverwing configuration COP migrated as HC changes at different AOA. The COP values is a mix of positive and negative indicated that it has migrated toward leading edge (LE) and returning migrated towards trailing edge (TE) in longitudinal position when HC increases from 20 % to 100 % (OGE) and as AOA increased. The COP location migrated from 0.7177013 m to

0.6753214 m in chord direction as the HC rise from 20 % to true flight (TF). The minimum and maximum increment as the HC rise is about 0.2663 % and -0.46898 % of its original position. It was also observed that the COP migrated as much as 4.23799 % towards leading edge from 0◦ to 8° and migrated back to trailing edge from 9◦ to 10°.

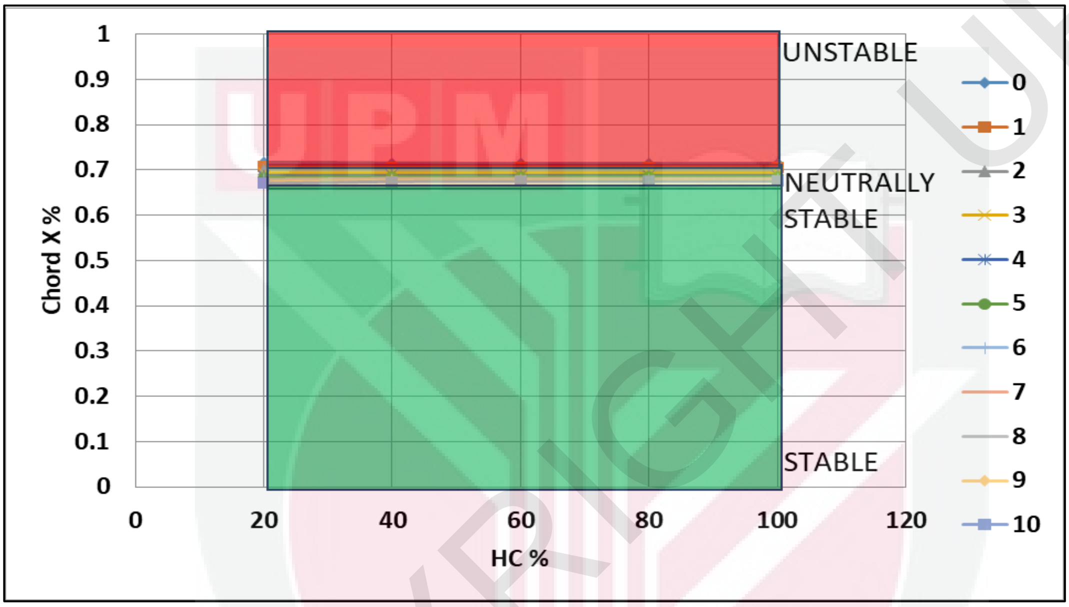

Figure 4.57: Clark Y with UHID Hoverwing configuration COP migration percentage increment from 20% HC to 100% HC° at various AOA

Table 58: Clark Y with UHID Hoverwing configuration COP migration percentage increment from 20% HC to 100% HC° at various AOA

HC %/AOA	0	1	2	3	4	5	6	7	8	9	10
20	0.717701	0.707983	0.700015	0.693434	0.687977	0.683451	0.679709	0.676636	0.674144	0.672162	0.670632
40	0.715663	0.706674	0.699359	0.693387	0.688513	0.684556	0.681376	0.678866	0.67694	0.675531	0.674582
60	0.715098	0.70621	0.698991	0.693112	0.688334	0.684475	0.681399	0.678997	0.677186	0.675896	0.675074
80	0.71503	0.706153	0.698946	0.693083	0.688323	0.684487	0.681437	0.679065	0.677287	0.676034	0.675252
100	0.715038	0.706156	0.698946	0.693083	0.688327	0.684496	0.681454	0.679092	0.677326	0.676087	0.675321

Figure 4.57 and Table 58 shows Naca4412 with New conceptual UHID Hoverwing configuration COP migration on every AOA increment. It was found that, when CG enters or moves inside the green region, it indicates

that it is stable longitudinally. The yellow to red region indicates that it will unstable when CG enters these regions. The location of COP is located at 67.53% Chord when it is OGE, and when the it flies closer to the ground (IGE) the location of COP move towards Leading Edge (LE), and it is located at 71.77% Chord when H/C = 0.2.

4.3.3 AWIG & DHMTU

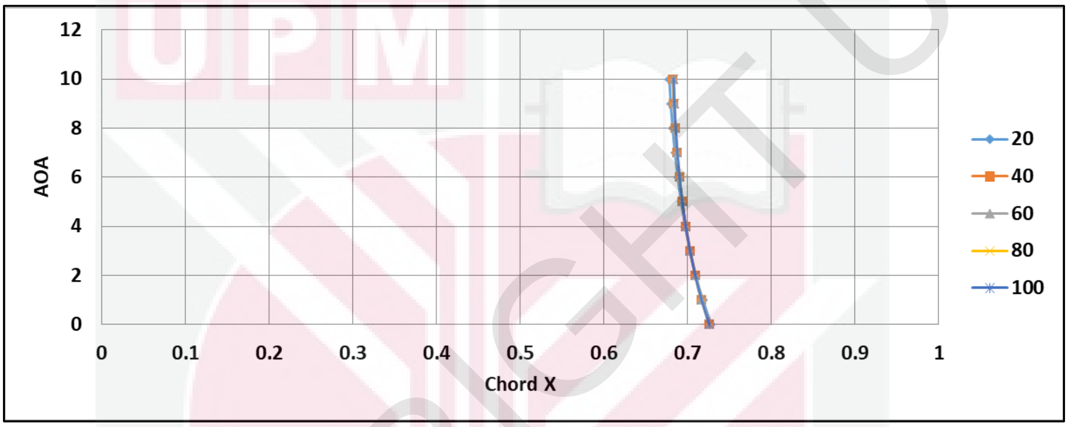

Figure 4.58: AWIG with UHID Hoverwing configuration COP migration

Table 59: AWIG with UHID Hoverwing configuration COP migration

HC %/AOA	0	1	2	3	4	5	6	7	8	9	10
20	0.728484	0.718359	0.709996	0.703041	0.697236	0.692387	0.688347	0.684999	0.682254	0.680038	0.678294
40	0.72659	0.717206	0.709509	0.703174	0.697961	0.693689	0.690218	0.687439	0.685265	0.683628	0.68247
60	0.726153	0.716874	0.709274	0.703035	0.697919	0.693747	0.690381	0.687711	0.685652	0.684135	0.683103
80	0.726149	0.716882	0.709296	0.703073	0.697976	0.693827	0.690486	0.687847	0.685821	0.684341	0.683349
100	0.726194	0.716921	0.709333	0.703111	0.698017	0.693873	0.690541	0.687911	0.685898	0.684432	0.683457

Figure 4.58 and Table 59 shows how AWIG with New conceptual UHID Hoverwing configuration COP migrated as HC changes at different AOA. The COP values is negative indicated that it has migrated toward trailing edge (TE) in longitudinal position when HC increases from 20 % to 100 %(OGE) and as AOA increased. The COP location migrated from 0.7284844 m to

0.6834567 m in chord direction as the HC rise from 20 % to true flight (TF). The minimum and maximum increment as the HC rise is about 0.22908 % and -0.51632 % of its original position. It was also observed that the COP migrated as much as 4.50277 % towards only leading edge from 0◦ to 10°.

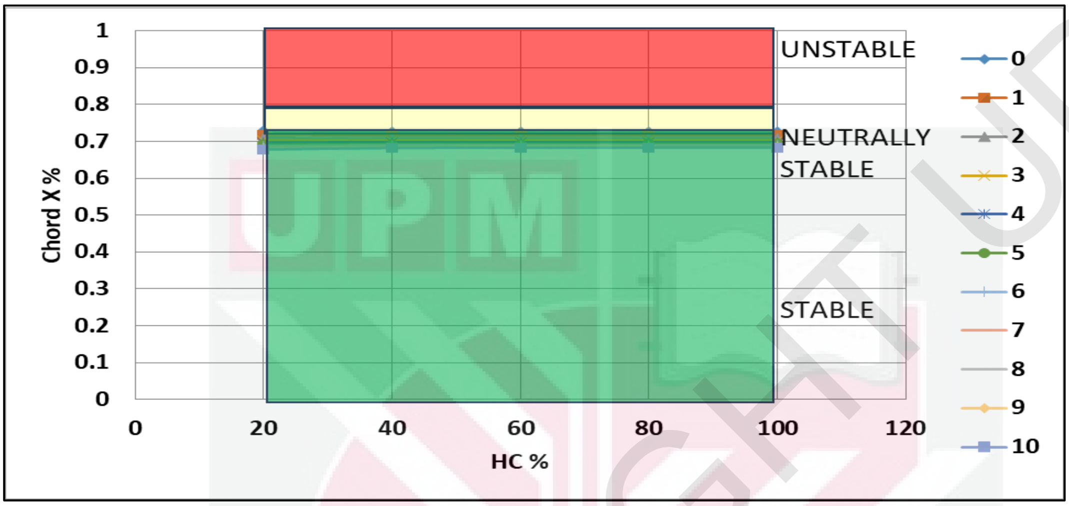

Figure 4.59: AWIG with UHID Hoverwing configuration COP migration percentage increment from 20% HC to 100% HC° at various AOA

Table 60: AWIG with UHID Hoverwing configuration COP migration percentage increment from 20% HC to 100% HC° at various AOA

HC %/AOA	0	1	2	3	4	5	6	7	8	9	10
20	0.728484	0.718359	0.709996	0.703041	0.697236	0.692387	0.688347	0.684999	0.682254	0.680038	0.678294
40	0.72659	0.717206	0.709509	0.703174	0.697961	0.693689	0.690218	0.687439	0.685265	0.683628	0.68247
60	0.726153	0.716874	0.709274	0.703035	0.697919	0.693747	0.690381	0.687711	0.685652	0.684135	0.683103
80	0.726149	0.716882	0.709296	0.703073	0.697976	0.693827	0.690486	0.687847	0.685821	0.684341	0.683349
100	0.726194	0.716921	0.709333	0.703111	0.698017	0.693873	0.690541	0.687911	0.685898	0.684432	0.683457

Figure 4.59 and Table 60 shows AWIG with New conceptual UHID Hoverwing configuration COP migration on every AOA increment. It was found that, when CG enters or moves inside the green region, it indicates that it is stable longitudinally. The yellow to red region indicates that it will unstable when CG enters these regions. The location of COP is located at

68.34 % Chord when it is OGE, and when the it flies closer to the ground (IGE) the location of COP move towards Leading Edge (LE), and it is located at 72.84 % Chord when H/C = 0.2.

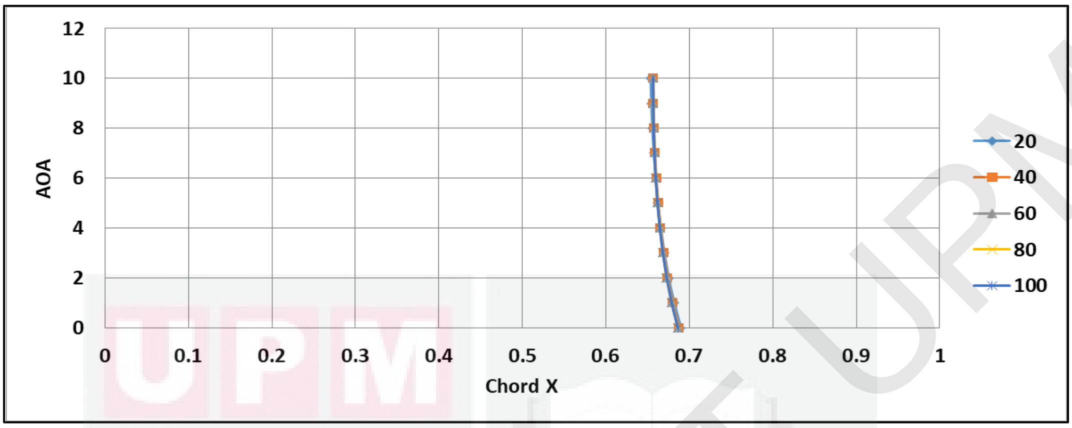

Figure 4.60: DHMTU with UHID Hoverwing configuration COP migration

Table 61: DHMTU with UHID Hoverwing configuration COP migration

HC %/AOA	0	1	2	3	4	5	6	7	8	9	10
20	0.690018	0.68182	0.675274	0.670005	0.665749	0.662319	0.659576	0.657416	0.655758	0.654539	0.65371
40	0.687617	0.680014	0.674011	0.669256	0.665504	0.662576	0.660339	0.658692	0.657558	0.656874	0.656593
60	0.686695	0.679174	0.673249	0.668575	0.664909	0.662071	0.659931	0.658387	0.657362	0.656795	0.656636
80	0.686435	0.678919	0.673003	0.668342	0.664692	0.661875	0.65976	0.658245	0.657253	0.656722	0.656603
100	0.686334	0.678811	0.672891	0.668229	0.664581	0.66177	0.659663	0.658159	0.657179	0.656662	0.65656

Figure 4.60 and Table 61 shows how DHMTU with New conceptual UHID Hoverwing configuration COP migrated as HC changes at different AOA. The COP values is positive indicated that it has migrated toward leading edge (LE) in longitudinal position when HC increases from 20% to 100%(OGE) and as AOA increased. The COP location migrated from 0.6900181 m to 0.6565597 m in chord direction as the HC rise from 20% to true flight (TF). The minimum and maximum increment as the HC rise is about 0.36845 % and -0.28502 % of its original position. It was also observed that the COP migrated as much as 3.34584 % towards leading edge from 0◦ to 6° and migrated back to trailing edge from 7◦ to 10°.

Figure 4.61: DHMTU with UHID Hoverwing configuration COP migration percentage increment from 20% HC to 100% HC° at various AOA

Table 62: DHMTU with UHID Hoverwing configuration COP migration percentage increment from 20% HC to 100% HC° at various AOA

HC %/AOA	0	1	2	3	4	5	6	7	8	9	10
20	0.690018	0.68182	0.675274	0.670005	0.665749	0.662319	0.659576	0.657416	0.655758	0.654539	0.65371
40	0.687617	0.680014	0.674011	0.669256	0.665504	0.662576	0.660339	0.658692	0.657558	0.656874	0.656593
60	0.686695	0.679174	0.673249	0.668575	0.664909	0.662071	0.659931	0.658387	0.657362	0.656795	0.656636
80	0.686435	0.678919	0.673003	0.668342	0.664692	0.661875	0.65976	0.658245	0.657253	0.656722	0.656603
100	0.686334	0.678811	0.672891	0.668229	0.664581	0.66177	0.659663	0.658159	0.657179	0.656662	0.65656

Figure 4.61 and Table 62 shows DHMTU with New conceptual UHID Hoverwing configuration COP migration on every AOA increment. It was found that, when CG enters or moves inside the green region, it indicates that it is stable longitudinally. The yellow to red region indicates that it will unstable when CG enters these regions. The location of COP is located at 65.65% Chord when it is OGE, and when the it flies closer to the ground (IGE) the location of COP move towards Leading Edge (LE), and it is located at 69% Chord when H/C = 0.2.

4.4 All Center of Pressure Migration – A Discussion

4.4.1 Rectangle and Inverse Delta with six types of airfoils

This study highlighted the center of pressure migration which in essence is caused by pressure distribution causes by the flow around the airfoils. From the simulation result obtained, a bar graph (see Figure 4.62) shows the COP percentage migration from 0-10 AOA rectangle configurations via six types of airfoils. The COP migration increase significantly as the chord length of the lifting surfaces increases. The migration of COP has significantly become lower as the AOA increase for Naca0012 and flat surfaces rectangular wing configuration when compare to other rectangle configurations. For Naca0012 and Flat surfaces, the percentage rate of change when AOA increased is roughly 7.3 % for both profiles. Naca0012 and flat rectangle wing have both 0.77381 % and 8.07323 % respectively. It is safe to make assumption now that the large increment in COP migration when AOA increases also indicated instability in longitudinal direction. However, for Naca0012 and Flat surfaces, their COP location almost constant as the AOA increased. It is safe to conclude that Naca0012 and Flat surfaces rectangular wing configuration maintained longitudinally stable as AOA increases compared to the remaining profiles of rectangular wing configuration. The result might be influenced by the fact that these two types of configurations having the same symmetrical curve on top and bottom surfaces.

As for inverse delta shape shown in Figure 63, Naca0012 and Naca4412 has about a maximum of 0.62379% and 41.96521 % of chord length respectively as it migrated from IGE to OGE from 20 % HC to 100 % (OGE). Clark Y, DHMTU and AWIG inverse delta configuration has a maximum of 44.4466 %, 45.37283 %, and 45.21554 % of AOA increment respectively. Flat surfaces inverse delta configuration has a maximum of 3.64756 %. This indicates that Naca 0012 inverse delta wing configuration is longitudinally stable in term of different ground effect HC value. The second best is flat surface inverse delta wing configuration.

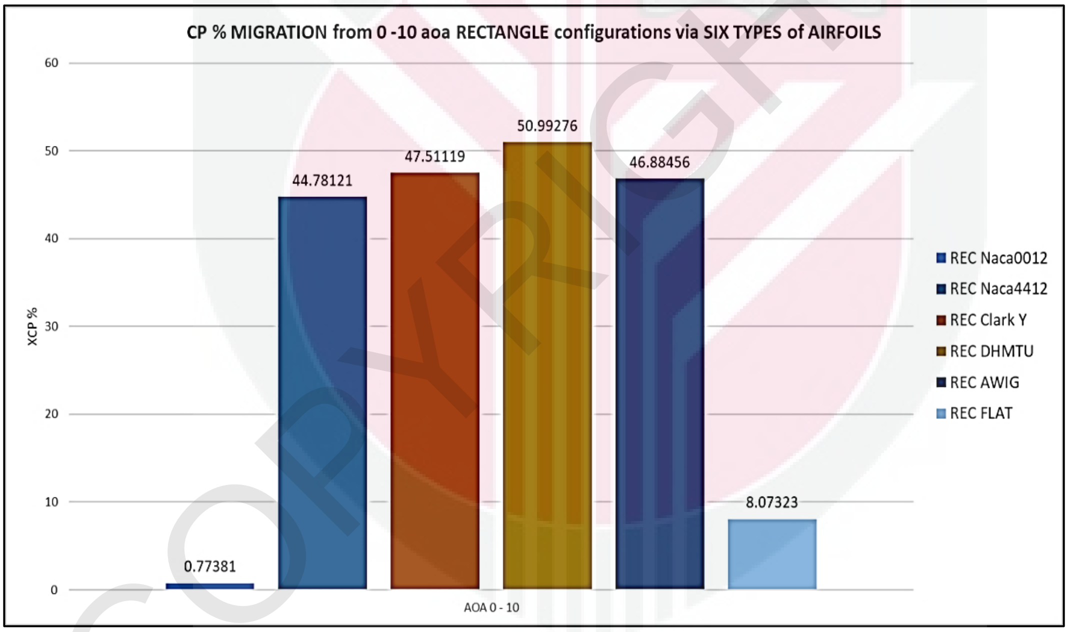

Figure 4.62: COP% MIGRATION from 0 -10 AOA RECTANGLE configurations via SIX TYPES of AIRFOILS

Naca0012 and Flat surface inverse delta configuration showed a lower COP migration as much as 0.2 % and 0.8 % (similar to rectangular wing configuration) respectively in term of percentage rate of change when AOA increased. This is a different case for Clark Y, DHMTU and AWIG rectangular wing configuration where the percentage rate of change when AOA increases is as large as 4.54 %. As conclusion for rectangle and inverse delta wing configurations, Naca 0012 profile has shown a remarkable result of maintaining stability in both ground effect envelope and AOA increment in comparison to the remaining profiles of inverse delta wing configurations. Flat surface, Clark Y, DHMTU and AWIG inverse delta wing configuration might have a longitudinal instability as HC increases due to the COP tend to migrate largely as the AOA increased.

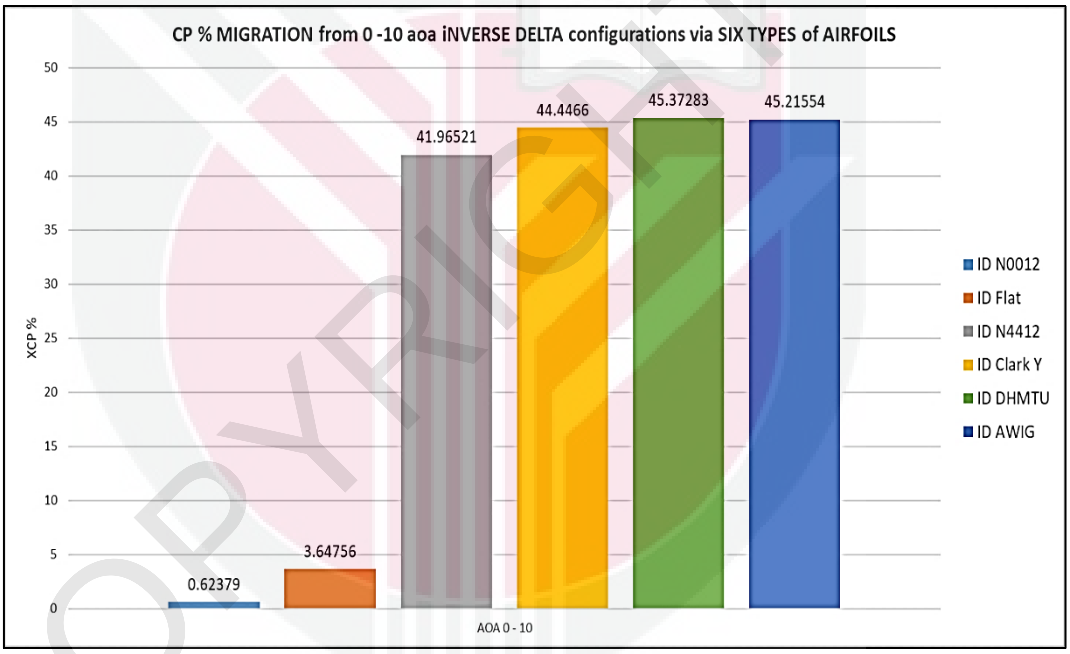

Figure 4.63: COP% MIGRATION from 0 -10 AOA INVERSE DELTA configurations via SIX TYPES of AIRFOILS

Ultimately, one can conclude that a satisfying configuration must have a minimal COP migration at different HC and AOA increment. However, the significant severances of ground effect are dependent on the total COP migration from 0° to 10°. In the first objective, the measurement outcome would be to investigate how COP behaves in relationship to various WIG craft design. Based on the research finding, a pitch up tendency occurred due to 'gap' distance of COP migration from the WIG craft/any aircraft Centre of Gravity (CG). As COP further distancing from its origin, moment force of COP will increase resulting instability in longitudinal direction. It is safe to conclude that the COP migration from 0◦ to 10° needed to be as less as possible to achieve sufficient stability in longitudinal direction IGE and OGE.

4.4.2 UH18-SPW Planform Area with Six types of Airfoils

This study highlighted the center of pressure migration which in essence is caused by pressure distribution causes by the flow around the airfoil. From the simulation result obtained, each configuration had showed an approximation distance of COP migration. From the excel spreadsheet data, each configuration stated that all configurations COP migration is less than 5% from its origin in longitudinal direction. To the author understanding, a pitch up tendency occurred due to 'gap' distance of COP migration from the WIG craft/any aircraft Centre of Gravity (CG).

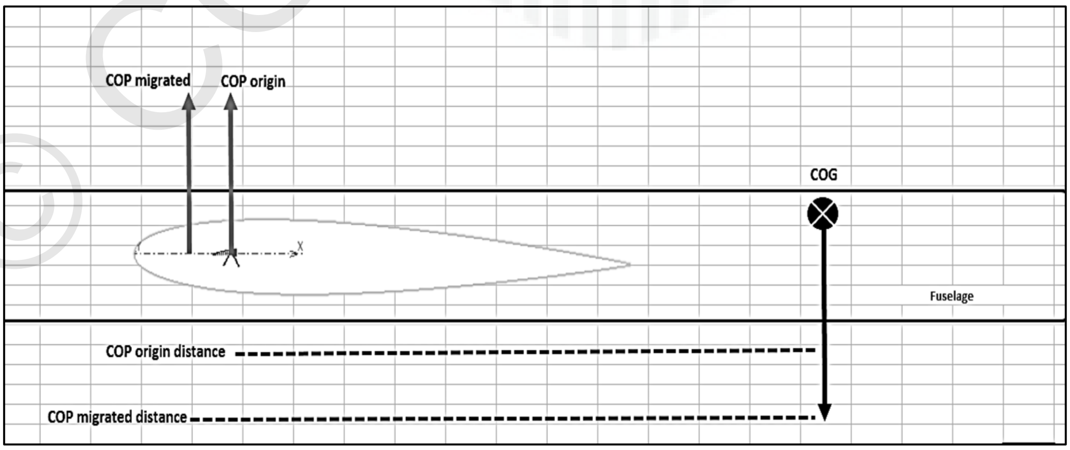

Figure 4.64: Illustration of moment force of COP in relation to CG

Therefore, as COP further distancing from its original position, moment force of COP will increase resulting instability in longitudinal direction. It is to the author assumption that COP moment force will drastically increases as the chord length of lifting surfaces increased. This is understandable as a full-scale WIG craft will experience the present of pitch up tendency much more in comparison to scale model. Figure 4.64 shows the illustration of moment force of COP in relation to Wig craft CG. Figure 4.65 shows all cop migration from 0-10 aoa with UH18 configurations via six types of airfoils as comparison result. From this Figure, it is clearly showed that Naca 0012 has the lowest COP migration as much as 0.82769% when comparing to other configurations. It is safe to assume that COP migration percentages and curve ideally should be as less and as vertical as possible. However, the significant severances of ground effect lie on the total COP migration from 0◦ to 10°. This is due to moment force of COP increases proportional to the distance from CG. Therefore, it is safe to conclude that the COP migration from 0◦ to 10° is needed to be as less as possible or zero.

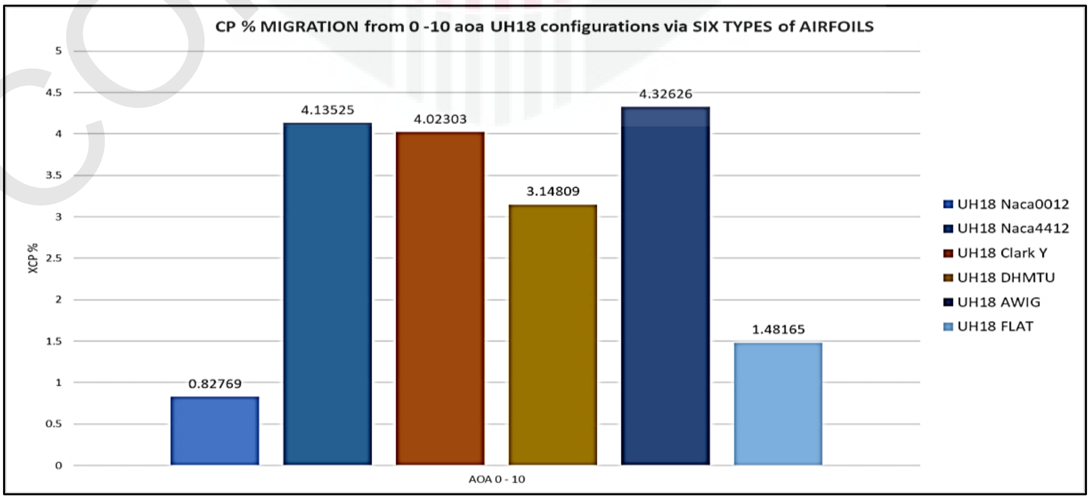

Figure 4.65: COP MIGRATION from 0 -10 AOA UH18 configurations via SIX TYPES of AIRFOILS

4.4.3 New conceptual UHID Hoverwing configuration with Six types of Airfoils

Figure 4.66 represents a comparative analysis of center of pressure (COP) migration of New conceptual UHID Hoverwing configuration with Six types of Airfoils. As the angle of attack (AOA) increases, all configurations exhibit a general upward trend in COP migration, indicating a rearward shift of the COP. This can influence stability and control surface such as flap and aileron on wing. Among the configurations, new conceptual UHID Hoverwing N0012 demonstrates the least COP migration (as much as 0.57241%), suggesting potential advantages in terms of stability and control. Conversely, New conceptual UHID Hoverwing AWIG exhibits the most significant COP migration, which could pose challenges in maintaining control at higher AOAs. The remaining configurations (New conceptual UHID Hoverwing Flat, DHMTU, N4412, and Clark Y) show intermediate levels of COP migration. The choice of airfoil configuration has implications for WIG craft design. Low COP migration configurations may offer enhanced stability and control but potentially compromise lift or increase drag. In contrast, high COP migration configurations could provide higher lift coefficients but require more complex control systems to manage stability. As conclusion for new conceptual UHID Hoverwing configuration with Six types of Airfoils, Naca 0012 profile has shown a remarkable result of maintaining stability in both ground effect envelope and AOA increment in comparison to the remaining profiles of inverse delta wing configurations. The final task is to investigate its COP migration on different tail position and wing area.

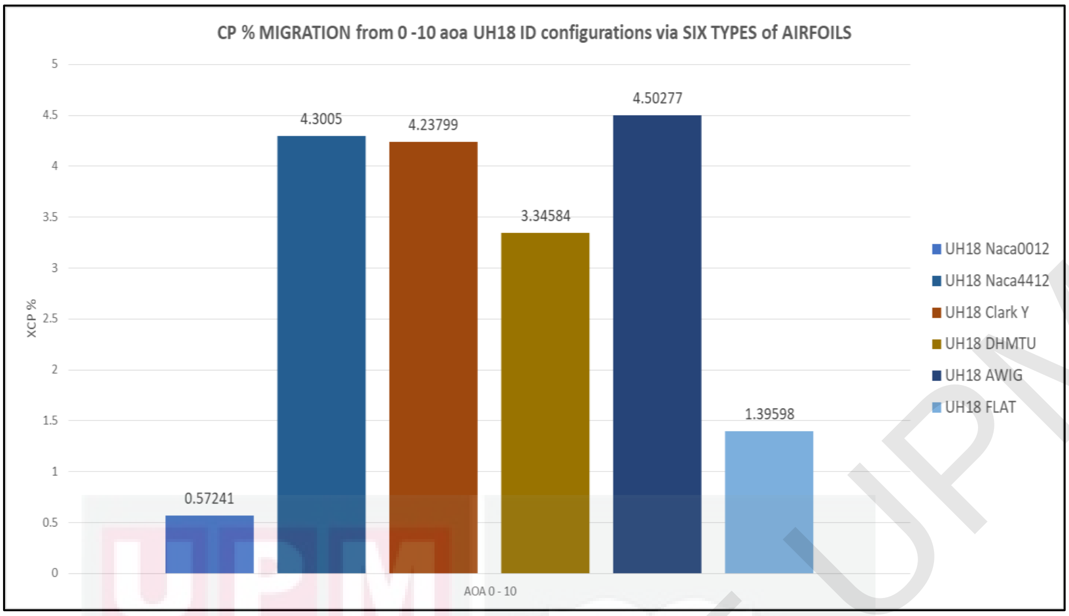

Figure 4.66: COP MIGRATION from 0 -10 aoa of New conceptual UHID Hoverwing configuration with Six types of Airfoils

Design Iteration

After done with investigation of UHID Hoverwing COP migration, two chosen parameters at tail elevator were analysis at various area and position from fuselage in order to determine whether the COP migration can be reduced again. Figure 4.67 and 4.68 shows the result of COP migration of UHID hoverwing of Naca 0012 on tail elevator position from fuselage and area respectively. From the graph shown, when moving the elevator position forward the COP migration reduced from 0.57241% to 0.33544%. This indicated that it can reduce up to 40% from its original position. When reducing the elevator area, the COP migration reduced from 0.57241% to 0.06288%. This indicated that the COP migration can reduce up to 89% from its original position. From the COP migration investigation, it can be concluded that reducing the elevator area derived a significant effect on this type of WIG craft. However, this may not necessarily be the same case for other type WIG craft. The final analysis is concluded by reducing the elevator area from the tail position that has the lowest COP migration and the result of this analysis will be presented in chapter 4.4.

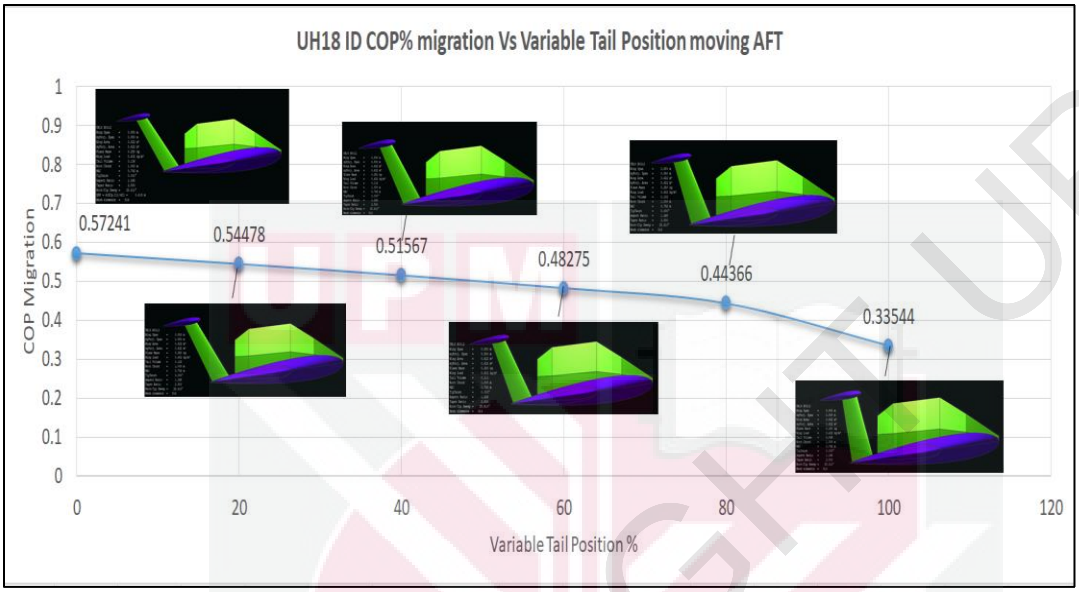

Figure 4.67: Naca 0012 with UHID Hoverwing configuration COP migration at various AOA with various Tail Position from fuselage

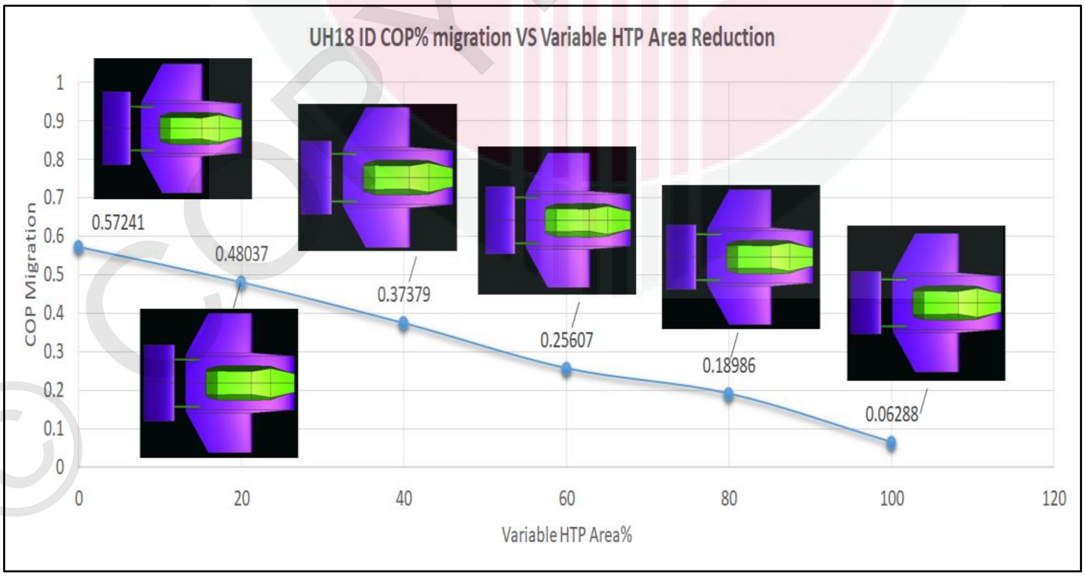

Figure 4.68: Naca 0012 with UHID Hoverwing configuration COP migration at various AOA with various Area

4.4.4 Control Approach from Center of Pressure migration

Theoretically, WIG craft stability hinges on understanding and managing COP migration. This dynamic interplay between design, pilot techniques, and active control systems is crucial for safe and controlled operation. There are several factors that need to be considered to achieve this. The first approach is designers can minimize COP movement by carefully crafting the wing shape, control surfaces, and weight distribution. This passive approach lays the foundation for stability. The second approach is the pilot's expertise plays a vital role. By understanding how COP movement from the aircraft's center of gravity (CG), they can adjust their control inputs accordingly. This proactive approach complements the efforts of design and active systems, ensuring the WIG craft remains balanced and maneuverable.

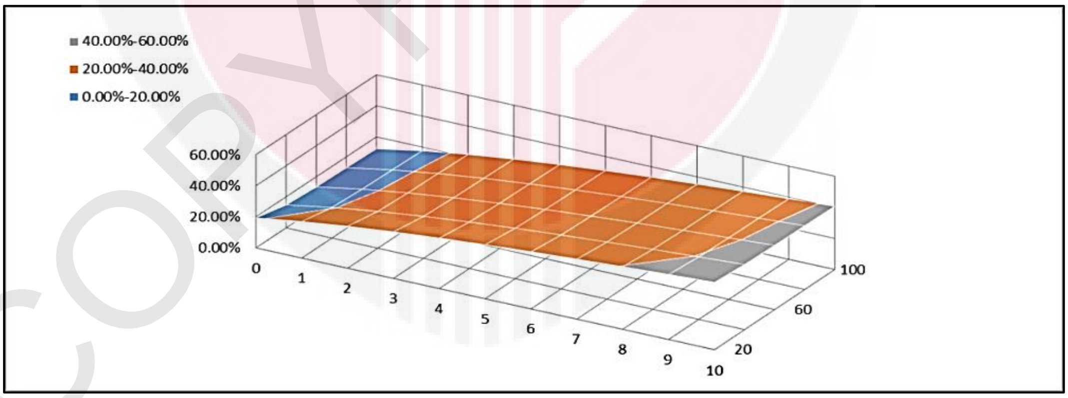

Figure 4.69: Example of control mapping of the Dragonfly DF2

The final approach is active control systems can add another layer of precision. Sensors vigilantly monitor COP location, feeding data into feedback loops that adjust control surfaces in real-time to maintain it within a safe range. This dynamic response helps counteract even the most sudden shifts. As an example, Figure 4.69 and Table 62 show the control mapping feedback of first iteration of Dragonfly DF2 for the pitching control system at tail plane. This works similarly to the engine volumetric efficiency mapping where the percentage amount of air fuel ratio (AFR) is being presetting for fine tuning later on. However, achieving such feat is a highly advanced engineering application because this requires a linear equation system incorporated into a highly none linear system. It should of interest to automatically counter the moment force created by COP migration to achieve longitudinal stability in and out of ground effect zone.

Table 63: Example of control mapping of the Dragonfly DF2

HC %/AOA	0	1	2	3	4	5	6	7	8	9	10
20	19.17%	23.38%	26.87%	29.82%	32.37%	34.62%	36.63%	38.46%	40.14%	41.69%	43.16%
40	14.71%	19.60%	23.60%	26.96%	29.85%	32.37%	34.60%	36.62%	38.46%	40.16%	41.75%
60	13.43%	18.48%	22.60%	26.06%	29.02%	31.60%	33.89%	35.95%	37.83%	39.56%	41.18%
80	12.93%	18.03%	22.20%	25.69%	28.68%	31.28%	33.59%	35.66%	37.55%	39.30%	40.92%
100	12.30%	17.46%	21.68%	25.21%	28.23%	30.86%	33.19%	35.28%	37.19%	38.95%	40.59%

4.5 Finalize conceptual Design of New Two-Seater UHID Hoverwing

From result of new conceptual UHID Hoverwing of Naca0012, after it being considered on various tail position and wing area in design iteration section, new conceptual UHID Hoverwing of Naca0012 with the lowest COP migration was proposed. From the design it can be seen that this design concept has decently shorter wingspan compare to other design. The horizontal tail stabilizer span also reduced significantly shorter compare to other design. Figure 4.70 and 4.71 shows the final design of new conceptual UHID Hoverwing.

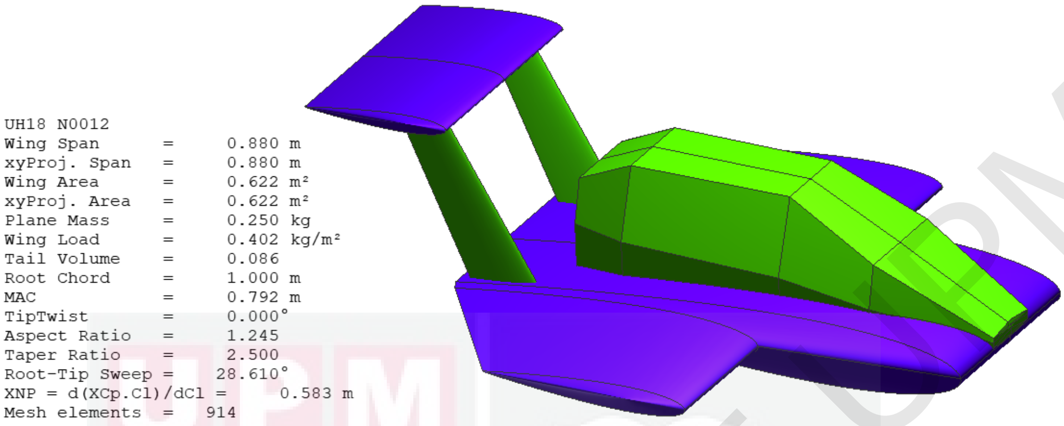

Figure 4.70: The new conceptual UHID Hoverwing of Naca0012

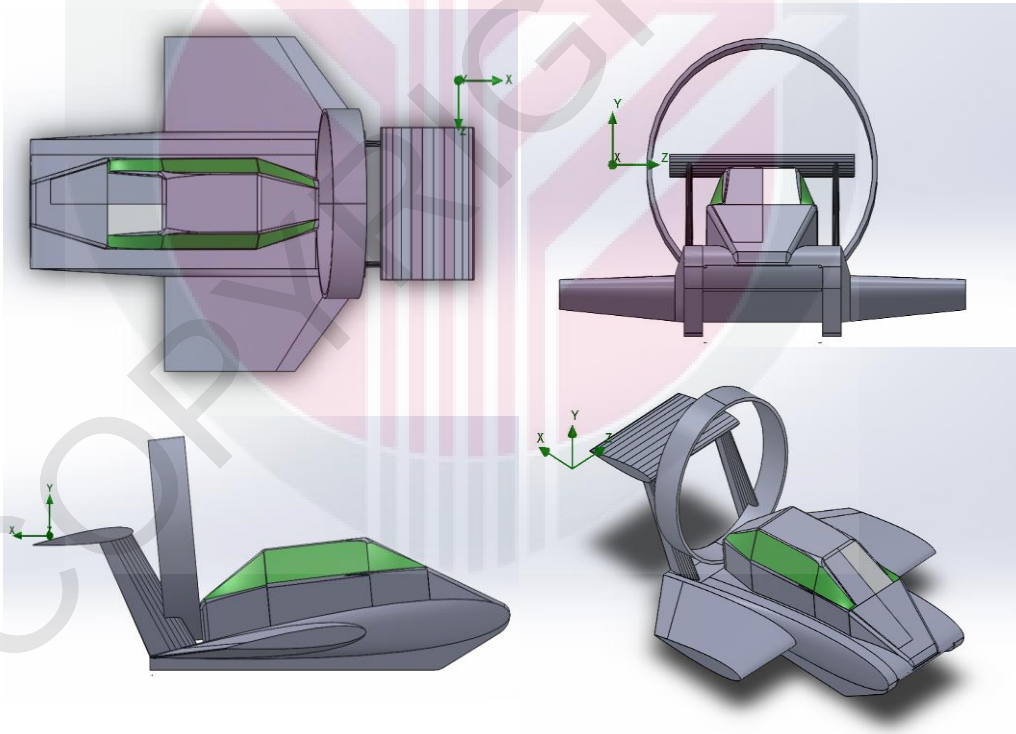

Figure 4.71: the new conceptual UHID Hoverwing of Naca0012 With lowest COP migration

4.6 Aerodynamic Performance Result of UH18-SPW with Naca 4412

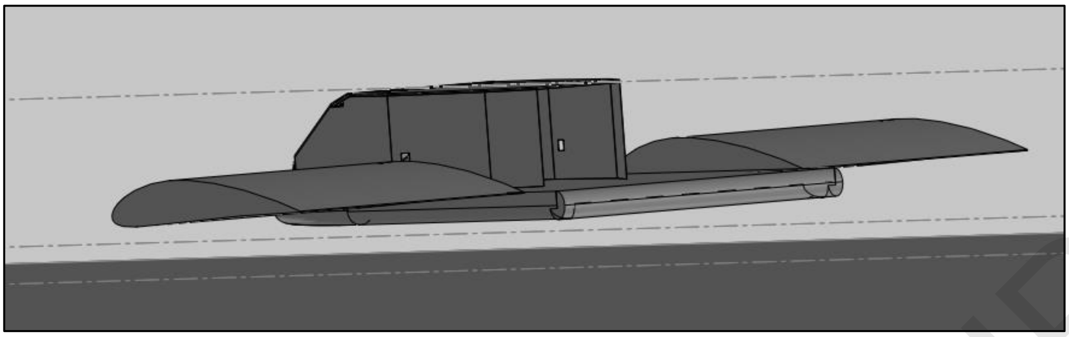

Figure 4.72: Cad model of UH18-SPW with Naca4412

As mentioned in chapter 3.8, the preliminary performance result obtained from the SolidWorks Flow Simulations is then verified by using UH18-SPW wind tunnel test analysis data produce by Steven Morris, 2008. It is important to verify the wind tunnel result with simulation result so that the different in data acquisition can be gauge. The initial task is to conduct a flow simulation analysis using SolidWorks Flow Simulation of UH18-SPW with Naca4412 CAD model (see Figure 4.72). The main values of interest here are preliminary data of lift, drag and moments (CL, CD, CM). When comparing to the aerodynamic performance data from Steven Morris 2008, the value of CL showed lower differences from 10% to 14%. The stall angle value shows a good agreement with UH18-SPW Naca4412 flow simulation which is 16° to 17° compared to Steven Morris, 2008 which is 14° to 16°. Figure 4.73 shows the CL graph of UH18-SPW obtained from flow simulation.

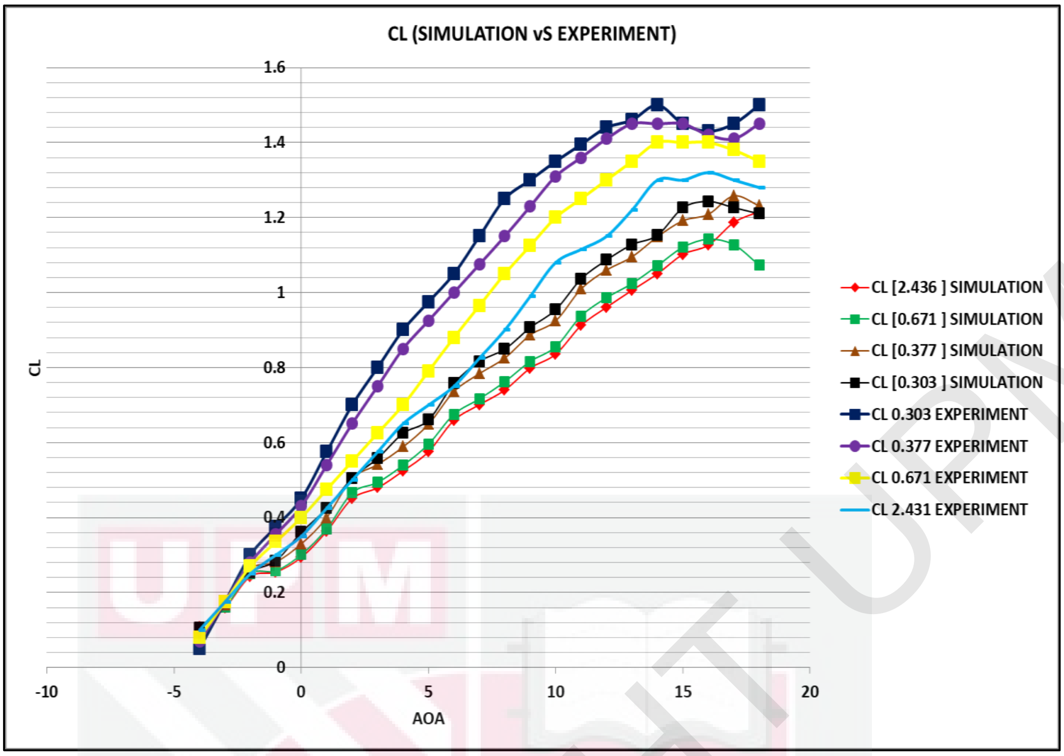

Figure 4.73: CL graph of UH18-SPW with Naca4412 (Experiment) VS UH18-SPW with Naca4412 (Simulation)

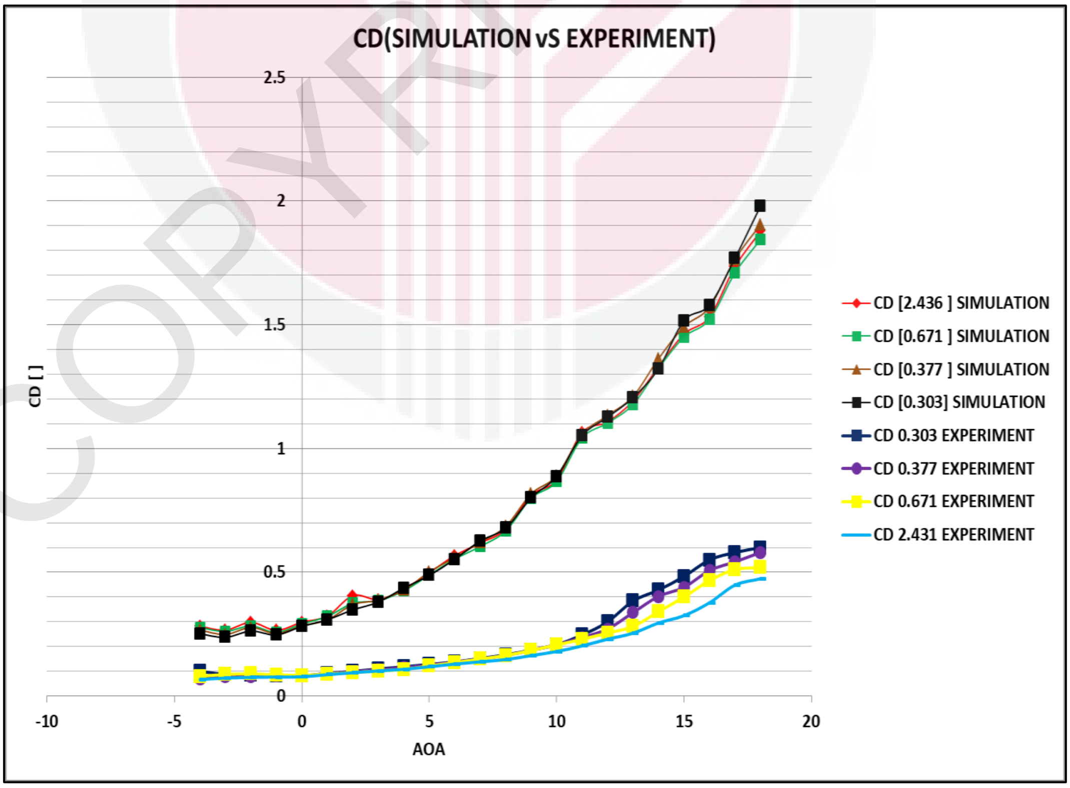

Figure 4.74: CD graph of UH18-SPW with Naca4412 (Experiment) VS UH18-SPW with Naca4412 (Simulation)

Throughout the simulations, drag result was shown to be higher as much as 62.5%. In some cases, lift remained relatively comparable even when drag was drastically different than Steven Morris, 2008 data [68]. Figure 4.74 shows the CD graph of UH18-SPW obtained from flow simulation. As for moment, it is shown that without a horizontal tail plane (HTP), the craft is longitudinal static unstable. This is similar with Steven Morris data where the CM graph shows that it is longitudinally unstable without horizontal tail plane HTP [60]. To the author understanding, CG location must be place in front of COP location in order to achieve negative slope. Figure 4.75 shows the CM graph of UH18-SPW obtained from flow simulation. As conclusion, other than similarity in graph pattern other aspect of the graph showed significant differences. This is due to both Re Number applied in Simulation and Experimental process was different due to limitation mention in chapter one

.

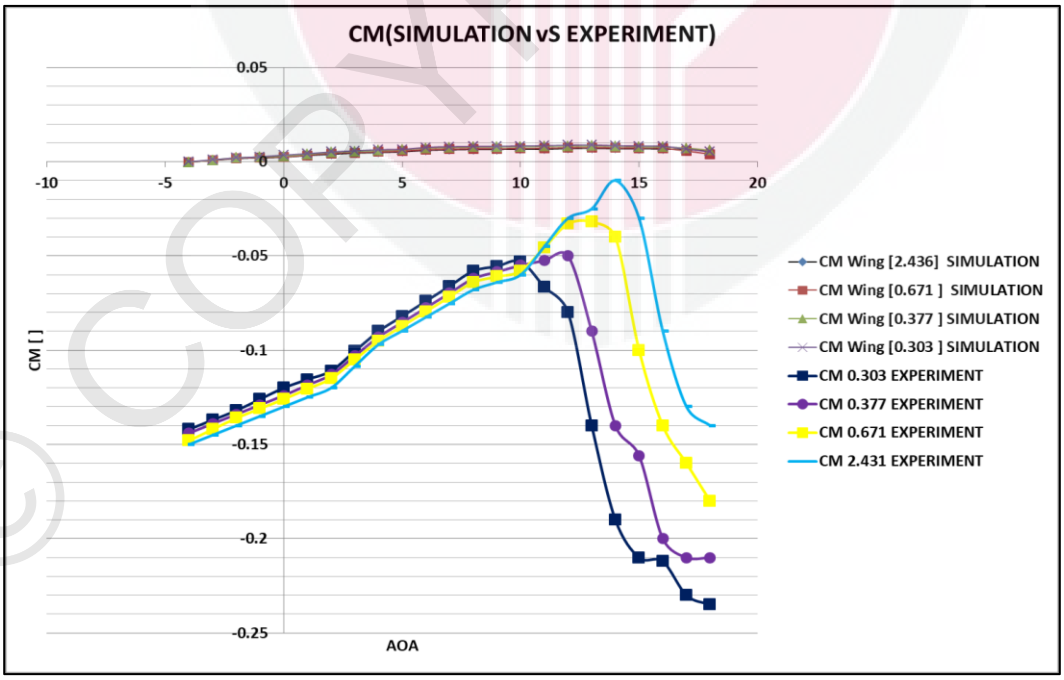

Figure 4.75: CM graph of UH18-SPW with Naca4412 (Experiment) VS UH18-SPW with Naca4412 (Simulation)

4.7 Aerodynamic Performance Result of New Two-Seater UHID Hoverwing

Through this ideology, by using XFLR5 the author has done multiple iterations of COP migration simulation in order to satisfy both requirements as discuss in previous chapter. The result of COP migration and aerodynamic performances of the conceptual Two-Seater UHID Hoverwing are shown in the following Figures of chapter 4.6.1.

4.7.1 Aerodynamic Performance Result of New Two-Seater UHID Hoverwing

After done with COP migration investigation, the next task is to look at the aerodynamic performance of conceptual Two-Seater UHID Hoverwing configuration which to conduct external flow simulation. The chosen software used for the generation and execution of the computational domain is Solidwork Flow simulation. It can obtain these values as well as able to display contour and vector plots. This gives excellent flow visualization of the ground effect. Figure 4.76 shows the CAD modeling of conceptual Two-Seater UHID Hoverwing using SOLIDWORK Workbench.

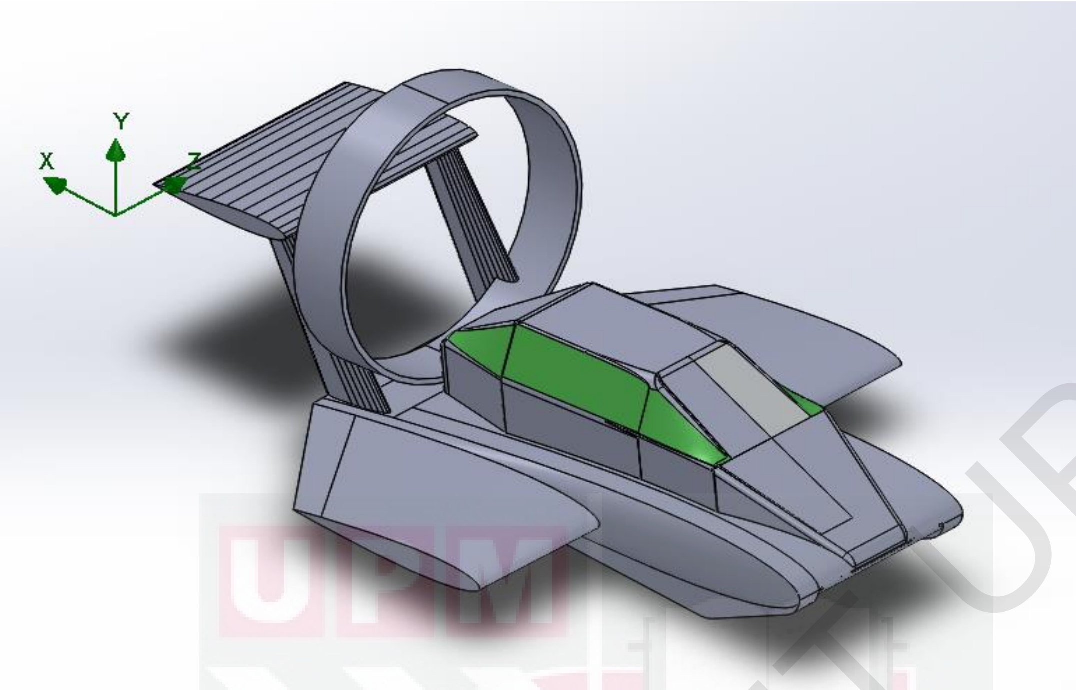

Figure 4.76: The conceptual Two-Seater UHID Hoverwing CAD using SOLIDWORK Workbench.

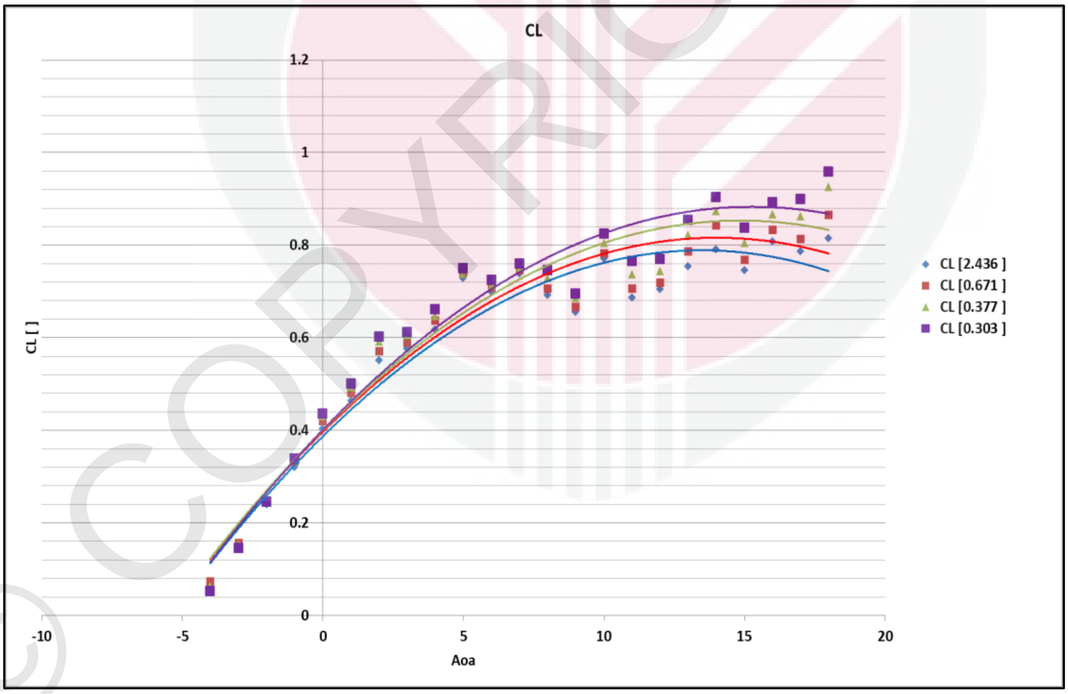

Figure 4.77: The conceptual Two-Seater UHID Hoverwing CAD using SOLIDWORK Workbench CL Vs AOA at Different HC

The blockage effect forming underneath the conceptual Two-Seater UHID Hoverwing model contributed to the increase in CL values as shown in Figure 4.77. This can be clearly seen when analyzing Figure 4.78 which shows the change in static pressure around the model. An extremely high-pressure region can be seen close to the leading edge. This transpires down towards the wall creating a cushion like effect which engulfs around the model underneath. This cushion-like effect has been observed fairly commonly when the ground effect has been studied by both (Satterfield, 2002) and (Abramowski, 2007). The same effect also showed underneath new conceptual UHID Hoverwing of Naca0012 wing surfaces as shown in Figure 4.79.

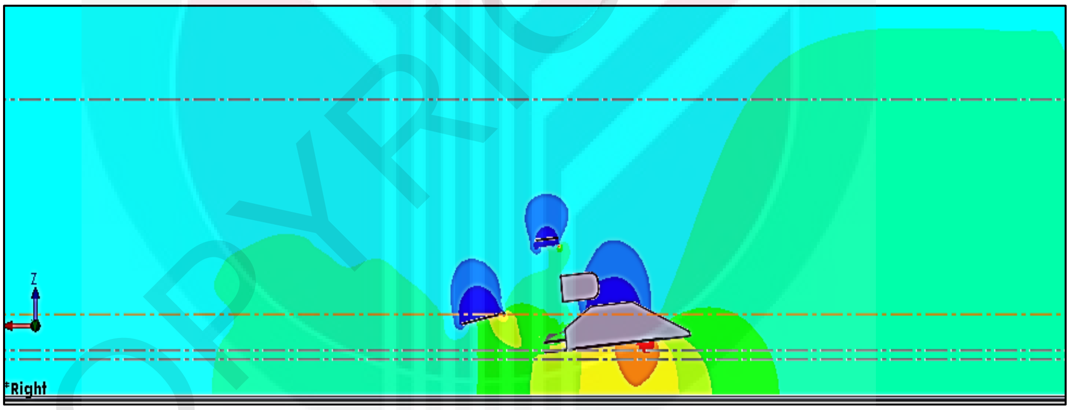

Figure 4.78: Static Pressure Contour around The conceptual Two-Seater UHID Hoverwing at a 0 degree A0A

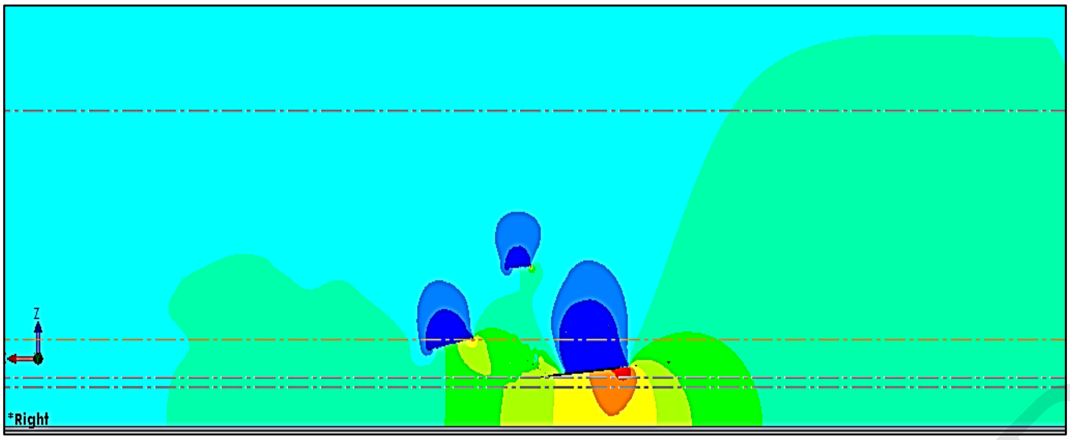

Figure 4.79: Static Pressure Contour around the conceptual Two-Seater UHID Hoverwing at a 0 degree A0A

The blue region shown in Figure 4.78 and 4.79 indicates a low-pressure act on the surface model. It can be observed that region with low pressure is tantamount to higher drag. This can be clearly seen when analyzing Figure 4.80 which shows the change in velocity around conceptual Two-Seater UHID Hoverwing at a 0-degree A0A. The high velocity region indicates the highest drag force.

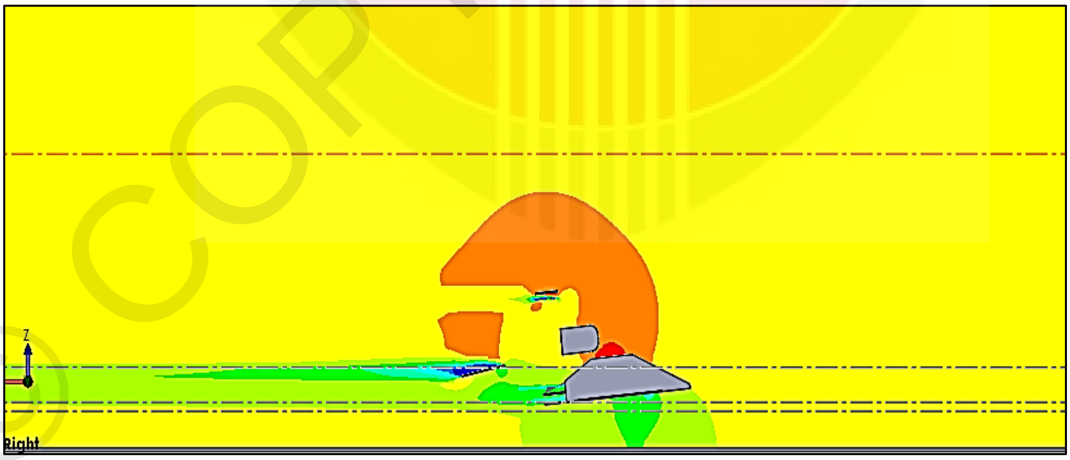

Figure 4.80: Velocity Contour around the conceptual Two-Seater UHID Hoverwing at a 0 degree A0A

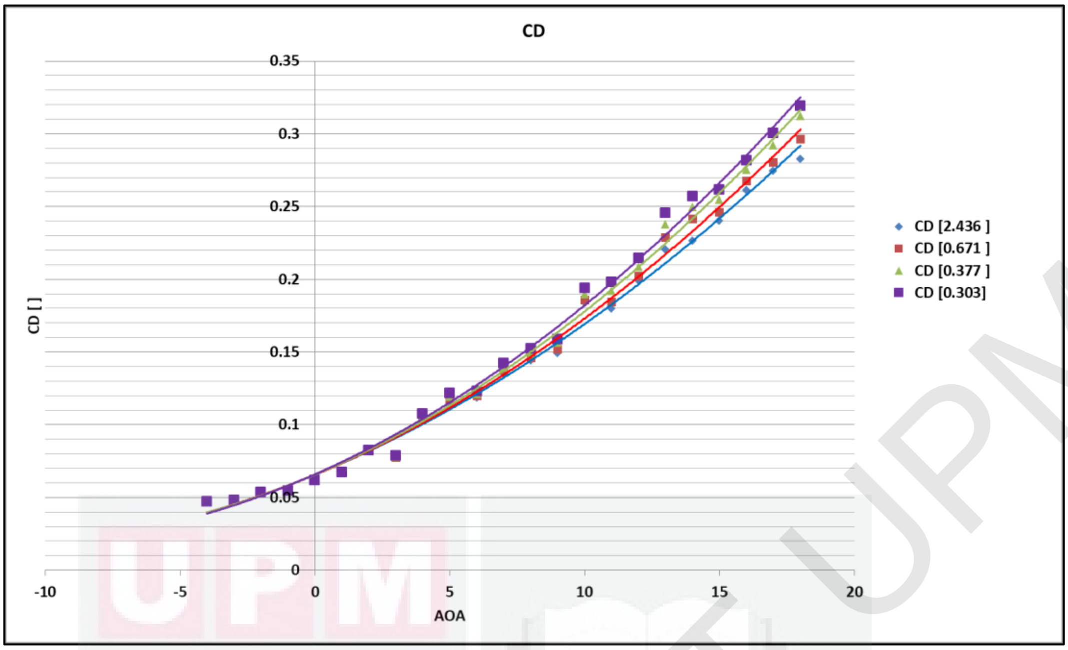

Figure 4.81: The conceptual Two-Seater UHID Hoverwing CD Vs AOA at Different HC

Changes in the CD values for the conceptual Two-Seater UHID Hoverwing as it was subjected to the Ground Effect are shown in Figure 4.81 as the conceptual Two-Seater UHID Hoverwing gets closer to the ground, it can be seen that there is a significantly rise in drag as AOA increases. The drag significantly increases from 0◦ AOA and the greatest drag increments for the new conceptual UHID Hoverwing of Naca0012 occurs at the highest 18◦ degree of AOA. This effect is particularly apparent as HC decreased. Currently there are no studies found, to have recorded such high reductions of drag values in ground effect condition.

The combination effect of the lift and drag result in an increase in the aerodynamic efficiency from -4º to 3º of conceptual Two-Seater UHID Hoverwing in ground effect due to an increase in the L/D ratio. This is in agreement with Steven Morris wind tunnel test where the aerodynamic efficiency is from -4º to 4º. After that, the efficiency slowly deteriorates until 18º. This is to show that different in ground plane heights also resulted in a significant change in the lift-to-drag ratio of the conceptual Two-Seater UHID Hoverwing. The overall trend as seen in Figure 4.82 is an increase in CL/CD ratio as ground clearance reduces especially on 0.303 HC. CL/CD increase proportional to reduction of the model height. Figure 4.82 also showed a value that is in good agreement with Steven Morris wind tunnel test with lower differences as much as 30 % to 35 %

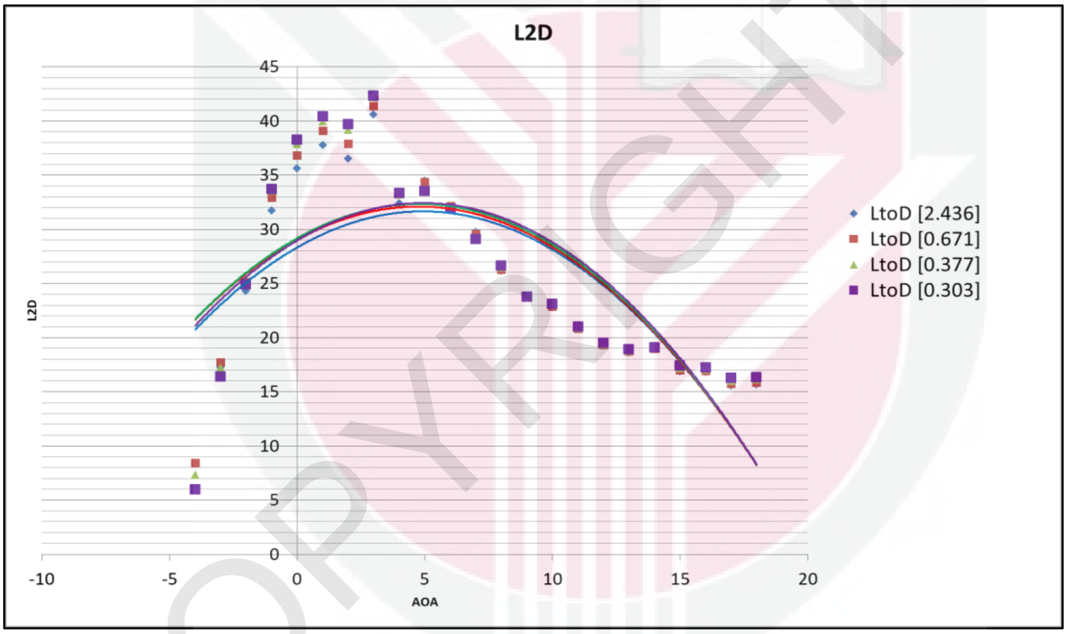

Figure 4.82: The conceptual Two-Seater UHID Hoverwing CLCD Vs AOA at Different HC

Figure 4.83 shows the change of Wing and fuselage moment coefficient against AOA with several different HC. Variations in the pitching moment with changing ground clearance can be seen for the conceptual Two-Seater UHID Hoverwing. The pitching moment acts at the center of pressure (COP) which is generally located 25% along the chord [94]. However as seen in literature the presence of ground effect results in a migration of the COP. A negative pitching moment is described as a nose pitch down motion of the airfoil. An increasingly negative pitch moment shows stability as it allows the airfoil to better counteract any disturbances such as gust. Theoretically, when COP has less migration the CM graph should sufficiently show a negative slope as long as the position of CG is forward of COP migration. This is the same case as when calculating the CM graph, the location of COP is considered fixed. From Figure 4.83, it can be seen that the model is longitudinally static stable even after inserting the COP location value in the CM graph calculation. The model is longitudinal static stable from 0º to 5º and the negative slope gradually becoming almost neutrally stable as it reaches 10º. The curve slope also achieved positive intercept. The several iterations change the location of COP thus having a significant effect on the CM graph.

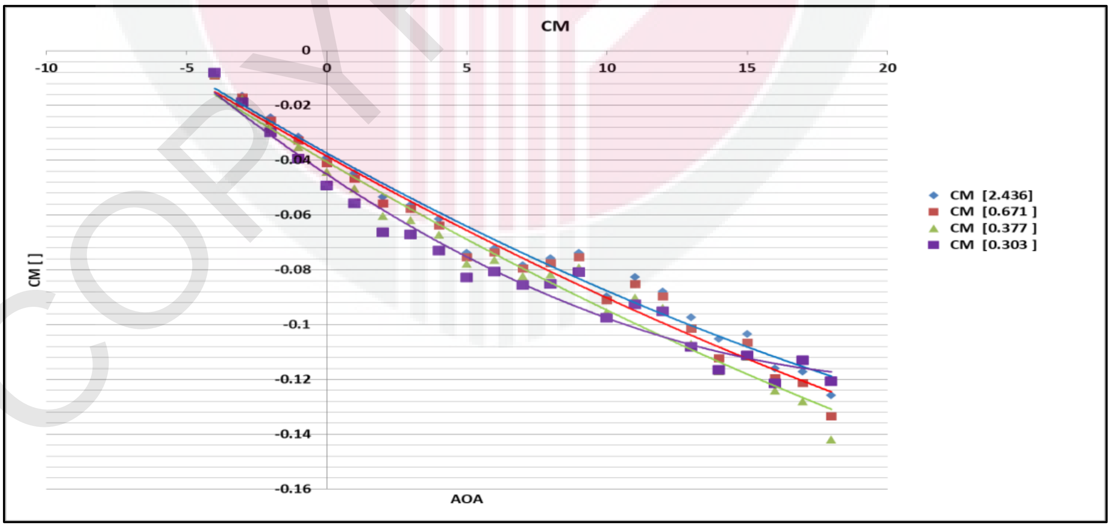

Figure 4.83: Wing and fuselage moment coefficient against AOA at Different HC

Figure 4.84 shows the conceptual Two-Seater UHID Hoverwing pressure flow trajectory in ground effect to out of ground effect. These Figures is a visualization of pressure contours and streamlines for conceptual Two-Seater UHID Hoverwing at three different heights above the ground: 0.03 meters (IGE), 0.1 meters (IGE), and 1 meter (OGE). The color code represents the pressure, with red being the highest pressure and blue being the lowest pressure. The length of the curve pattern represents the distance that the air travels behind conceptual Two-Seater UHID Hoverwing. The Figure also shows that the pressure flow trajectory for the Dragonfly is significantly affected by its height above the ground. At the lowest height (0.03 meters), the pressure flow trajectory is very close to the ground. This is because the conceptual Two-Seater UHID Hoverwing is flying very close to the ground and is experiencing a strong ground effect. As the height of the conceptual Two-Seater UHID Hoverwing increases (0.1 meters and 1 meter), the pressure flow trajectory becomes less affected by the ground and more similar to the flow pattern of a conventional aircraft. The pressure signatures in the Figure show that the conceptual Two-Seater UHID Hoverwing is generating a significant amount of lift due to the ground effect. The pressure is highest under the lifting surfaces of the conceptual Two-Seater UHID Hoverwing and decreases as the air moves away from it. The length of the curve patterns also shows that the air is traveling further behind the craft at the lower heights. This is because the ground effect is channeling the airflow and preventing it from spreading out as much.

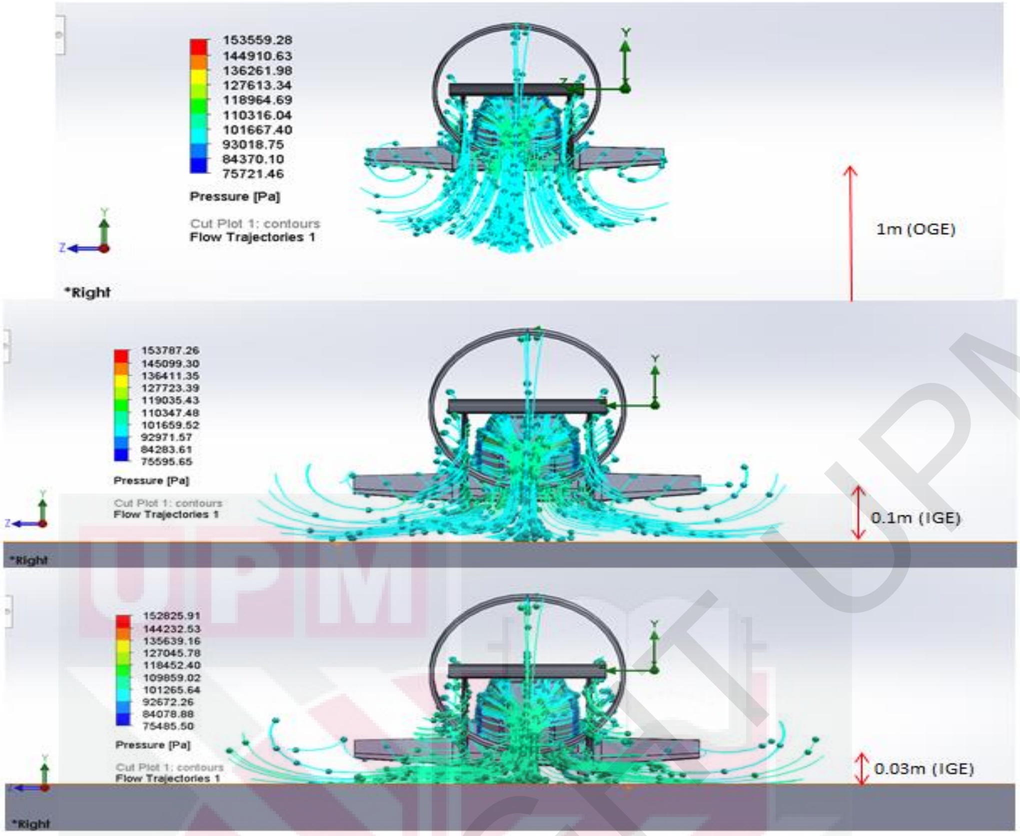

Figure 4.84: The conceptual Two-Seater UHID Hoverwing pressure flow trajectory IGE to OGE

Figure 4.85 shows the conceptual Two-Seater UHID Hoverwing velocity flow trajectory in ground effect to out of ground effect with the same standard color codes, pattern curves and height from ground level as discussed earlier. At the lowest height (0.03 meters), the air flow is closest to the ground, and the velocity decreases rapidly as the distance behind it increases. This is because the conceptual Two-Seater UHID Hoverwing is flying very close to the ground and is experiencing a strong ground effect. This effect creates a cushion of air that the craft rides on, reducing the amount of lift that needs to be generated by the lifting surfaces. The air flow separates from the ground much sooner, and the velocity decreases more gradually as the distance behind the conceptual Two-Seater UHID Hoverwing increases.

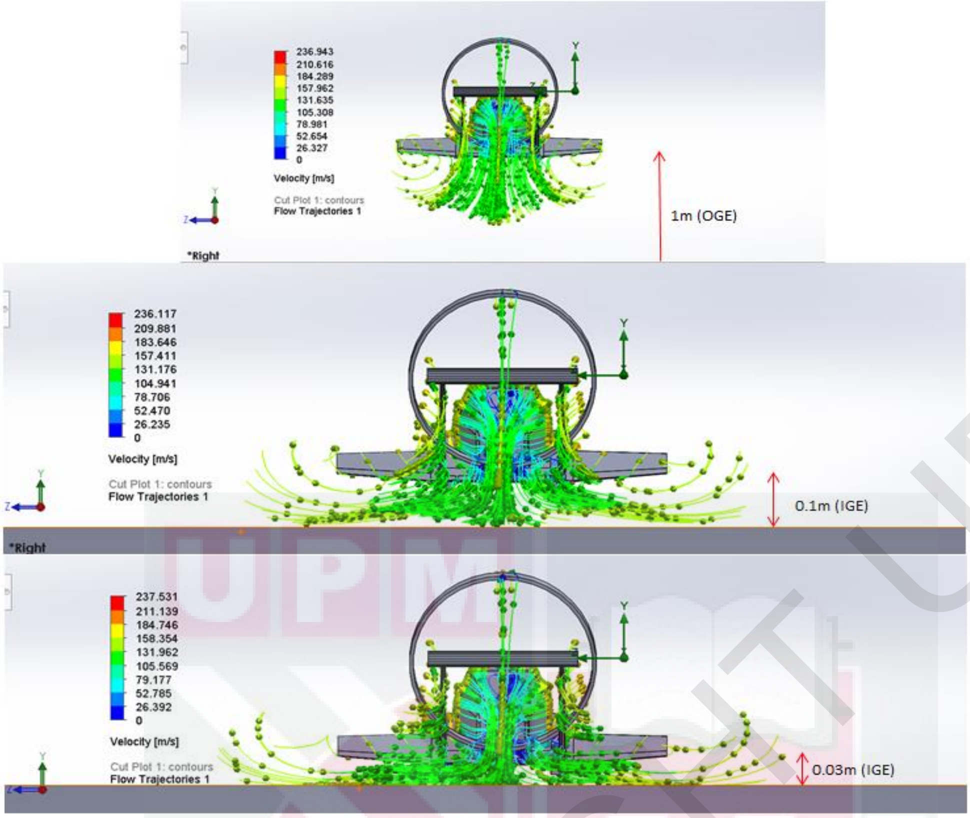

Figure 4.85: The conceptual Two-Seater UHID Hoverwing velocity flow trajectory IGE to OGE

4.8 Aerodynamic Performance and Center of Pressure Migration of Two-Seater UHID Hoverwing Result Discussion

In this chapter, the measurement outcome of objective three is been answered. The result of individual type was compared and discussed to determine the best aerodynamic performance. Data acquisition such as COP migration percentage, maximum CL, and CD, stall angle and CM graph curve was used in determining the final outcome. Based on aerodynamic data result specification comparison between UH18-SPW with Naca 4412 and conceptual Two-Seater UHID Hoverwing as shown in table 64, the chosen WIG craft as final outcome is the conceptual Two-Seater UHID Hoverwing and the reason are discussed in the next paragraph.

Table 64: Aerodynamic Data Result Specification of all Hoverwing types

DATA TYPE	COP %	CL max	AOA Stall	CD max	CM Curve
UHID Hoverwing	0.00046	0.902	14º	0.319	Stable
UH18-SPW N4412	13.48	1.5	14º	0.6	Unstable

From Table 63, it can be seen that conceptual Two-Seater UHID Hoverwing configuration has the lowest maximum lift coefficient which about 0.902. However, it also has the average drag coefficient which about 0.319 at high angle of attack. The center of pressure migrated about 0.00046 % from its original location. The pitching moment curve is positive for both altitudes, indicating it is a longitudinal static unstable. As for UH18-SPW with Naca 4412, this configuration has the maximum lift coefficient and highest stall angle which about 1.5 and 14° when comparing to all types. It also has the highest drag coefficient which about 0.6 when compared to conceptual Two-Seater UHID Hoverwing. The center of pressure migrated by 13.48 % indicating it to be the second highest migration when comparing with all types. The pitching moment curve is positive, indicating instability in longitudinal direction.

As a conclusion, this study aimed to improve the design of Wing-in-Ground-Effect (WIG) craft by understanding the existing designs. Through investigation of the COP migration of various lifting surfaces configurations and existing WIG craft, this analysis provided insights into how pressure distribution changes across the lifting surfaces as the WIG craft transitions between flight modes (in ground effect to out of ground effect flight). Based on established design requirements and the learning from existing WIG craft, the study came to a conclusion of new conceptual design for a two-seater Hoverwing craft. Finally, the study compared the performance of the proposed design with existing WIG craft (baseline references). This comparison would reveal potential improvements in areas like efficiency, stability, or payload capacity.

CHAPTER 5

CONLCUSION & RECOMMENDATION

As final conclusion, the thesis has successfully investigated and determined the relationship between Center of Pressure (COP) migration and WIG craft instability. This analysis provided insights into how pressure distribution changes across the wings as the aircraft transitions between flight modes. Based on the analysis established, the study develops a new conceptual design of two-seater WIG craft, analyze it and compared the performance with other existing WIG craft. Based on the process mentioned above, it is concluded the new conceptual Two-Seater UHID Hoverwing have the most advantages among other WIG craft. The conclusions are elaborated further in the next sub chapter.

5.1 Center of Pressure Migration In & Out Of Ground Effect for Cambered, Flat Airfoil & Bixel Patent

All type of aircraft flies through ground effect at some point. Although there are few aircraft that has been designed to be precise on ground effect are either unsuitable or unable to take them into flight that is OGE (free flight). Those that can fly OGE are only capable of short distance hops into free flight or in a form of small capacity such as UH18-SPW [53]. Ultimately, one can conclude that a satisfying configuration must have a minimal COP migration in term of HC and AOA increment. However, the significant severances of ground effect depend on the total COP migration from 0◦ to

10°. To the author understanding, a pitch up tendency occurred due to ‘gap’ distance of COP migration from the WIG craft/any aircraft Centre of Gravity (COG). Therefore, as COP further distancing from its origin, moment force of COP will increase resulting instability in longitudinal direction. From the result and discussion of this study, it is safe to conclude that the COP migration from 0◦ to 10° needed to be as less as possible to make sure the flight achieves sufficient stability in longitudinal direction IGE and OGE.

5.2 New Conceptual Design of two-seater WIG craft – UHID Hoverwing

Based on the design process outcome, the thesis successfully produces a new conceptual design of two-seater WIG craft that utilize flat wing configuration to enhance longitudinal stability. The design also intended to have a quality of enhanced lift, drag, and stability while traveling at different height to ground level conditions. From the analysis result shown, a flat surface profile and all Bixel AR double wing configurations are operational capable in term of longitudinal static stability in or out of ground effect condition. However, in term of lift capability Flat airfoil produce less lift compared to camber profiles [107]. From the COP migration simulation data obtained, it is proven that a flat or symmetrical airfoil [108] does have much lesser migration as ground clearance and AOA increase or decrease. Since the effect of COP migration tends to significantly increases proportionally to the chord lifting surfaces, this is not in flat or symmetrical cases as COP location of this type of airfoil tend to rarely making a large movement as ground clearance and AOA increase or decrease. Hence, Bixel claimed wasn't far from the truth as theoretically increasing chord lifting surfaces of this type of WIG craft can achieve 4 times ground clearance than conventional aircraft since it should be stable longitudinally.

5.3 Aerodynamic Performance and Stability of the Proposed new conceptual Two-Seater UHID Hoverwing

The thesis has successfully shown the preliminary aerodynamic performances of new conceptual Two-Seater UHID Hoverwing. The new conceptual Two-Seater UHID Hoverwing is able to accommodate maximum payload of 546 kg at 14º AOA and takeoff weight of 454 kg at 5º AOA. The location of center of pressure (COP) migrates from inside ground effect to outside ground effect as the new conceptual Two-Seater UHID Hoverwing lift causing less stability and manageable control response. Choosing the right-wing profile and platform of maximum lift and minimum drag is the tradeoff. The new conceptual Two-Seater UHID Hoverwing also has a minimum fuel capacity and stay operating long enough for commercialization. The wingtip may also have an impact when turning as the hoverwing operate under ground effect.

5.4 Contribution of Knowledge through the Discovery of New Finding

This thesis presents a novel graphical approach to analyzing the behavior of the Center of Pressure movement for a various type of wings and existence WIG craft configurations in ground effect and out of ground effect across various Angles of Attack. This graphical method offers a deeper understanding of how the COP migrates under different flight conditions. The thesis goes beyond just analysis, it also introduces a design process for developing a novel 2-seater hoverwing concept. This design leverages the insights gained from the COP analysis, potentially leading to a more optimized hoverwing configuration. Lastly, the applications of this research extend beyond hoverwings. The graphical method for COP movement analysis can be applied to other flying vehicles, such as Wing-in-Ground effect (WIG) craft. This could be instrumental in developing active control systems for these vessels, allowing for more precise and stable flight control. Overall, this thesis contributes valuable knowledge to the understanding and design of hoverwings and other WIG crafts.

5.5 Future Recommendation

The thesis has highlighted the center of pressure (COP) migration which in essence is caused by pressure distribution caused by the flow around the airfoil. The COP migration has been investigated and the result has been obtained. Although the objectives of this thesis have being carried successfully, the accuracy of the result is still preliminary level at best. This is due to the lack of tools such as XFLR5 which only used thin wing VLM method to predict the pressure around lifting surfaces. This is less desirable as theoretically pressures on both upper and lower surfaces are needed to accurately calculate the COP location. Nevertheless, the XFLR5 instantaneous displayed COP location on lifting surfaces is one of the remarkable functions of this aerodynamic software since through this method multiples reconfiguration of lifting surface to improve COP migration can be done in less time. Unlike other CFD software although they do offer various improvement in term of result accuracy, unfortunately they did not provide COP location display function like XFLR5. These increases the task times as one has to calculate COP migration on every configuration manually unless in the future this function has been embedded into CFD software.

The performance analysis described in the previous section has not been validated experimentally. Therefore, further analysis must be carried out in wind tunnel experiments. However, the successful flight test of the RC model provides a proof of concept for the subsequent future full scale engineering design and prototype fabrication. The preliminary aerodynamic analysis indicated that the new conceptual Two-Seater UHID Hoverwing is able to operate with maximum payload and minimum fuel consumption and it is able to achieve longitudinal stability in and out of ground effect zone.

REFERENCE

[1] T. M. Buildar, "WIG Short Theory," *Turkstra.com,* 2021.

[2] W. S. Ruchała, "GROUND EFFECT INFLUENCE ON THE AERODYNAMIC CHARACTERISTICS OF ULTRALIGHT HIGH-WING AIRCRAFT – WIND TUNNEL TESTS," *Journal of KONES Powertrain and Transport, Vol. 24, No. 2,* p. 1, 2017.

[3] Z. Z. A. P. A. H. A. M. Matdaud, "Stabilizing Attitude Control For Mobility Of Wing In Ground (WIG) Craft – A Review," *Southeast Asia Workshop on Aerospace Engineering,* p. 3, 2019.

[4] C. Dritsas, "Flight Dynamics of a Wing in Ground Effect Air Vehicle Utilizing a RAM Air Wing," *Cranfield University,* p. 242, 2006.

[5] S. Fluck, "Thesis Ground Effect Vehicles: Models and Technology," *2011 ,* p. 17.

[6] M. B. Y. M. S. J. Adi Maimun, "AERODYNAMIC CHARACTERISTICS OF A WIG CRAFT BY NUMERICAL SIMULATION," *International Conference on Marine Technology,* p. 9, 2012.

[7] A. D. K.M. Saridakis, "Soft computing in engineering design – A review," *Machine Design Laboratory, Department of Mechanical Engineering & Aeronautics, University of Patras, Patras 26500, Greece,* 2007.

[8] Gor Carvalho Santos De Oliveira Luis Felipe De Aguilar Paulinyi, "AERODYNAMIC STUDY OF FORMULA 1 WING IN GROUND EFFECT USING COMPUTATIONAL FLUID DYNAMICS," *24th ABCM International Congress Of Mechanical Engineering December 3-8, Curitiba, PR, Brazil,* p. 11, 2017.

[9] Albert Landis, "CFD analysis of RAM air flow in an aircraft air conditioning system," *The University of Leeds School of Chemical and Process Engineering,* p. 65, 2018.

[10] C. J. T. B. C. K. C. J. G. H. Wanga, "Computational Aerodynamics and Flight Stability of Wing-InGround (WIG) Craft," *7th Asian-Pacific Conference on Aerospace Technology and Science, 7th APCATS,* p. 10, 2013.

[11] D. P. P. P. Beverly Beasley, "Morphing Wing Geometry," *Virginia Tech Aerospace Engineering,* p. 52, 2003.

[12] C. T. a. S. A. Rattapol Sakornsin, " Experimental Investigation of the Ground Effect of Ground Effect of WIG Craft-NEW1 Model," *Innovation Aviation & Aerospace Industry-International Conference 2020 (IAAI 2020, Chumphon Thailand),* p. 6, 2020.

[13] M. S. S. Mohammad Tavakoli, "A Practical Method for Investigation of Aerodynamic and Longitudinal Static Stability of Wing-in-Ground Effect," *INTERNATIONAL JOURNAL OF MARITIME TECHNOLOGY,* p. 9, 2015.

[14] A. A. K. P. V. S. a. E. A. P. V I Chernousov, " Ground effect aerodynamics of twin fuselage aircraft," *IOP Conf. Series: Materials Science and Engineering,* p. 9, 2022.

[15] A. Nunthasitthakorn, "Longitudinal Stability of a Small Commercial WIG Craft," *School of Aerospace, Mechanical and Manufacturing Engineering, RMIT University,* p. 8, 2011.

[16] G. K. Taylor, "ARE YOU MISSING THE BOAT? THE EKRANOPLAN IN THE 21ST CENTURY ITS POSSIBILITIES AND LIMITATIONS," *18th Fast Ferry Conference,* p. 12, 2002.

[17] A. B. Liang Yun, "High Performance Marine Vessels," *Springer Science+Business Media, LLC,* p. 378, 2012.

[18] C.-s. H. C.-H. B. Juhee Lee, "Influence of Wing Configurations on Aerodynamic Characteristic of Wings in Ground Effect," *Hoseo University, Asan Chungnam 336-795, Republic of Korea,* p. 11, 2010.

[19] M. Z. M. R. A. E. M. F. &. H. F. Wiriadidjaja S, " Wing-in-ground-effect craft as a potential domestic transport vehicle," *AIAA Applied Aerodynamics Conference,* 2016.

[20] N. Kornev, " Investigation of influence of non linear and unsteady effect on the stability of WIG craft under pertubation cause by wind and waves," *Universitat Rostock,* p. 17, 2011.

[21] N. Kornev, " COMPLEX NUMERICAL MODELING OF DYNAMICS AND CRASHES OF WING-IN-GROUND VEHICLES," *California Institute of Technology, Pasadena, CA, 91125, USA,* p. 9, 2003.

[22] H. Z.-B. S.N. Skinner ∗, "State-of-the-art in aerodynamic shape optimisation methods," *University of Glasgow, School of Engineering, Glasgow G12 8QQ, UK,* p. 30, 2016.

[23] N. Kornev, "On Unsteady Effects in WIG Craft Aerodynamics," *International Journal of Aerospace Engineering,* p. 5, 2019.

[24] S. K. M. K. Hiromichi Akimoto, "Wing in surface effect ship with canard configuration," *x Inderscience Enterprises Ltd,* p. 16, 2014.

[25] A. S. T. Abdulhalim, "The effect of aspect ratio on aerodynamic performance and flow separation behavior of a model wing composed from different profiles," *JOURNAL OF ENERGY SYSTEMS,* p. 13, 2018.

[26] D. S. C. E. S. C. F. V. a. P. T. Cristina Riso, "Parametric Roll maneuverability Analysis of a High-Aspect-Ratio-Wing Civil Transport Aircraft," *AIAA SciTech Forum, Orlando FL,* p. 28, 2020.

[27] C. Hiemcke, "Design of a wing section in ground effect:application to high speed ground transportation," *Iowa State University,* p. 369, 1994.

[28] A. B. J. D. Liang Yun, "Wig Craft and Enkranoplan Ground Effect craft Technology," *Springer Science+Business Media,* p. 17, 2010.

[29] C. H. H. K. S. K. a. J. L. Kyoungwoo Park, "Effect of Endplate Shape on Performance and Stability of Wings-in Ground (WIG) Craft," *World Academy of Science, Engineering and Technology International Journal of Aerospace and Mechanical Engineering Vol 2 No 11,* p. 7, 2008.

[30] B. Tae-Cheol Jung, "Design of Air Cushion Vehicles Using Artificial Intelligence:Expert System and Genetic Algorithm," *Ryerson University Toronto,* p. 161, 2002.

[31] C. G. Bixel, "Hovercraft Ground-Effect Vehicle," *US Patent 5105898,* p. 10, 1989.

[32] J. SIDERITS, "HOVERCRAFT: BODY AND FRAME," *Faculty of the Mechanical Engineering Technology Program of the University of Cincinnati,* p. 38, 2011.

[33] Y. S. Ong, "Artificial Intelligence Technologies in Complex Engineering Design," *UNIVERSITY OF SOUTHAMPTON,* p. 132, 2002.

[34] C. Krishnamoorthy and S. Rajeev, "Artificial Intelligence and Expert Systems for Engineers," *CRC Press LLC,* p. 254, 1996.

[35] C. T. L. a. E. T. T. Wong, "CFD Simulation of a Wing-In-Ground-Effect UAV," *International Conference on Aerospace and Mechanical Engineering (AeroMech17),* p. 9, 2018.

[36] R. K. A. Michael Grabis, "Computational Fluid Dynamics Analysis of Inverted, Multi-Element Airfoils in Ground Effect," *Washington University in St. Louis,* p. 90, 2019.

[37] D. K. E. R. R. G. S. N. V. R. N. U. V. Zubin Zaheer, " CFD analysis of the performance of different airfoils in ground effect," *International Conference on Aerospace and Mechanical Engineering, ICAME'18 ,* p. 8, 2018.

[38] R. B. S. H. F. K. G. T. Klaus Matjasic, "THE HOVERWING CONCEPT - A NEW GENERATION OF HIGH SPEED MARINE CRAFT," *Nato Conference,* p. 11, 2003.

[39] P. A. C. Wei Yang, "WIG craft serves niche transportation needs," *World Review of Intermodal Transportation Research, Vol. 3, No. 4,* p. 13, 2011.

[40] K. F. H. Alan, "Ground Effect on Lift Generating Body," *National University of Singapore,* p. 250, 2013.

[41] B. N. G. H. Q. Y. S. J. T. B. W. a. L. S. B. G. Ng Dyi En, "Wing in

Ground (WIG) Effect Vehicle," *National University of Singapore,* p. 18, 2004.

[42] J. Quah Yong Seng, "Stability, Performance & Control for a Wing in Ground Vehicle," *National University of Singapore,* p. 58, 2005.

[43] A. Nebylov, "WIG-Craft Flight Control Systems Development," *State University of Aerospace Instrumentation, 67, Bolshaya Morskaya str., Saint-Petersburg, 190000, Russia,* p. 11.

[44] J. Junde, "Aerodynamics and Propulsion for an Inverted Delta Wing-InGround Effect Aircraft," *National University of Singapore,* p. 76.

[45] L. Qihui, "Stability Control and Performance for an Inverted Delta Wing-In-Ground Effect Aircraft," *National University of Singapore,* p. 92, 2006.

[46] D. D. S. S. V. N. Alexander Nebylov, "FLIGHT AUTOMATIC CONTROL SYSTEMS FOR THE WING-IN-GROUND EFFECT CRAFT BUCHON-1," *State University of Aerospace Instrumentation, 67, Bolshaya Morskaya, Saint-Petersburg, 190000 Russia,* p. 6, 2007.

[47] P. C. M. a. M. C. P. C. M. Daniel James, "Aerodynamically Alleviated Marine Vehicle (AAMV):Bridging the Maritime-to-Air Domain," *Cranfield University, UK,* p. 11, 2015.

[48] Eric Leonhardt, "The Ekranoplan Vehicle Design Project," *Western Washington University,* p. 8, 2004,.

[49] S. O. Michael Halloran, "Wing In Ground Effect Craft Review," *The Sir Lawrence Wackett Center For Aerospace Design And Technology. Royal Melbourne Institute Of Technology, Melbourne,* p. 88, 1999.

[50] W. Y. a. Y. L. Zhigang YANG, " Analysis of Two Configurations for a Commercial WIG Craft based on CFD," *Shanghai Automotive Wind Tunnel Center, Tongji University, Shanghai, China,* p. 9, 2018.

[51] W. Pearce, " Lun-class / Spasatel Ekranoplans," *Old Machine Press,* p. 10 , 2019.

[52] N. D. E. Benedict, " Structure design and analysis for a small-scale wing in ground (WIG) vehicle," *National University of Singapore,* p. 96, 2005.

[53] E. v. d. V. J. H. E.K. den Breejen, "" Wing in ground vehicles operating as high-speed passenger ferries, A feasibility and profitability study",," *TU Delft Mechanical, Maritime and Materials Engineering. Delft University of Technology,,* p. 49, 2018.

[54] H. Hameed, "The design of a four-seat reverse delta WIG craft," *The Maldives National Journal of Research. Maldives National University,* p. 10, 2018.

[55] Z. P. &. K. Szafran, " Ground effect" Inter-Modal Fast Sea Transport," *Instiute of Aviation, Warsaw, Poland,* p. 317, 2014.

[56] B. J. P. Cadete, "Aero-Structural Optimization of Sailplane Wings," *Academia DaForca Aerea,* p. 124, 2011.

[57] L. Hainan England WIG Manufacturing Co., "CYG-11," *Haikou Meilan District Gui Ling Road No. 351,* 2020.

[58] M. A. A. T. A. M. R. S. a. E. H. Razali Abidin, "Preliminary Development of a Wing in Ground Effect Vehicle," *AIP Conference Proceedings 1930, 020004 ,* p. 7, 2018.

[59] M. K. M. Graham Taylor, "RE-DEFINING SEA LEVEL: THE HOVERWING WING IN GROUND EFFECT VEHICLE," *Paper for The Hovercraft Society, Air Cushion Technology Conference & Exhibition, England 14th & 15th October,* p. 8, 2003.

[60] R. B. a. J. S. Steven Morris, " Analysis of a Hoverwing in Ground Effect," *U.S. Air Force Academy, CO, 80841,* p. 3, 2008.

[61] Jeff Salton, "New Zealand's Home-Made 'Hoverwing' Flies 5 Feet Above Water," *The Nelson Mail,* 2010.

[62] A. F. T. M. R. M. S. R. S. W. Leon Bennett, "Wing in Ground Effect (WIG) aircraft Aerodynamics," *University of Adelaide Australia,* p. 59, 2016.

[63] ,. R. N. B. Iaroslav V. Zagumennyi, "Ground Effect in Hydrodynamics of a Strip in a Stratified Fluid," *Procedia IUTAM 8,* p. 10, 2013.

[64] S. Jamshed, " Introduction to CFD," *TU Delft Mechanical, Research Gate, Institute of Space Technology, Karachi campus,* p. 4, 2015.

[65] D. P. d. S. a. A. C. Julien Alexandre dit Sandretto, "Appropriate Design Guided by Simulation: An HovercraftApplication," *U2IS, ENSTA ParisTech, Universit´e Paris-Saclay,* p. 14, 2016.

[66] B. S. a. P. I. Yaakov Abudaram, " Wind Tunnel Testing of Load-Alleviating Membrane Wings at Low Reynolds Numbers," *47th AIAA Aerospace Sciences Meeting Including The New Horizons Forum and Aerospace Exposition,* p. 16, 2009.

[67] R. d. K. ,. a. B. G. R. Bleischwitz, "Aeromechanics of membrane and rigid wings in and out of ground-effect at moderate Reynolds Numbers," *University of Southampton, Southampton, SO17 1BJ, UK,* p. 23, 2016.

[68] J. S. Wallace, "Investigation Of Solidworks Flow Simulation As A Valid Tool For Analyzing Airfoil Performance Characteristics In Low Reynolds Number Flows," *Oklahoma State University Stillwater, Oklahoma,* p. 31, 2017.

[69] M. Sosnowski, "THE INFLUENCE OF COMPUTATIONAL DOMAIN DISCRETIZATION ON CFD RESULTS CONCERNING AERODYNAMICS OF A VEHICLE," *Journal of Applied Mathematics and Computational Mechanics,* p. 11, 2018.

[70] W. L. a. R. L. C. Irian Ordaz, "Automated Tetrahedral Mesh Generation for CFD Analysis of Aircraft in Conceptual Design," *Aerospace research central,* 2014.

[71] A. K. A. K. C. Hussain H. Al-Kayiem*, "An Investigation On The Aerodynamic Characteristics Of 2-D Airfiol In Ground Collision," *Journal*

of Engineering Science and Technology , UniversitiTeknologi PETRONAS, 2011.

[72] A. V. H. T. G. S. M. Aananthan M, "Wing in Ground Effect- 2d Analysis Using Ansys," *Journal of Engineering Research and Application, School of Engineering and Technology,vidya Nagar, Palissery..*

[73] A. Z. Z. H. M. S. R. A. A. P. a. M. T. A. Surjatin Wiriadidjaja, "Wing In Ground Effect Craft: A Study in Aerodynamics," *International Journal of Engineering & Technology,* 2018.

[74] C. G. a. J. M. Tom McLaughlin, "Analysis of a Hoverwing in Ground Effect," *46th AIAA Aerospace Sciences Meeting and Exhibit,* 2008..

[75] Z. M. A. Z. M. T. Afifi.A Pua'at, "Case Study on Aerodynamic Stability of Bixel WIng In Ground Effect Craft," *Southeast Asia Workshop on Aerospace Engineering (SAWAE),* 2019.

[76] G. D. McBain, "Theory of Lift, Introductory Computational Aerodynamics in MATLAB/Octave," *Wiley,* p. 10, 2012.

[77] T. Vogeltanz, "Application for Calculation of Mean Aerodynamic Chord of Arbitrary Wing Planform," *American Institute of Physics,* p. 5, 2016.

[78] D. R.H.Barnard, " Aircraft Flight A Description Of The Physical Principles Of Aircraft Flight," *Longman,* p. 39, 1995.

[79] F. T. J. Y. a. J. L. A. Shahzad, "Aerodynamic Hovering Performance of Rigid and Flexible Wing Planform Shapes," *20th Australasian Fluid Mechanics Conference,* p. 1, 2016.

[80] M. N. Landell-Mills, " How airplane wings generate lift is disputed," *Research Gate,* p. 43, 2019.

[81] P. Puttkammer, " Boundary Layer over a flat plate," *Universiti of Twente,* p. 49, 2013.

[82] G. M. Craig, "Stop Abusing Bernoulli, How Airplane Really Fly," *Regenerative Press, Anderson, Indiana,* p. 22, 1997.

[83] D. L. G. a. J. Katz, "Trapped Vortex in Ground Effect," *AIAA JOURNAL, San Diego State University, San Diego, California 92182,* p. 675, 2003.

[84] V. J. C. G. S. S.N Logu, "DESIGN AND FABRICATION OF RC PLANE WITH FLEXIBLE WINGS," *International Journal of Advance Engineering and Research Development,* p. 5, 2018.

[85] E. Geller, "HANG GLIDER STABILITY AND CONTROL," *3750 79th Ave. SE Mercer island WA 98040,* p. 10, 2003.

[86] B. G. Newman, "The Aerodynamics Of Flexible Membranes," *Department Of Mechanical Engineering, Mcgill University, Montreal, Quebec H3A 2K6, Canada,* p. 107, 1982.

[87] M. S. B. A. Aziz, " Numerical And Experimental Investigations Of 2d Membrane Airfoil Performance," *Universiti Sains Malaysia,* p. 3, 2012.

[88] M. V. C. a. M. Spottiswoode, " Modelling the flight dynamics of the hang glider," *THE AERONAUTICAL JOURNAL,* p. 20, 2006.

[89] I. Wanjohi, "Aeroelastic Analysis of a Flexible Membrane Wing," *Embry-Riddle Aeronautical University Daytona Beach, Florida Summer,* p. 87, 2004.

[90] D. G. a. R. S. Jan Hummel, "Automatic measurement and characterization of the dynamic properties of tethered membrane wings," *Faculty of Aerospace Engineering, Delft University of Technology, 2629 HS Delft, the Netherlands,* p. 15, 2019.

[91] V. Y. Mudkavi, "Powered Hang Gliding," *National Aerospace Laboratory,* p. 12, 2003.

[92] N. K. T. H. B. L. W. D. Andreas Groß, "FLIGHT STABILITY AND SAFETY OF WIG CRAFT WITH AND WITHOUT FEEDBACK CONTROL," *ASME 2014 12th Biennial Conference on Engineering Systems Design and Analysis ESDA2014 June 25-27,* p. 12, 2014.

[93] N. Hall, "Aerodynamic Center-AC," *Glen Research Center, Nasa*

Aeronautic and Space Administration, 2015.

[94] 1. 1. Anderson, "Fluids – Lecture 3 Notes," *Massachusetts Institute of Technology,* p. 3, 2008.

[95] H. Mahmood, "A CFD STUDY ON THE GROUND EFECT," *Department of Mechanical, Aerospace and Civil Engineering,* p. 42, 2015.

[96] N. U. Rathod, "Aerodynamic Analysis of a Symmetric Aerofoil," *Department of Mechanical Engineering, BMS college of Engineering, Bangalore, India,* p. 3973, 2014.

[97] A. T. A. R. R. V. S. K. E. U. Z. A. J. M. M. Nikhil S. Pillai*, "Investigation on airfoil operating in Ground Effect region," *International Journal of Engineering & Technology, 3 (4),* p. 5, 2014.

[98] E. I. A. Amin, "Efficiency of Wing-In-Ground Marine Crafts," *Faculty of Engineering, Port Said University,* p. 217, 2006.

[99] L. S. Ko, "An experimental investigation of the aerodynamic and vortex flow field of reverse delta wing," *Montreal Quebec, Canada,* p. 195, 2017.

[100] A. Nuhait, "Aero-elastic Behavior of Flat Plate Moving Near Ground," *Virginia Polytechnic Institute and State University,* p. 37, 2014.

[101] T. Abramowski, " NUMERICAL INVESTIGATION OF AIRFOIL IN GROUND PROXIMITY," *JOURNAL OF THEORETICAL AND APPLIED MECHANICS 45, 2, Warsaw,* p. 436, 2007.

[102] A. Z. M. T. A. A. H. Afifi.A.Puaat, "CENTER OF PRESSURE MIGRATION INVESTIGATION OF DIFFERENT WING CONFIGURATION," *Journal of Aeronautics, Astronautic and Aviation,* p. 7, 2022.

[103] A. Deperrois, "Overview of the theoretical background in XFLR5," *Rev. 1.1,* p. 20, 2019.

[104] D. G. D. Dr. A. Sobachkin, "Numerical Basis of CAD-Embedded CFD,"

Dassault Systèmes, 175 Wyman Street, Waltham, Massachusetts, 02451-1223, USA, p. 7, 2014.

[105] D. A. R. ,. D. P. S. F. S. Alexandre Medina, "STUDY OF THE FLOW OVER AN OSCILLATING NACA0012 AIRFOIL," *VIII Congresso Nacional de Engenharia Mecânica , 10a 15 deagostode,* p. 4, 2014.

[106] P. M. S. A. Ihsan Y. Hussain, "Aerodynamic Characteristics of CLARK-Y Smoothed Inverted Wing with Ground Effects," *International Journal of Computer Applications (0975 – 8887),* p. 50, 2016.

[107] H. O. B. G. a. I. C. Justin Winslow, "Basic Understanding of Airfoil Characteristics at Low Reynolds Numbers (104–105)," *Journal of Aircraft,* p. 1060, 2018.

[108] H. Liu, "AERODYNAMIC CHARACTERISTICS OF THE FLAT PLATE AIRFOIL AT LOW REYNOLDS NUMBERS," *The Johns Hopkins University,* p. 61, 2021.

[109] D. K. B. J. K. B. J. U. K. J. K. Debolina Dasgupta, "DESIGN OF RC AIRCRAFT," *IIT Madras, Chennai,* p. 163, 2013.

[110] V. N. P. M. N. L. I M Dantsevich, "Research of wing in surface effect ship configuration and development of an experimental model of increased stability," *IOP Conf. Series: Materials Science and Engineering 873,* p. 9, (2020).

APPENDICES

Appendix A

UHID Hoverwing Model Drawing

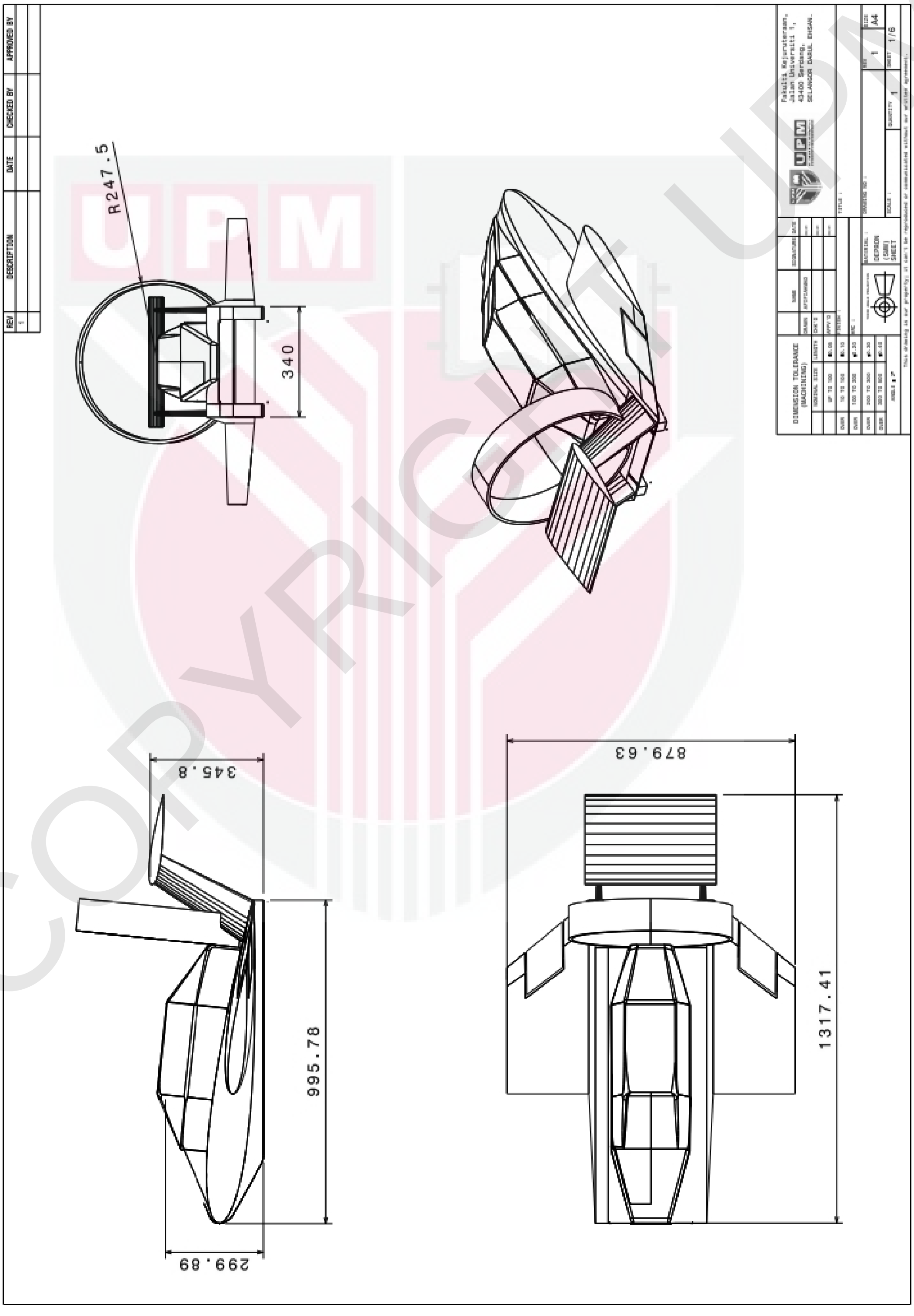

Appendix B

Chord Pressure distribution on Lifting Surfaces (Root to Tip)

Naca0012 Rectangular & Inverse Delta Wing

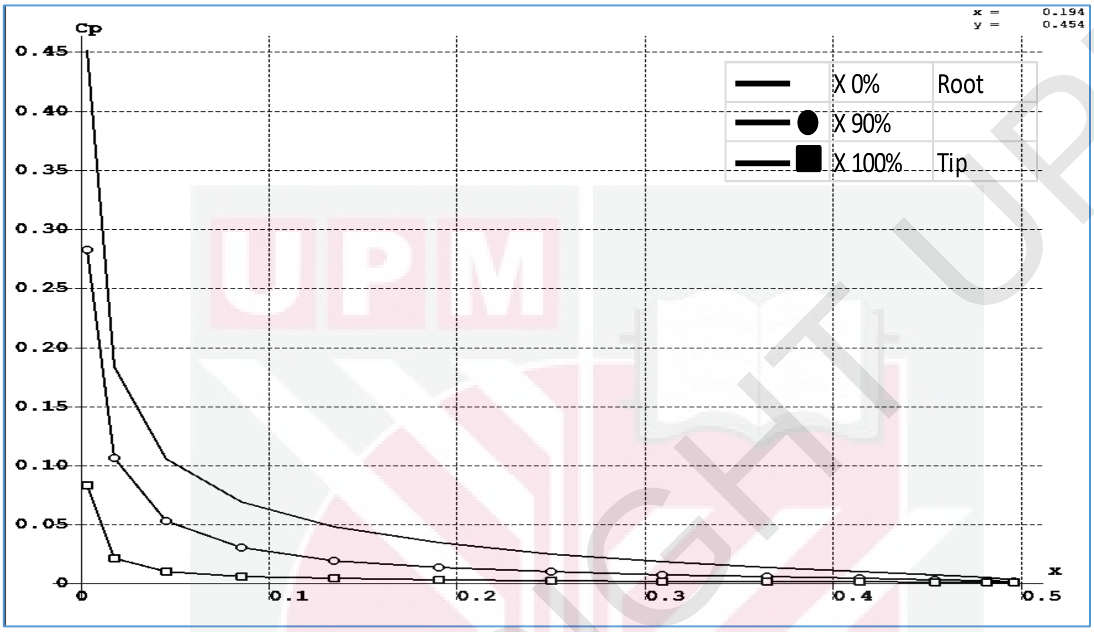

Naca0012 rectangular wing chord pressure distribution TF at 1 degree AOA

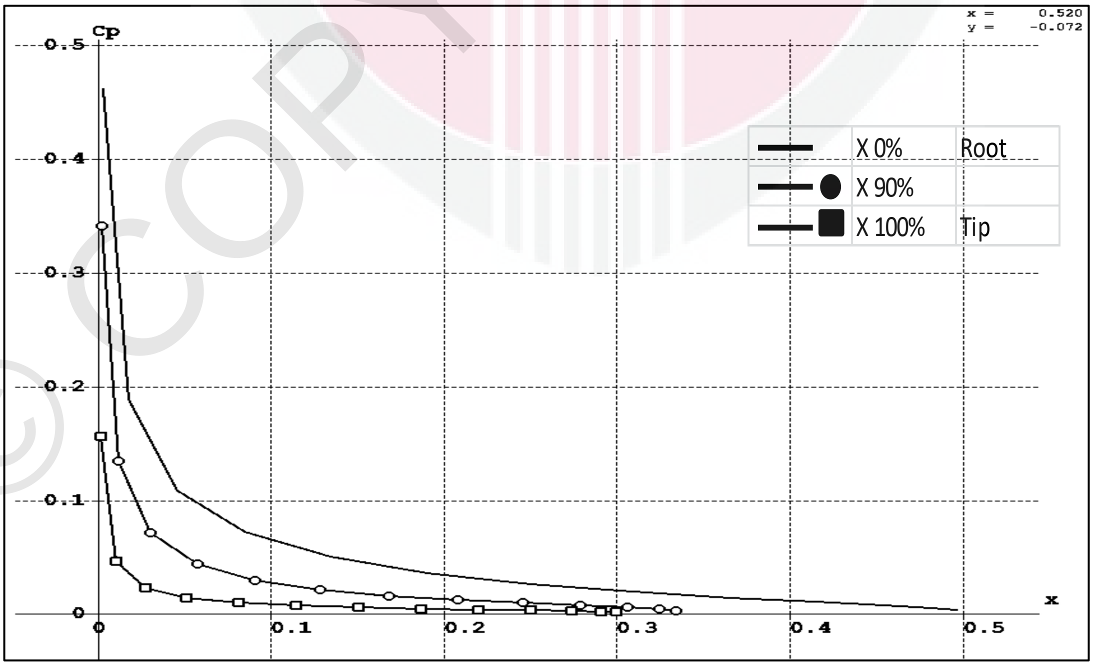

Naca0012 Inverse Delta chord pressure distribution TF at 1 degree AOA

Flat Surface Rectangular & Inverse Delta Wing

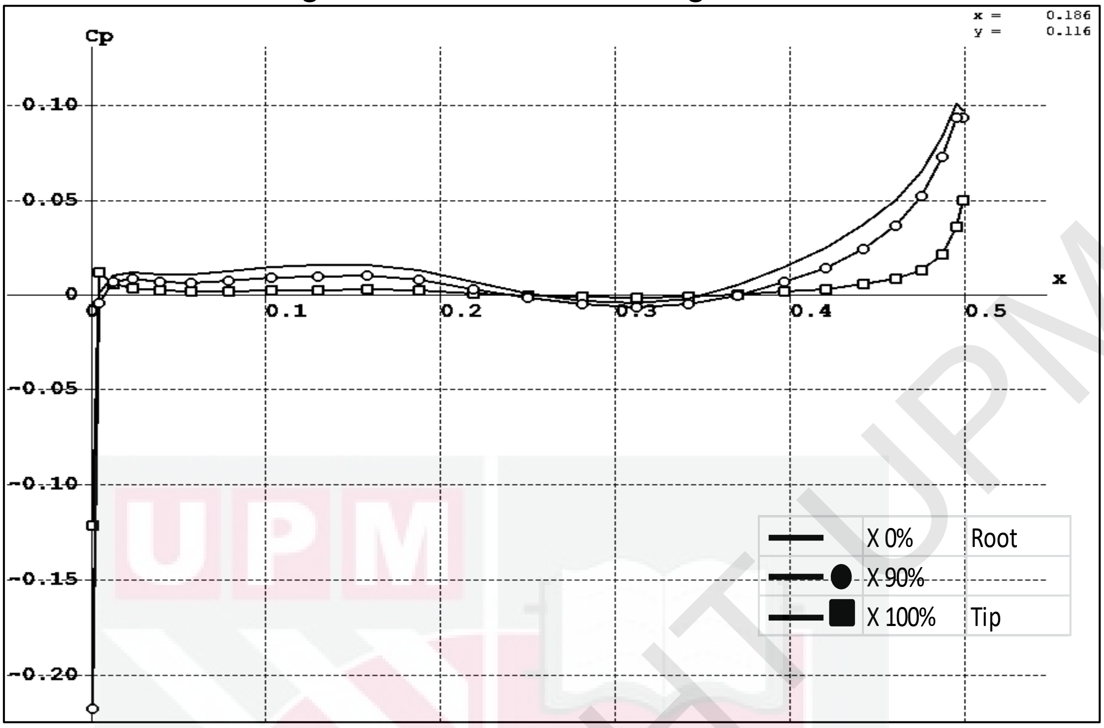

Flat Surface rectangular wing chord pressure distribution TF at 0 degree AOA

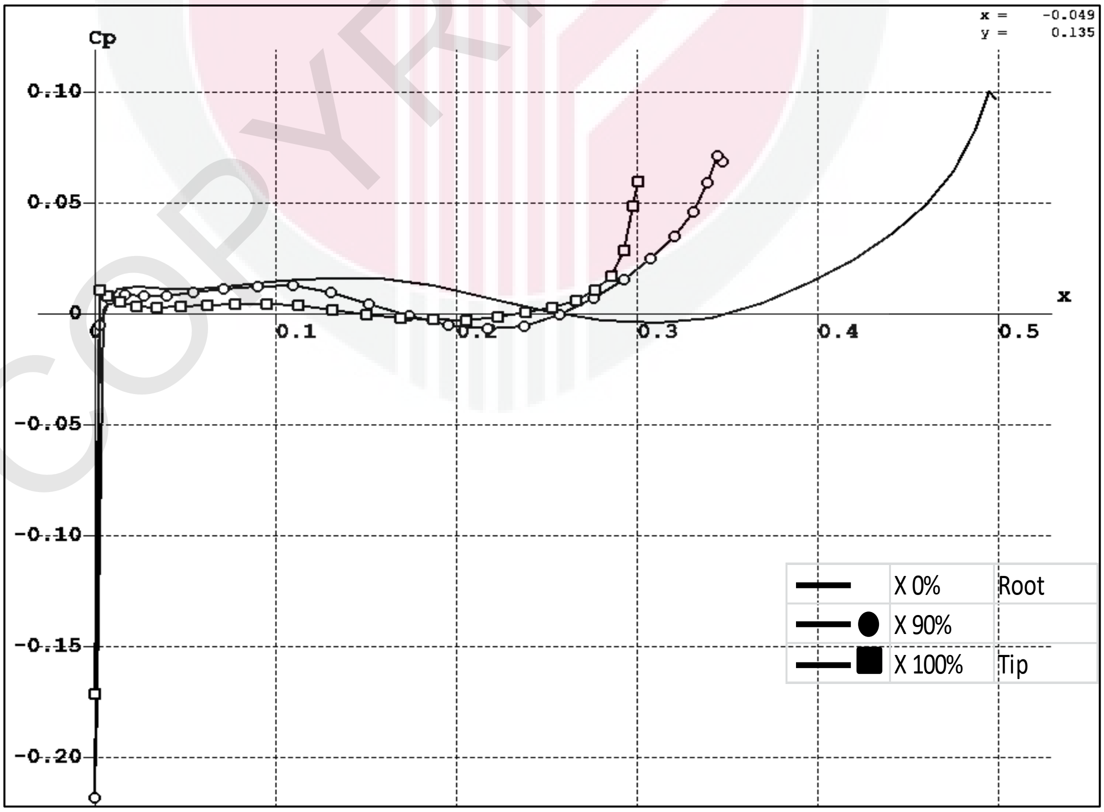

Flat Surface Inverse Delta chord pressure distribution TF at 0 degree AOA

Naca4412 Inverse Delta Wing

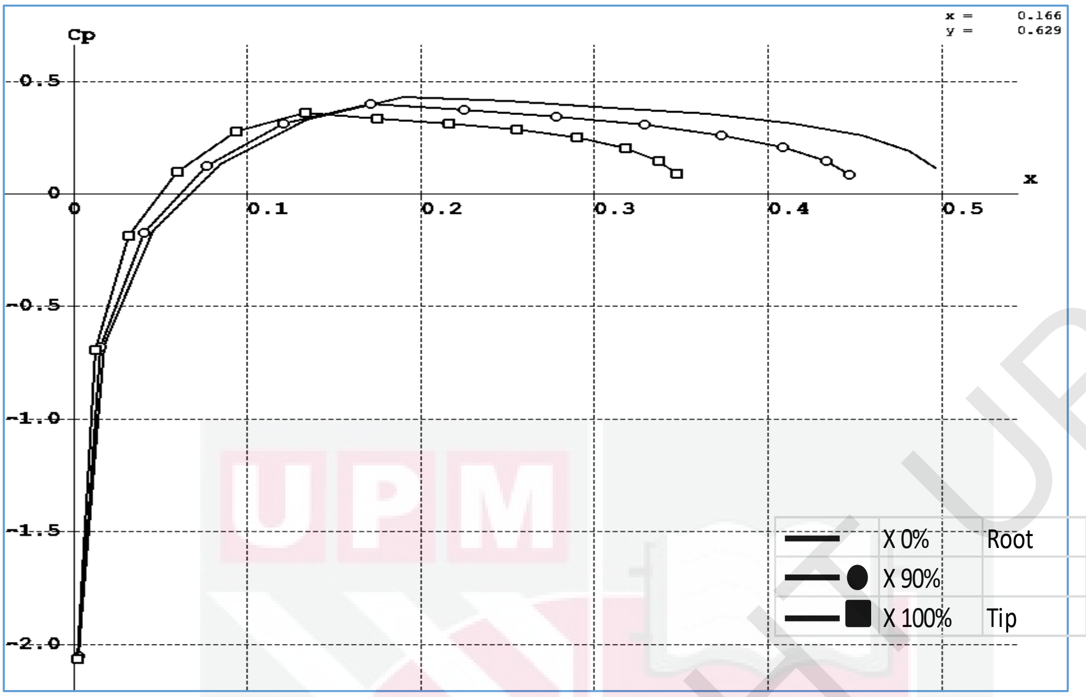

Naca4412 Inverse Delta chord pressure distribution TF at 0 degree AOA

Clark Y Rectangular & Inverse Delta Wing

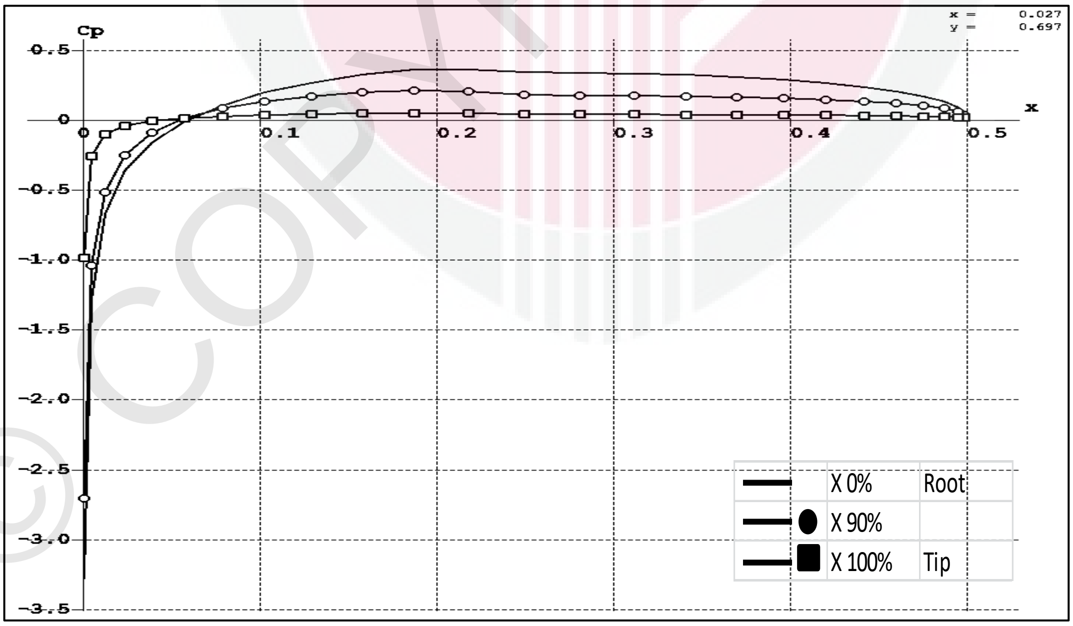

Clark Y Rectangular chord pressure distribution TF HC at 0 degree AOA

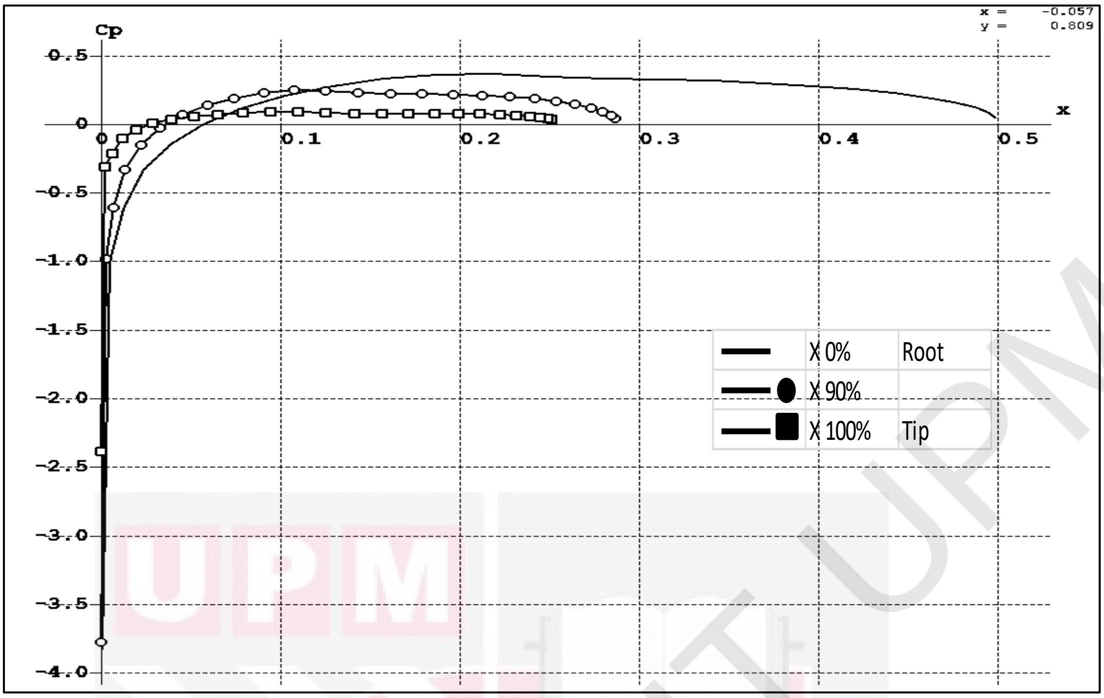

Clark Y Inverse Delta chord pressure distribution TF HC at 0 degree AOA

AWIG Rectangular & Inverse Delta Wing

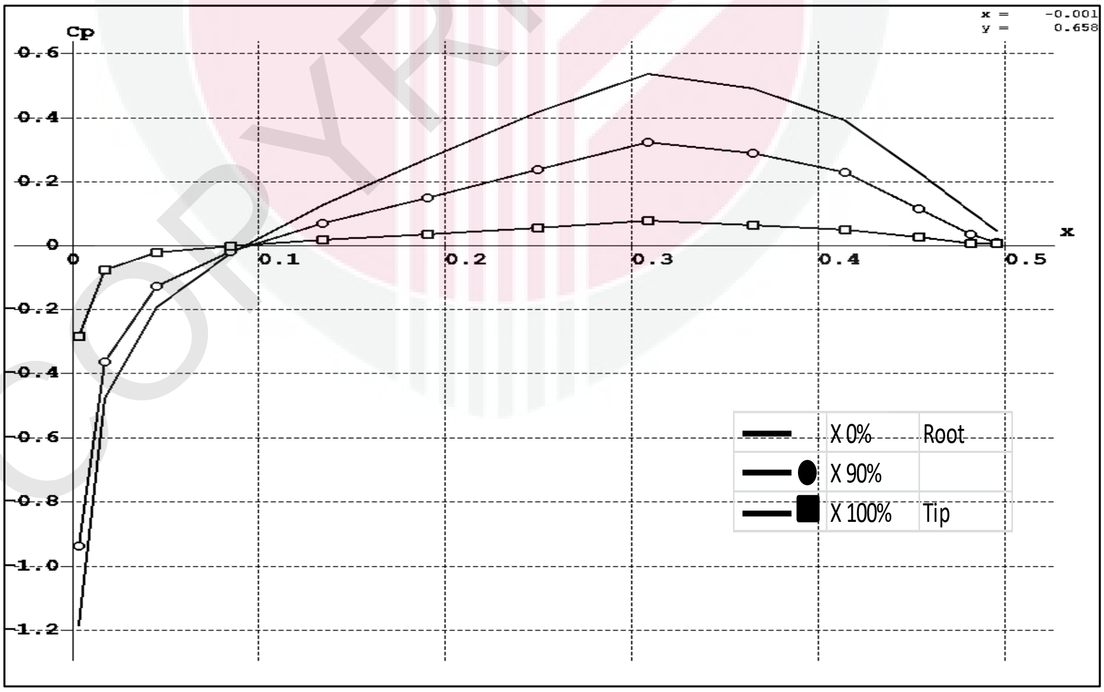

AWIG Rectangular chord pressure distribution 60% HC at 0 degree AOA

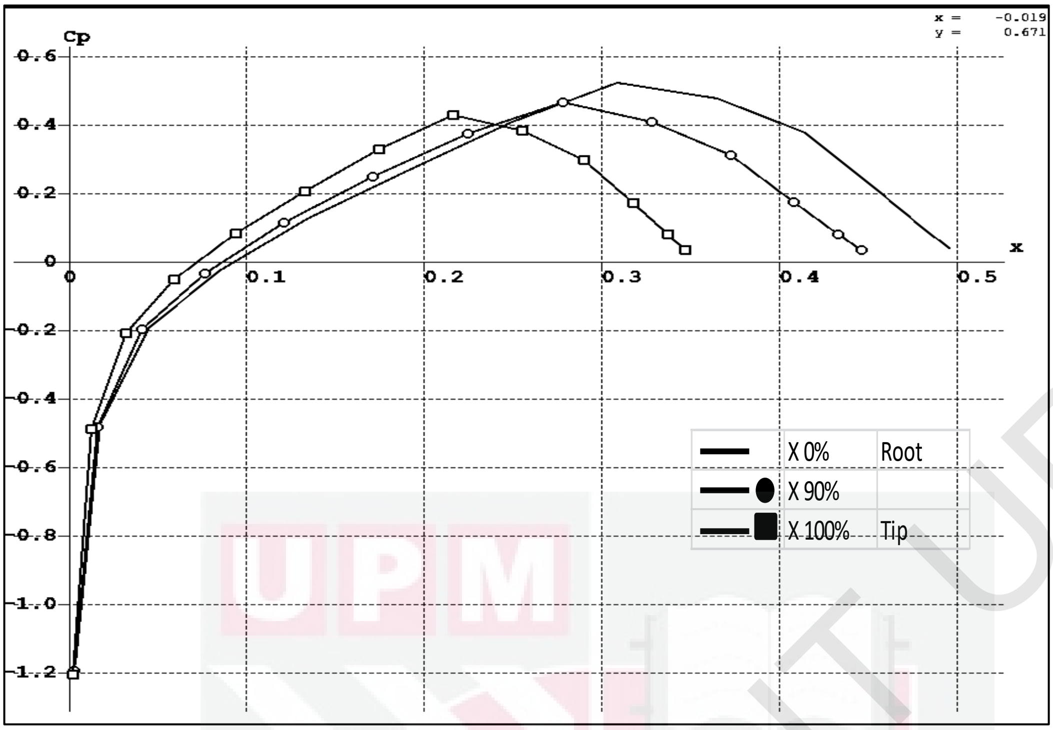

AWIG Inverse Delta chord pressure distribution TF HC at 0 degree AOA

DHMTU Rectangular & Inverse Delta Wing

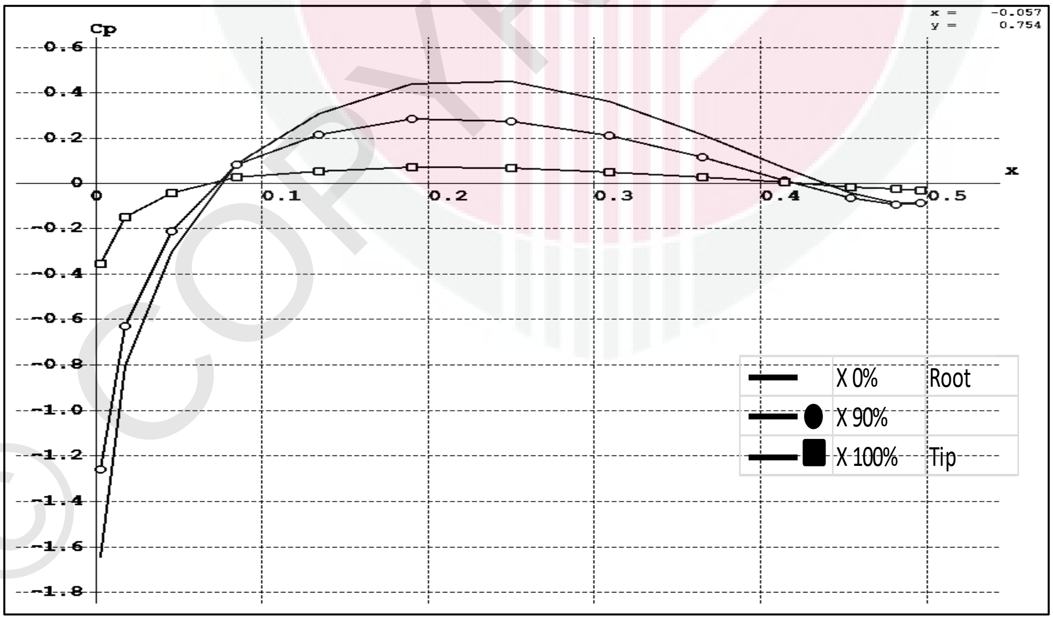

DHMTU Rectangular chord pressure distribution TF HC at 0 degree AOA

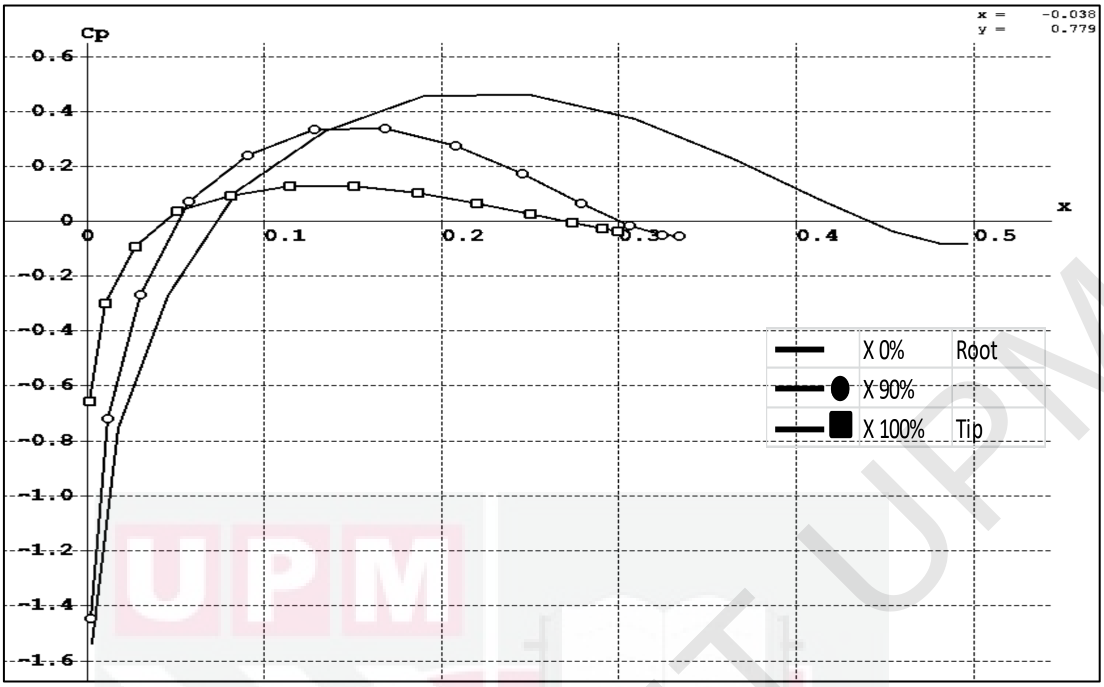

DHMTU Inverse Delta chord pressure distribution 60% HC at 0 degree AOA

Chord Pressure distribution on Profiles with UH18 Plan form (Root to Tip)

Naca 0012 & Flat Surface

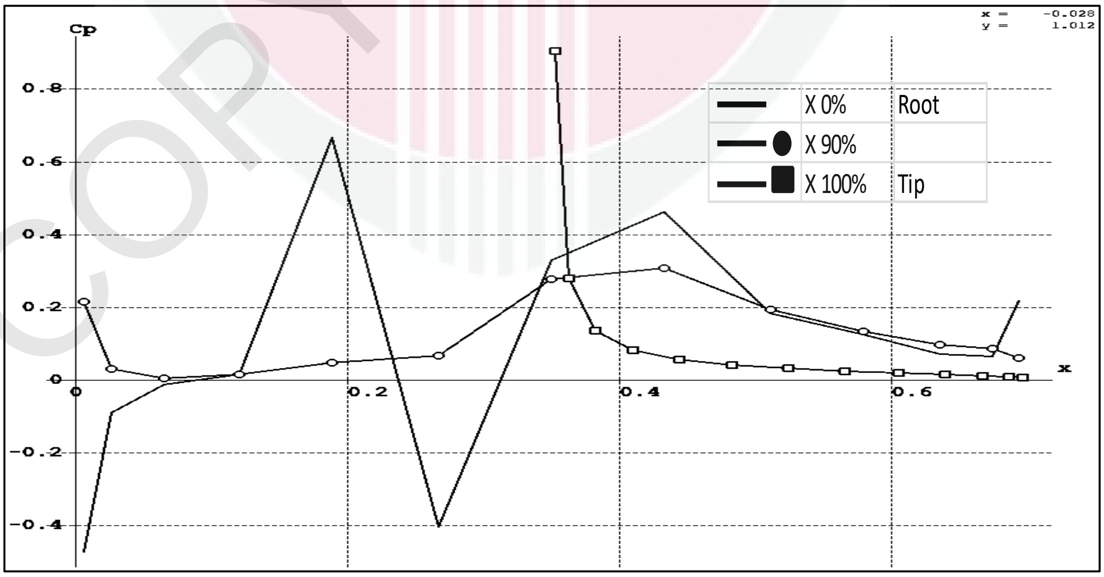

Naca0012 UH18 Planform chord pressure distribution TF HC at 0 degree AOA

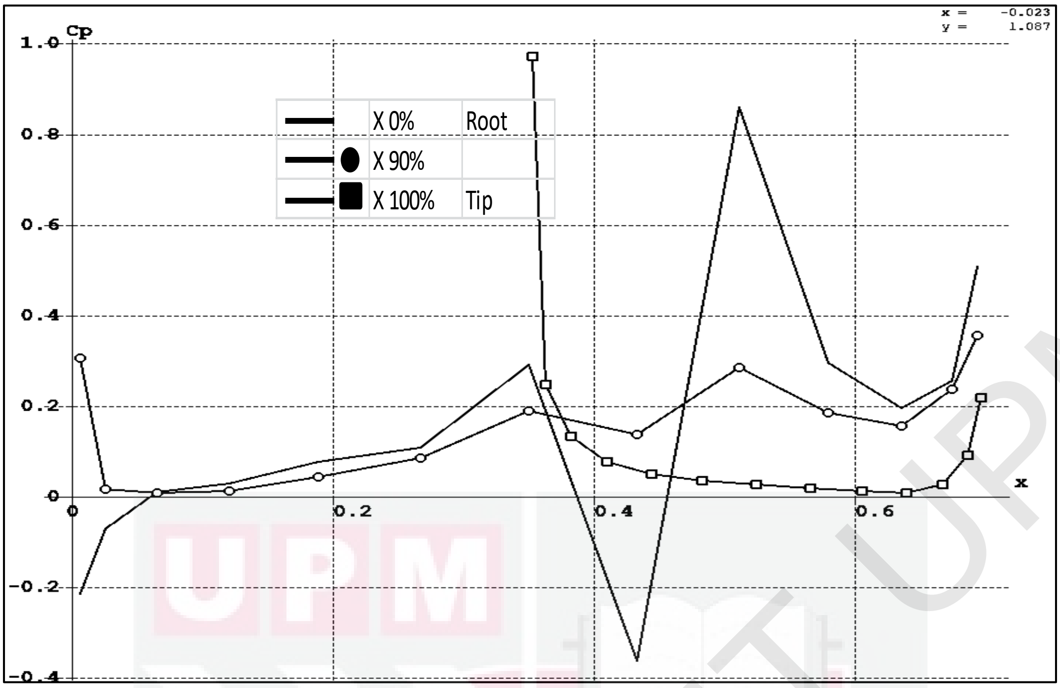

Flat Surface UH18 Planform chord pressure distribution TF HC at 0 degree AOA

Naca 4412 & Clark Y

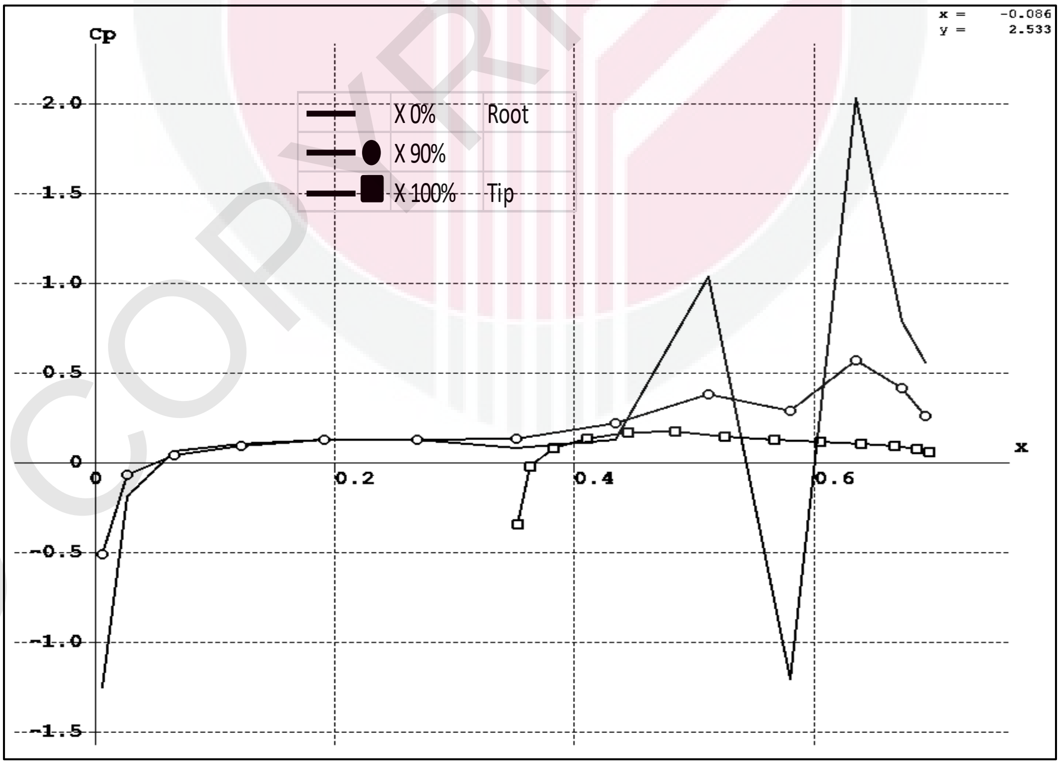

Naca4412 UH18 Planform chord pressure distribution TF HC at 0 degree AOA

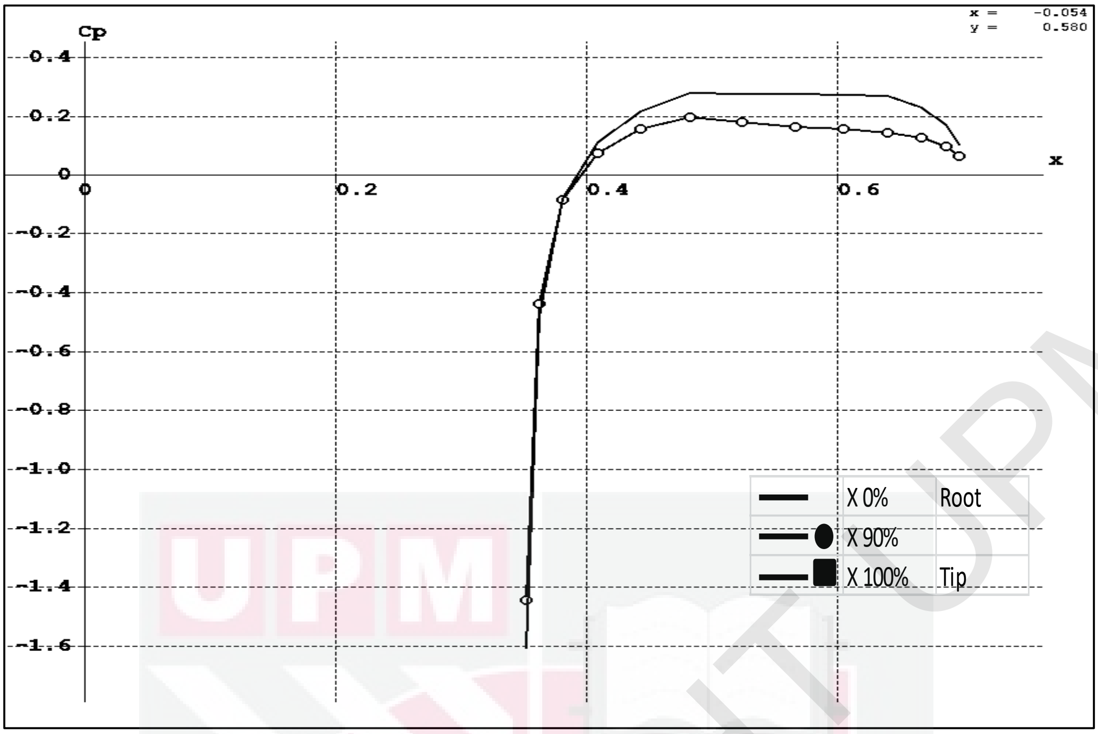

Clark Y UH18 Planform chord pressure distribution TF HC at 0 degree AOA

AWIG & DHMTU

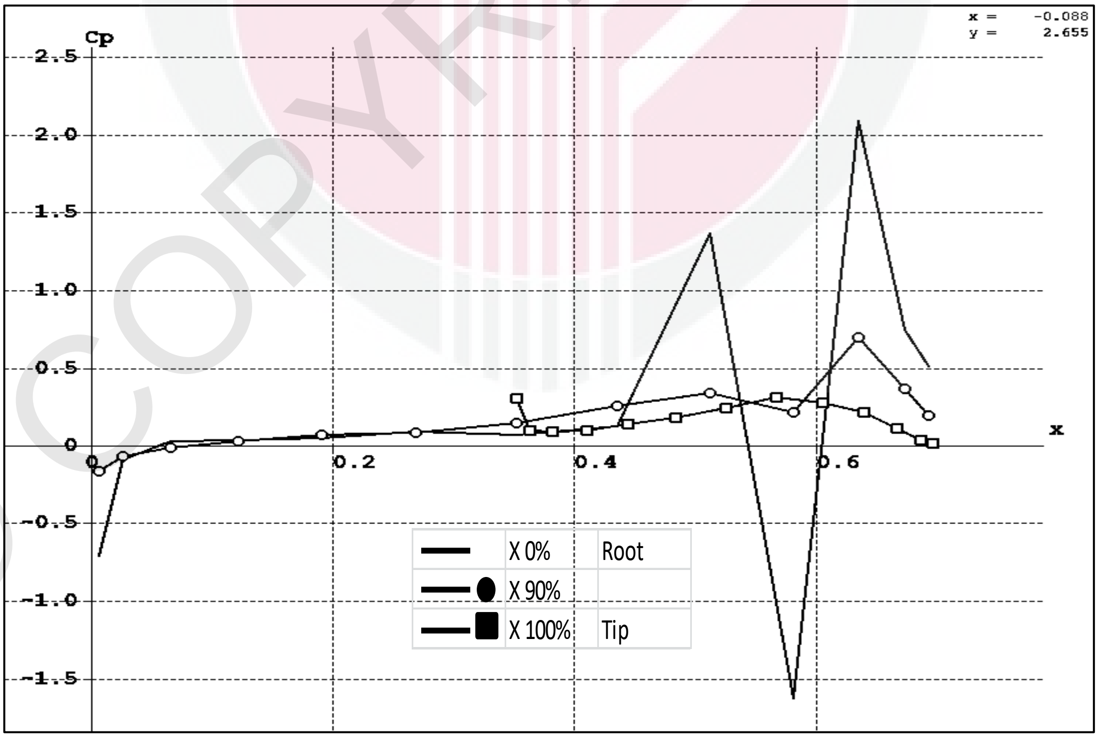

AWIG UH18 Planform chord pressure distribution TF HC at 0 degree AOA

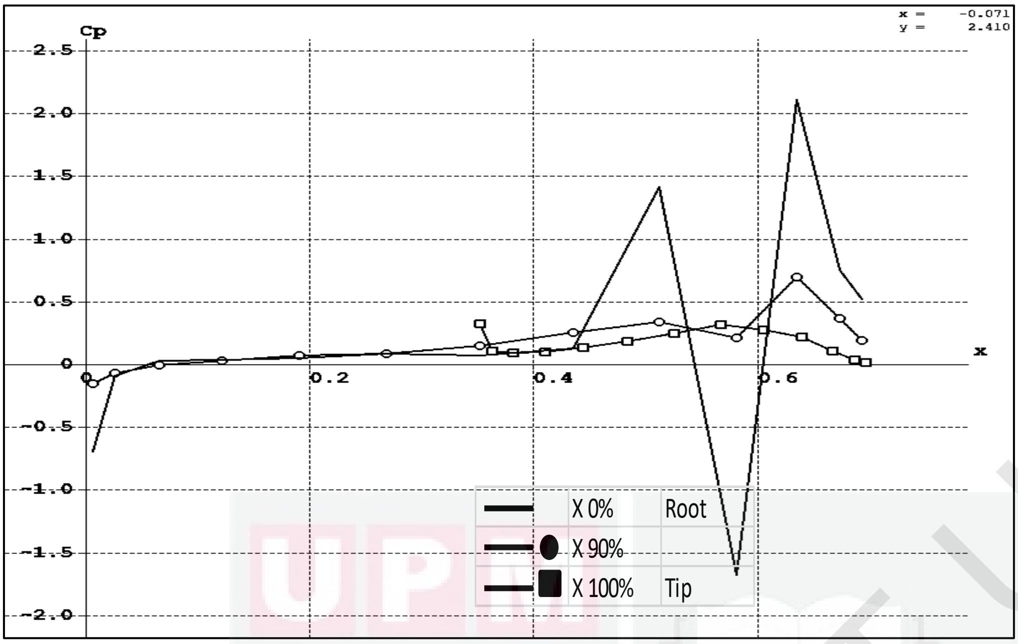

AWIG UH18 Planform chord pressure distribution 80% HC at 0 degree AOA

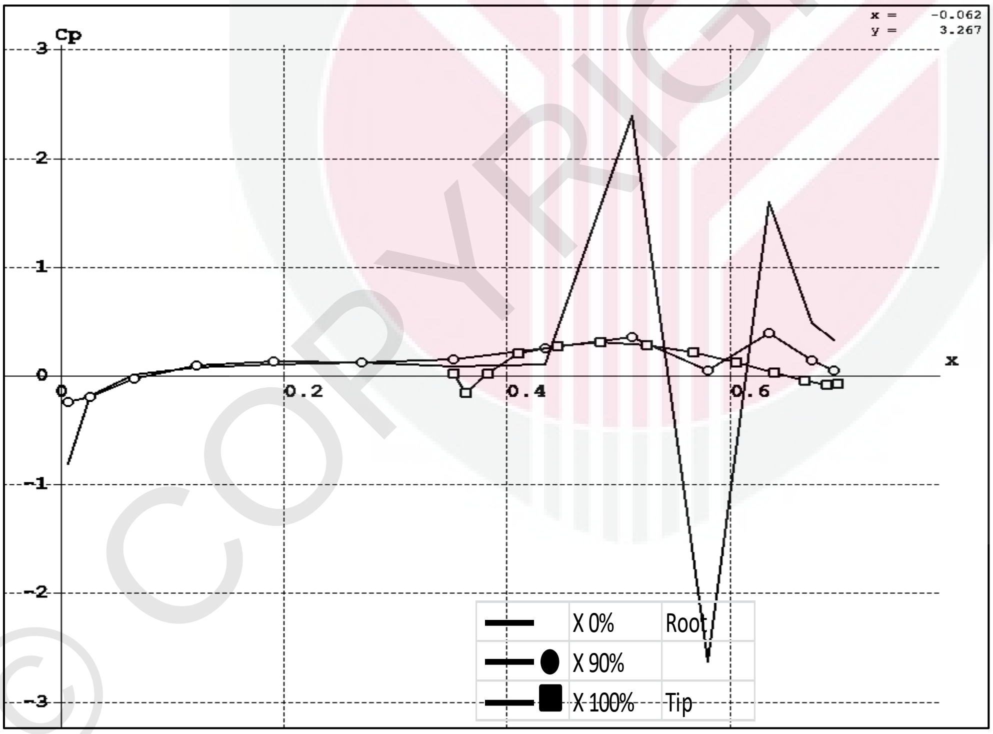

DHMTU UH18 Planform chord pressure distribution TF HC at 0 degree AOA

LIST OF PUBLICATIONS

CONFERENCE

Afifi.A Pua’at , Zulkifli Matdaud, Amzari Zhahir, Mohamed Tarmizi, Ahmad and Aziz Hassan," Case Study on Aerodynamics Stability of Bixel Wing-In-Ground Effect Craft", Southeast Asia Workshop on Aerospace Engineering (SAWAE 2019).

A,Afifi.A Pua'at, Amzari Zhahir, Aziz Hassan , Ahmad, M.T" Review on the Development of Wing-In-Ground Crafts", E3S Web Conf. Volume 477, 2024 International Conference on Smart Technologies and Applied Research (STAR'2023)

JOURNAL

Surjatin Wiriadidjaja, Amzari Zhahir, Zahratu Hilall Mohamad, Shikin Razali, Ahmad Afifi Puaat, Mohamed Tarmizi Ahmad" Wing-in-ground-effect craft: A case study in aerodynamics", International Journal of Engineering & Technology, 2018.

Afifi.A Pua’at, Amzari Zhahir, Mohd Faisal Abdul Hamid, Ezanee Gires ,Mohamed Tarmizi Ahmad, and Aziz Hassan" Investigation on the Centre of Pressure Migration for Different Wing Configurations", Journal of Aeronautics, Astronautics and Aviation, 2022) .

RESEARCH GRANT

A. Zhahir, M.F. Abdul Hamid, E. Gires and A. Pua'at. Industrial Research Grant (Tan Sri Syed Azman Syed Ibrahim Endowment Fund), Grant No. 2/2020 [Aerodynamic Performance of Two Seater DragonFly Hoverwing] worth RM 40,000 and was successfully completed on 31 December 2022.